The University Of Sheffield.

Department of Electrical and Electronic Engineering

Communication Research Group

High Gain Wide Bandwidth Layered Dielectric Resonator Antennas

By:

Abdulmajid A. Abdulmajid

Department of Electronic and Electrical Engineering

University of Sheffield

A thesis submitted in partial fulfilment of the requirements for the degree of Doctor of Philosophy

September 2019

Dedicated to:

To the soul of my grandfather **Abdulmajid**, may Allah have a mercy on him.

To my father **Abdulalhag** and mother **Sitalkil**.

To my wonderful family, my wife **Muna** and my kids.

To my brothers and sisters.

Acknowledgements

I would like express the deepest appreciation to my supervisor Dr. Salam Khamas for his unlimited support throughout my PhD study, without his encouragement and enlightening ideas this thesis would not have been possible.

Special thanks go to Mr Steven Marsden for his technical support throughout lab experiments. Many thanks as well to Dr Shiyu Zhang at Loughborough University, Loughborough, UK., for granting access to mm-wave lab. The author also would like to thank C. Majewski and W. Birtwistle at the Centre of Advanced Additive Manufacturing, University of Sheffield, Sheffield, U.K., for granting access to their facilities and their technical assistance with the laser sintering process.

I would also like to thank the Ministry of Higher Education in Libya for their financial support especially Dr Atef Saeeh my academic advisor at Libyan cultural affair London, UK.

To all relatives, friends, my colleagues in the communication group at the University of Sheffield, thank you for your support;

Finally, and most importantly, a huge thank you to my wife Muna for her full support and looking after our kids throughout PHD course.

Publications

Journal articles

[1] A. A. Abdulmajid, Y. Khalil, and S. Khamas, "Higher-Order-Mode Circularly Polarized Two-Layer Rectangular Dielectric Resonator Antenna," IEEE Antennas and Wireless Propagation Letters, vol. 17, pp. 1114-1117, 2018. (Chapter 3)

[2] A. A. Abdulmajid and S. Khamas, "Higher Order Mode Layered Cylindrical Dielectric Resonator Antenna," Progress In Electromagnetics Research, vol. 90, pp. 65-77, 2019. (Chapter 4)

[3] A. A. Abdulmajid, S. Khamas, and S. Zhang “Wide Bandwidth High Gain Circularly Polarized Millimetre-wave Rectangular Dielectric Resonator Antenna,” Progress In Electromagnetics Research M, vol. 89, pp.171-177, 2020. (Chapter 5)

[4] A. A. Abdulmajid, S. Khamas, and S. Zhang "Wideband Millimetre-Wave Three-layer Hemispherical Dielectric Resonator Antenna “, submitted to Microwave and Optical Technology Letters, 2019. (Chapter 5).

Conference proceedings papers

[1] A. A. Abdulmajid, Y. Khalil, and S. Khamas, "Higher Order Mode Layered Rectangular Dielectric Resonator Antenna," presented at the Loughborough Antennas & Propagation Conference 2018 (LAPC 2018), Loughborough, UK, 2018. (Chapter 3)

[2] A. A. Abdulmajid, S. Khamas, and Khalid Al-Khateeb, "High Gain Rectangular Dielectric Resonator Antenna with a Superstrate for X band Applications," Accepted for publication in Antennas & Propagation Conference 2019 (APC 2019), Birmingham, UK, 2019. (Chapter 2)

Book Chapter

[1] A. A. Abdulmajid, Y. Khalil, and S. Khamas. High gain Circularly Polarized Multi-layer Rectangular DRA. In Advances in Networks, Security and Communications. Vol.2. Ed.by Sergey Y. Yurish, IFSA Publishing, 2019. (Chapter 2&3).

List of Abbreviations

DRA	Dielectric Resonator Antenna
RDRA	Rectangular Dielectric Resonator Antenna
CDRA	Cylindrical Dielectric Resonator Antenna
HDRA	Hemispherical Dielectric Resonator Antenna
LHCP	Left Hand Circular Polarization
RHCP	Right Hand Circular Polarization
LDRA	Layered Dielectric Resonator Antenna
DWM	Dielectric Waveguide Model
CST MWS	Computer Simulation Technology Microwave Studio
BW	Bandwidth
AR	Axial Ratio
TE	Transfer Electric
TM	Transfer Magnetic
HE	Hybrid Electric
λ_0	Wavelength
λ_g	Guide Wavelength
ε_r	Dielectric Constant

Abstract

Dielectric resonator antennas (DRAs) are promising candidates for the next-generation wireless communication systems since they offer wider bandwidth and higher radiation efficiency. In addition, higher gain can be accomplished by exciting a higher order resonance mode in order to meet the high-frequency application requirements. However, several challenges exist in the design of higher-order mode DRAs such as the narrow bandwidth and the possibility of impractical dimensions. This thesis presents a novel design approach that offers high gain in conjunction with wide impedance and axial ratio bandwidths by utilizing layered DRAs that are excited in higher order mode. A number of known approaches for gain enhancement have been investigated such as higher order mode operation of standalone DRAs, dielectric superstrate as well as DRA arrays. Generally, each of these design approaches is associated with at least one of key limitations such as narrower impedance bandwidth, impractical dimension, considerable sensitivity to fabrication errors and the requirements for a complex and lossy feed network in the case of arrays. On the other hand, the reported literature designs that incorporate multi-layer DRAs have been limited only for impedance bandwidth improvements. This research extends the potential of incorporating a dielectric coat layer to enhance the gain and axial ratio as well as impedance bandwidth.

X-band and mm wave rectangular DRAs that operate at multi-high order modes have been considered, where each one of them has been coated by an additional dielectric layer that has increased the order of the excited modes so that an enhanced gain of ~12dBi can be accomplished in conjunction with wider matching impedance and axial ratio bandwidths as well as a considerable robustness to fabrication errors. The proposed design concept offers an alternative approach to the existing mechanisms that are either based on a lower gain single mode operation or a higher order mode operation with narrow bandwidth and noticeable sensitivity to fabrication tolerances. This framework has been applied to cylindrical DRA that offered a remarkably gain of ~ 14 dBi, which is the highest for a single wideband DRA and in line with those offered by arrays. Therefore, the proposed layered DRA designs represent alternative to the classical approach of employing arrays for gain enhancement with additional appealing radiation characteristics. Moreover, the proposed concept has been adopted to design a high gain wide band mm-wave hemispherical DRA.

However, owing to the nature of the modal field distribution inside the DRA, the design has been modified to utilize a two-layer dielectric coat in order to create a multi-stage transitional region between the DRA element and free space. This has provided an enhanced gain of 9.5dBi in conjunction with a wide impedance bandwidth. Several prototypes have been fabricated and measured at the x-band and mm-wave frequency range with good agreement between simulated and measured results.

Contents

List of figures

List of tables

Chapter 1

Introduction

1.1 Dielectric Resonator Antennas

The last few decades have witnessed a significant growth in wireless communication systems. In order to acquire a much wider bandwidth with reduced interference, higher carrier frequencies such as X- and mm-wave bands are presently needed more than ever to replace the already congested lower frequency spectrums. Microstrip antennas are not the most suitable choice for the next generation communication system owing to their well-known limitations such as narrow bandwidth, low gain and above all metallic and surface wave losses, which can be considerable at higher frequencies. On the other hand, dielectric resonator antennas (DRAs) are more favorable due to higher radiation efficiency, wider bandwidth, smaller size, various geometries, easy excitation, low profile and light weight. Therefore, key limitations of micro-strip antennas can be eliminated by utilizing DRAs. The aforementioned advantages paved the way of DRAs to be an ideal candidate for higher frequency applications [1-5].

Dielectric resonator antennas have been introduced by Long et al. in earl 1980s [6], where it has been demonstrated that cylindrical DRs can be used as energy storage devices, which represents an advantage to use such resonators as radiating elements. Since then, many investigations have been reported that are focused on DRAs with different shapes and their radiation characteristics have been examined [6-8]. As DRAs proved themselves as good radiating elements, numerous studies have been concentrated on improving the characteristics of such antennas. Bandwidth and gain enhancement techniques have been going on to satisfy the requirements of the recent wireless technology advancements [9-11]. In addition, considerable efforts have been directed towards the design and optimization of DRA arrays, where, a linear DRA array has been first introduced in the early 1980's [7]. In addition, the first study of a planar array has been reported by Haneishi and Takazawa [8].

As mentioned earlier, in comparison to microstrip antenna, DRAs offer wider impedance bandwidths in the order of 10% by fabricating the antenna using a material with a typical dielectric constant, ε_r, of ~10 [1]. This can be attributed to the fact that the microstrip antenna radiates only through two narrow radiation slots. However, the DRA radiates through the whole antenna surfaces excluding the grounded part. It should be noted that the DRA size is linearly proportional to $\lambda_o/\sqrt{\varepsilon_r}$, where λ_o is the free space wavelength at the resonance frequency [12]. Therefore, a substantial reduction in the antenna size can be accomplished using a higher permittivity material. Additionally, DRAs are available with different geometries such as rectangular, cylindrical, hemispherical, triangular and many others, as depicted in Figure 1.1. Compared to cylindrical and hemispherical configurations, a rectangular DRA geometry requires a simpler fabrication process and provides two aspect ratios that can be varied in order to excite different modes.

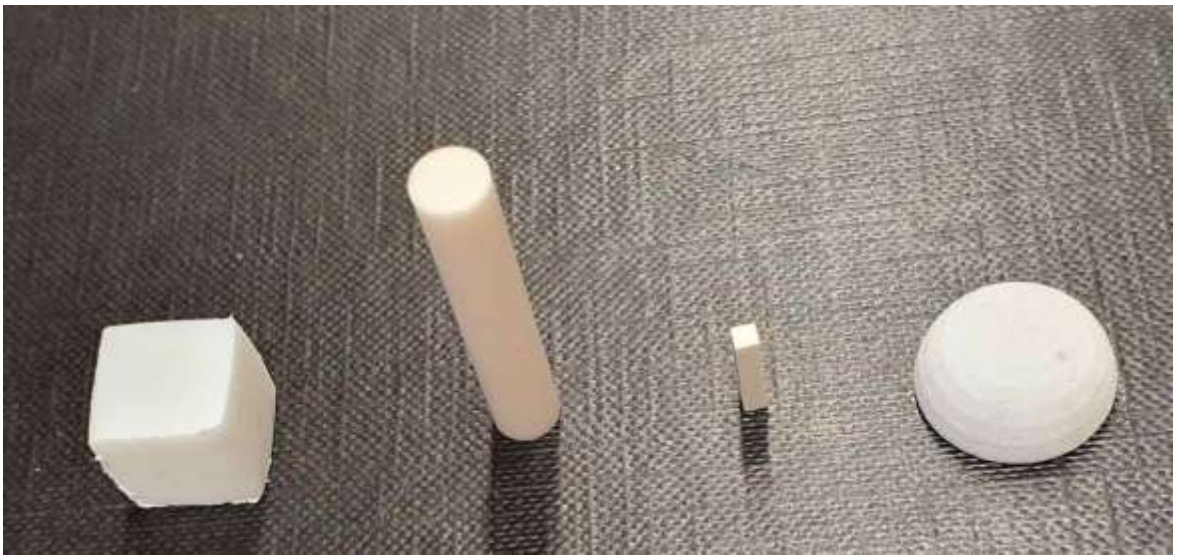

Figure 1.1: Dielectric resonator antennas of various geometries.

For most practical applications, power can be coupled into DRA through one or more ports, and the strength of the coupled depends on the type, size and location of the feeding element. The power can be coupled to the DRA using slot aperture [13], coplanar wave guide [14], probe [15], microstrip line [16] and coaxial feed [17]. However, a number of limitations exist in most feeding mechanisms, which makes the slot aperture as the most popular. For example, when taking a probe fed DRA, a hole is required to be drilled in a hard ceramic, and if drilled inaccurately, the DRA performance is affected because of the small DRA size at a high frequency range. On the other hand, a microstrip line feed impacts the antenna radiation

characteristics as the line is not isolated from the DRA. In addition, when the DRA is placed directly on the top of the transmission line strip, unwanted air gaps are formed between the resonator and ground [18-20]. In this study, a slot coupling has been chosen for multiple reasons such as ease of fabrication and the isolation of the antenna from the ground plane that results in minimizing spurious radiation from the feed network. Moreover, similar to the slot antenna, the rectangular DRA radiates like a horizontal magnetic dipole when excited by a centrally fed slot, hence the undesirable cross-polarized fields will be minimized because the radiated fields of the DRA and slot are similar to each other.

1.2. High Gain Dielectric Resonator Antenna

1.2.1 Higher Order Mode DRAs

It is well known that with the increase in the operating frequency, a smaller DRA size is expected. For example, a rectangular DRA that has a respective length, width and height of 10mm, 5mm and 2.5mm at 10GHz, will exhibit a considerably smaller respective dimensions of 1mm, 1mm and 5mm when operating at 60GHz [21, 22]. Thus, proving a precise DRA fabrication becomes a key requirement at higher frequencies. On the other hand, larger DRA dimensions support higher order operation at higher frequencies. A recent study has investigated the excitation of higher order mode by changing the RDRA height to $\sim\lambda_0/3$, $\lambda_0/2$ and$\sim\lambda_0$ in order to excite the TE_{111},TE_{115} and TE_{119} modes, receptivity, for higher gain [23, 24]. The gain enhancement can be explained by studying the DRA inner magnetic field distribution in which the maximal field spots can be represented as short magnetic dipoles, where a maximum gain can be achieved when the separation distance between the adjacent magnetic dipoles is $\sim 0.4\lambda_o$. Moreover, the higher order mode operation can be classified as single mode and multi-resonance modes operations. The single higher order mode DRA operation can be achieved using a width to height aspect ratio range of ~0.25 to 1.5 [25]. Furthermore, that study paved the way to choose a single, or multi, mode operation on the basis of the aspect ratio, where it has been demonstrated that by utilizing an aspect ratio of less than 0.25, a multi-higher order mode operation is triggered.

In addition, the dielectric waveguide model (DWM) has been employed to investigate higher order mode rectangular DRA, where it has been shown that a more directive radiation pattern

can be achieved by increasing the mode order, where it has been reported that the pattern of the TE_{917} resonance mode is more directive compared to that of the TE_{111} mode [26]. Furthermore, a slot-fed rectangular DRA with a low relative permittivity of 6.15 offered a higher gain of 10dBi along with an impedance bandwidth of 20% by optimizing the size of the ground plane when the $TE_{\delta 33}$ mode is excited [27]. An alternative study has demonstrated that a rectangular DRA that is designed for 5G applications and operates in the higher order mode of $TE_{1\delta 3}$ offers a gain of 9dBi with an impedance bandwidth of 4.7% [28]. Furthermore, gain enhancement has been demonstrated by exciting the $HE_{12\delta}$ resonance mode where a gain of up to 8dBi has been achieved in conjunction with a narrower bandwidth of ~6% [29]. In addition, a dual-band dual-polarized cylindrical DRA has been reported by utilizing strip and slot excitations in order to excite the HE_{111} mode and the HE_{113} higher order mode that offered a ~7% impedance bandwidth as well as a gain of ~8.9dBi at 6.4GHz [30]. In another study, a cylindrical DRA that operates in various resonance modes such as TE_{211}, TM_{212} and TM_{121} has been reported, with narrow impedance bandwidth of 1.5% and gain of 3.6dBi at the TE_{211} resonance frequency [31]. In addition, the $HEM_{12\delta}$ higher order mode has been successfully excited using a microstrip line with a bandwidth of 5.6% and a gain of 7.8dBi at 5.46GHz [32]. Furthermore, an air-filled cavity in the ground plane has been proposed, where both of the $HEM_{11\delta}$ and $HEM_{12\delta}$ modes have been experimentally realized with a ~10dBi gain together with a narrower impedance bandwidth of 2.6% [33]. Recently, a higher order mode cylindrical DRA characterized by a high gain has been investigated experimentally, where a gain of 12dBi has been obtained through the combination of the HEM_{123} and HEM_{133} higher order hybrid modes, albeit with a relatively narrower impedance bandwidth of ~2.6% [34]. The same modes have been generated by employing a slot-fed excitation, where a gain of 11.6dBi has been achieved with an impedance bandwidth of 3.5% [35]. Additionally, a cylindrical DRA that is excited by a microstrip coupled slot has been investigated experimentally resulting in a wider bandwidth of ~61% and higher gain up to 8.7dBi by exciting the $HEM_{31\delta}$ and $HEM_{13\delta}$ higher order modes [36]. However, this approach involved some complexity in terms of the feed design and convoluted fabrication. Therefore, increasing the mode order results in a considerably higher gain [23, 26], which represents a key requirement at higher frequency communications. However, and as mentioned earlier, higher order modes are usually associated with a narrower bandwidth, which can be attributed to the fact that the DRA

effective dielectric constant increases with the mode order, where the effective permittivity increase with antenna size [25].

Alternative approaches to enhance the DRA gain have been reported in the literature. For example, a defected ground structure of a dual band RDRA has been reported in [37], where a directivity of 10dBi has been achieved at 18GHz with a narrow bandwidth of less than 4%. In another investigation, DRA gains of 7dBi and 10dBi have been measured when a dielectric image line has been coupled to the DRA through a narrow rectangular sot aperture [38, 39]. In a subsequent study, a uniaxial anisotropic material has been incorporate inside a rectangular DRA in order to increase the radiation from the antenna side walls [40], which has improved the gain of the TE_{111} mode to 8dBi in conjunction with a 20% impedance bandwidth. In addition, the gain can be improved using a dielectric superstrate on the top of the DRA, resulting in a considerable gain enhancement. It should be noted that this approach is common among patch antennas design [41-43]. However, a dielectric superstrate used to enhance the gain of 60 GHz rectangular dielectric resonator antenna operating at its higher order mode, where ~14dBi was obtained at 60GHz associated with 17.4% impedance bandwidth when the TE_{311} mode has been excited [44] . Furthermore, an investigation applied a superstrate above a cylindrical DRA for an enhanced gain of ~18dBi in conjunction with 10% impedance bandwidth were noted by exciting $HE_{11\delta}$ mode [45].

1.2.2 High Gain DRA Arrays

The DRA arrays represent ideal candidates for applications that require higher gain. In the early 1980s, DRA array for millimeter wave applications has been investigated experimentally using a dielectric waveguide feed [7]. Later, a novel design of X-band CP rectangular DRA arrays using cross slot feeding mechanism has been introduced, where a 20% axial ratio bandwidth has been achieved in conjunction with 20dBic gain by using 4×4 DRA elements that are separated by a distance of $0.7\lambda_o$ [46]. Moreover, an array of four rectangular DRA elements that are separated by a half wavelength has been reported with an impedance bandwidth of ~0.5% and a ~5dBi gain at an operating frequency of 40.3GHz [47]. In a subsequent study, a 21.3dBi gain has been measured by using a rectangular DRAs array with 8×8 elements and an impedance bandwidth of ~18% in conjunction with 21.3 dBi [48] . In another investigation, 128 rectangular DRAs have been itched on a Silicon substrate

using micromachining techniques to achieve a gain of ~11dBi along with a 15% impedance bandwidth for mm wave applications [49]. High gain rectangular DRA antenna arrays utilizing a dielectric layer on Bismuth Titanate ceramics has investigated in [50], where the antennas have been designed and constructed with a combination of two, four, and six elements that offered gains of 7 and 7.6 and 8dBi respectively. However, the impedance bandwidth has not been reported. Furthermore, a linear rectangular DRA array with a modified feeding line structure has been proposed for 5G applications, where four elements have been used to provide respective impedance bandwidth and gain of 20% and 12dBi [51]. Moreover, DRA array with a direct microstrip line fed has been reported in another study, where four rectangular DRAs have been employed, resulting in a gain enhancement of 14.8dBi at 7GHz in conjunction with a narrow impedance bandwidth of 3.1% [52]. However, the employed feeding microstrip line has not isolated the DRA from the feed network, therefore the spurious backward radiation has not been eliminated completely. Another study has utilized a higher order mode four cylindrical DRA elements operating at the HE_{133} resonance mode at a center frequency of 25GHz with a maximum measured gain of 10.8dBi and a narrow impedance bandwidth of 2.2% [53]. A significantly higher gain of 13.4dBi has been achieved when an aperture coupled rectangular DRAs array has been designed with parasitic elements using eight elements that are separated by distance of half of wavelength [54]. However, the narrow impedance bandwidth of 0.4% represents the main limitation. Further, a series-fed in order to improve front to back ratio linear substrate-integrated dielectric resonator antenna array has been investigated experimentally for millimeter-wave applications [55] with an impedance bandwidth of ~10% at 34.5GHz and an average gain of 11.8dBi. Additionally, a wide band rectangular DRA array that has been fed using an array of slots that are excited by a printed microstrip line has considered [56] an impedance matching bandwidth of 63% along with an 11.5dBi gain. A wideband artificial grid dielectric resonator antennas (GDRAs) operating at 32GHz have been recently proposed offering wide impedance bandwidth of 18.46%, high gain up to 12dBi [57]. On the other hand, using antenna arrays for gain enhancement has a number of limitations. For example, the overall size will be increased considerably for increased number of elements, hence, a more complex feed network results in a higher cost is required. In addition, considerable ohimc losses are expected at higher frequencies. Furthermore, the limited impedance bandwidth falls short of meeting the requirements of new generation commutations system, which may be considered as the key limitation of antenna arrays.

1.3 Circular polarization DRAs

The earlier DRAs studies have focused mainly on linearly polarized radiation [23, 24, 26]. However, circularly polarized DRAs have received an increased interest recently since their radiation is less sensitive to atmosphere conditions and insensitive to the transmitting and receiving antennas orientation. For example, a quadrature-fed circularly polarized rectangular DRA has been proposed in [58] by exciting the TE_{111} and TE_{113} resonance modes with a maximum gain of 6dBic . In addition, a higher order mode dual-band CP chamfered RDRA has been reported using a single feed point [59]. The two bands have been achieved by exciting the TE_{111} and TE_{113} resonance modes with respective impedance and axial ratio bandwidths of 11.4% and 1.4% as well as a gain of ~7dBic for the TE_{113} mode. In a recent study, a cross slot-fed dual band circularly polarized DRA that operates in the TE_{111} and TE_{113} higher order modes has been presented with respective impedance and axial ratio bandwidths of 8.4% and 2.2% as well as a gain of ~4.3dBic for the TE_{113} mode[60]. Therefore, TE_{113} represents the highest mode order that has been considered for a circularly polarized DRA radiation. On the other hand, a number of papers have focused on the design of circularly polarized cylindrical DRAs. For example, a cross-slot-fed CP cylindrical DRA that operates at the $HE_{11\delta}$ lower order mode has been reported with respective impedance and AR bandwidths of 28% and 4.7% [61] . However, the modest gain of ~3.5dBic at 5.75GHz represents a key limitation of this approach. An alternative approach has been proposed in [62], where a cylindrical DRA that is fed by a number of slot apertures has been optimized to provide a comb-shape with a wide axial-ratio bandwidth of ~4% and a 3.5dBic gain. Furthermore, a CP cylindrical DRA fed by a quadruple strip has been investigated experimentally, where four vertical conformal strips have been placed around the DRA circumference in order to achieve wide axial ratio, AR, and impedance bandwidths of 25.9% and 34.5%, respectively, with a broadside gain of 5dBic [63]. In another study, a single probe feeding has been utilized to excite several CP cylindrical and rectangular DRAs, where it has been noted that two orthogonal resonance modes, TM^{x}_{110} and $TM^{y}_{110,}$ can be excited by changing the probe length to achieve maximum AR and impedance bandwidths of 1.2% and 5.7%, respectively [64]. A study of a dual-band CP cylindrical DRA that operates in the HE_{111} and HE_{113} higher order modes have been presented with respective impedance and AR bandwidths of 23.5% and 7.4% and a maximum gain of 7dBic [65]. In addition, respective impedance and axial ratio bandwidths of 25.36% and 3.23% have been

achieved in conjunction with a 6.5dBic gain using a single probe excitation of an elliptical CDRA [66]. Circularly polarized hemispherical DRAs have received attention, for example, a hemispherical DRA has been excited using dual conformal-strips, where a 21% axial ratio has been measured in the fundamental broadside TE_{111} mode [67]. Similarly, 2.4% AR bandwidth has been achieved when a single parasitic patch used for CP radiation of a hemispherical DRA [68]. However, in both studies the impedance bandwidth and gain have not been reported. Furthermore, aperture-coupled hemispherical DRAs with a parasitic patch has been studied rigorously [69], where respective AR and impedance bandwidths of 22% and 7.5% have been measured by exciting the TE_{111} mode,. A recent investigation utilized unequal and adjacent-slided rectangular DRA fed by coaxial probe in order to obtain a circularly polarized radiation for Wi-Fi wireless communication [70] with measured input reflection coefficient and axial ratio bandwidth of 26% and 26.85%, respectively. A wideband high-gain CP RDRA loaded with partially reflective surface excited by a microstrip line through modified stepped ring cross-slot presented in [71], ~55% and 54% and impedance and axial ratio bandwidths was obtained over frequency range 4.5-7.5 GHz with 10.7 dBic gain by exciting TE_{111} and TE_{113} modes.

1.4 Multi-layer Dielectric Resonate Antenna

The impedance bandwidth can be significantly increased by the addition of a dielectric coat to the DRAs as the second layer acts as a transition region between the antenna and air. As a result, the quality factor is reduced with increased bandwidth. Wideband multi-layer hemispherical DRAs have been reported in [72] utilizing a slot aperture to feed the DRAs, where a bandwidth of 55% has been achieved by exciting the TE_{111} and TE_{221} resonance modes. In addition , a three-layer HDRA fabricate from low permittivities of 9, 4 and 3 respectively, excited by coaxial probe was presented in [73], a bandwidth of 62.75% in conjunction with low gain 3.2 dBi was measured when low order modes TM_{101} and TM_{102} were excited. Similarly, a three-layer hemispherical DRA has been reported, where it has been demonstrated that through optimization of the outer layer permittivity, a broadband coupling has been established with the rectangular feeding waveguide to provide an impedance bandwidth of 9.6% and gain of 6.4 dBi by exciting TE_{113} mode [74]. A wide impedance bandwidth ~25% was measured when a conformal strip utilized feeding three-

layer HDRA that supported low order mode TE_{111} [75]. Furthermore, microstrip line slot-coupled to the three-layer HDRA resulted wide impedance bandwidth 29% and 4.4 dBi gain when fundamental mode TE_{111} excited[76]. Comparison of the performance of a two-layer hemispherical DRA with that of a single layer counterpart has been implemented [77]. The study demonstrated a wide bandwidth of 31.9% in conjunction with a gain of 2.5dBi at 3.6GHz for a layered hemispherical DRA compared to a bandwidth of 14% for a single layer DRA operating at the lower order mode of TM_{101}.

On the other hand, DRA stacking represents an alternative approach to enhance the impedance bandwidth. For example, four rectangular DRAs have been stacked on top of each other in order to achieve an impedance and axial ratio (AR> 3dB) bandwidths of 21% and 6%, respectively, in conjunction with a gain of 6dBi [78]. Similarly, an impedance bandwidth of 40% and a gain of 9dBi have been achieved by stacking two rectangular DRAs with different permittivities [79]. The bandwidth enhancement of cylindrical DRAs have also received a considerable attention by employing novel techniques such as introducing air gaps and DRA stacking, as well as coating, using various materials. For example, the first experimental results for a multi-layer wideband cylindrical DRA have been reported with an impedance bandwidth of 30% that has been achieved when ε_{r2} is half of ε_{r1} [80]. Additionally, a wider bandwidth of 66% has been achieved conjunction with a 5.5dBi gain for a stacked cylindrical DRA that consists of three segments placed on top of each other with respective dielectric constants of 6.15, 2.32 and 10.2 for the bottom, middle and top layers, respectively [81]. In a later study, a wideband four-element cylindrical DRA array has been proposed with a 47% impedance bandwidth and ~4dBi gain, where the $TM_{01\delta}$ mode has been excited by utilizing a central probe to feed the antenna [82]. In a subsequent publication, a two-layer half-split cylindrically shaped DRA has been reported with simulated impedance bandwidth of 88% and an average gain of 8.36dBi [83]. An alternative investigation has demonstrated that a substantial enhancement in the bandwidth can be achieved by stacking two cylindrical DRAs vertically [84], where a 55% impedance bandwidth and 5dBi gain have been obtained. In addition, a wideband two-layer transparent cylindrical DRA has been demonstrated experimentally, where a conformal conducting strip has been utilized in order to excite the $HE_{11\delta}$ mode with a 30% impedance bandwidth and a 7dBi gain [85].

Therefore, a number of studies have proposed layered DRAs as a solution to the narrower bandwidth issue. Nevertheless, improvement of the gain has not been considered. Furthermore, the impact of the outer dielectric layer on higher order modes operation and axial ratio of DRAs have not been considered earlier. All these limitations will be addressed in a simple design for a rectangular DRA. Furthermore, the incorporation of a dielectric coat has been demonstrated for linearly polarised cylindrical and hemispherical lower order mode DRAs. However, layered rectangular DRA is considered in this work and the impact of the dielectric coat on the performance of higher order modes and/or circularly polarized DRAs has not also been considered earlier.

1.5 Millimeter-wave DRAs

Millimetre-Wave frequencies are acquiring more research attention due to potential applications in5G communication systems and radar. With the increasing demand for wireless mobile devices and services, the new wireless applications require high data rates up to 1Gbit/s that can only be supported by the fourth generation (4G) wireless networks. Therefore, the investigations have started on the fifth generation (5G) wireless systems to achieved higher data rates, where the mm-wave frequency band is utilized [86, 87]. Further, the mm-waves signals can penetrate through fog and dust [25]. However, the electromagnetic energy at the mm-wave band is absorbed by oxygen, which considerably attenuates the signal over the communications channel and necessitates the use of an efficient high gain antenna [88]. As mentioned earlier, since DRAs fabricated from low loss dielectric materials, then they are most suitable for millimetre-wave band applications. Moreover, even mm wave horn antennas suffer from a number of drawbacks such as high cost and large size make that make such antennas heavy and bulky [89]. Unfortunately, antenna arrays with low gain elements are incapable of meeting the high gain requirements because of the potentially high ohmic losses in the feed network. Furthermore, microstrip antennas are not really qualified to play a key role in the 5G communication systems owing to well-known limitations such as narrow impedance bandwidth of 2-5% and considerably lower radiation efficiency due to the increased ohmic and surface wave losses at the millimeter-wave frequencies [51]. Therefore, a higher order mode DRA represents a suitable choice to address the aforementioned limitations as it offers enhanced gain in conjunction with high radiation efficiency as well as other appealing features such as small

size, different shapes, easy excitation, low profile and lightweight [23, 90]. However, the narrow impedances bandwidth represents a key challenge that need to be addressed for higher order mode DRAs. A high gain cylindrical DRA with a superstrate and aperture coupling has been considered for millimetre underground communication applications with respective impedance bandwidth and gain of 18% and 11dBi gain. In addition, a millimetre wave rectangular DRA that is fed by a coplanar waveguide has been reported with a bandwidth of 29% and gain of 3.6 dBi. Moreover, a higher order mode mm-wave cylindrical DRA has been proposed in [91] with 25% impedance bandwidth and gain of 8.6dBi by exciting the HEM_{113} and HEM_{115} resonance modes. Besides, an impedance bandwidth of 24% has been achieved when a stacked rectangular resonator fed by coplanar waveguide has been employed for underground millimetre wave communications [92]. On the other hand, circularly polarized DRAs have so far received limited attention in the mm-wave band compared to those at lower frequency bands. This is despite the fact that CP radiation offers advantages such as minimizing the impact of atmosphere attenuation as well as eliminating the need for alignment between the receiving and transmitting antennas. In addition, a hybrid microstrip/elliptical DRA that is fed by dual-orthogonal slots has been utilized to obtain an impedance and CP bandwidths of 12% and 10%, respectively, as well as a high gain of more than 9dBi [93]. Moreover, a low permittivity DRAs were excited with $\varepsilon r \sim 4$ fabricated of polymer-based materials resulted in BW of 27% over the 23 – 30 GHz and low gain of 5 dBi [94]. A new hybrid millimetre waves CDRA composed of a dielectric resonator and superstrate for underground applications having an impedance bandwidth of 19% and gain of 11 dBi was reported in [95]. Furthermore, wide respective impedance and CP bandwidths of 13.1% and 9.7%, have been attained by proposing a hybrid microstrip/DRA configuration that provided a high gain of 13.5dBi [96]. A circularly polarized millimetre wave hybrid microstrip/DR antenna operating at 60GHz and excited $HEM_{15\delta}$ mode has been simulated in [97] respective impedance and AR bandwidths of 15% and 11.6% in conjunction with a gain of 12.3dBic. Another 60GHz rectangular DRA has been investigated experimentally using a coplanar wave guide feed with a low gain of up to 3.6dBi and an impedance bandwidth of 29.2% by exciting the TE_{111} [98]. A rectangular DRA that is excited by a narrow slot aperture cut on the substrate integrated waveguide has been considered by exciting the TE_{111} resonance mode at 37.43GHz, where a gain of 5.5dBi has been attained together with an impedance bandwidth of 11.5% [99]. Furthermore, a hollow cylindrical DRA placed on a low-cost FR-4 surface and fed by a coaxial probe

reported has been reported for 5G systems with an impedance bandwidth and gain of 54% and 4dBi respectively [100]. Recently, a novel millimetre wave DRA arrays design has been investigated experimentally using the substrate integrated technology, where gain and impedance bandwidth of ~14dBi and 13.3%, respectively, have been measured [101]. A cross slot feeding dual-band CP corner-truncated RDRA operating at TE_{111} and TE_{113} modes for millimetre-wave band was reported in [102], the proposed design offered ($|S11| < -10$ dB) are 17.0% (20.5-24.3 GHz) and 15.2% (26.1-30.4 GHz), while the AR bandwidths are 12.8% (21.2-24.1 GHz) and 5%(27.4-28.8GHz). Low gains are 5 and 8 dBic was a limitation of this approach.

1.6 Problem Definition

It is well known that employing a higher order mode DRA to improve the gain results in a number of challenges such as narrower impedance and axial ratio bandwidths. Increase the antenna profile provides a DRA that is hard to fabricate and easy be break due to the fragility of ceramic that the antenna is made of. Furthermore, mm-wave antennas arrays have number of limitations as has been mentioned earlier. It is mainly for these reasons that the presented work has been carried out to address the mentioned limitations by considering alternative methods to improve the antenna performance to be suitable for Mm-wave and X band communications. In this thesis, a novel design that combines high gain, wide impedance and axial ratio bandwidths with improve fabrication error tolerance will be introduced and supported by practical measurements.

1.7 Thesis aims and objectives

The primary aim of this project is to investigate novel DRA designs with improved performance for mm-wave and X band communication systems. The specific objectives to achieve the main aim are set:

1. Propose an alternative design of higher order mode rectangular DRA for linear and circular polarizations, which has been accomplished by utilizing layered rectangular DRA, where, incorporating an outer dielectric layer improves the impedance and axial ratio bandwidths as well as gain high for a reduced antenna profile.

2. Achieve a gain that is comparable to, or exceeds, an array gain, albeit using a single DRA element instead of the array.

3. Utilize the proposed layered DRA concept in the mm-wave frequency band, from 20 to 30GHz.

4. The fourth main objective is engaging the 3D printing technology to print multiple shapes of outer layer coats, which are considered complex in traditional subtractive methods.

1.8 Thesis Structure

The thesis consists of six Chapters as shown below;

Chapter 1: Presents an introduction, literature review, research contribution and thesis layout.

Chapter 2: Investigates different approaches for the gain enhancement of rectangular DRA such as; higher order mode operation, incorporating a dielectric superstrate and antenna arrays.

Chapter 3 and 4: Present layered rectangular and cylindrical DRAs that operate at their higher order modes for linear and circular polarization with improved performance and close agreement between simulated experimental results.

Chapter 5: Presents wide bandwidth, high gain mm-wave layered hemispherical and rectangular DRAs for 5G applications. The simulation results are supported by practical measurements.

Chapter 6: Presents the conclusions and future work suggestions.

Chapter 2

High Gain Rectangular Dielectric Resonator Antenna

2.1 Introduction

This chapter introduces the rectangular dielectric resonator antenna (RDRA) as one of three regular geometries that will be considered throughout this research. Considering, the considerable wave attenuation due to atmosphere condition at higher frequencies, a higher antenna gain is need to compensate for this loss and maintain a reliable communication. Common approaches to enhance the DRA gain include the excitation of higher order modes [23], using a dielectric superstrate [43] as well as employing DRA arrays [8]. However, higher order mode operation is usually associated with narrow bandwidths, superstrate incorporates increase the size and fabrication complexity and arrays suffers from feed network complexity and losses as well as an increased size. In this work, higher order mode DRAs will be considered with enhanced radiation properties that address the aforementioned limitations.

Generally, altering the DRA aspect ratio can generate several of modes and hence the antenna may support several resonance modes, out of which the lower frequency dominant modes are usually considered while higher order modes are excited at the higher frequencies. Furthermore, when the rectangular DRA's aspect ratio falls between ~0.25 and 1.5, a single higher order mode operation can be achieved [25]. Otherwise, a multi-higher order modes operation is established. A comparison between single and multi-higher order mode DRA designs will be presented based on the width to height, *w/h*, aspect ratio, when the DRA is assumed to have a square cross section. Additionally, the impacts of fabrication errors for both single and multi-higher order modes will be studied using the time domain solver of the CST microwave studio as well as the dielectric waveguide model (DWM) [26, 103]. The outline of this Chapter is illustrated in Figure 2.1.

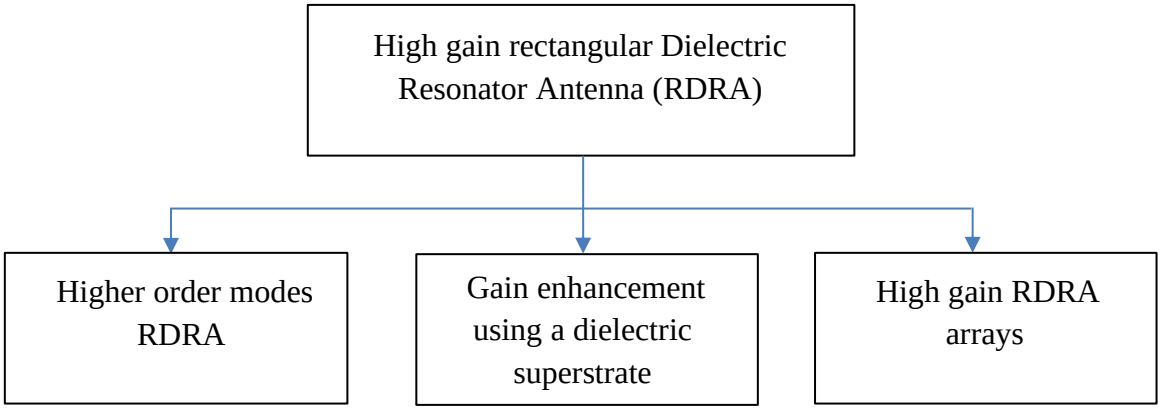

Figure 2.1: Chapter two overview.

2.2 Excitable Rectangular DRA Modes

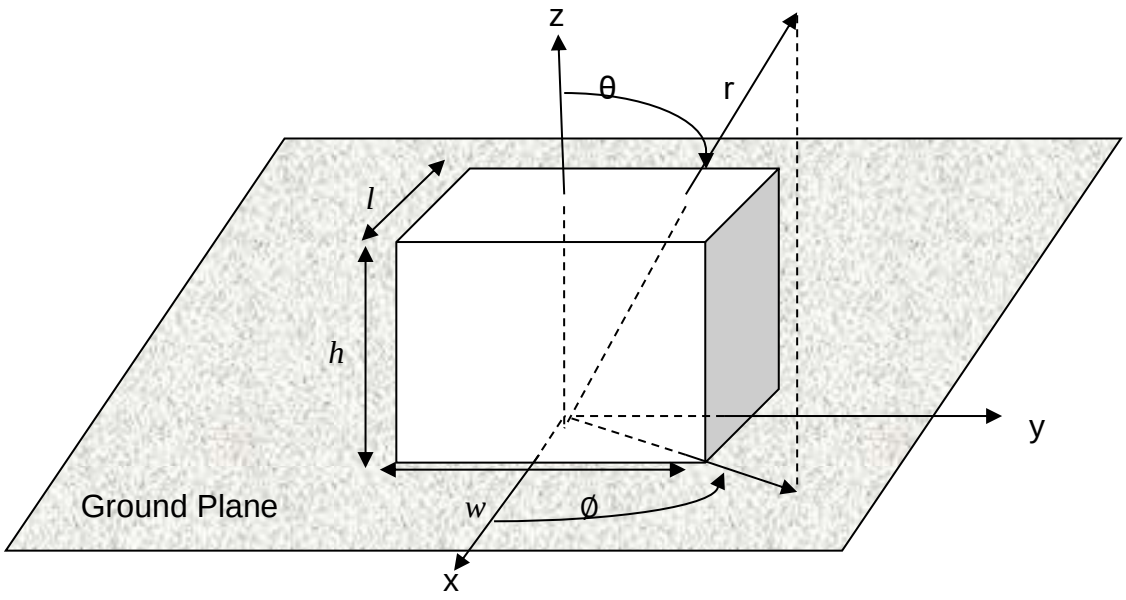

Figure 2.2 :Geometry of a rectangular DRA mounted on ground plane.

Figure 2.2 shows the rectangular DRA placed on the ground plane In should be noted that the transverse magnetic, TM, modes cannot be generated at the presence of a ground plane, that is because these modes requires the E field to be maximum at z=0 which is not agreed with the boundary condition. In addition, the resonance frequency of each of the TE and TM modes depends on the DRA's dimensions and permittivity. These resonance frequencies can be predicated using the Dielectric Waveguide Model (DWM). The

magnetic fields inside a rectangular DRA with respective width, length and height of *w*, *l* and *h* can be expressed as [104, 105];

$$H_x = \frac{(K_y^2+K_z^2)}{(jw\mu_0)} cos(k_x x)\, cos(k_y y)\, cos\,(k_z z) \quad (2\text{-}1)$$

$$H_y = \frac{(k_y k_x)}{(jw\mu_0)} sin(k_x x)\, sin(k_y y)\, cos\,(k_z z) \quad (2\text{-}2)$$

$$H_z = \frac{(k_z k_x)}{(jw\mu_0)} sin(k_x x)\, cos(k_y y)\, sin\,(k_z z) \quad (2\text{-}3)$$

$$E_x = 0 \quad (2\text{-}4)$$

$$E_y = K_z\, cos(k_x x)\, cos(k_y y)\, sin\,(k_z z) \quad (2\text{-}5)$$

$$E_z = -K_y\, cos(k_x x)\, sin(k_y y)\, sin\,(k_z z) \quad (2\text{-}6)$$

Where,

$$k_x = \frac{m\pi}{w}, k_y = \frac{n\pi}{l}$$

$$k_z\, tan(k_z h/2) = \sqrt{(\varepsilon_r - 1)k_0^2 - k_x^2}$$

and k_0 represents the free-space wavenumber, which is defined as

$$k_0 = \frac{2\pi}{\lambda_0} = \frac{2\pi f_0}{c}$$

The relationship between the wavenumbers in all directions and the free space wave number is

$$k_x^2 + k_y^2 + k_z^2 = \varepsilon_r k_0^2 \quad (2\text{-}7)$$

$$k_0 = \frac{2\pi}{\lambda_0} = \frac{2\pi f_0}{c} \quad (2\text{-}8)$$

in which λ_0 represents the free-space wavelength, and c is the speed of light. Substitution of equation (2-8) in equation (2-7) produces the modes resonance frequency as:

$$f_0 = \frac{c}{2\pi\varepsilon_r}\sqrt{k_x^2 + k_y^2 + k_z^2} \quad (2\text{-}9)$$

A MATLAB code has been developed to solve equation (2-9). For example, the effects of varying the RDRA dimensions and ε_r on the resonance frequencies of higher order mode have been calculated using equation (2-9) and tabulated in Table 2-1 compared to those obtained from CST simulations. It is worth mentioning that, the difference between simulated and calculated resonance frequencies can be attributed to the absence of feed network in the calculations.

Table 2-1: Effects of rectangular DRA dimensions and dielectric constant on higher order modes

No	RDRA dimensions (mm)			Dielectric constant (ε_r)	Simulated (f_0) (GHz)	Calculated (f_0) (GHz)	Resonance mode
	l	*w*	*H*				
1	4	4	40	10	11.3	12.2	TE_{117}
2	16	4	4	10	16.9	16	TE_{513}
3	5	10	5	15	12.7	12.4	TE_{131}
4	15.2	7.6	3.1	11	17.7	16.8	TE_{531}
5	10	10	10	20	16.4	15.6	TE_{353}

As mentioned earlier, the DRA-source coupling strength can be optimised by extending the strip transmission line beyond feeding the slot in order to create what is known as a matching stub. As an example, a rectangular DRA has been simulated using a low loss Alumina having dielectric constant of ε_r=10 and loss tangent of $\tan\delta < 0.002$, with dimensions of l=w=4mm, h=40mm. The DRA has been placed on commercially available, Rogers RO4535, substrate of respective length and width of 150mmand 100mm thickness 0.8mm, dielectric constant of 3.5 and loss tangent of 0.0037. The length and width of the slot have been chosen as ls= 6mm and w_s =1mm, respectively. It should be noted that the guided wavelength, λ_g, is 15mm at 11.2GHz. The reflection coefficient is illustrated in Figure 2.3 where it can be noted that a considerable coupling has been achieved by employing an optimum stub length 6mm. However, the mount of coupling found to be reduced at l_{stub} of 4 and 7 mm.

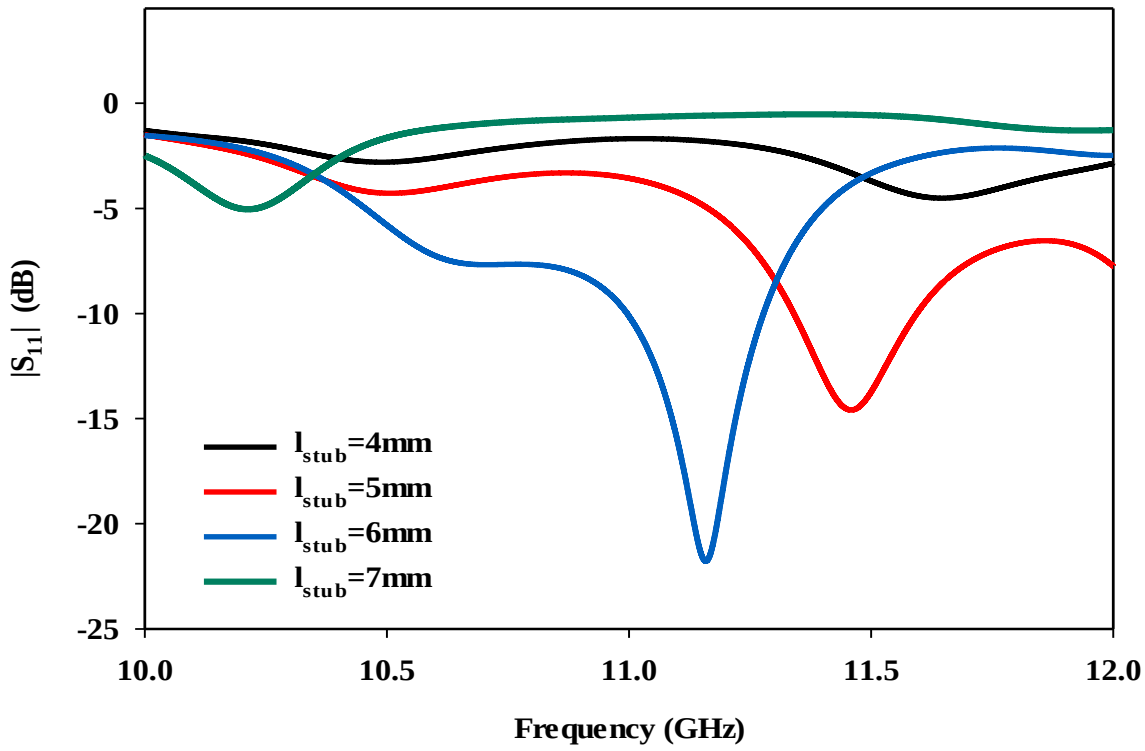

Figure 2.3: Effects of stub length on the DRA return losses.

2.3 DRAs measurements procedures

In order to validate the CST MWS results a real antenna needs to be fabricated then tested, measuring S_{11} is straightforward once the antenna connected to the network analyser after the connection cable being calibrated. However, the far-field measurements like an axial ratio (AR) and gain is not direct. Where E_R is the right-hand CP electric field component, and E_L the left-hand CP electric field component can be calculated using the following equations [106], The AR can be calculated by following expression

$$E_R = \frac{1}{\sqrt{2}}\left(E_\phi + jE_\theta\right) \tag{2-10}$$

$$E_L = \frac{1}{\sqrt{2}}\left(E_\phi - jE_\theta\right) \tag{2-11}$$

$$\mathrm{AR} = \frac{|E_R|+|E_L|}{|E_R|-|E_L|} \quad (2\text{-}12)$$

The electric field component in the ϕ-direction denoted by E_ϕ, E_θ represents the electric field component in the θ-direction. In order to determine both experimentally, the component of Eϕ can be obtained when receiving horn antenna fixed inside the anechoic chamber in one direction at ϕ = 0°, in meanwhile, transmitting DRA rotated at each elevation angle θ (θ = 0^0, 45^0, 90^0 and 360°), the difference between received power should not exceed 3 dB, which is the value of the axial ratio. The same procedure repeated for the measurement of E_θ with the horn antenna rotated at ϕ= 90°.

In order to measure the antenna gain, a comparison method has been applied in which another horn antenna has been used at the receiving end, where the gain of DRA can be from known gain of the reference horn using equation (1-7) [107].

$$G_{\text{DRA in dB}} = G_{\text{Horn in dB}} + 10\,log_{10}\left(\frac{P_{DRA}}{P_{Horn}}\right) \quad (2\text{-}13)$$

2.4 DRAs design from simulation

In this research CST MWS [103] used to build the DRAs, where some parameter must be set up properly such as frequency range to simulate the antenna , defining the port to energize it, the mesh cells and the kind of simulation that will be performed, the type of mesh that used called hexahedral mesh which computational volume is discretized by means of variable size rectangular cuboids (x,y,z). the antenna structure using the CST MWS tools illustrated in Figure 2.4 . The CST MWS produced graphics showing the results once all the necessary parameters have been set for the simulation. The antennas performance such as impedance bandwidth and resonance frequency cab be gained in the $|S_{11}|$ graphics.
Furthermore, the initial set of resonator geometries is obtained by magnetic wall method (i.e. numerical implementation of DWM). the method is done by performing modal analysis of the resonator in Eigenmode solver of CST MWS. In the simulations, all of the resonator's walls are set as perfect magnetic conductors (PMC), except the bottom wall which is considered perfect electric conductor (PEC). The antenna and its feed network radiation losses have taken into account by adding the loss tangent in the material properties.

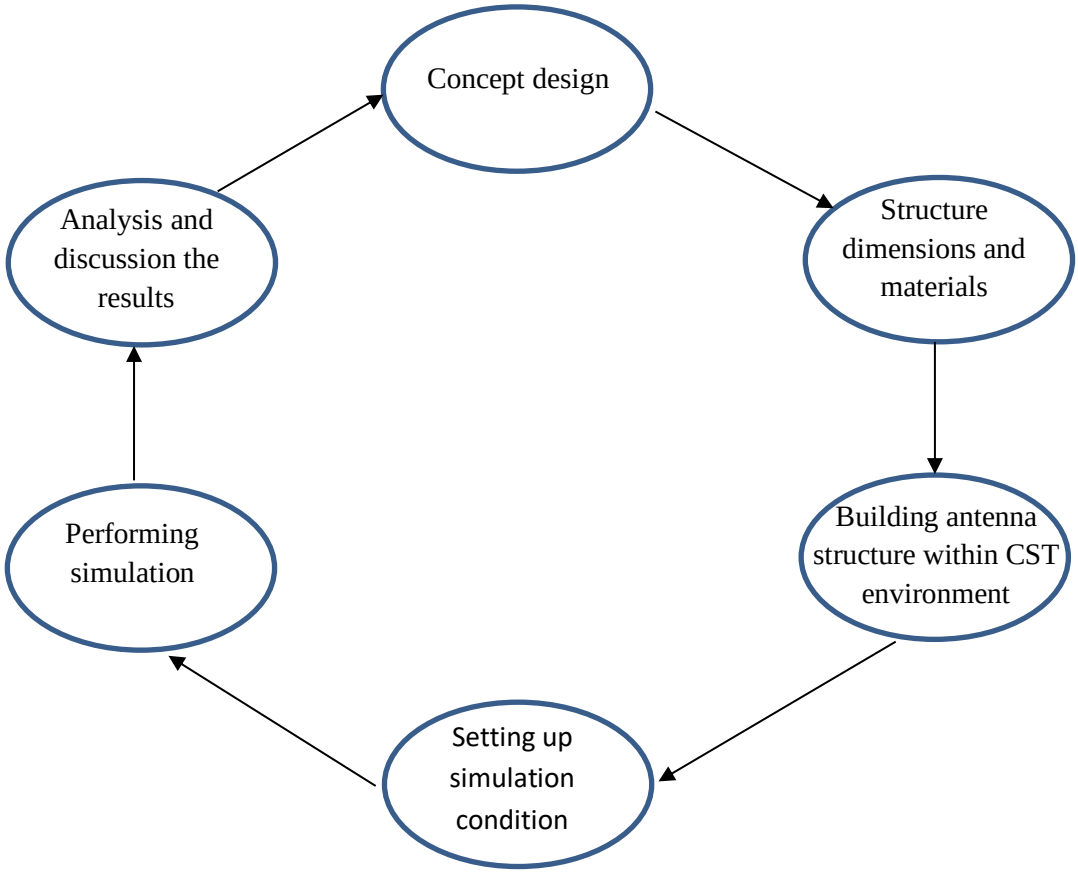

Figure 2.4: Dielectric resonator antenna design by simulation with CST MWS.

2.5 Higher-Order Mode Rectangular DRA

The higher order operation of any DRA can be classified into single and multi-mode operations that can be controlled by adjusting the DRA aspect ratio with strengths and limitations that will be addressed in this section.

2.5.1 Single Higher-Order Mode Operation

As explained earlier, when the rectangular DRA aspect ratio falls between 0.25 and 1.5 a single higher order mode operation can be achieved, where at distance between one mode and another is ~10%. Single mode operation requires a lower RDRA profile with wide impedance bandwidth and far field patterns that have not interference from adjacent mode patterns. However, the overlapping between the equivalent short magnetic dipoles, inside

the DRA, results in a lower gain. The effects of the aspect ratio on the RDRA resonance modes, impedance bandwidth and fabrication errors tolerance have been investigated. Three rectangular DRAs have been simulated using Alumina ε_r=10 with loss tangent of 0.0001, and open stub length of 6 mm to operate at a single mode such as TE_{111}, TE_{115} and TE_{119} with a frequency range of 10 to 12GHz. The DRAs have been placed on same feed network that has been used in section 2.2. The dimensions for the three DRAs are presented in Figure 2.5 and summarised in Table 2-1.

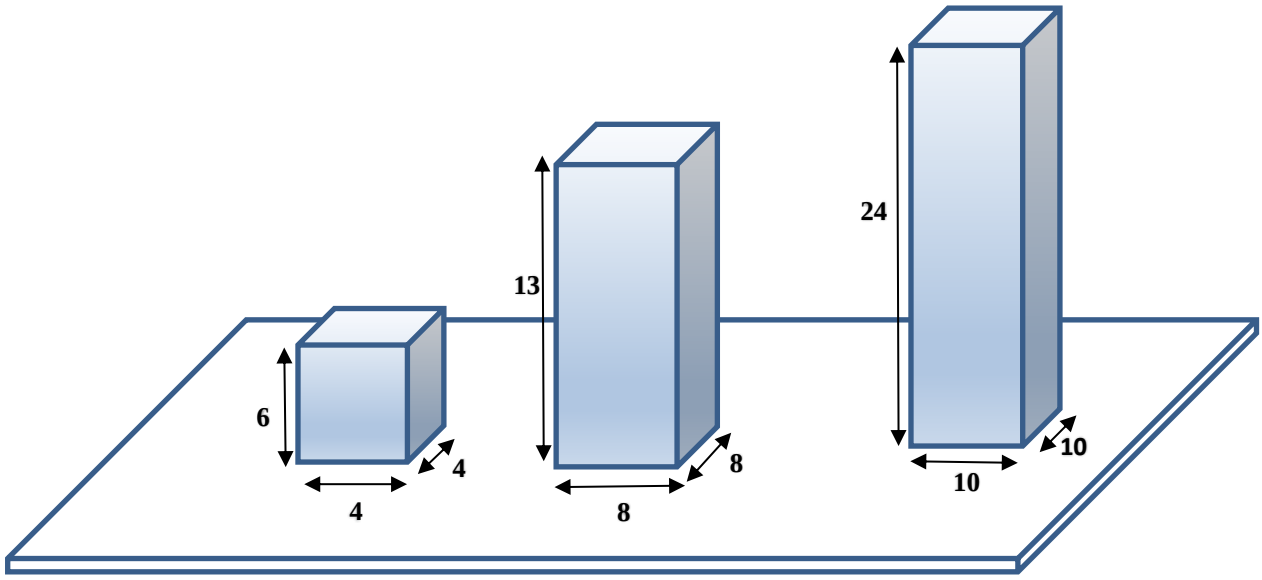

Figure 2.5: DRA operating in a single higher order mode with dimension given in mm.

Table 2-2: Dimensions and volumes of three rectangular DRAS operating in the TE_{111}, TE_{115}, TE_{119} resonance modes

Resonance modes	Resonance frequencies (GHz)	RDRA dimensions $l \times w \times h$ (mm)	Volume lwh (mm^3)
TE_{111}	10.7	4×4×6	96
TE_{115}	11.6	8×8×13	832
TE_{119}	11.3	10×10×24	2400

As expected, in order to excite a higher order mode, the RDRA volume needs to be increased significantly. For example, the volume of a DRA excited in the TE_{119} mode is larger than those required to excite the TE_{111}, TE_{115} modes by 25 and 2.9 times, respectively. The return losses are illustrated; in Figure 2.6, where it can be observed that the -10dB impedance bandwidths are 4 %, 3.7 % and 3.5% for the TE_{111}, TE_{115} and TE_{119} modes, respectively. The reduction in the impedance bandwidth can be explained as a result of the fact that the effective DRA permittivity increases for higher order mode operation [26]. The magnetic field distributions inside the DRAs are illustrated in Figure 2.7, where it can be noticed that the spacing between short magnetic dipoles, *s*, is 5.7mm ($0.22\lambda_0$) for the TE_{115} mode at 11.6GHz and 5mm ($0.19\lambda_0$) for the TE_{119} mode at 11.3GHz, in conjunction with respective gains of 6.8dBi and 7.6dBi. In both cases, the distance *S* is less than $0.4\lambda_0$, which results in an overlapping between the short magnetic dipoles. Therefore, decreasing the *w/h* aspect ratio represents the best solution to eliminate such overlapping and improve the gain by forcing the DRA to work in a multi-higher order mode. Figure 2.8 presents the far field patterns of the DRAs presented in Figure 2.3, where it can be observed that the TE_{119} mode provides a considerably more directive pattern compared to that of the TE_{111} resonance mode. This is due to the fact that the higher height needed for the TE_{119} mode provides a larger separation distance of 5mm between adjacent short magnetic dipoles, which increases the forwarded power to the main lobe rather than side lobes for higher gain and directivity. It should be pointed out that the RDRA dimensions play an important role in generating the higher order modes since the increment of the antenna height leads to an increased number of magnetic dipoles inside the DRA, which results in a higher gain when S exceeds $0.4\lambda 0$. A comparison between single-higher order modes in terms of impedance bandwidth and gain is illustrated in Figure 2.9 , where the existence of the classical inverse gain-bandwidth relation is evident.

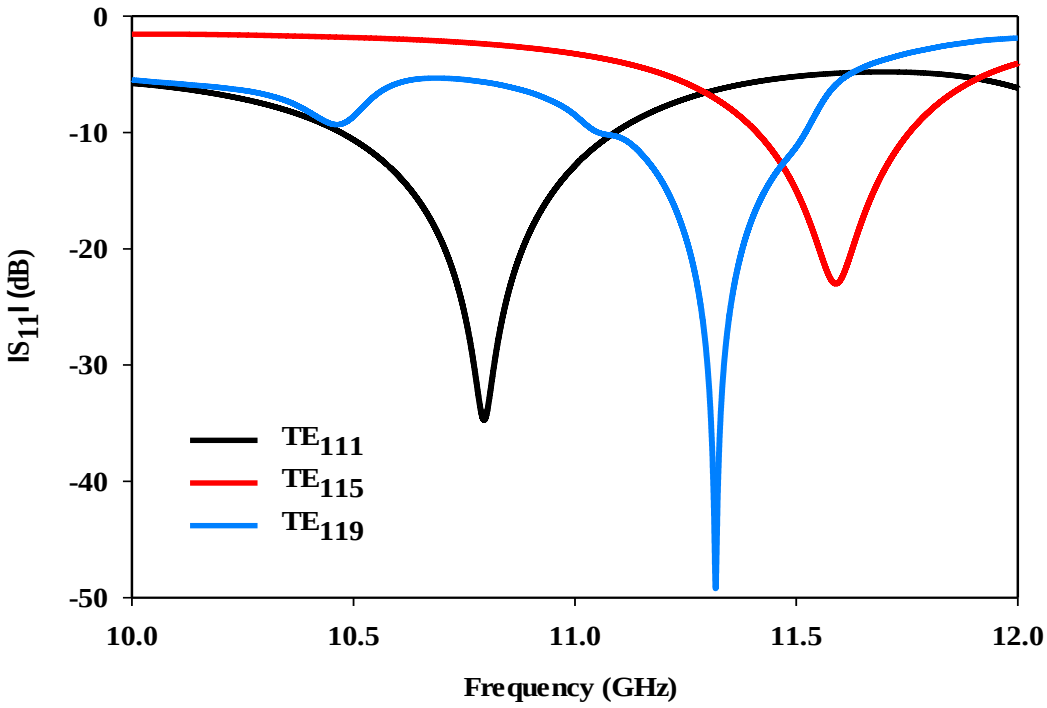

Figure 2.6: Reflection coefficients of rectangular DRAs excited in the TE_{111}, TE_{115} and TE_{119} modes.

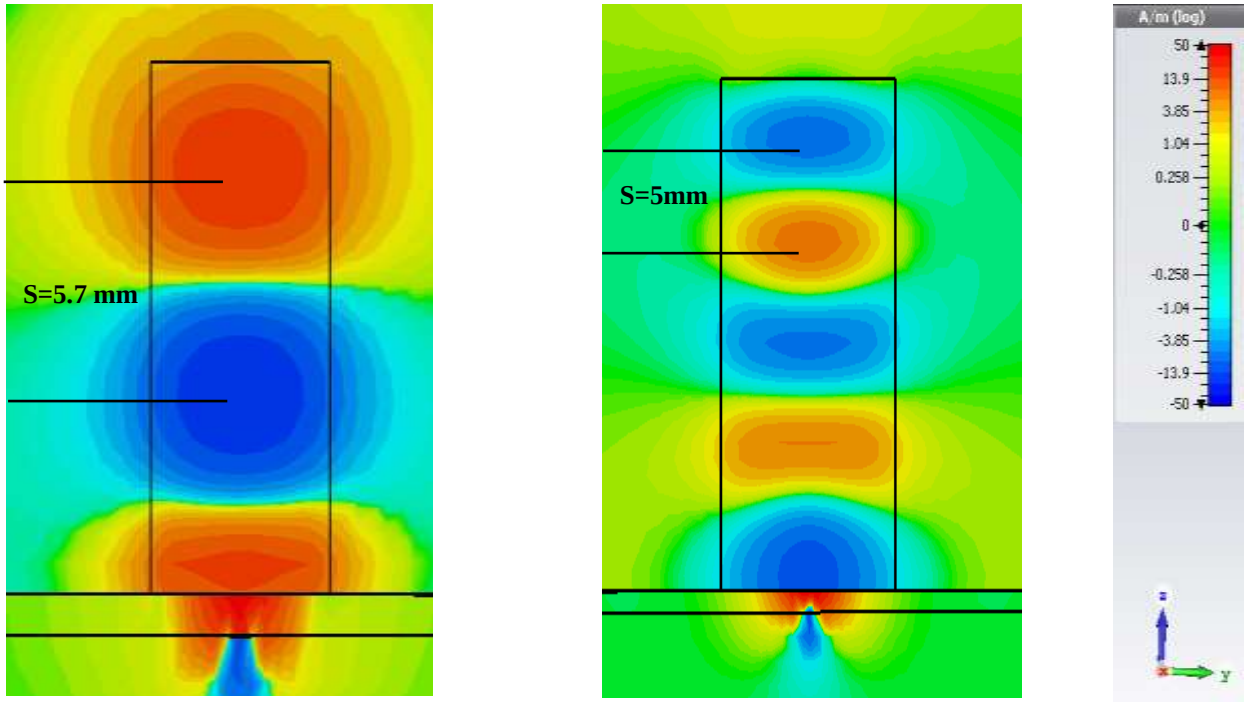

Figure 2.7: Magnetic fields for the TE_{115} and TE_{119} modes.

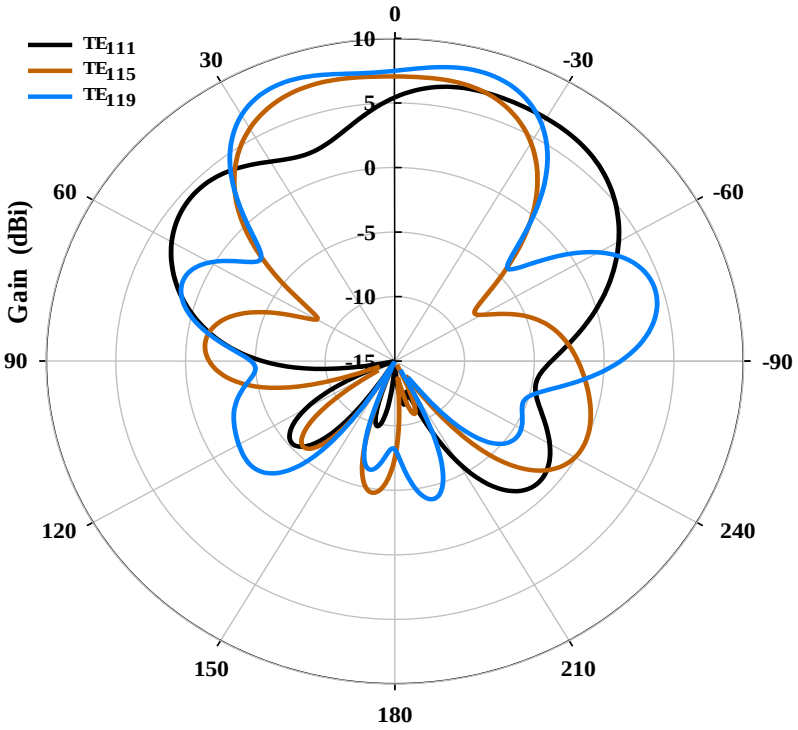

(a)

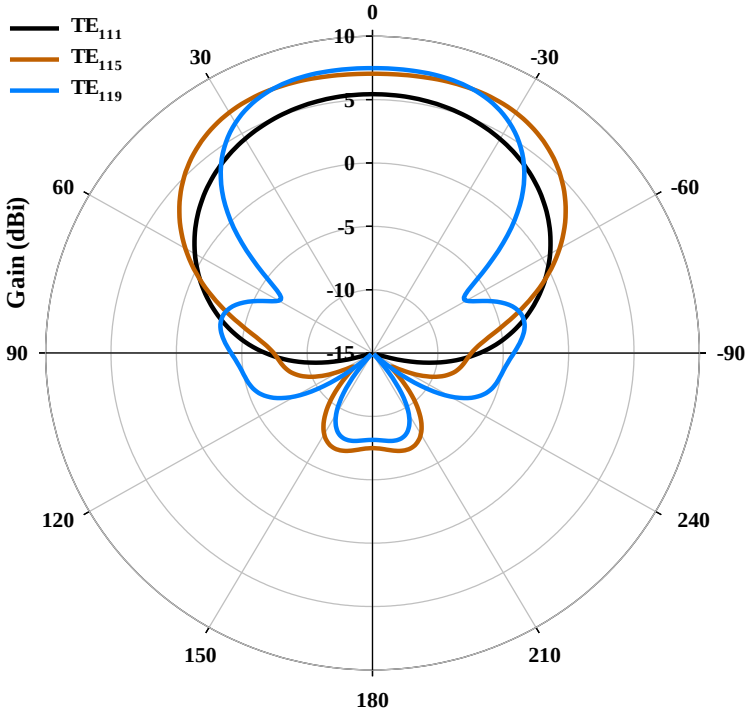

(b)

Figure 2.8: Radiation patterns of rectangular DRAs operating at the TE_{111}, TE_{115}, and TE_{119} modes at 10.8, 11.6 and 11.3GHz, a) E-Plane and b) H-Plane.

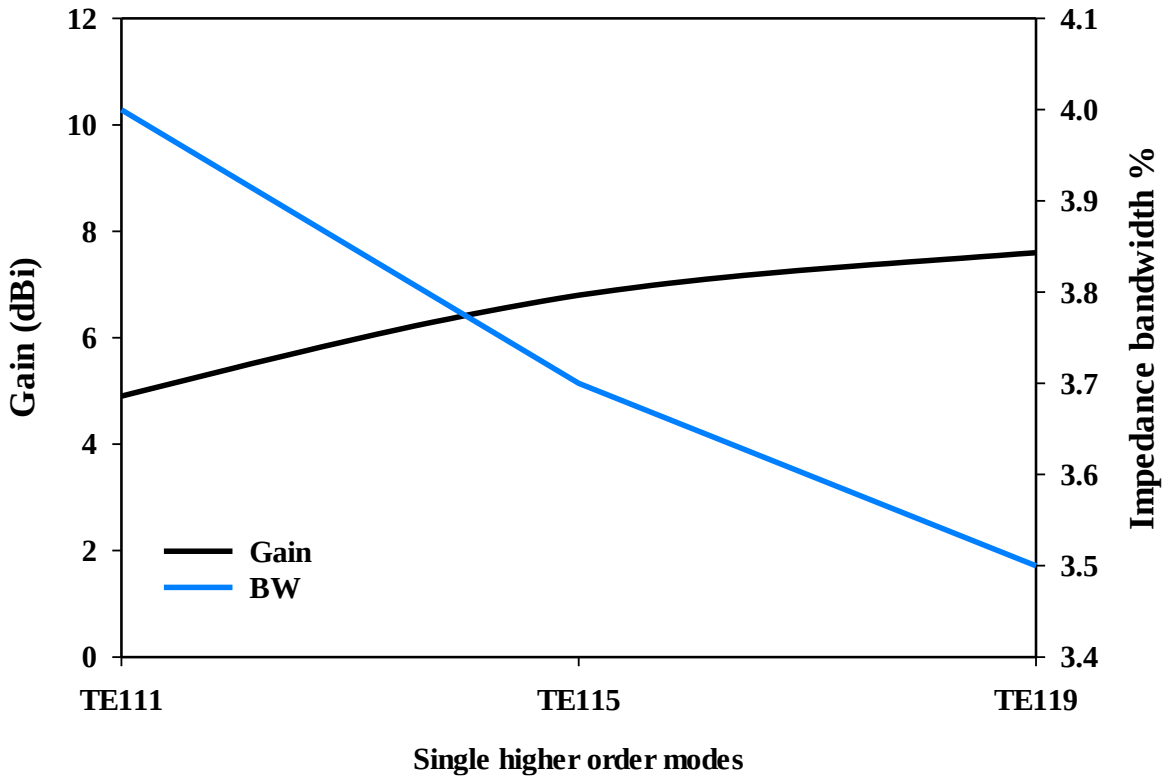

Figure 2.9: Gain and bandwidth for various higher order modes.

Table 2-3: Comparison of frequency shifts (Δf) of the TE_{111}, TE_{115} and TE_{119} modes for different fabrication errors.

Fabrication error (mm)	TE_{111} mode	TE_{115} mode	TE_{119} mode
	Δf %	Δf %	Δf %
0.01	0.06	0.054	0.017
0.05	0.39	0.27	0.10
0.1	0.77	0.55	0.18

The DRA dimensions have been altered slightly to take account of potential fabrication errors. The frequency shifts of the TE_{111}, TE_{115} and TE_{119} modes due to three different fabrication errors of 0.01, 0.05 and 0.1mm have been investigated as demonstrated in Table 2-3. In each case the error has been added to the DRA dimensions (width, length and height), then a new resonance frequency has been calculated. For instance, when there is fabrication error of 0.01 mm the single higher order mode, $TE_{119,}$ for which the RDRA volume is 2400

mm^3, is less affected by fabrication errors compared with the TE_{111} and TE_{115} modes where the RDRA volumes are of 96 and 832 mm^3, respectively. It is worth mentioning that, due to increment of antenna volume the TE_{119} mode operation is less affected by the fabrication error compared to theTE_{115} and TE_{111} modes.

2.5.2 Multi- Higher Order Mode Operation

In this section, a comparison between five RDRA's of different heights with fixed width and length will be implemented. It has been demonstrated that a RDRA having a lower height and operating at a lower order mode offers a reduced gain [24]. As mentioned earlier, by increasing the DRA height, the distance between short magnetic dipoles will be increased, which improves the antenna's gain. At the same time, when the DRA aspect ratio is less than 0.25 a multi-higher order mode operation will be triggered, where overlapping between short magnetic dipoles will not take place. Despite the fact that the gain will be enhanced, the antenna profile will be increased significantly, which results in a long and thin fragile DRA. To demonstrate this concept five rectangular DRAs, all with ε_r=10, have been considered at the higher order modes of TE_{115}, $TE_{117,}$ $TE_{119,}$ $TE_{11,11}$ and $TE_{11,13}$ over a frequency range of 10 to 12GHz. The DRA dimensions are listed in Table 2-4. The same feed network and slot utilized in Section 2.2 have been employed. It is worth mentioning that an aspect ratio of less than 0.25 has been used for the four DRAs in order to ensure a multi-mode operation. More importantly, the DRA heights have been increased in order to fulfil the requirement of separating the magnetic fields maxima by a spacing of $0.4\lambda_o$ [23]. With reference to Figure 2.10, the simulated -10dB impedance bandwidths are ~2.2% and 1.7% for the TE_{117}, and TE_{119} modes at 11.4GHz and 12.3GHz respectively. A comprehensive comparison between higher orders modes is presented in Table 2-4 and Figure 2.11, where it is noted that increasing the mode order provides a higher gain in conjunction with a lower impedance bandwidth. However, as the antenna height needs to be increased, the DRA dimensions will be impractical and difficult to fabricate. For instance, the antenna height needs to be increased up to 70mm in order to achieve a gain of ~11dBi, which results in a considerably narrower bandwidth, higher profile and fragile DRA.

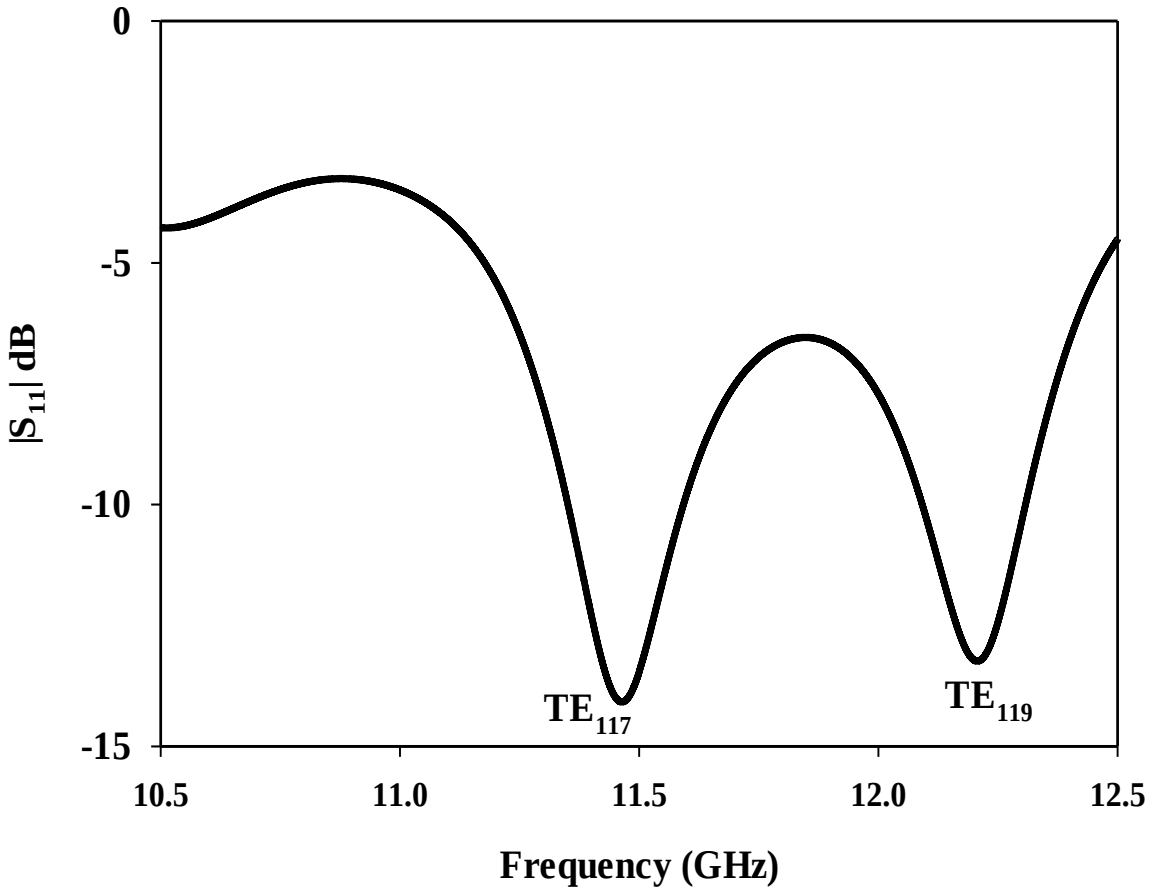

Figure 2.10: $|S_{11}|$ of RDRA excited in the TE_{117} and TE_{119} modes.

Table 2-4: Comparison between the gains of higher order mode RDRAs at 11.4GHz.

Resonance Mode	RDRA dimensions $l \times w \times h$ (mm^3)	Volume lwh (mm^3)	w/h	Gain (dBi)
TE_{115}	4×4×30	480	0.13	8.2
TE_{117}	4×4×40	640	0.1	8.6
TE_{119}	4×4×50	800	0.08	9.1
$TE_{11,11}$	4×4×60	960	0.06	10.3
$TE_{11,13}$	4×4×70	1120	0.057	10.8

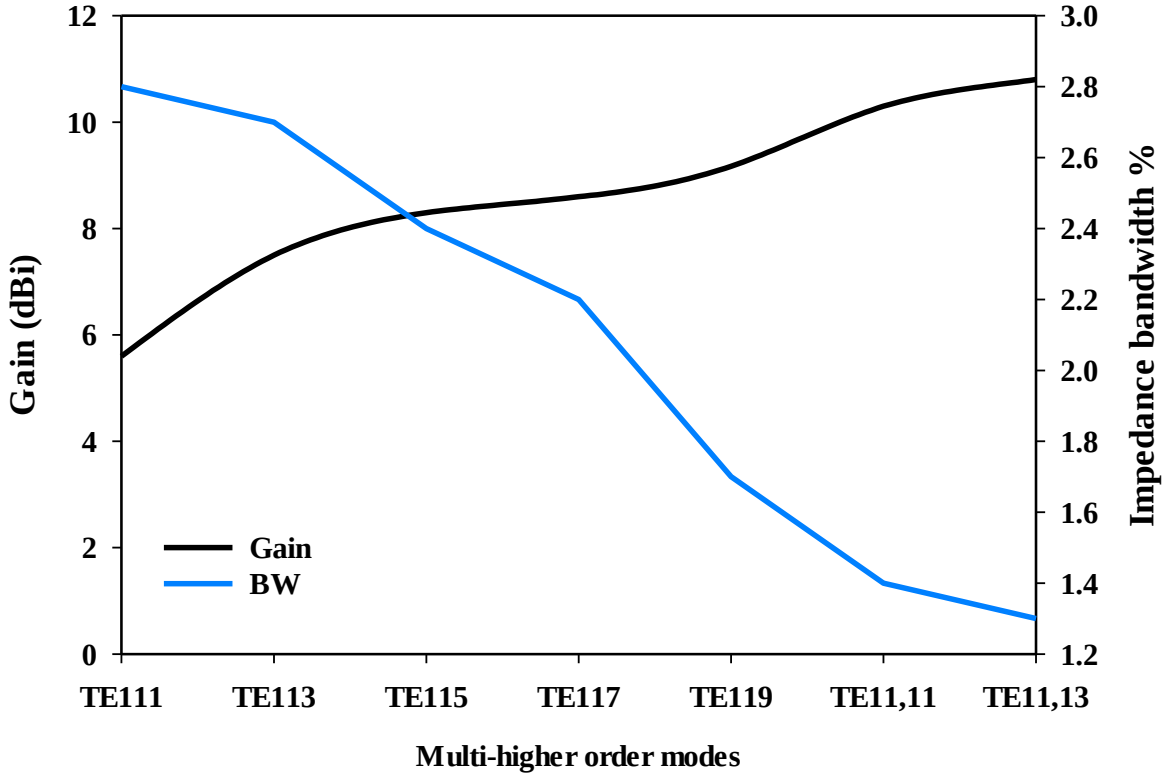

Figure 2.11: The gain and impedance bandwidth of higher order mode RDRAs.

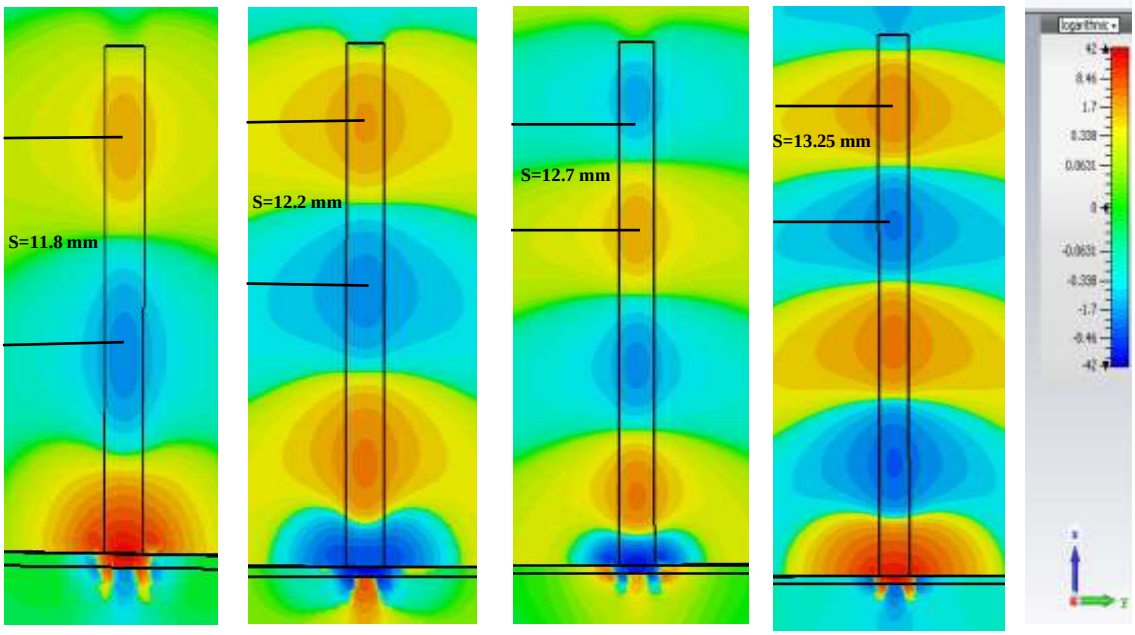

Figure 2.12: Simulated magnetic fields at the TE_{115}, TE_{117}, TE_{119} and $TE_{11,11}$ resonance modes at 11.4 GHz.

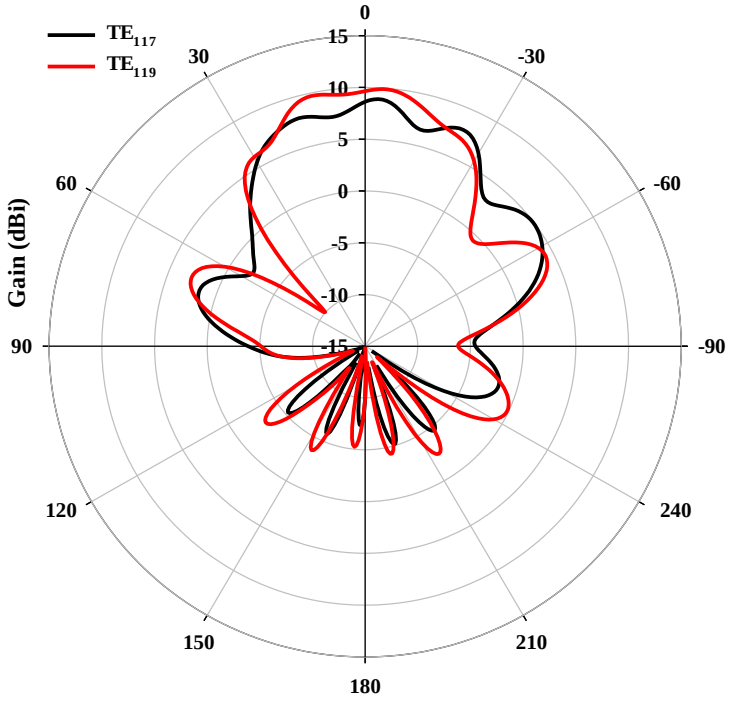

(a)

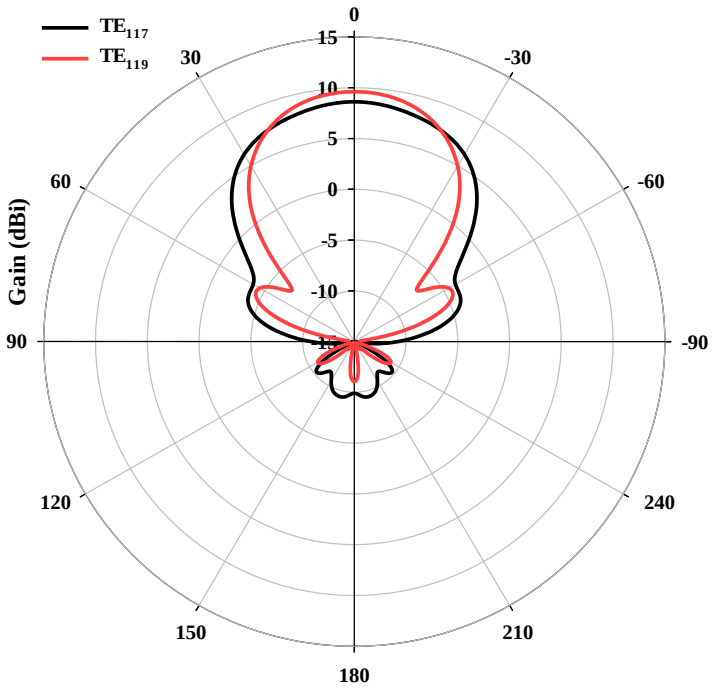

(b)

Figure 2.13: Radiation patterns of rectangular DRAs operating in the TE_{117} and TE_{119} modes at 11.4GHz and 12.2 GHz respectively a) E-Plane b) H-Plane.

Figure 2.12 illustrated the magnetic field distribution inside the considered rectangular DRAs, where it can be noticed that an increment of the spacing between the short magnetic dipoles is linked to the mode's order. For example, for the $TE_{115,}$ $TE_{117,}$ TE_{119} and $TE_{11,11}$ modes, the respective distances between adjacent magnetic dipoles are 11.8, 12.2, 12.7 and 13.25mm, which corresponding to $0.44\lambda_0$, $0.46\lambda_0$, $0.47\lambda_0$, and $0.5\lambda_0$ respectively. As a result, increasing the mode order results in a higher gain as illustrated Figure 2.13 and 2.14 resulted in an increment of the gain, where the power will be forwarded to main lobe than side lobes. In comparison with Table 2-3, Table 2-5 demonstrated that the multi-higher order modes are more affected to fabrication errors with lower bandwidth, higher profile and gain compared to a single higher order mode operation. This could be attributed to the fact that, the multi-higher order mode's RDRAs have thinner width and length than single higher order mode's RDRAs. To sum up, designing RDRAs to operate at its single and multi-higher order modes cannot meet the new communication systems the required high gain and wide bandwidth, this changed will be addressed in the next chapter.

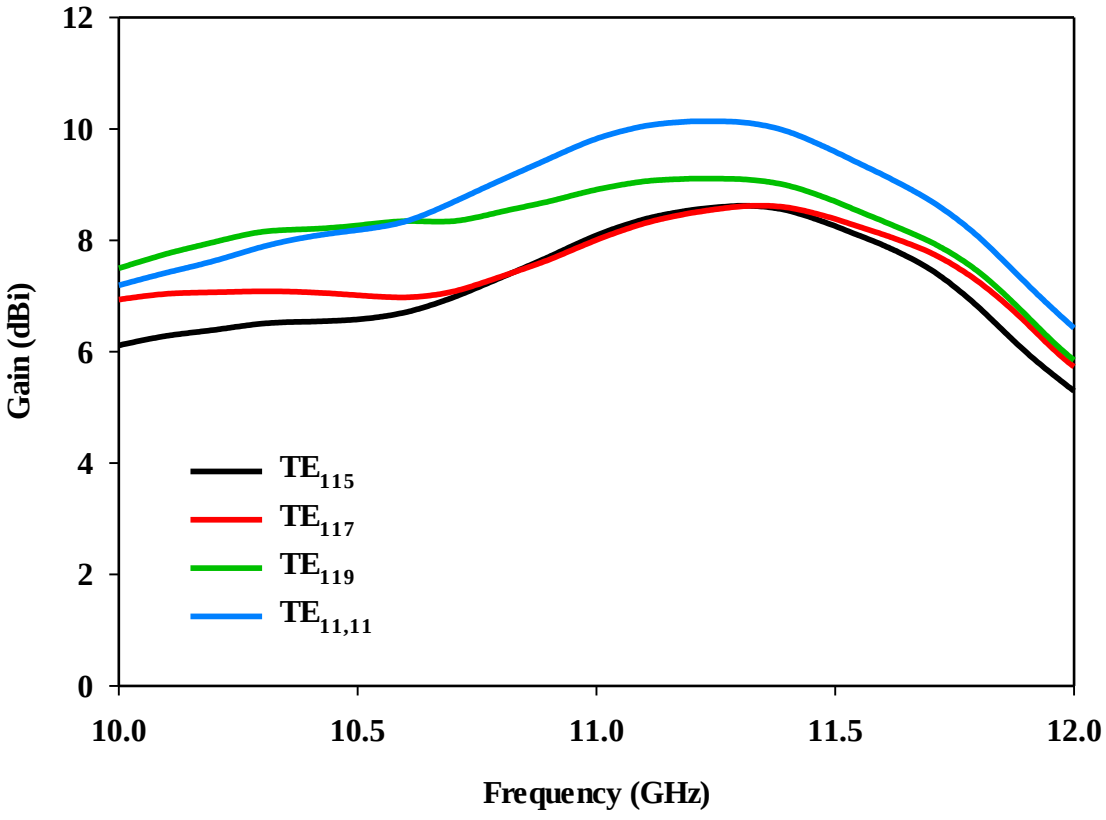

Figure 2.14: Rectangular DRAs gain at the TE_{115}, TE_{117}, TE_{119} and $TE_{11,11}$ resonance modes.

Table 2-5: Comparison of frequency shifts (Δf) of the TE_{111}, TE_{115} and TE_{119} modes for different fabrication errors.

Fabrication error (mm)	TE_{111} mode	TE_{115} mode	TE_{119} mode
	Δf %	Δf %	Δf %
0.01	0.39	0.24	0.20
0.05	1.16	1.08	0.98
0.1	2.35	2.21	2.08

To demonstrate aforementioned analysis and simulations, measurements have been implemented using rectangular DRA which has dimensions $w=l$=4mm and h=40mm, the proposed antenna was fabricated using an alumina dielectric material with $\varepsilon_{r=}$ 10 a loss tangent of tan δ<0.002 provided by a T- CERAM company. Figure 2.15 shows the microstrip feedline etched on a Rogers 4350 substrate having a dielectric constant of $\varepsilon_{rs=}$3.48, with a loss tangent 0.0037, a thickness of h=0.8 mm, and a size of 150×100 mm^2 which has fabricated at Wrekin-circuits workshop. 6×1 mm^2 slot aperture etched on the ground plane. Figure 2.16 (a) and (b) illustrates the RDRA on the ground plane and inside the anechoic chamber. The reflection coefficients were measured using a Keysight E5071C vector network analyser, whereas radiation pattern and gain were measured using an NSI near field system. The dimensions of the DRA are tuned to give a resonance frequency of 11.33 GHz excited in the TE_{117} mode.

(a) (b)

Figure 2.15: Photographs of feed network a) bottom view b) top view

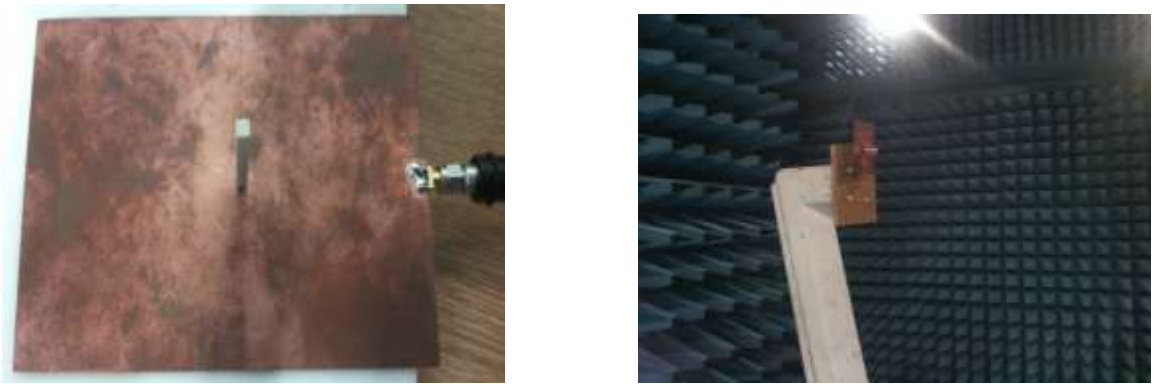

(a) (b)

Figure 2.16: Photographs of RDRA a) on the ground plane b) inside the anechoic chamber

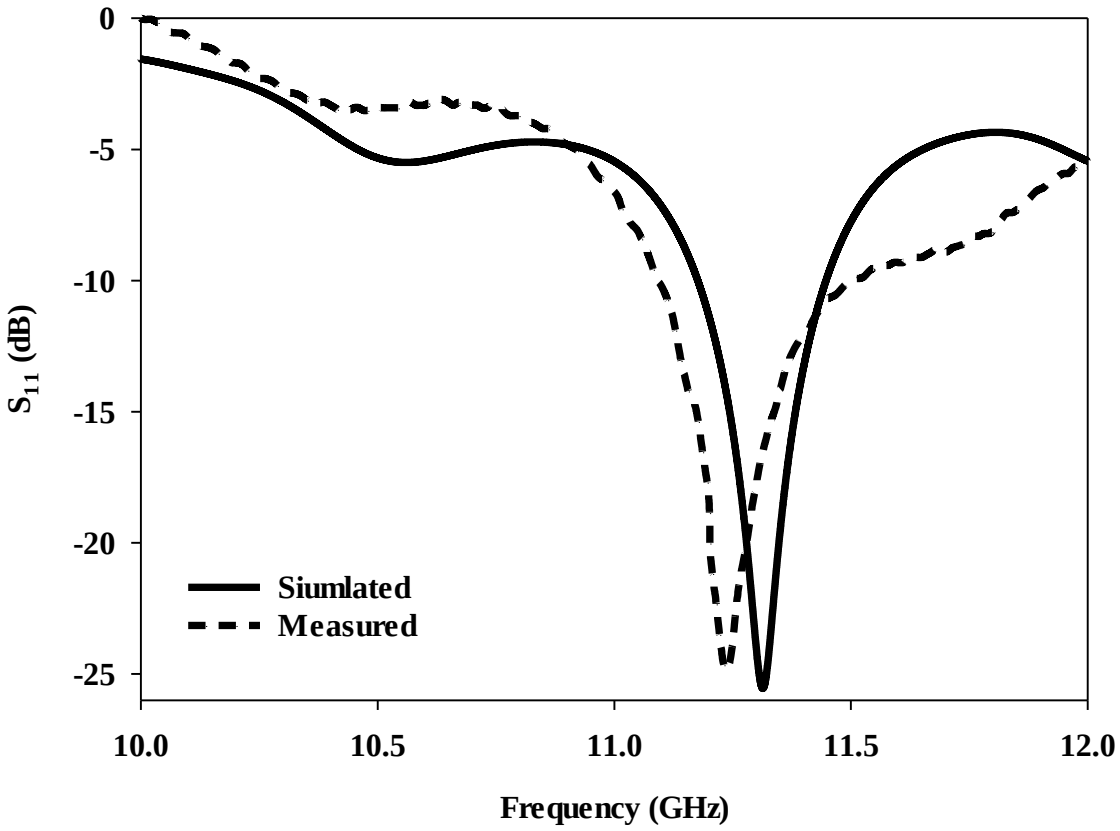

Figure 2.17: measured and simulated reflection coefficients of RDRA exited in the TE_{117}

Figure 2.17 shows the simulated and measured reflection coefficients of the proposed RDRA, and reasonable agreement between them is observed. Once again, with reference to the figure, the simulated and measured ($|S_{11}| > 10$-dB) impedance bandwidths are given by 2.38 % (11.17–11.44 GHz) and 2.43% (11.12–11.43 GHz), respectively. The measured resonance frequency (minmum $|S_{11}| > -10$ dB) is 11.24 GHz, agreeing well with simulated (11.33 GHz) values.

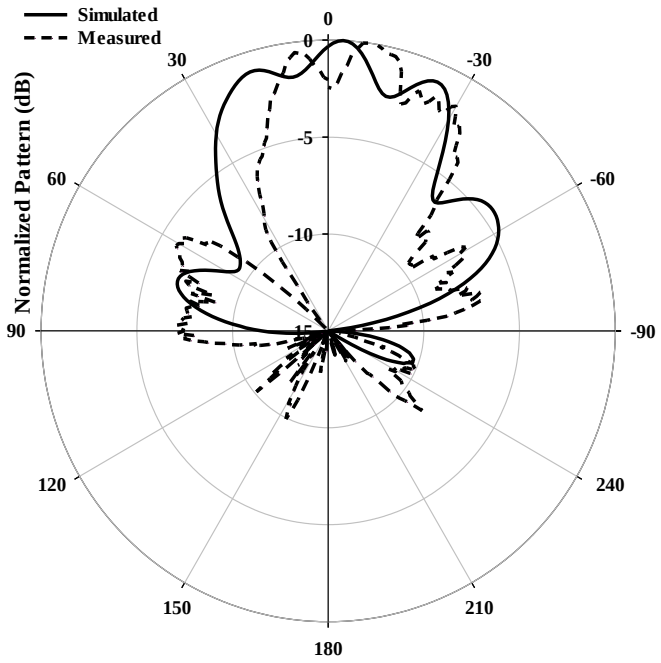

(a)

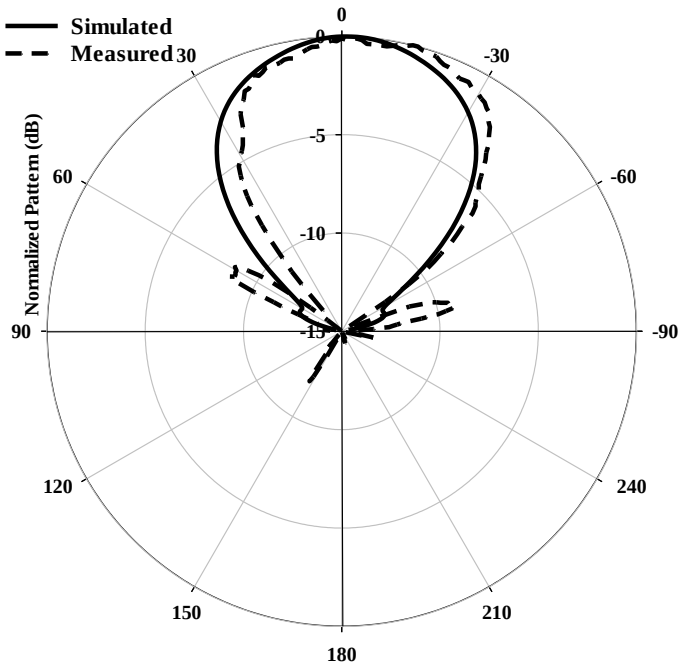

(b)

Figure 2.18: Simulated and measured radiation patterns a) E- Plane and b) H- Plane of the DRA excited in the TE_{117} mode (at 11.24 and 11.33 GHz).

The normalized simulated and measured radiation patterns of the TE_{117} mode at 11.24 GHz and 11.3 GHz are shown Figure 2.18. The agreement between measured and simulated radiation pattern is very close. However, the ripples in E-plane in the measured pattern are

primarily due to diffraction from finite ground plane, and because of SMA connector since it becomes electrically large at high frequencies. The measured and simulated antenna again which are ~ 8.6 dBi at around ~11.3 GHz are illustrated in Figure 2.19.

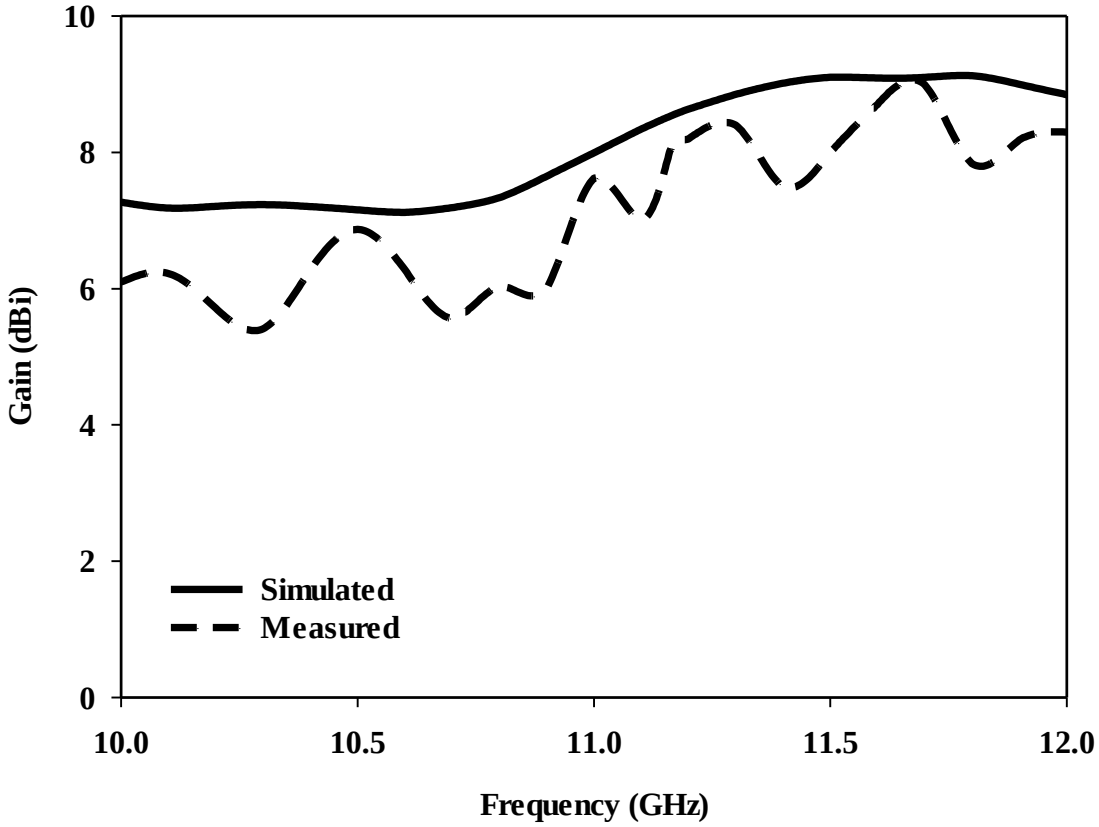

Figure 2.19: Simulated and measured antenna gain as a function of Frequency

2.6 Rectangular DRA operating in the TE_{511} and TE_{533} higher order modes

In this section, a rectangular DRA that is working in the TE_{511}, TE_{533} will be investigated. The dimensions of the DRA are based on those reported in [26] using DWM calculations and demonstrated using CST MWS [103] in this research with feed network. The DRA dimensions are 15.24×7.62×3.1 mm^3 that supports resonance modes at 17.7 and 19.6GHz. It is worth mentioning that the DRA has a rectangular cross section and the dimensions support a multi-higher order operation. It should be noted that a y-directed slot has been utilized to excite the DRA with respective length and width of 4 and 0.5mm. In addition, an optimum stub length of 7 mm has been employed. With reference to Figure

2.20, it can be noted that impedance bandwidths of 1.6% and 0.75% have been achieved at the TE_{511} and TE_{533} resonance modes, respectively.

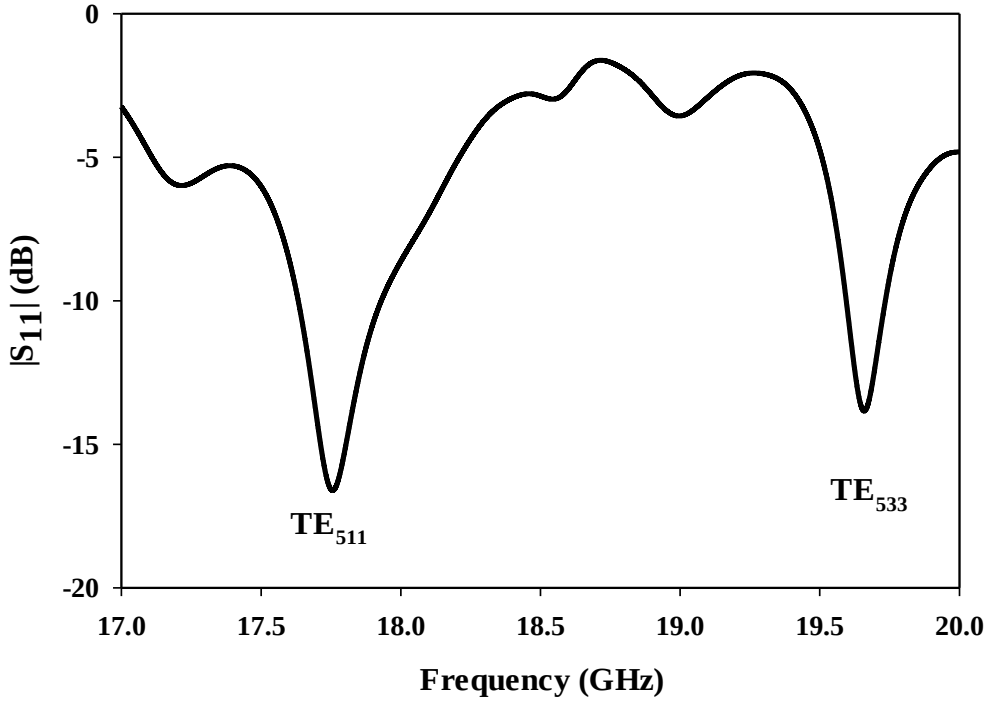

Figure 2.20: Return losses of a rectangular DRA excited in the TE_{511} and TE_{533} modes.

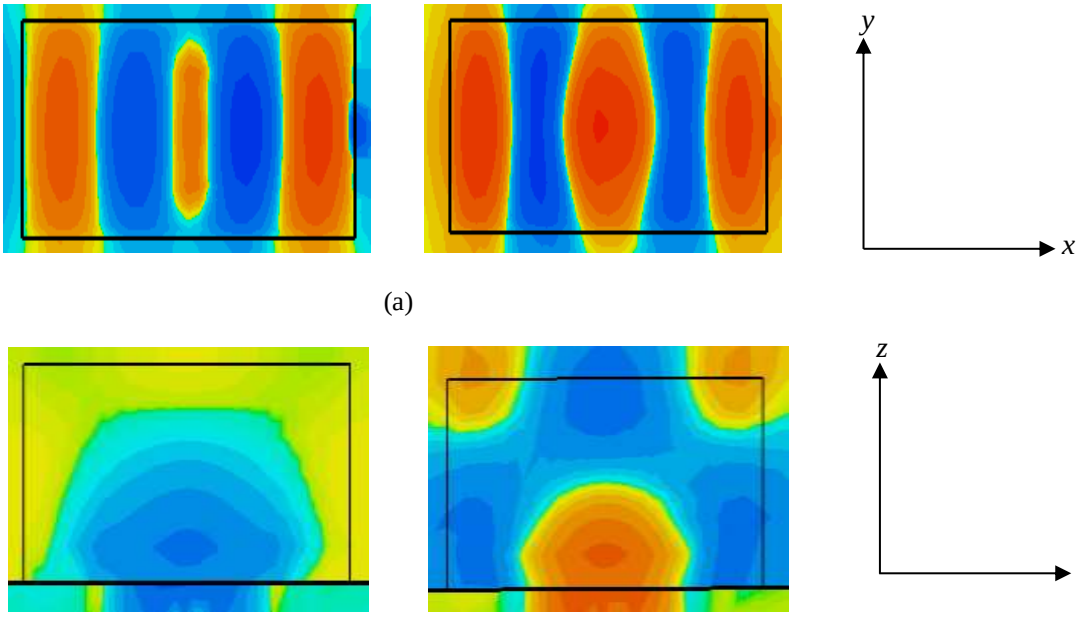

Figure 2.21: Magnetic fields of the TE_{511}, TE_{533} and resonance modes at, 17.7 GHz and 19.6 GHz, respectively (a) xy plane, (b) yz plane.

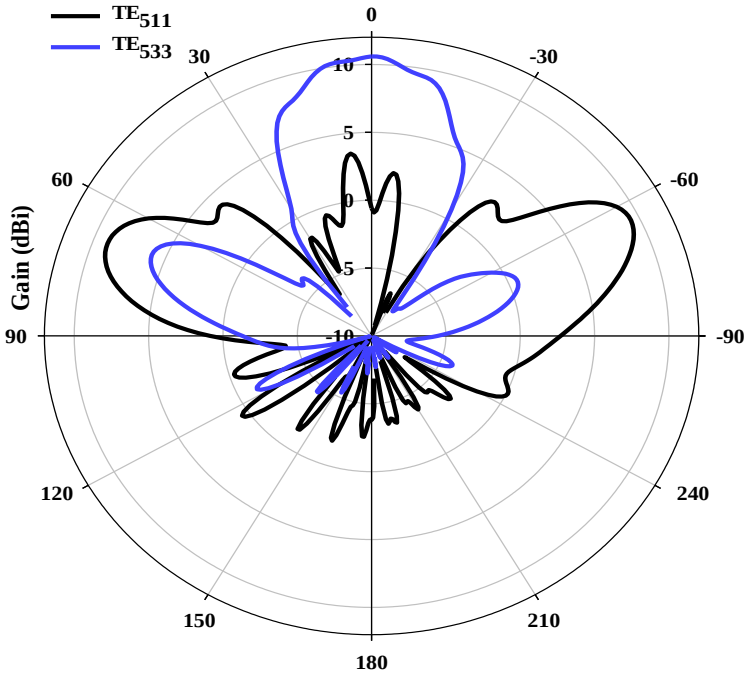

(a)

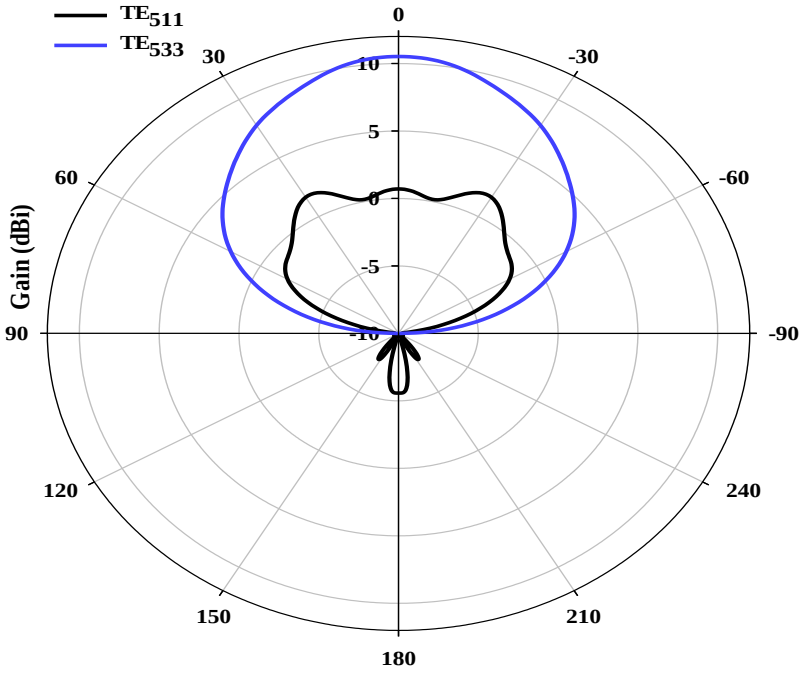

(b)

Figure 2.22: Radiation patterns of rectangular DRAs operating in the TE_{511}, TE_{533} modes at 17.7 GHz and 19.6 GHz respectively; a) E- Plane, b) H- Plane.

As explained earlier, higher order modes can be treated as magnetic dipole arrays with an elements number that depends on the excited mode. In the earlier simulations of this Chapter it has been demonstrated that increasing the antenna height results in higher order of the mode along the *z*-axis. However, in the current example, the antenna's length has been increased in order to excite higher number of short magnetic dipoles along the x–axis as demonstrated in Figure 2.21. The radiation patterns are illustrated in Figure 2.22, from which it can be noticed that gains of 10.3, and10.5dBi have been achieved for the TE_{511} and TE_{533} modes, respectively with strong side lobes in both of the principle planes due to the increase the number of magnetic dipoles along the *x*-axes. Due to inequality of antennas width and length, hence, short magnetic dipoles distribution, the TE_{511} mode is more directive in the E plane compared to the H plane. Although a high gain has been achievable when the number of short magnetic dipoles is increased along the *x* axis, the impedance bandwidth still narrow.

2.7 Gain enhancement using dielectric superstrate

In this section, DRA gain enhancement is considered theoretically and experimentally when a dielectric superstrate is incorporated in the configuration. By optimising the thickness of the dielectric superstrate most of the electromagnetic wave are radiated into free space and can be bent in a prescribed direction resulting in the increment of the gain in that direction. In another word, the director acts as a reflector to redirect the propagation density from the back lobe to the main lobe [108]. Hence, increasing the directivity for the same radiation efficiency. Simulations have been conducted using CST MWS in order to investigate the impacts of the dielectric superstrate surface on the antenna gain and impedance bandwidth. As seen in Figure 2.23 a dielectric superstrate with respective thickness and dielectric constant of 3.5mm and 3.5 with loss tangent of 0.0027 has placed on top of a rectangular DRA that supports the TE_{117} and TE_{119}, i.e. a multi-mode operation, as has been explained in Table 2-4. It should be noted that the superstrate permittivity has been chosen according to the available material for fabrication, while the optimum height has been determined using CST parameter sweep. With reference to Figure 2.24, it can be observed that a maximum gain of 16.2dBi in conjunction with a ~2% impedance bandwidth have been achieved when the dielectric superstrate surface are is $60mm^2$, which corresponds

to a size of $2.3\lambda_o$. On the other hand, it can be noted from the same figure that the widest impedance bandwidth of 2.83% has been achieved, albeit with a gain of 14.9 dBi, when the superstrate surface is reduced to~40mm^2 corresponding to a superstrate size of $1.5\lambda_o$. Further investigations demonstrated that the maximum gain and impedance bandwidth 16.2 dBi and 2%, respectively, can be achieved when the dielectric superstrate relative permittivity range from 3 to 4, when the surface fixed at 60mm2 as demonstrated in Figure 2.25, therefore a superstrate with a surface area of 60mm^2 has been chosen for measurements. In order to demonstrate aforementioned results, a rectangular DRA has been built using an Alumina that has permittivity of 10 and loss tangent of 0.0001 placed on the ground plane of 100×150mm^2. The dielectric superstrate has been fabricated using 3D printing technology with a polyimide that has dielectric constant of 3.5 and loss tangent of 0.0027. The proposed antenna illustrated in Figure 2.26, and during the measurement a foam substrate has been utilized to provide a mechanical support to the superstrate.

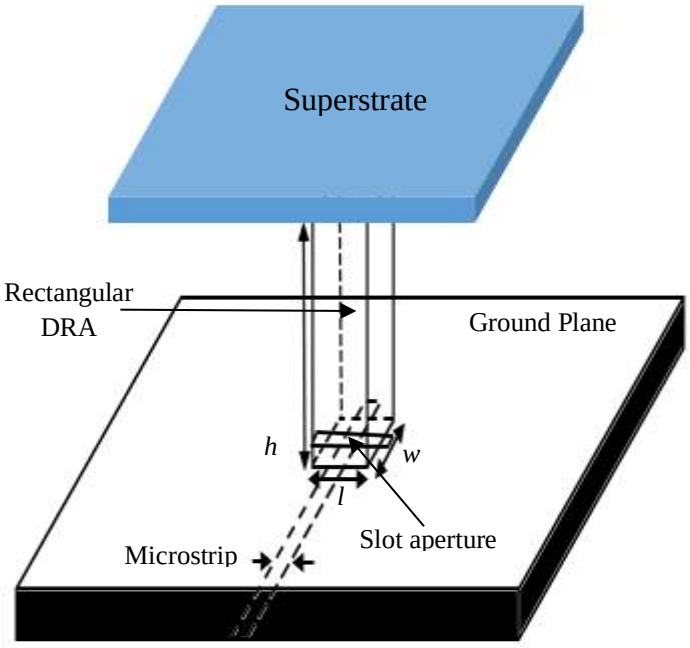

Figure 2.23: Rectangular DRA loaded by a dielectric superstrate.

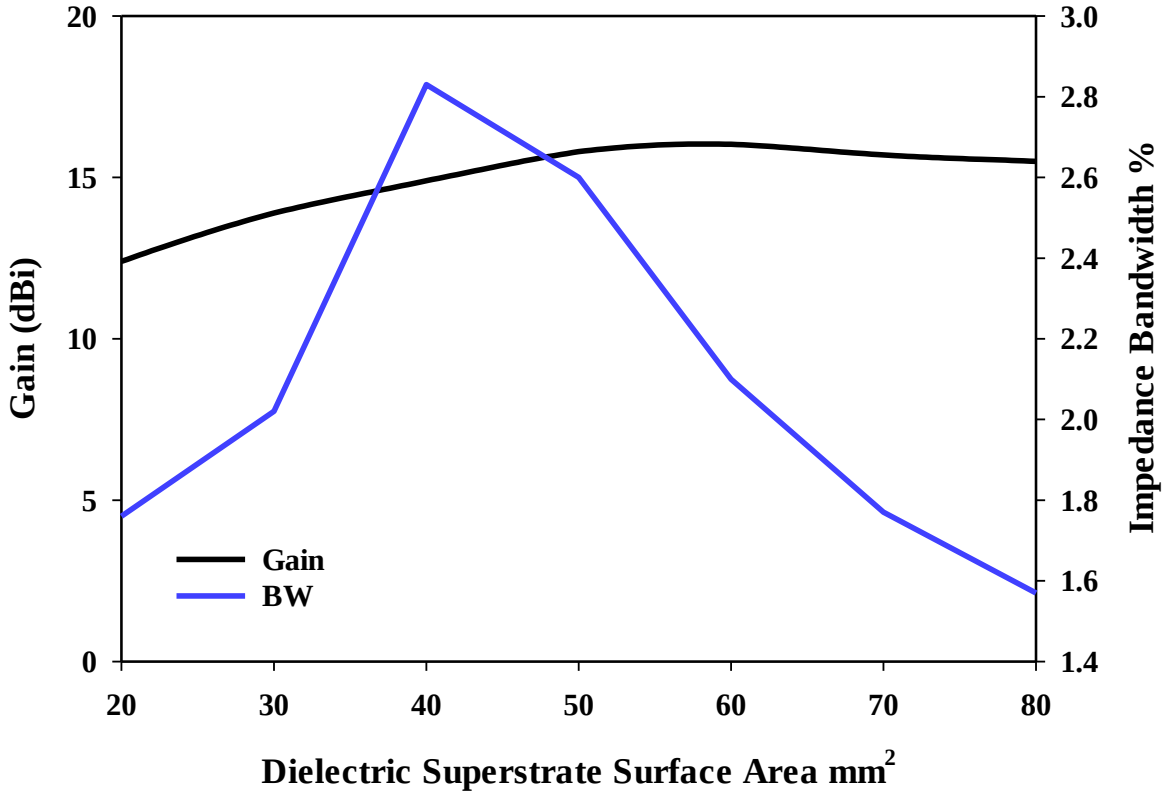

Figure 2.24: Maximum bandwidth and gain as functions of dielectric superstrate surface.

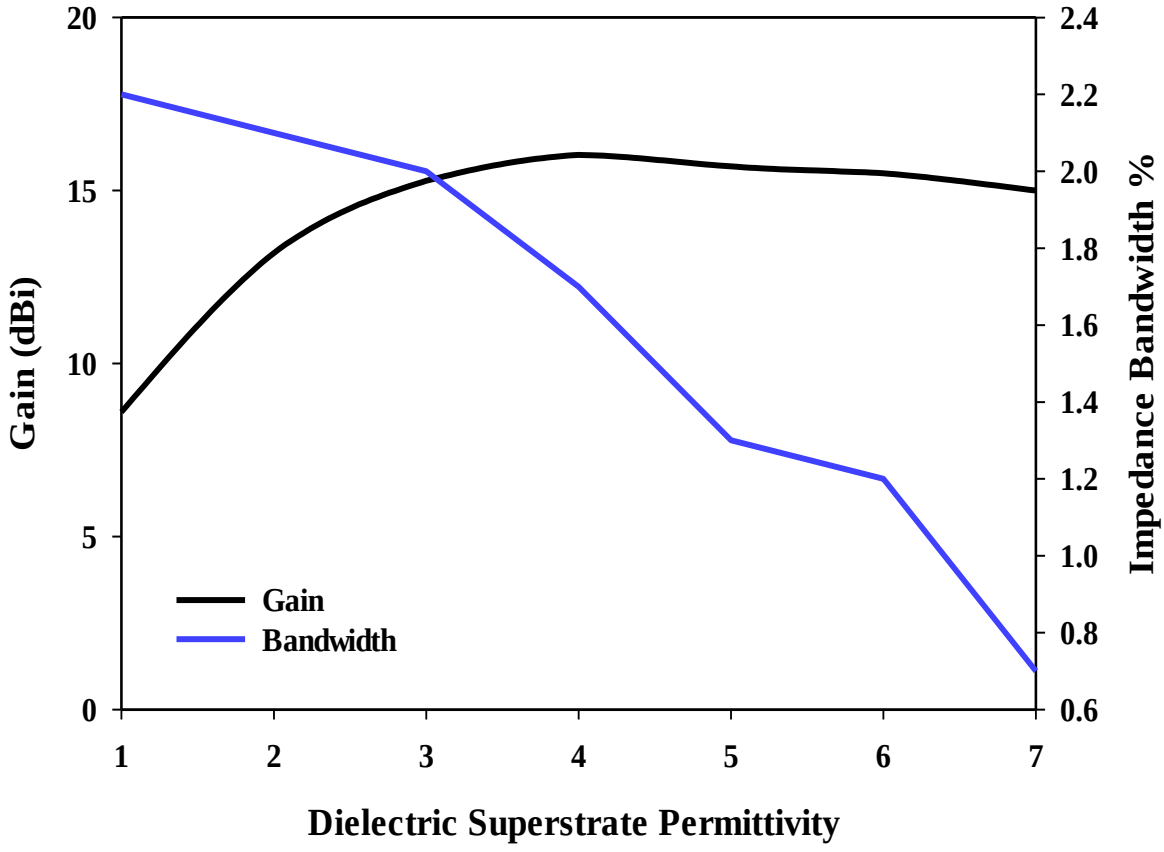

Figure 2.25: Maximum bandwidth and gain a function of dielectric superstrate permittivity.

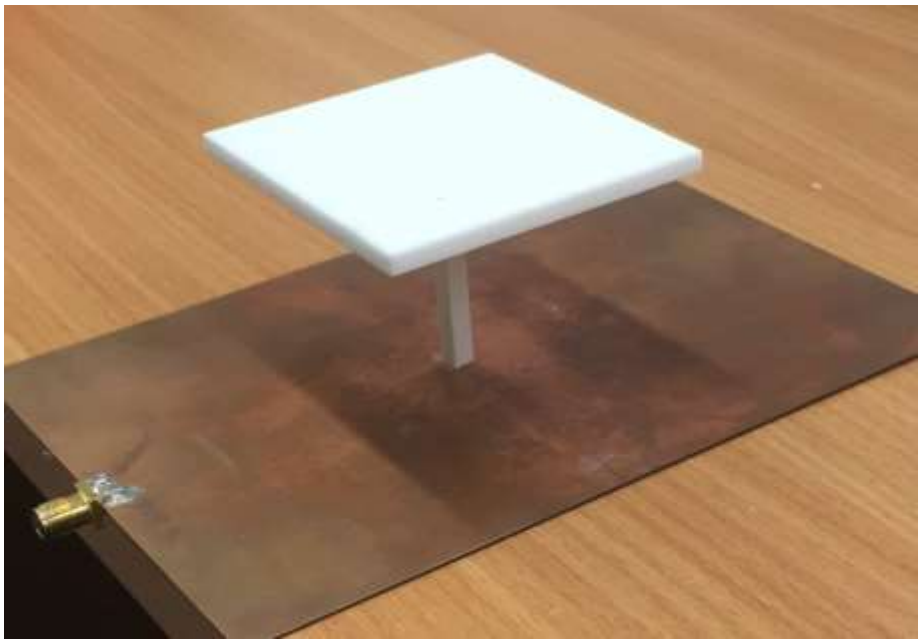

Figure 2.26: Dielectric superstrate overhead rectangular DRA.

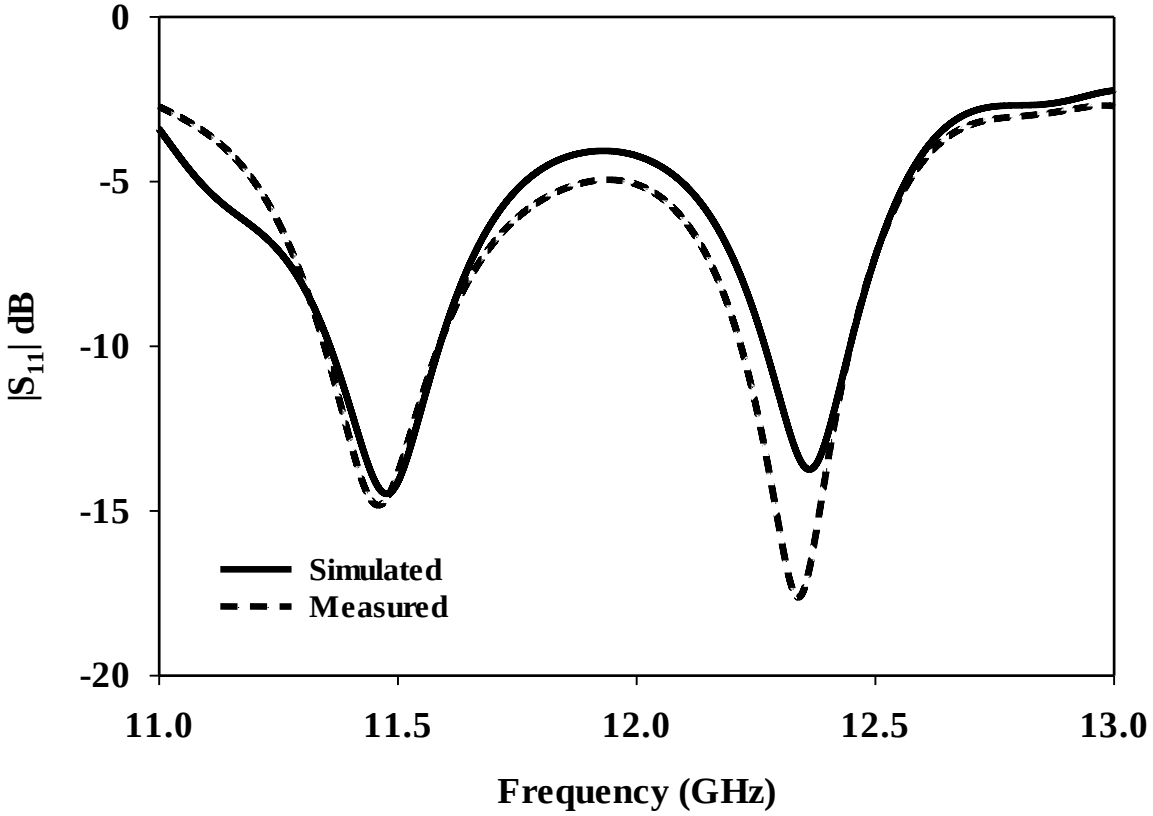

Figure 2.27*:* Reflection coefficients of superstrate loaded RDRA.

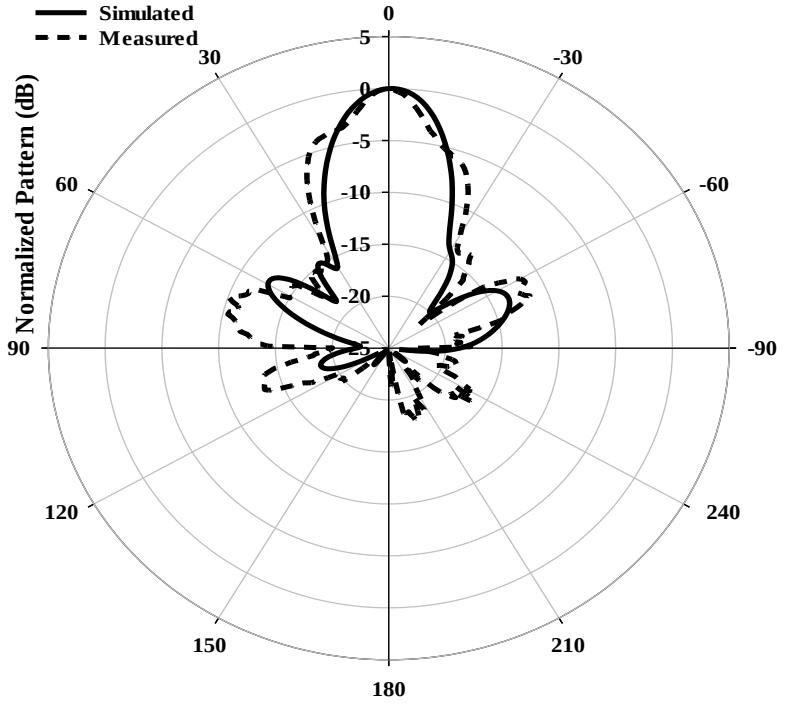

(a)

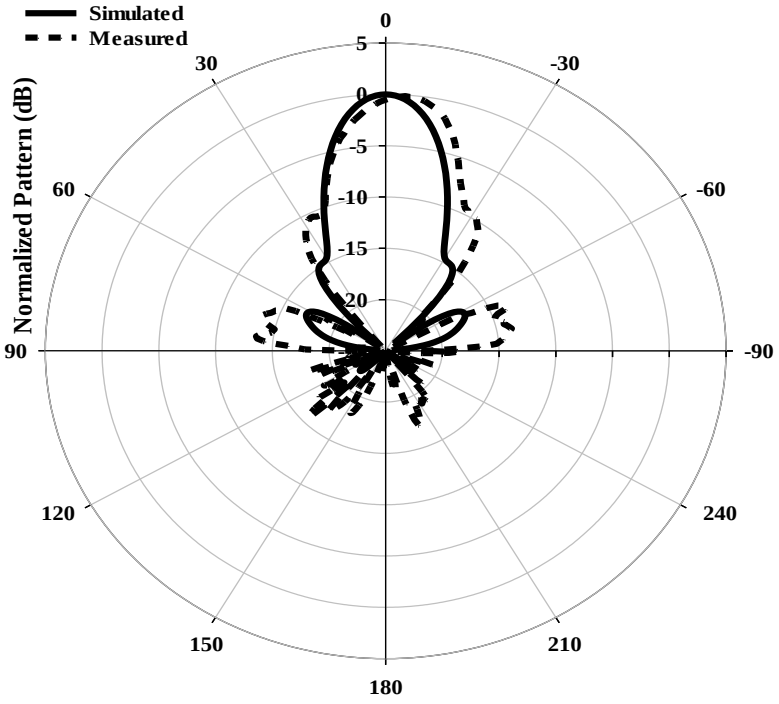

(b)

Figure 2.28: Radiation patterns of dielectric superstrate loaded RDRA at 11.4GHz. (a) $\phi = 0$. (b) $\phi = 90$.

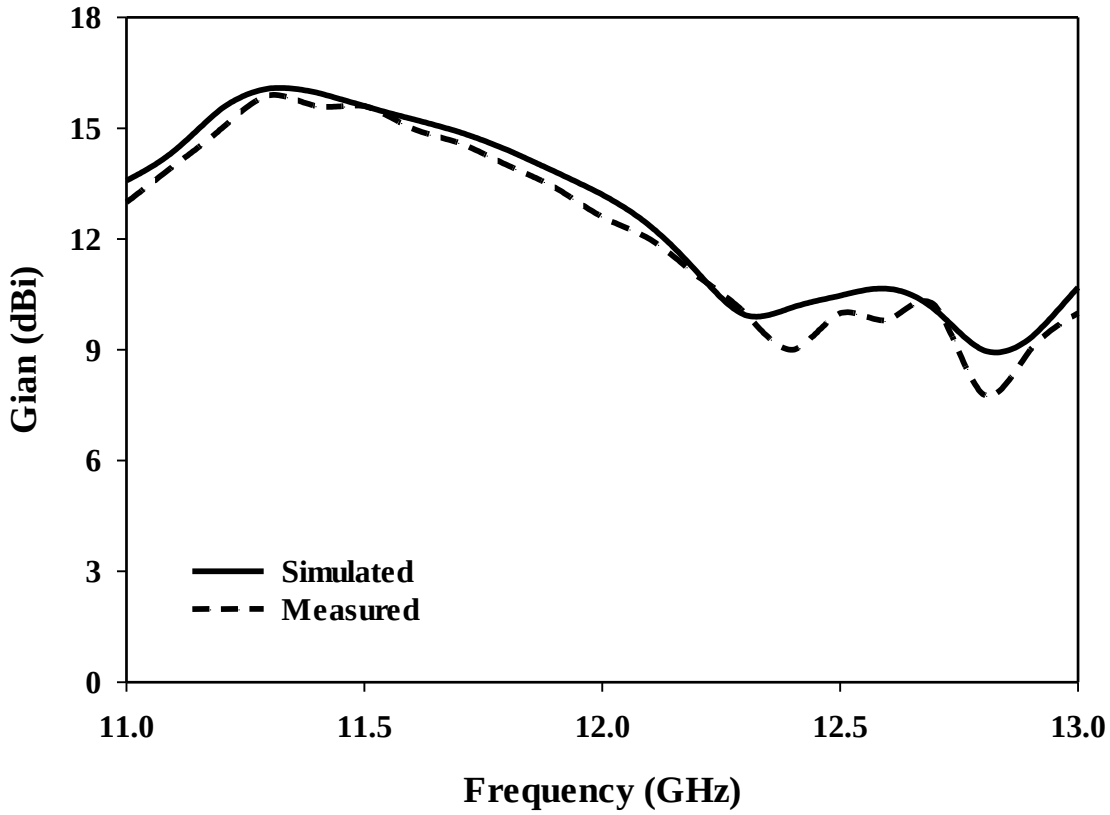

Figure 2.29: Simulated and measured gain for superstrate loaded RDRA.

The reflections coefficient has been measured using an E5071C vector network analyser and the results are illustrated in Figure 2.27, where it can be observed that a close agreement has been achieved between the simulated and measured results for the TE_{117} and TE_{119} resonance modes. The far field patterns have been measured using NSI system. Figure 2.28 presents a close agreement between the measured and simulated far field patterns for the TE_{117} mode at 11.4GHz. However, as noted in Figure 2.29, a slight drop in measured gain to 15.8dBi has been achieved compared to the simulated gain 16.2dBi. This marginal discrepancy could be attributed to experimental errors such as the superstrate may have not aligned precisely with respect to the DRA center. These results demonstrate that a considerable gain enhancement may be achieved with the aid of a dielectric superstrate albeit with noticeable limitations such the narrow bandwidth and the significantly increase DRA size.

Table 2-6: Comparison of the performances of the proposed design and those available in the literature

Ref	Technique	Number of elements	Operating at GHz	BW %	Gain dBi
Proposed design	Superstrate	1	11.47	2	16.2
[101]	array	4	30	1.6	13.6
[56]	array	4	1.9	4	13
[53]	array	4	25.5	2	16.3
[109]	Superstrate	1	61.34	13	14
[110]	Superstrate	1	7.9	15	11.34

Table 2-1 presents a comprehensive comparison between gain and bandwidth of the proposed design with those previously reported in literature. From these results it can be noted that the achieved gain is higher, or comparable to, that of reported DRA arrays albeit without the complexity, losses, increased size and cost of utilizing an array. On the other hand, using dielectric superstate has improved the gain significantly in conjunction with narrow impedance bandwidth.an alternative design that addressing the gain mad BW challenges will be addressed in the next chapter.

2.8 Higher order mode rectangular DRA arrays

Another well know approach for gain enhancement is to employ an antenna array. In this section, higher order modes rectangular DRAs array will be investigated, where five rectangular DRA arrays have been considered with elements that support one of the following resonance modes for each array; TE_{111}, TE_{113}, TE_{115}, TE_{117} and TE_{119}. It is worth mentioning that the DRAs dimensions are same as those used in section 2.4.2 and illustrated earlier in Table 2-4. Figure 2.30 illustrates four RDRA elements that are separated by distance of d and fed using a slot aperture size of 1×4.6 mm^2 through the feeding network. A summary of the simulated gain and impedance bandwidth for higher order modes is Table 2-7 and Figure 2.31, 2.32, 2.33 and 2.34, where it can be observed that, for the lower order mode TE_{111} single element the gain and bandwidth 5.6dBi, and 2%, respectively, at an

operating frequency of 11.9GHz. However, by utilizing an array of six elements that are separated by distance of *d* which is $0.8\lambda_0$, the gain and bandwidth improves to 13.4dBi and 6.8%, respectively, at 11.5GHz. On the other hand, respective gain and bandwidth of 9.9dBi and 2.3% can be achieved using a single DRA element that operates in the TE_{119} higher order mode at 11.9GHz compared to gain and bandwidth of 17dBi and 6.9% for six higher order mode DRAs array at 11.5GHz with a separation distance of $0.8\lambda_0$ between adjacent elements. Comparison between these results demonstrate that respective gain enhancements of 7.8 and 7.1dBi have been achieved for lower order and higher order mode DRA arrays with identical bandwidths.

The mutual coupling between neighbouring elements plays a key role in terms of radiation pattern distortions. This phenomenon has been analysed using CST MEWS[103], where two RDRA elements of the aforementioned arrays that support the TE_{113}, TE_{115} and TE_{119} and separated by distance *d* that varies between 12 to 20mm , i.e. $0.5\lambda_0$ to λ_0. As can be noted from Figure 2.35, the mutual coupling has increased by increment the excited mode order and decreased by increasing the separation distance. Although these results are promising for gain enchantment using higher order mode RDRA arrays, considerable back lobes exist as illustrated in Figure 2.33. This can be attributed to the increased number of slot apertures that can be considered as a key limitation for any array since it increases the radiation leakage to the lower half-space. Moreover, the complexity of the feed network also is a serious challenge where the loss is expected at high frequencies. Furthermore, utilising several RDRAs, each with a height of 50mm, increases size and volume of the antenna considerably with a higher risk of the long and thin DRAs to be broken since the fragility of ceramic that the antennas are made from. Finally, the Ohmic losses of the feed network can be increases substantially at higher frequencies and hence reduces the radiation efficiency. Designing a simple model that can address all aforementioned challenges will be taken into account in this research.

Table 2-7: Gain and bandwidth of RDRA arrays

Mode	TE_{111}		TE_{113}		TE_{115}		TE_{117}		TE_{119}	
	Gain dBi	BW %	Gain dBi	BW %	Gain dBi	BW %	Gain dBi	BW %	Gain dBi	BW %
Single element	5.62	2.02	7.8	2.19	9.4	2.27	8.6	2.2	9.96	2.25
2 elements	6.7	3.35	9.37	3.6	10.4	3.78	11.1	3.73	11.6	3.5
4 elements	10.3	4.5	12.5	4.38	13.5	4.30	14.1	4.30	14.5	4.28
6 elements	13.4	6.8	14.7	6.8	15.7	6.9	16.7	6.9	17.1	6.9

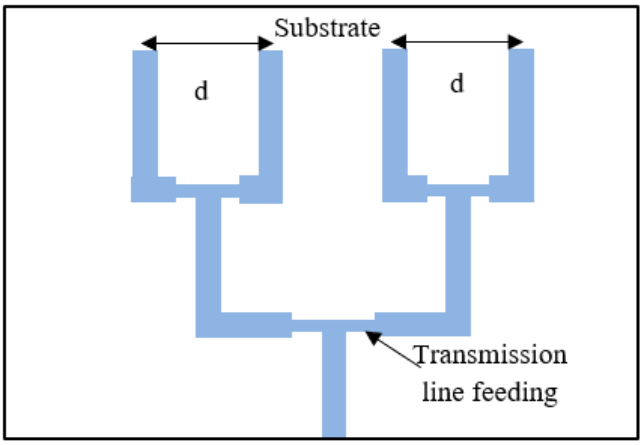

(a)

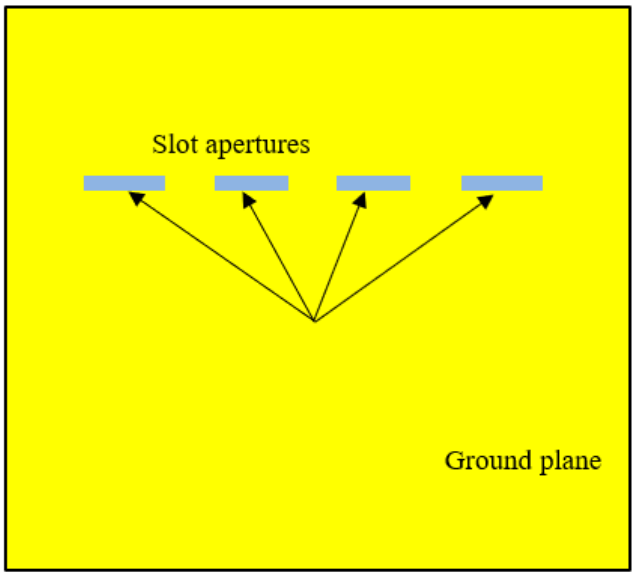

(b)

Figure 2.30: Four elements RDRAs array feed network (a) bottom view (b) top view.

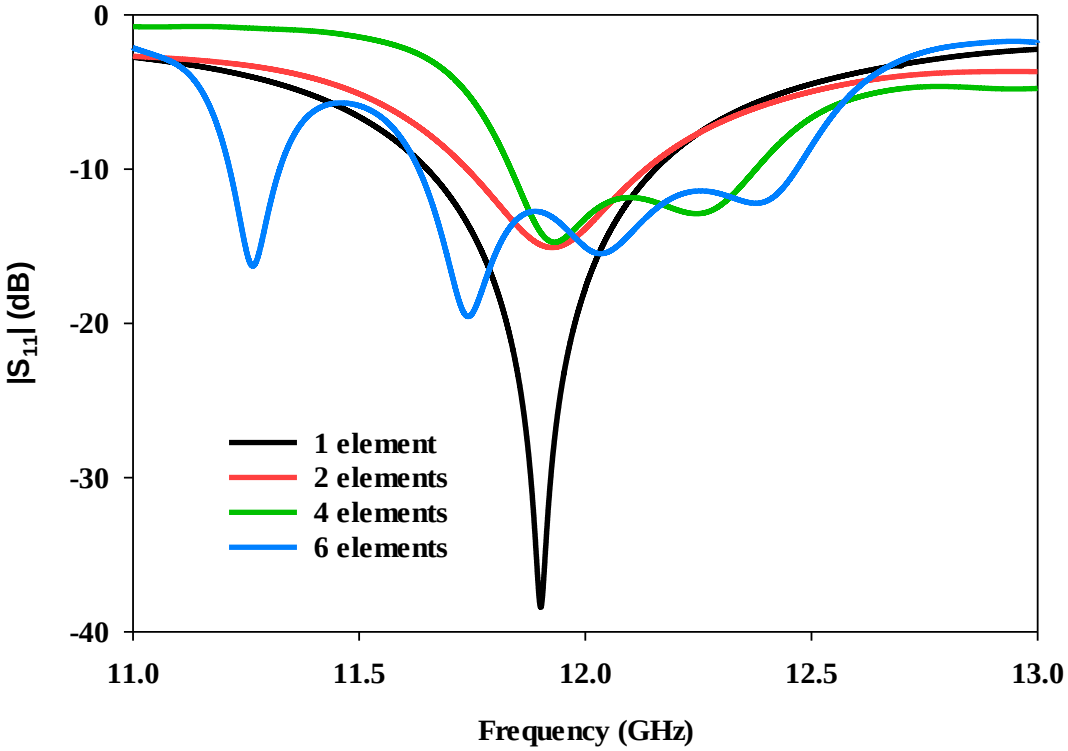

Figure 2.31: Reflection coefficient for RDRAs array TE_{111} mode

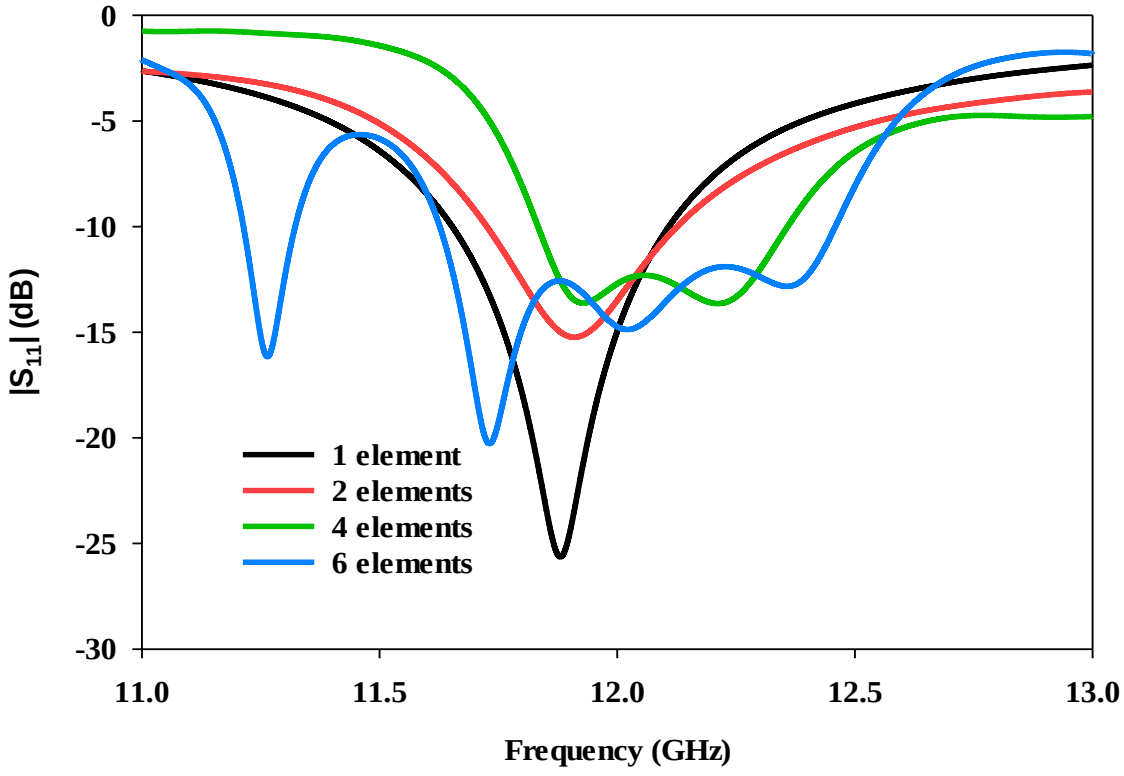

Figure 2.32: Reflection coefficient for RDRAs array (a) TE_{111} mode and (b) TE_{119} mode.

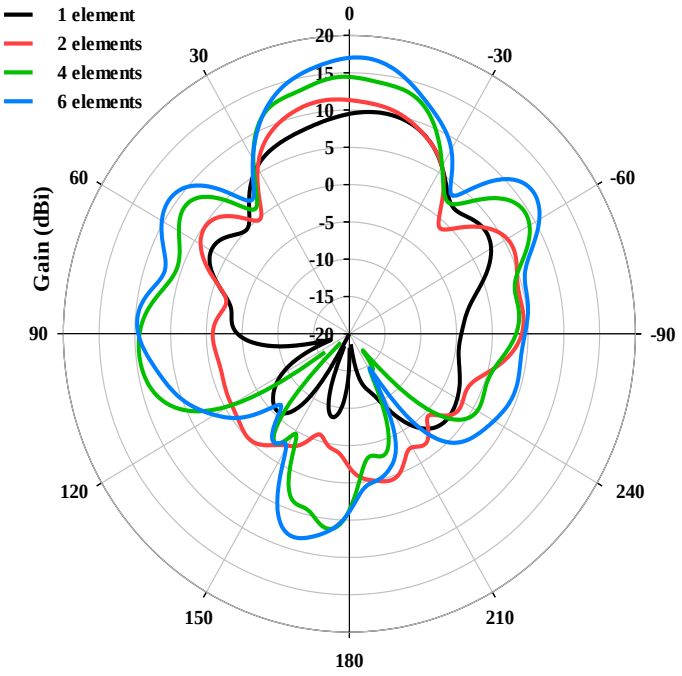

(a)

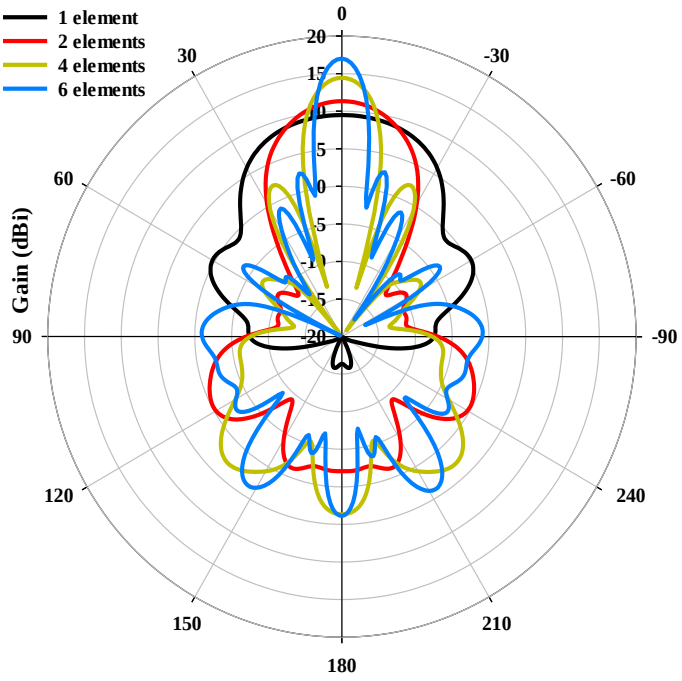

(b)

Figure 2.33: Radiation pattern of TE_{111} mode RDRA arrays. (a) E-plane. (b) H-plane.

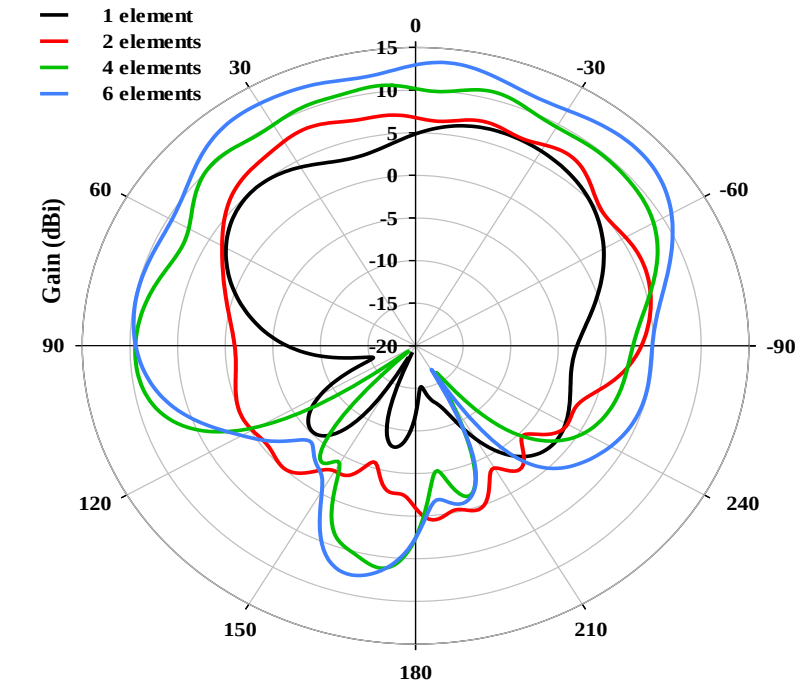

(a)

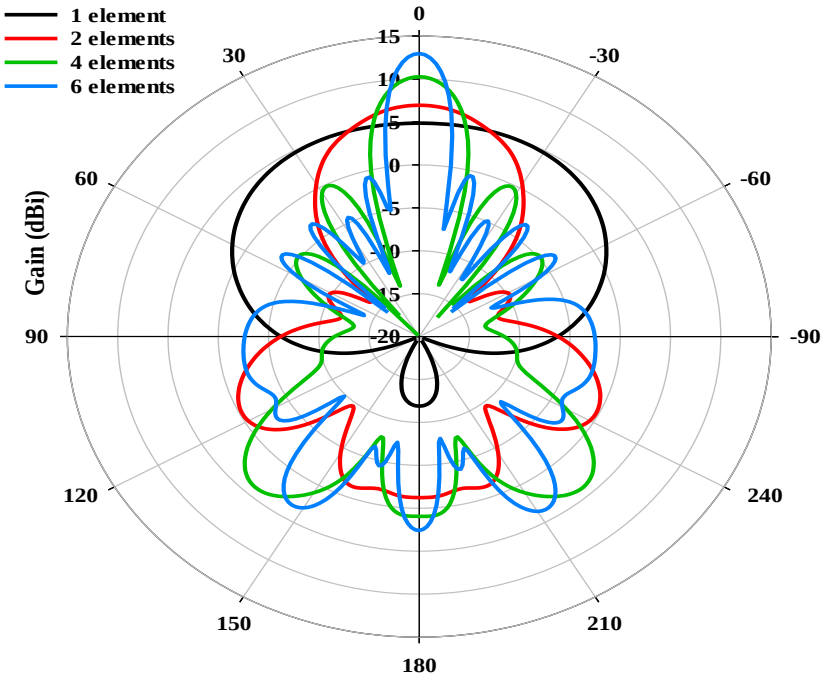

(b)

Figure 2.34: Radiation pattern of TE_{119} mode RDRA arrays. (a) E-plane. (b) H-plane.

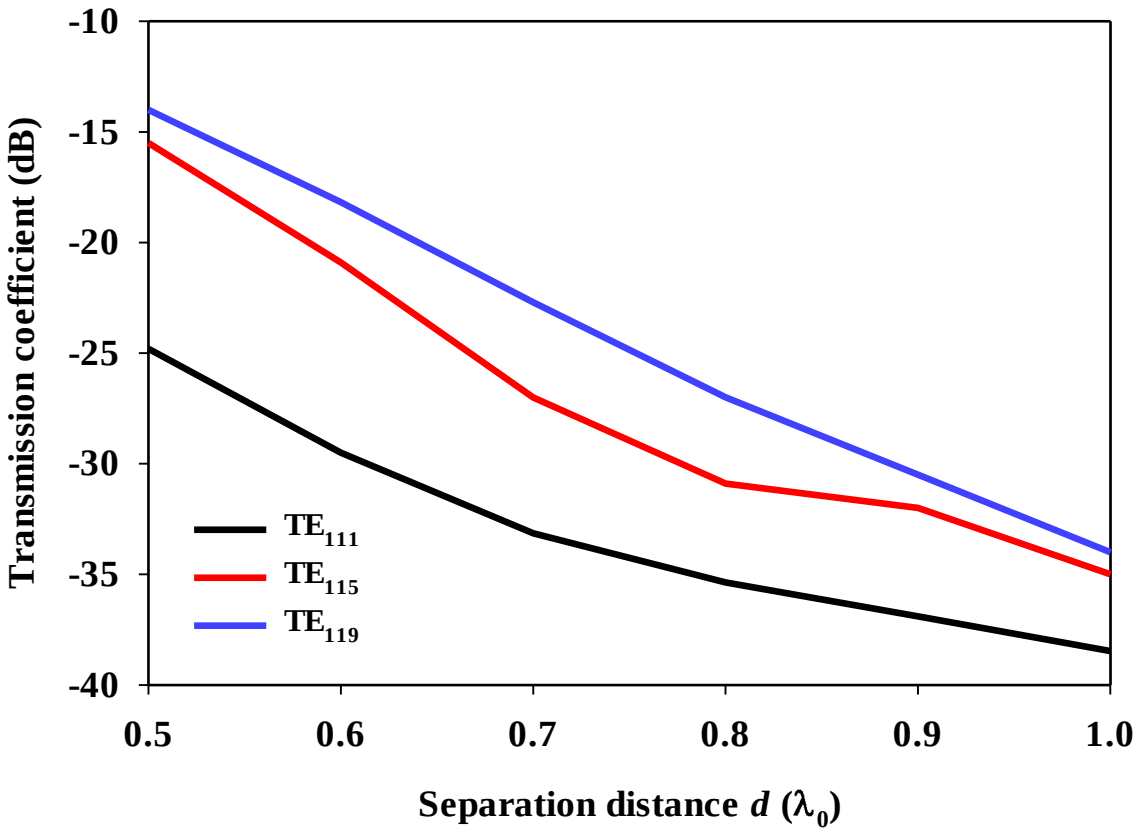

Figure 2.35: Transmission coefficient as a function of element spacing for TE_{111}, TE_{115} and TE_{119} mode at 15 GHz.

2.9 Conclusion

The impacts of the aspect ratio on the impedance bandwidths and gain of an X-band rectangular DRA have been studied, where it has been noticed that a single higher order mode operation, where the aspect ratio of more than 0.25, offers wider impedance bandwidth and lower gain due to the overlapping between the short magnetic dipoles. In addition, a single mode operation is less affected by fabrication errors compared to a multi-higher order mode operation. On the other hand, a multi-higher order mode operation, in which the aspect ratio is less than 0.25 and greater than 0.1, offers narrower bandwidth in conjunction with higher gain due to eliminating any overlapping between adjacent magnetic dipoles inside the DRA. For example, the gain of a DRA operating in the single higher order mode of TE_{119} is 6.4dBi compared to ~9 dBi in a multi-modes' region. Moreover, further gain enhancement requires a longer DRA that results in impractical and fragile antenna with an extremely narrow bandwidth. Therefore, alternative approaches have been considered to achieve a more practical higher gain DRA. For example, incorporating a dielectric superstrate has

increased the gain considerably up to 16dBi with no improvement in the impedance bandwidth as well as a considerably larger DRA footprint. Furthermore, employing array has also been considered for a higher gain and wider bandwidth DRA. However, factors such as the increased size, feed network complexity and considerable back lobe radiation represent serious limitations combine with the increased feed network losses at higher frequencies. Considering all these limitations, a new approach needs to develop to design a high gain wide-band DRA with more practical dimensions and improved fabrication tolerance. Such approach will be presented in the next Chapter.

Chapter 3

Higher Order Mode layered Rectangular Dielectric Resonator Antenna

3.1 Introduction

The limitations of single and multi-higher order mode DRA designs have been outlined in Chapter 2, where it has been demonstrated that a lower gain can be achieved when the rectangular DRA operates in a single higher order mode compared to that of a multi-higher order modes operation. This can be explained as a result of the overlapping between the short magnetic dipoles that are separated by a distance of less than $0.4\lambda_o$. However, this gain enhancement is usually associated with a narrow impedance bandwidth. As mentioned earlier, and according to arrays' theory, maximum gain can be achieved when the separation distance between two adjacent magnetic dipoles is $\geq 0.4\lambda_o$. As for an increased DRA height, i.e. a lower aspect ratio, the distance between short magnetic dipoles increases, which eliminates the overlapping between short magnetic dipoles, thus increasing the gain. Additionally, it has also been demonstrated in Chapter 2 using a dielectric superstrate can increase the gain significantly. However, it is associated with narrow impedance bandwidth and the size of the director increased the antenna size. Furthermore, using DRA array for gain enhancement may not represents an ideal solution for higher gain enhancement due to the complexity and potentially high ohmic losses of the feed network at higher frequencies. In order to address these challenges, a layered rectangular DRA will be investigated that operates in the higher order modes of TE_{119}, $TE_{11,11}$ and $TE_{11,13}$ for linear and circular polarizations. The simulations have been implemented using CST microwave studio [103], where the impacts of different dielectric coating permittivities on the impedance bandwidth and gain have been studied. Moreover, a prototype of the layered higher order mode DRA has been built and measured with close agreement between experimental and simulated results. This Chapter is focused on demonstrating the potential of a layered higher order

mode rectangular DRA as a solution to the bandwidth limitations of a multi-higher order modes single layer counterpart. The outline of this Chapter is illustrated in Figure 3.1.

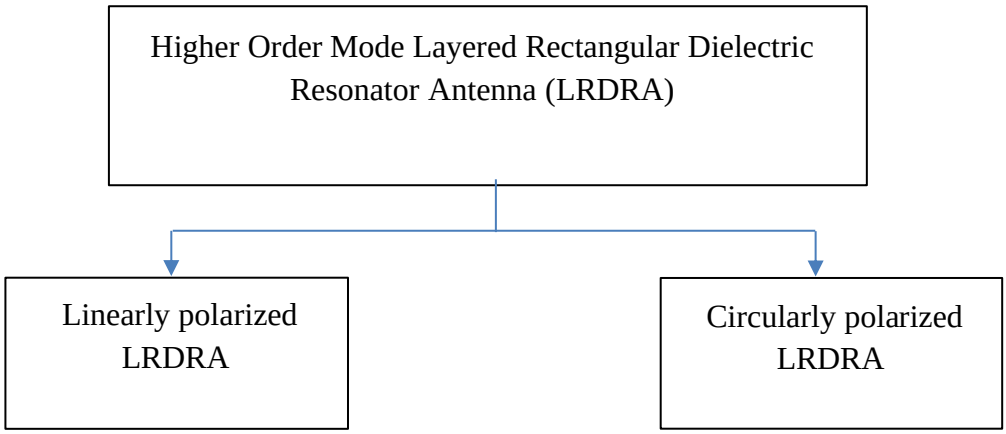

Figure 3.1: Chapter three overview.

3.2 Linearly Polarized Higher Order Mode RDRA

3.2.1 Antenna Configuration

In order to demonstrate the potential of a layered higher order mode DRA, simulations have been implemented to investigate the effects of using a coating dielectric layer with a different permittivities. A rectangular DRA operating at a frequency range of 10 to 12GHz has been considered using an inner layer with ε_{r1}= 10 and a loss tangent of tan $\delta < 0.002$ as well as respective length, width and height of l_1= $w_{1=}$ 4mm and h_1 =40mm coated with a layer that has a dielectric constant of $\varepsilon_{r2,}$ optimised dimensions of l_2 and w_2, however, the height of outer layer has been fixed at h_2=41mm. The resulting design for the linearly polarized layered RDRA is presented in Figure 3.2. The proposed antenna has been placed on a Rogers RO4535 substrate length, width and thickness of 150mm, 100mm, 0.8mm, respectively, and a dielectric constant of 3.5 with a loss tangent 0.0037. A copper ground plane has been placed on the top side of the substrate, while a microstrip transmission line has been printed on the lower side. A slot has been created in the ground plane with dimensions of 1×6mm^2, which has been used to excite the DRA.

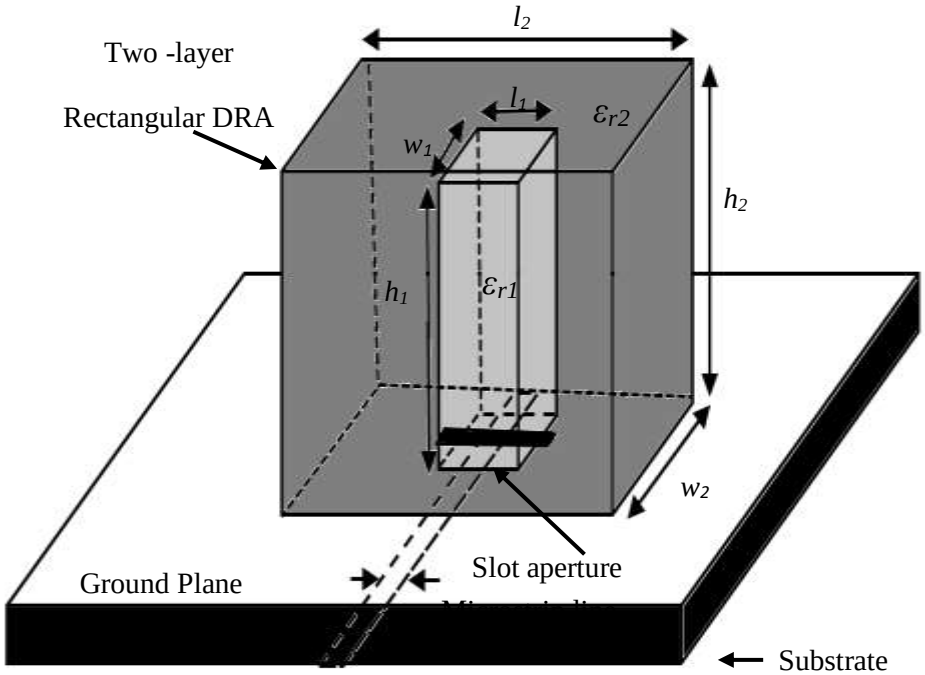

Figure 3.2: Configuration of the LP layered RDRA.

3.2.2 Parametric study

The reflection coefficient and gain have been studied as a function of the dielectric coat permittivity when the outer layer dimensions have been optimised for each value of ε_{r2}. The inner layer, DRA, dimensions have been fixed at $w_1 \times l_1 \times h_1 = 4 \times 4 \times 40$ mm^3. The results are illustrated in Figure 3.3 and Figure 3.4 as well as Table 3-1, where it can be observed that increasing ε_{r2} provides a wider bandwidth in conjunction with a shift in the resonance frequency. The narrowest bandwidth of 2.4% has been achieved at the absence of the dielectric coat. In contrast, employing a coat layer with ε_{r2}=4 provides a considerably wider bandwidth of ~12% compared to 10%, 2.75%, 1.5% for ε_{r2}=2, 6 and 10, respectively. This can be attributed to the aforementioned fact that the second layer can serve as a transition region between the DR antenna and the free space, which increases the impedance bandwidth [12]. It is worth mentioning that by increasing the outer layer permittivity the optimum outer layer dimensions of length and width have been decreased to 25, 20, 15 and 10mm when ε_{r2}= 2, 4, 6 and 10, respectively. This could be attributed to the fact that by increasing the permittivity of a dielectric material, a reduced size will be expected. Furthermore, once the outer layer permittivity exceeds half that of the original DRA's permittivity, the impedance bandwidth will be decreased as has been confirmed in earlier

studies [111, 112]. Moreover, it has been observed that, the lowest gain of 7.4 dBi at 10GHz has been achieved at ε_{r2}= ε_{r1}=10. However, the highest gain of 12.2 dBi at 10.8GHz has been achieved when at ε_{r2}=2.

Table 3-1: Impedance bandwidth and gain of layered rectangular DRA with various outer layer permittivities.

Outer layer dimensions $w_2 \times l_2 \times h_2$ (mm^3)	ε_{r2}	Resonance Frequency (GHz)	Resonance mode	Bandwidth %	Gain (dBi)
no coating	1	11.3	TE_{117}	2.4	8.6
25×25×41	2	11.3	$TE_{11,11}$	10	12.2
20×20×41	4	10.7	$TE_{11,11}$	12	11.14
15×15×41	6	10.25	$TE_{11,13}$	2.75	10
10×10×41	10	10.1	$TE_{11,13}$	1.47	7.4

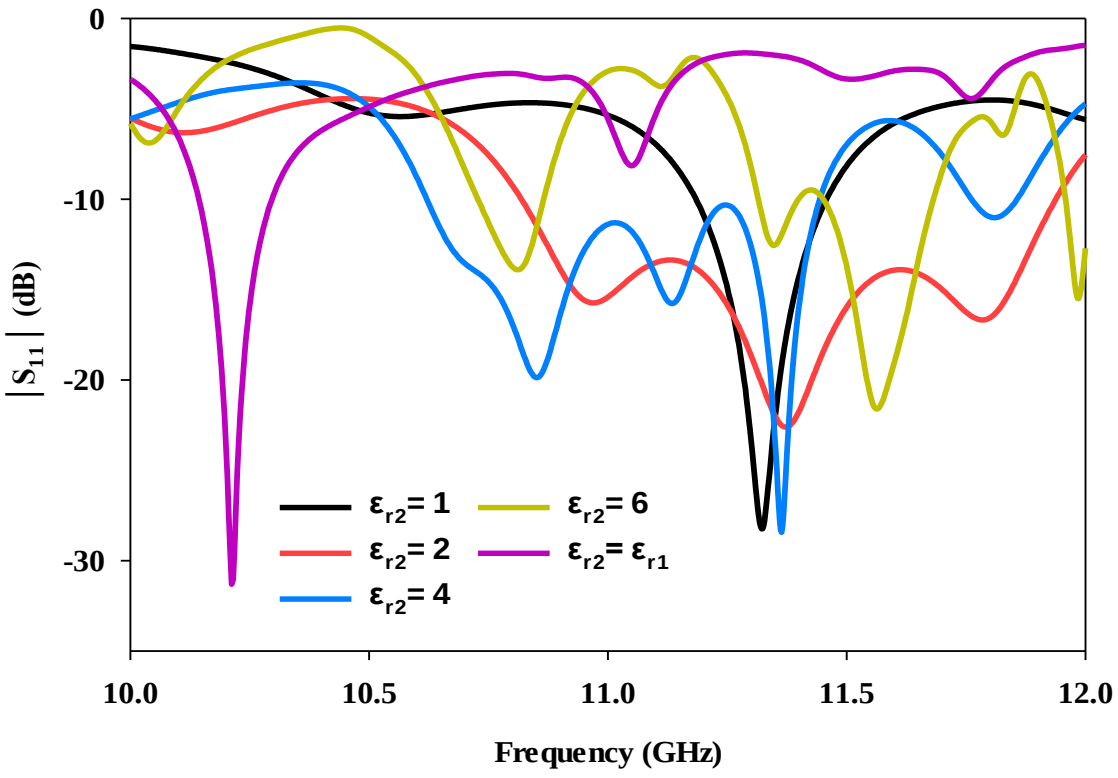

Figure 3.3: Reflection coefficient of a layered rectangular DRA when ε_{r2}= 1, 2, 4, 6 and $\varepsilon_{r2=}$ ε_{r1}=10.

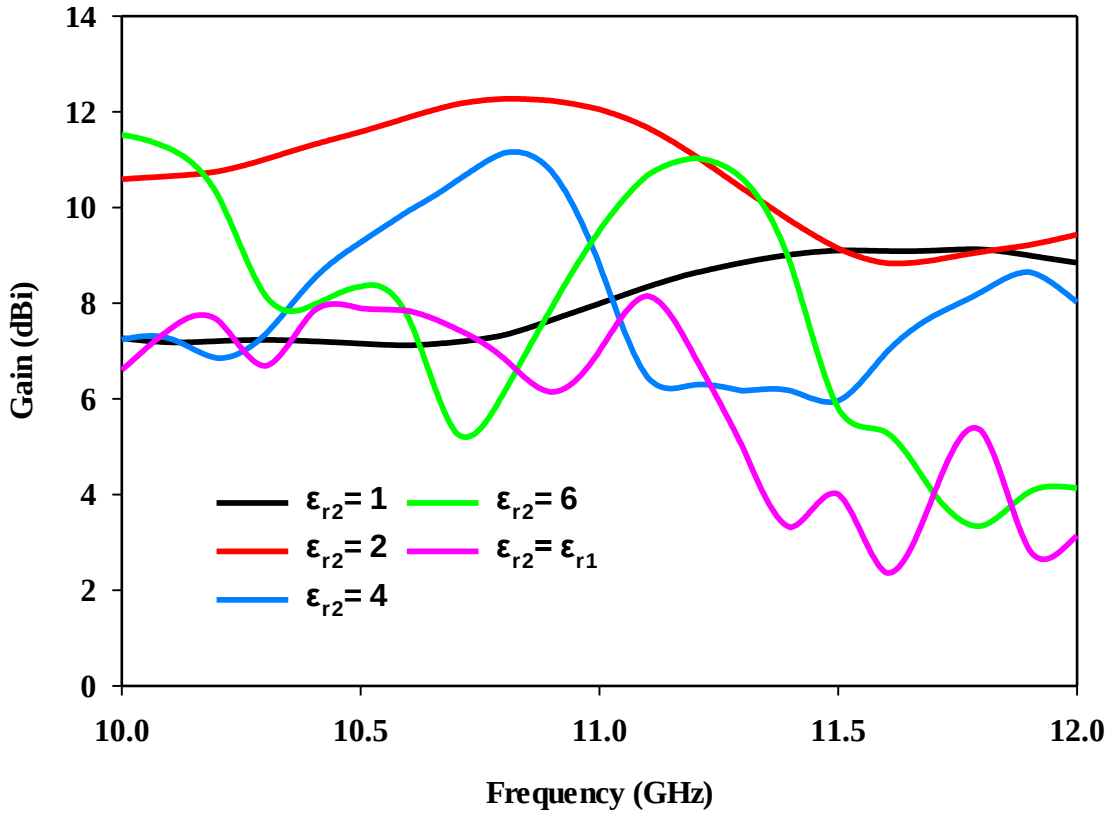

Figure 3.4: Gain of a layered rectangular DRA when ε_{r2}= 1, 2, 4, 6 and ε_{r2}= ε_{r1}.

3.2.3 Effects of the dielectric coat on the resonance modes

In order to demonstrate the effects of a dielectric coat on the performance, a rectangular DRA operates at multi-higher order modes of $TE_{11,11}$ has been considered with an outer layer that has a dielectric constant of ε_{r2}= 3.5 and a loss tangent of tanδ<0.0027. It is worth mentioning that, the lower relative permittivity of 3.5 has been chosen based on availability of material that can be utilized fabrication. The proposed antenna has been compared to a single layer DRA that has been simulated for a single, $TE_{11,11,}$ mode operation with the dimensions shown in Figure 3.5. Figure 3.6 illustrates the return losses, $|S_{11}|$, for the layered rectangular DRA, where it can be observed that adding the outer dielectric layer has improved the impedance bandwidth from 2.18% to ~12%, which is approximately by a factor of 6 times. Moreover, the dielectric coat provided a stronger physical support to the original antenna and reduced the height from 60 to 40mm. The magnetic field distribution inside the DRAs is illustrated in Figure 3.7. In the case of the 60mm height single layer DRA, only the $TE_{11,11}$ mode has been excited at 11.33GHz resulting in a gain of 10dBi. The separation distance between adjacent short magnetic dipoles is 13.25mm, which corresponds to more than $0.44\lambda_o$, hence overlapping between the magnetic dipoles has been eliminated

[23]. However, in the case of ε_{r2}=3.5, both of the $TE_{11,11}$ and $TE_{11,13}$ modes have been excited at 11.4GHz and 11.8GHz, respectively. The distance between the short magnetic dipoles is 6.4mm at the $TE_{11,11}$ at 11.4GHz, which corresponds to more than 0.44λg, which results in a slightly higher gain of 10.6dBi. In addition, when the DRA is surrounded by another dielectric medium, the maximum gain can be achieved when the adjacent magnetic dipoles are separated by a distance of ~0.4λ_g, where $\lambda_g = \lambda_0/\sqrt{\varepsilon_{r2}}$, which results in a lower profile and a more practical configuration. With reference to Figure 3.8, it can be noticed that at the absence of the dielectric coat, the $TE_{11,11}$ mode radiation pattern is slightly less directive than that of a layered DRA, which means the outer layer maintained a higher gain even with a lower profile. As mentioned earlier, increasing the spacing between the short magnetic dipoles results in higher gain and directivity, where the power will be forwarded to the main lobs than distributed to the side lobs.

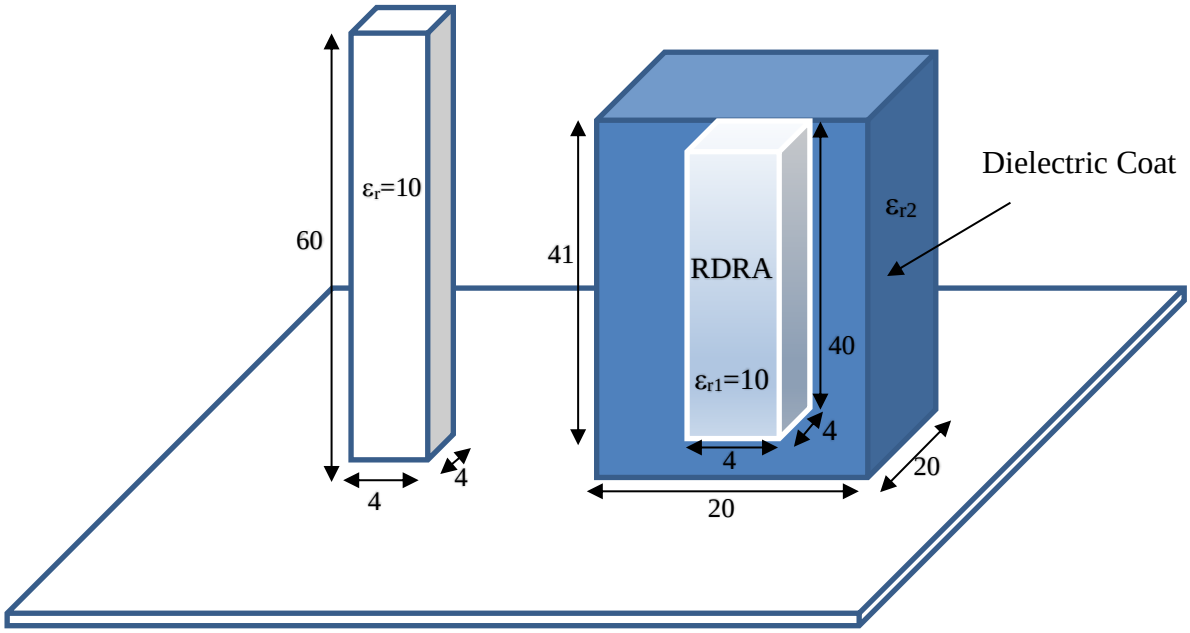

Figure 3.5: Configuration of the RDRA and layered RDRA with dimensions given in mm.

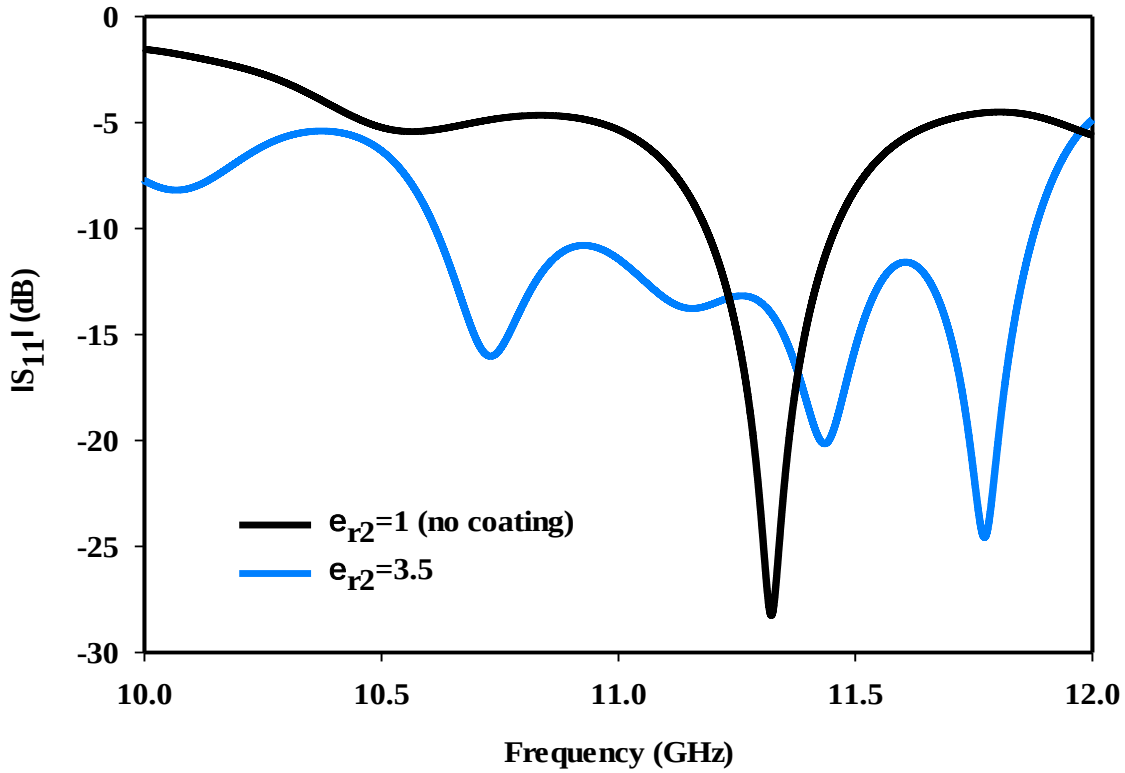

Figure 3.6: $|S_{11}|$ of a rectangular DRA excited in the $TE_{11,11}$ mode when ε_{r2}= 1 and ε_{r2}= 3.5.

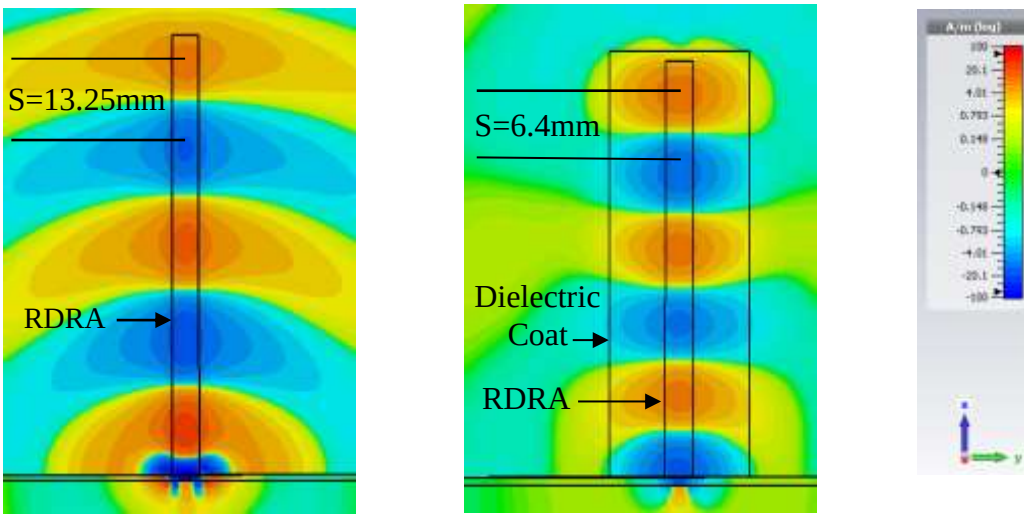

(a) (b)

Figure 3.7: Magnetic field of the $TE_{11,11}$ resonance mode when a) ε_{r2}= 1 and b) ε_{r2}=3.5.

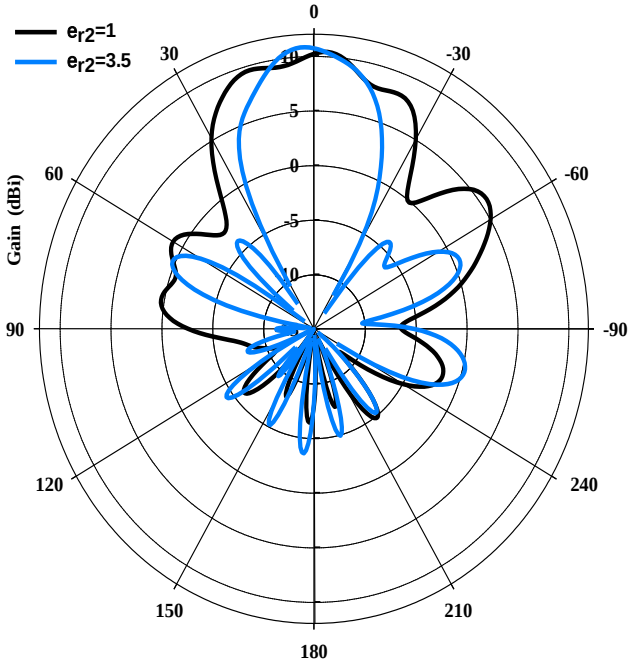

(a)

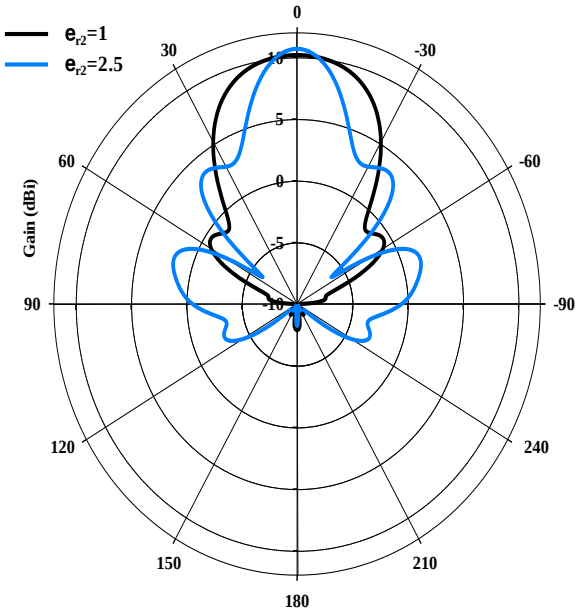

(b)

Figure 3.8: Radiation pattern of DRA operating in the $TE_{11,11}$ mode at 11.33 and 11.4 GHz when ε_{r2}= 1 and 3.5, respectively. a) E- Plane and b) H- Plane.

The impact of fabrication errors have been investigated by studying the resonance frequency variation for fabrication errors of 0.05 mm, 0.1 mm, and 0.2 mm. In each case the error has been added to the DRA element dimensions and the resonance frequency has been

monitored. At the absence of the dielectric coat, the RDRA height has been increased to 60mm in order to excite the $TE_{11,11}$ mode at 11.3GHz.

Table 3-2: Impact of fabrication errors on the resonance frequency shift (Δf) of the $TE_{11,11}$ mode operation with and without the dielectric coat.

Fabrication error (mm)	$TE_{11,11}$ mode (ε_{r2}=1)		$TE_{11,11}$ mode (ε_{r2}=3.5)
	CST Δf (%)	DWM Δf (%)	CST Δf (%)
0.05	1.1	1.06	0.24
0.1	2.18	2.12	0.48
0.2	4.23	4.16	0.97

Table 3-3: Comparison of the bandwidth and gain for rectangular DRAs

f_o (GHz)	Dielectric constant ε_r	Excitation technique	Bandwidth%	Gain dBi	Reference
11.3	10	Slot aperture	11.7	10.6	Proposed DRA
9.9	10.2	Slot aperture	30	6	[78]
14.8	10.8	Slot aperture	3	-	[113]
2.44	38	Probe	5.5	-	[64]
3.7	10	Slot aperture	32	2	[58]
11	10	Slot aperture	2	10	[23]
24	10	Slot aperture	5	9	[25]
17.3	10	Slot aperture	1.19	9.05	[26]
5.8	20	Microstrip line	6.4	2.4	[90]
15.2	10	Slot aperture	3	10	[114]
28	10	Modified structure	6.5	6.17	[51]
6.7	20	Microstrip line	5.8	8	[52]
5	10.8	Slot aperture	11.4	6.2	[59]
4.3	9.3	Spiral strip	12.5	5	[115]

As illustrated in Table 3-2, the impact of fabrication errors on the layered RDRA is considerably smaller than that of a single layer counterpart operates in the same resonance frequency. This can be attributed to the fact that for the layered DRA, the dimensions variation is taking place in the vicinity of reduced wave reflections at the DRA surface compared to the case of a single layer DRA. Therefore, the fabrication tolerance has been improved at the presence of a dielectric coat. Finally a comparison between the performance of the proposed layered rectangular DRA and that of reported DRAs in the literature is shown in Table 3-2 in terms of bandwidth and gain.

3.4. Effect of Outer Layer on Single-Higher Order Mode RDRAs

In this section, a rectangular DRA the supports TE_{119} single-higher order mode will be investigated, it is worth noting that, the proposed antenna dimensions has already used in Chapter two and illustrated in Table 2-2. The proposed antenna coated by dielectric coat has permittivity of 3.5 with dimensions of $20 \times 20 \times 25$ mm^3. With reference to the Figure 3.9, TE_{119} modes has been generated 11.1GHz with respective impedance bandwidth of 5% respectively in conjunction with 9.55 dBi as illustrated Figure 3.10.

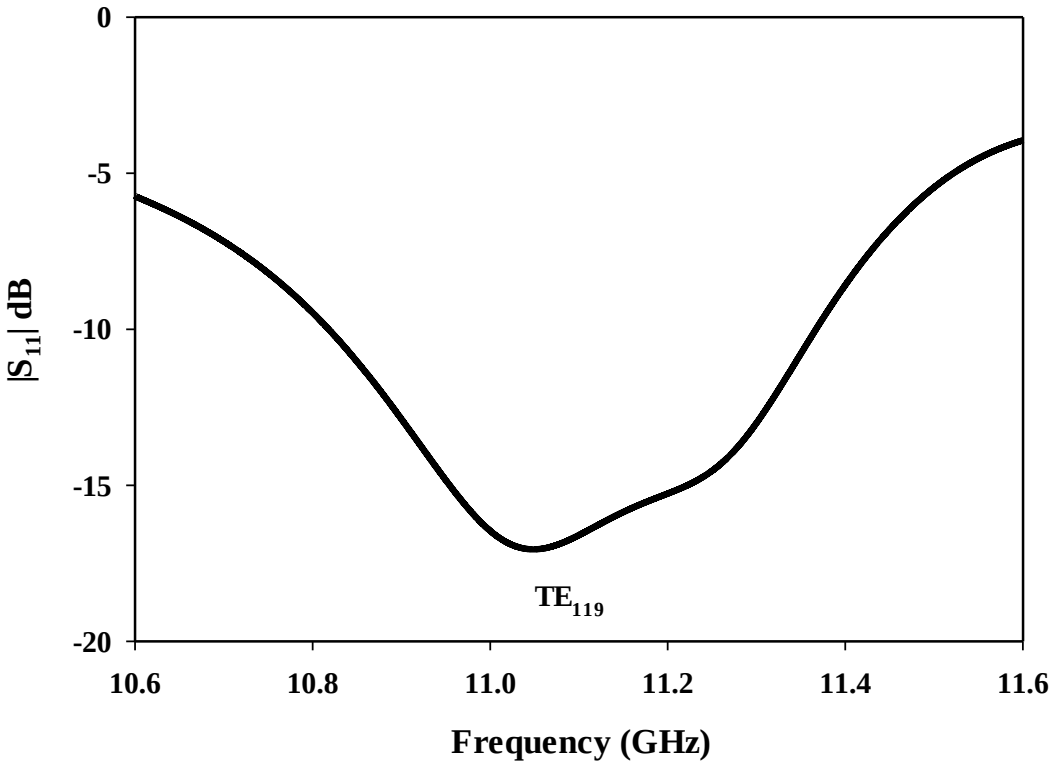

Figure 3.9: $|S_{11}|$ of layered single higher order modes supporting the TE_{119}.

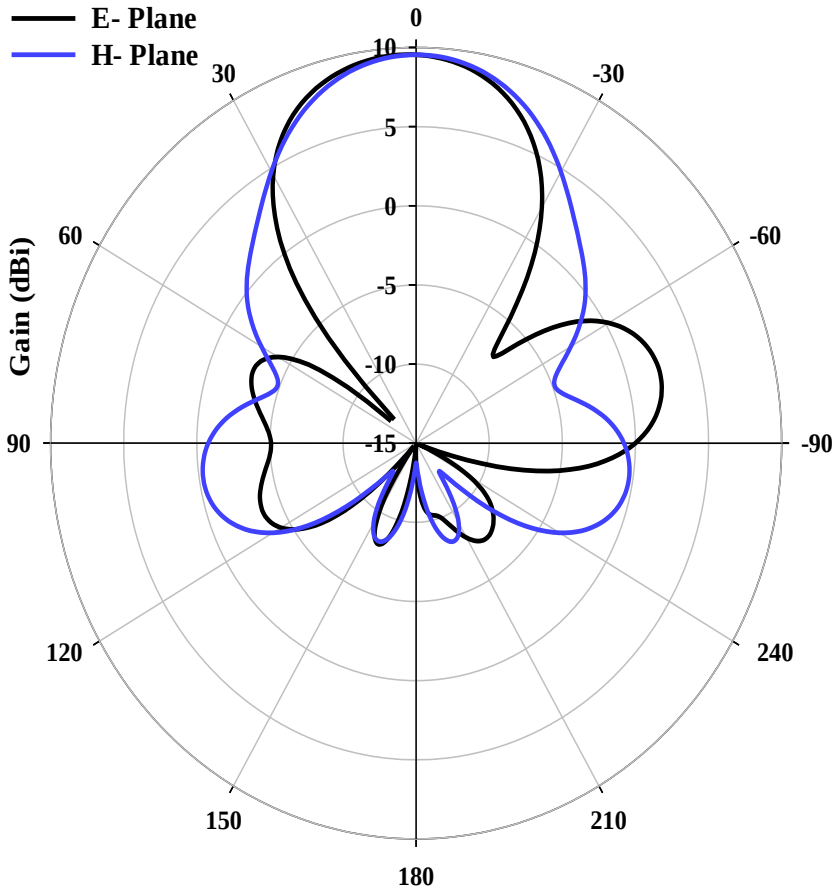

Figure 3.10: Far-field radiation patterns single higher order mode TE_{119} layered DRA at 11.1 GHz.

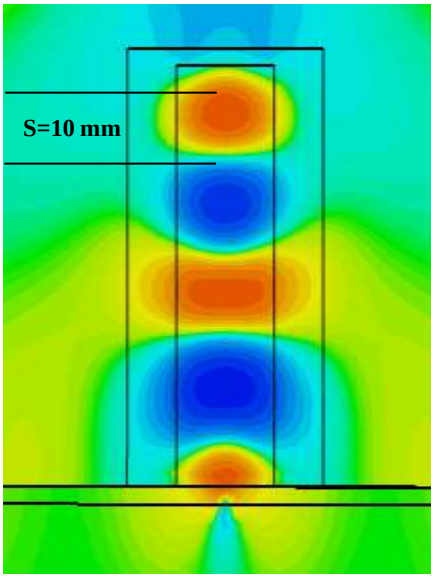

Figure 3.11: Hx-field distributions within the single higher order mode TE_{119} layered DRA at 11.1 GHz

Again, the overlap between short magnetic dipoles took place as seen in Figure 3.11 where the higher-order mode operation is clearly visible and the distance between short magnetic dipoles is 10 mm corresponding to 0.37 λ_g, which is considered less than 0.4 λ_g. The impedance BW improved slightly compared to the single layer, where 3.7% BW has been achieved, this is because no nearby modes to combine with. Furthermore, the overlapping between short magnetic diploes resulting lower gain than multi higher order mode as seen in section 3.2. These results demonstrated that using layered RDRA approach cannot support single higher order mode.

3.5 Layered RDRA Operating in the TE_{313} and TE_{315} Modes

For a DRA that works in the TE_{313} and TE_{315} modes, the required dimensions are 19×5×5 mm^3 coated by dielectric coated that has permittivity of 3.5 and dimensions of 30×30×6 mm^3. Once more, an *x*-directed slot has been placed in the ground plane with respective length and width of 6 and 1 mm, an open stub length of 4mm.

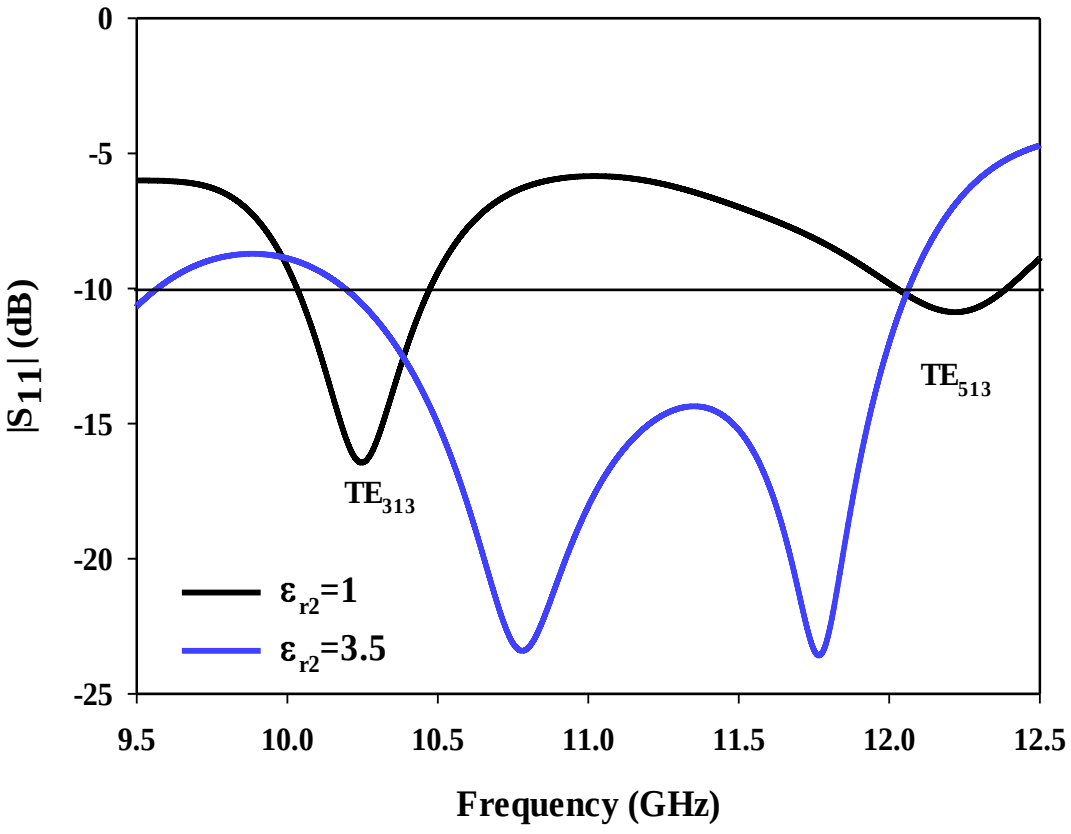

Figure 3.12: Simulated return loss of TE_{313} and TE_{513} modes with and without dielectric coat.

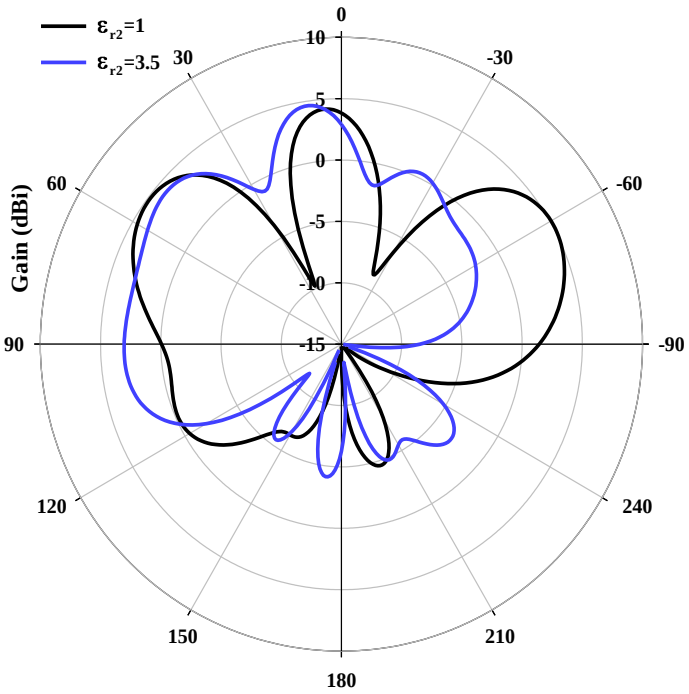

(a)

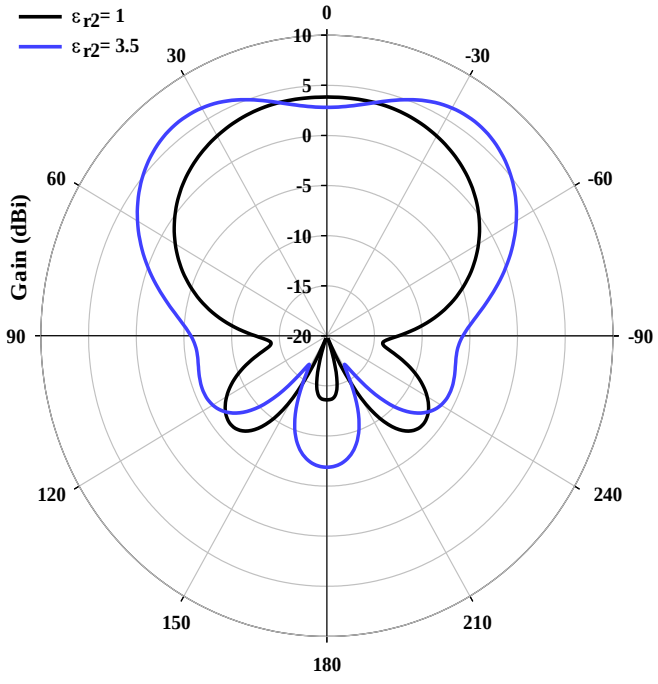

(b)

Figure 3.13: far field radiation pattern for a layered RDRA supporting the TE_{315} mode at 12.11 and 11.7 GHz when ε_{r2}= 1 and 3.5 (a) $\phi=0^0$ (b) $\phi=90^0$.

Figure 3.12 presents the reflection coefficient of proposed design. As it can be seen, at absence of outer layer dual resonances are clearly discernible 10.25 and 12.11 GHz with respective impedance BW 4.29% and 3% for TE_{313} and TE_{315} respectively. Once the outer layer took place, both of modes merged together to form wide impedance bandwidth up to 16.7 % from 10.2 to 12.1 GHz. In addition, a gain of 5.6 dBi has been achieved when the RDRA stand alone. However, a slight improvement of gain noted when outer layer incorporated 6.42 dBi as seen in Figure 3.13.

3.3 Experimental Results

3.3.1 Linearly Polarized Higher Order Mode layered DRA

In order to demonstrate the potential of a layered rectangular DRA, measurements have been implemented using commercial materials for the inner and outer layers. Figure 3.14 illustrates the proposed two-layer rectangular DRA and feed network configuration. The proposed antenna inside the anechoic chamber is illustrated in Figure 3.15. The inner layer represents the actual DRA element that has been fabricated using Alumina with a dielectric constant of 10 and a loss tangent of less than 0.002. The DRA dimensions have been chosen as l_1=w_1=4mm and h_1=40mm. The second layer has been fabricated by utilizing 3D printing technology of a Polyamide layer with a dielectric constant of 3.5 and a loss tangent of less than 0.0027. The optimized dielectric coat dimensions have been determined as l_2=w_2=20mm and h_2=41mm. h_2 value has been chosen in order to ensure fully protection to the inner layer. It should be noted that a central air-gap tunnel has been created in the outer layer to accommodate the DRA. The resonance frequencies of the DRA modes have been determined using the dielectric wave guide model [24] and CST Eigen mode solver [103] for the single and two layer DRAs, respectively. The layered DRA has been placed on a 150×100mm^2 ground plane and excited using a 50Ω microstrip-feed line through a 6 ×1 mm^2 slot aperture that has been etched on a Rogers RO4350 substrate with dielectric constant of 3.48 and a loss tangent of 0.0037. Furthermore, the reflection coefficient has been measured using an E5071C vector network analyzer, whereas radiation patterns and gain have been measured using an NSI near field system.

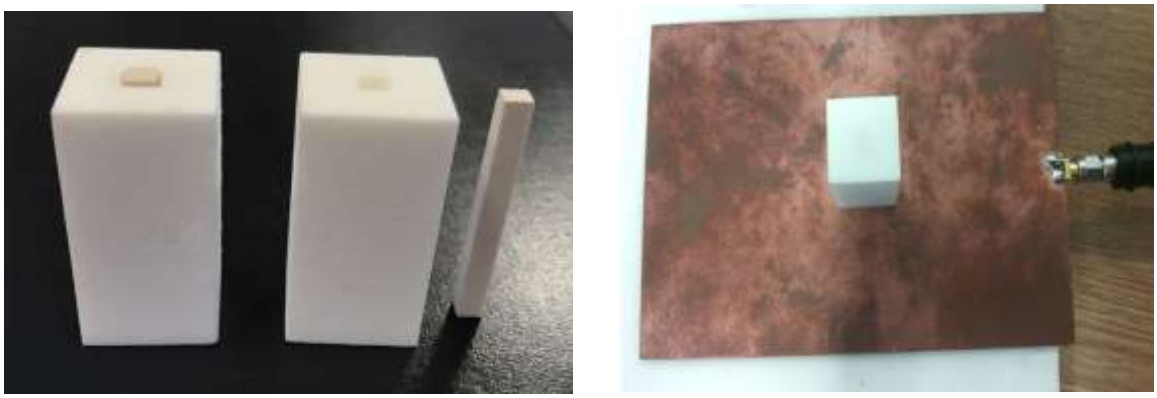

(a) (b)

Figure 3.14: a) The outer dielectric coat and original rectangular DRA before and after assembly, b) Photographs of layered RDRA on the ground plane.

Figure 3.15: Layered rectangular DRA inside the anechoic chamber.

Figure 3.16 presents the reflection coefficients and gain of the layered DRA with a close agreement between simulated and measured impedance bandwidths of ~11.6% and ~11.8%, respectively. However, a slight gain drops to ~9.5dBi can be observed in the measured results compared to a maximum simulated gain of 10.4dBi, which may be attributed to experimental errors as well as the existence of un-eliminated air-gap spots between the DRA and the dielectric coat. In addition, these results demonstrate that the layered DRA supports a multi-mode operation, which also contributes to the bandwidth and gain enhancement.

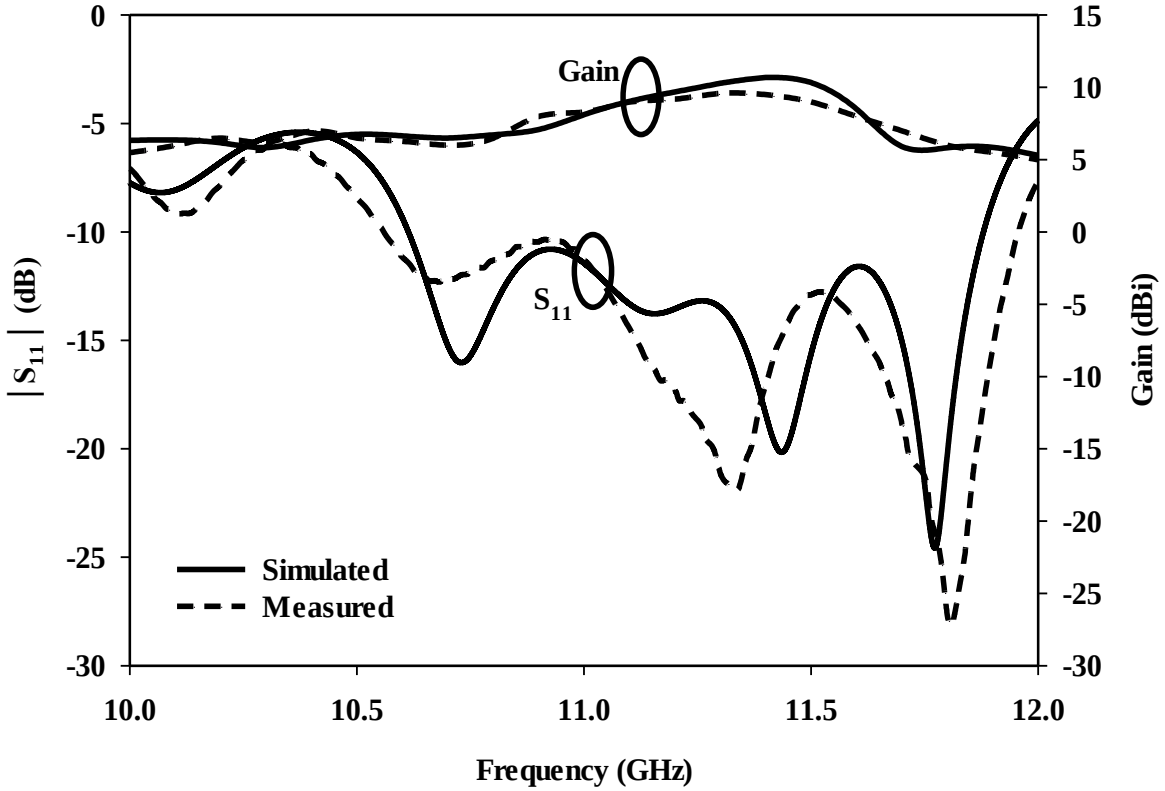

Figure 3.16: Reflection coefficient and gain of a layered RDRA operates in multi-higher order modes.

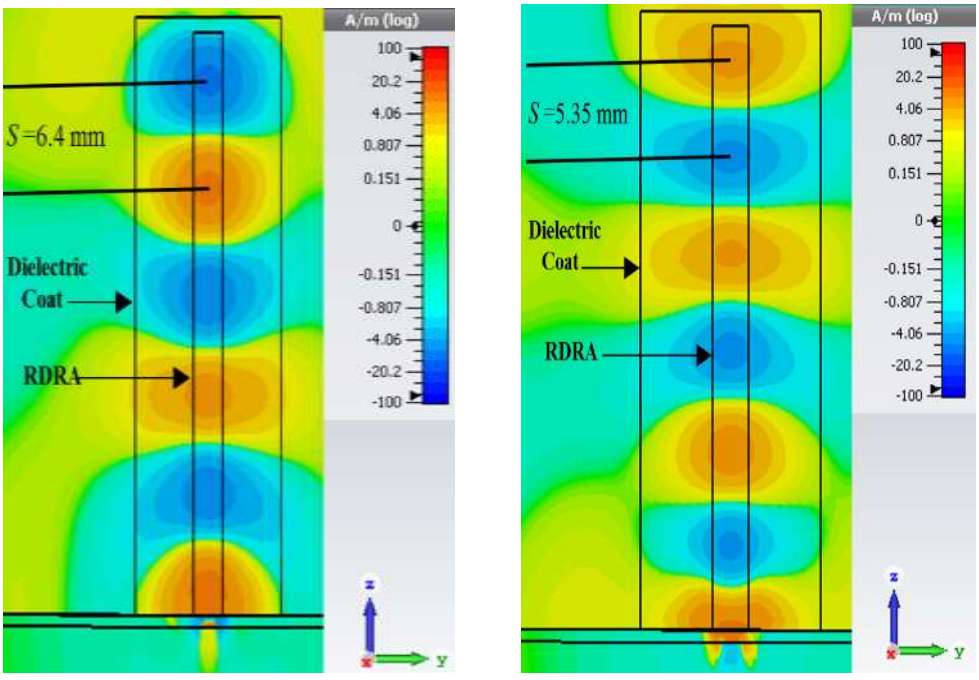

(a) (b)

Figure 3.17: Magnetic fields of a layered DRA operates in two resonance modes; (a) $TE_{11,11}$ (b) $TE_{11,13}$.

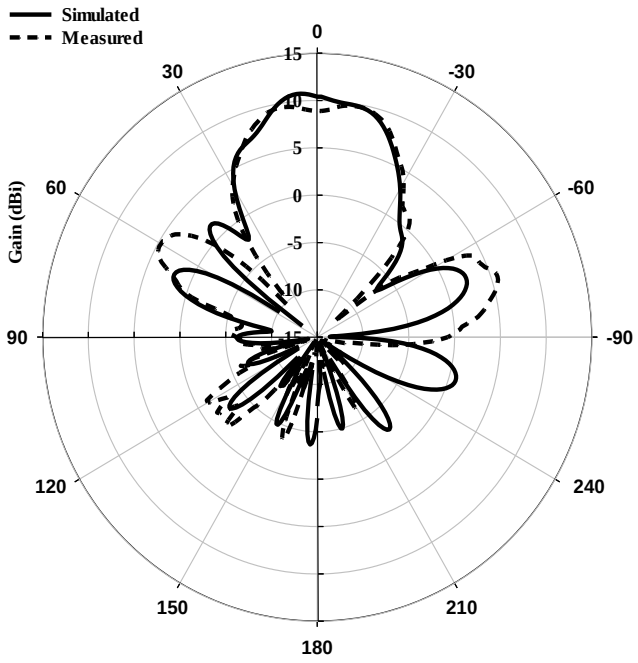

(a)

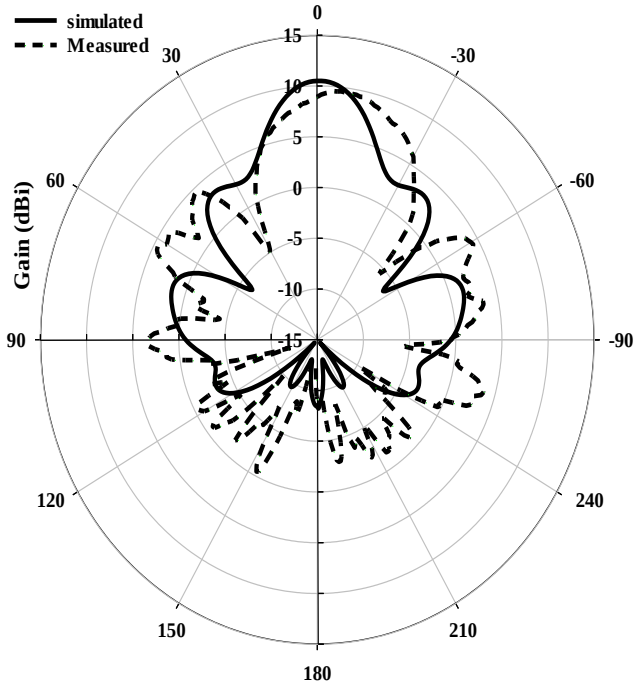

(b)

Figure 3.18: Radiation patterns of a layered DRA operating in the $TE_{11,11}$ mode at 11.3GHz; a) E- Plane and b) H- Plane.

Figure 3.17 presented the magnetic field distribution inside the layered DRAs, where it can be noted that by adding the dielectric coat, the $TE_{11,11}$ and $TE_{11,13}$ resonance modes have been excited at 11.3 and 11.7GHz, respectively. As mentioned in Chapter 2, for a single layer configuration, the DRA height needs to be increased to 50, 60 and 70mm in order to

excite the TE_{119}, $TE_{11,11}$ and $TE_{11,13}$ modes, respectively. As illustrated in Figure 3.17, the distance between adjacent short magnetic dipoles is S=6.4mm for the $TE_{11,11}$ mode, which corresponds to more than $0.44\lambda_g$ at 11.3GHz. As a result, a higher gain of 10.4dBi has been achieved at this frequency. However, it can also be observed that for the $TE_{11,13}$ mode, the separation distance is 5.35mm, which corresponds to less than $0.44\lambda_g$ at 11.8GHz, hence a lower broadside gain of ~6dBi has been achieved at this frequency point. Figure 3.18 illustrates the measured and simulated radiation patterns of the layered DRA at 11.3GHz with reasonable agreement.

3.6. Circularly Polarized Higher Order Mode layered RDRA

3.6.1 Single Layer Circularly Polarized Higher Order Mode RDRA

A comparison between three RDRA's of different heights with fixed width and length that support circular polarization will be implemented. It has been demonstrated that a RDRA having a lower height and operating at a lower order mode offers a reduced gain [24]. More importantly, the DRA heights have been increased in order to fulfil the requirement of separating the magnetic fields maxima by a spacing of $0.4\lambda_o$ [23]. To demonstrate this concept three rectangular DRAs, all with ε_r=10, have been considered at the higher order modes of TE_{115}, $TE_{117,}$ $TE_{119,}$ over a frequency range of 10 to 12GHz. The DRA dimensions are listed in Table 2-4. With reference to the table, using higher order mode for circular polarization can enhance only the RDRA gain. However, the impedance and axial ratio bandwidths have not been improved.

Table 3-4: Comparison between the BW, AR and gains of multi-higher order mode RDRAs at 11.4GHz.

Resonance Mode	RDRA dimensions $l \times w \times h$ (mm^3)	Volume lwh (mm^3)	w/h	BW %	AR %	Gain (dBi)
TE_{115}	4×4×30	480	0.13	2.9	2.5	7
TE_{117}	4×4×40	640	0.1	2.8	2.4	7.5
TE_{119}	4×4×50	800	0.08	2.6	2	8.5

The fabricated DRA supports the multi-mode of TE_{117} and TE_{119} at 11.2, 12.1 GHz has been placed on unequal arms cross slot with length of 4.4mm and 5mm, width of 1mm. the prototype of rectangular DRA and its feed network illustrated in Figure 3.19. The simulated and measured reflection coefficients are presented in Figure 3.20, with respective impedance bandwidths of 1.9% and 1.8%. The measured resonance frequency is 11.2GHz, which agrees well with the simulated counterpart. It is worth pointing that the TE_{119} mode exists at 12.1 GHz, However. It was not exited. The broadside simulated and measured gain are depicted in Figure 3.21, where a good agreement with simulated and measured results of ~7.5dBic at 11.2GHz. With reference to the Figure 3.22, a reasonable agreement has been achieved between the measured and simulated radiation patterns of a single layer rectangular DRA at 11.3GHz, where it can be noticed that the EL components are greater than ER counterparts by ~10dB. The simulated and measured axial ratios are depicted in Figure 3.23 , the simulated circular polarization bandwidth extends from 11.1 to 11.37 GHZ, which corresponds to a 3-dB axial ratio bandwidth of 2.4% that agrees well with a measured bandwidth of 2.3% over a frequency range of 11.1 to 11.4GHz.

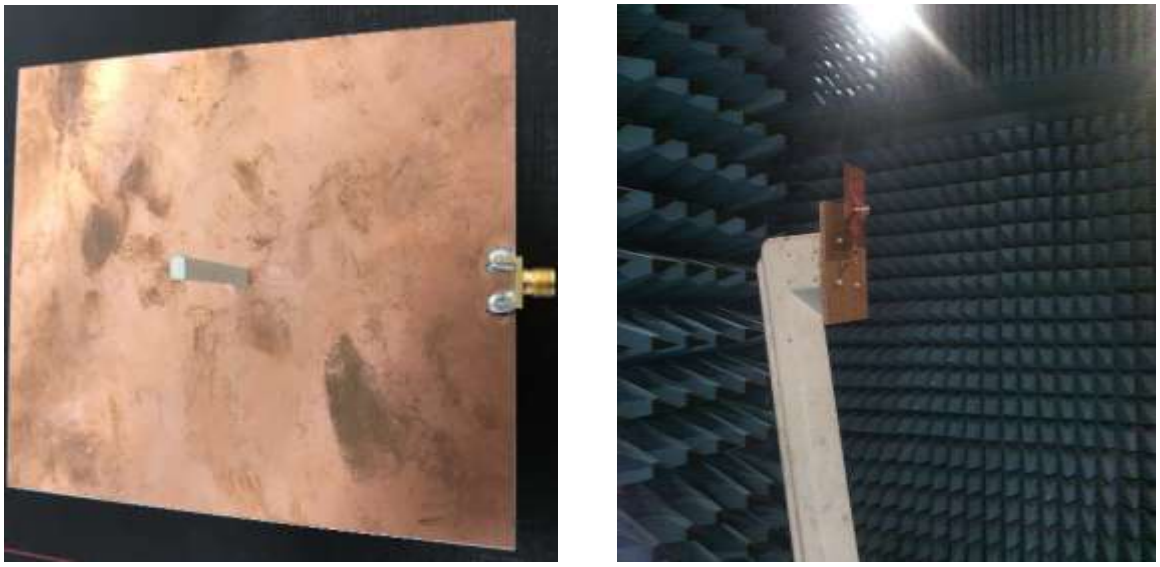

(a) (b)

Figure 3.19: Photographs of RDRA a) on the ground plane b) inside the anechoic chamber

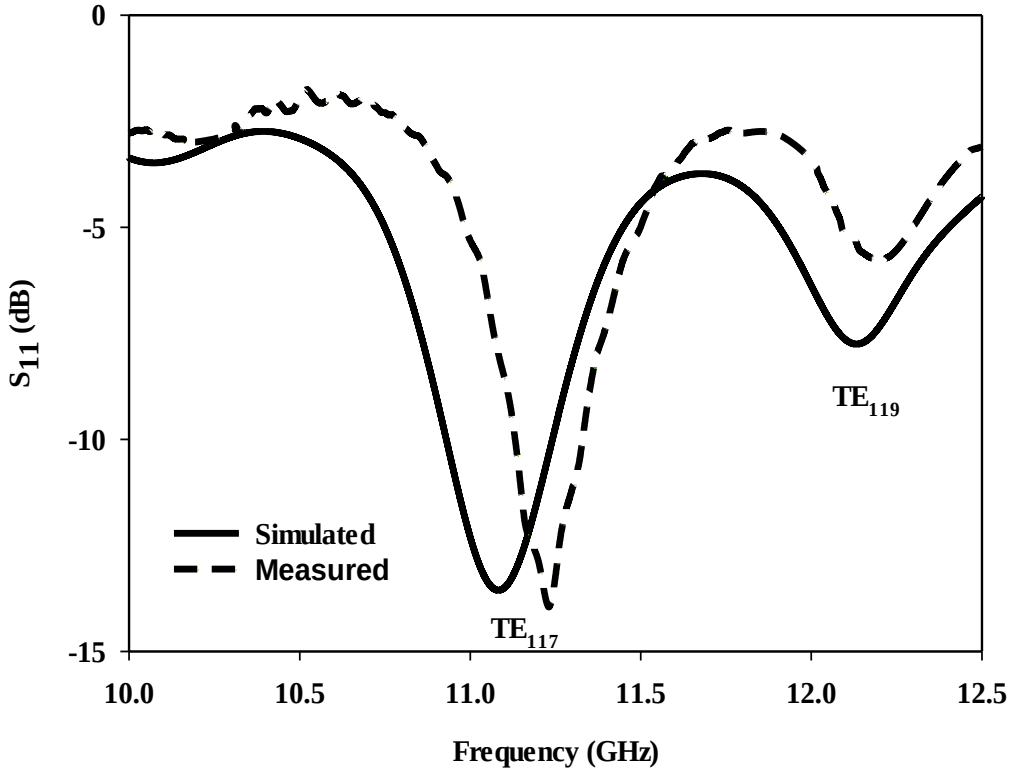

Figure 3.20: Reflection coefficient of a multi-mode RDRA operating in the TE_{117} and TE_{119} mode.

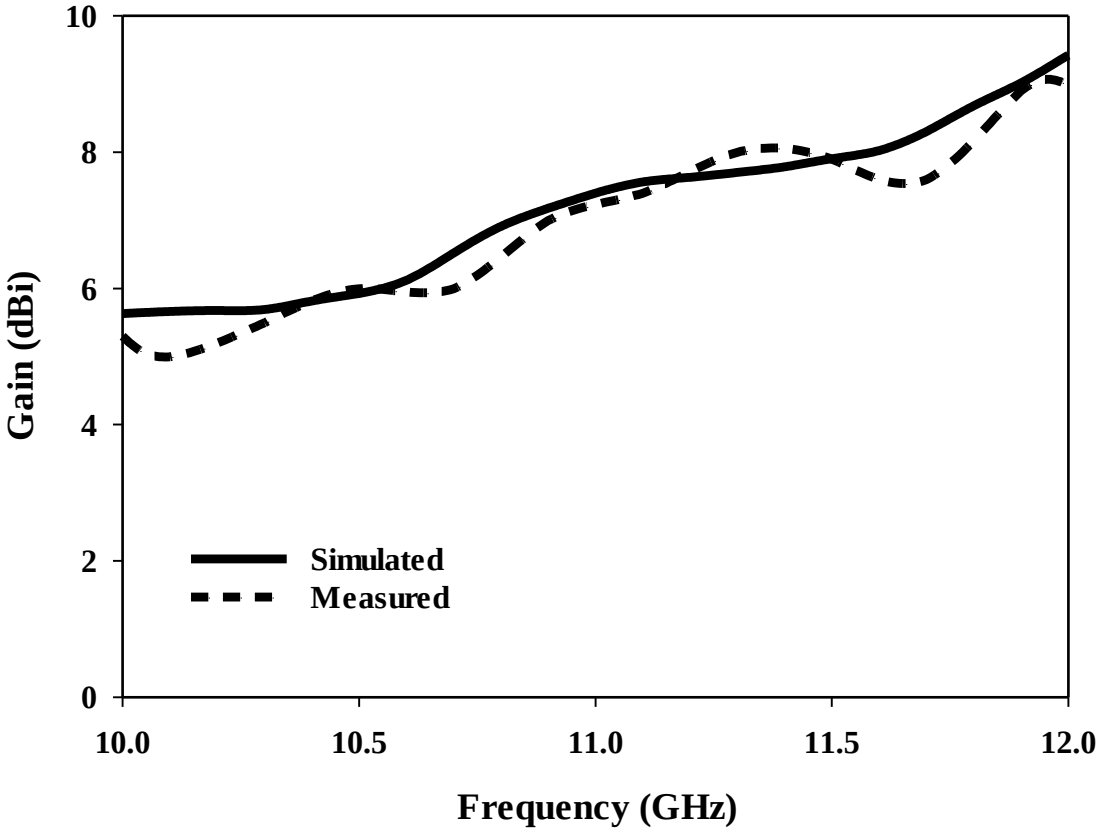

Figure 3.21: Simulated and measured Gain of a single-layer higher-order-mode DRA.

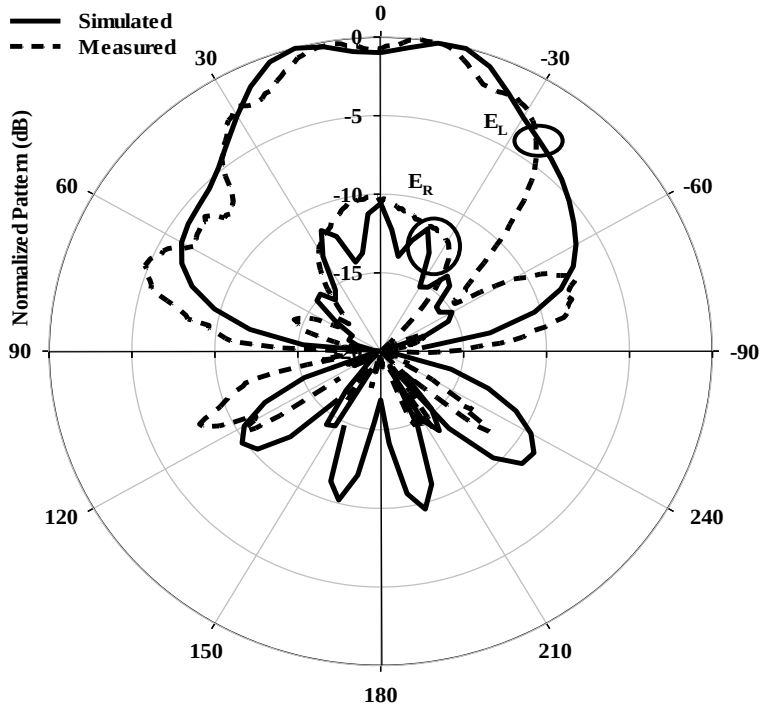

(a)

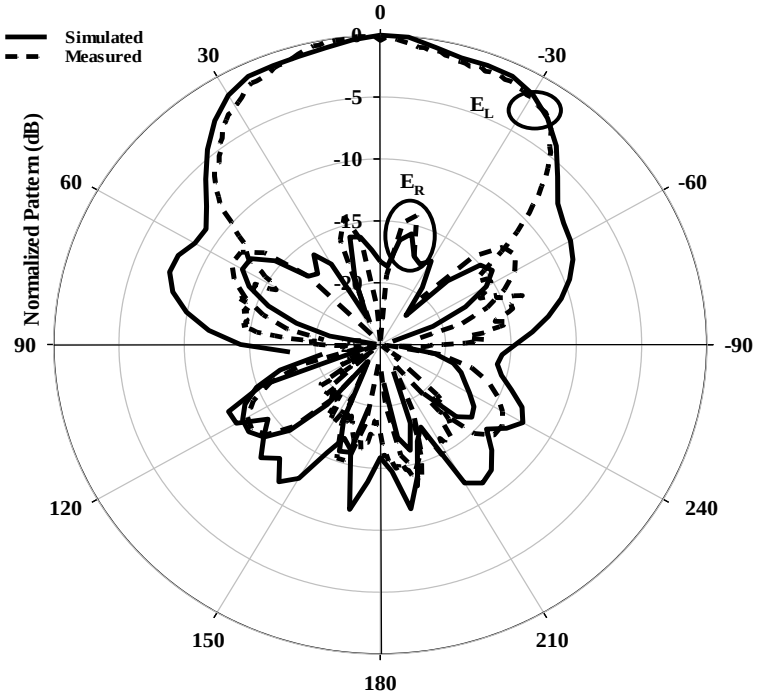

(b)

Figure 3.22: Radiation patterns of a multi-mode DRA excited in the TE_{117} mode at 11.3GHz a) ϕ=0 b) ϕ=90.

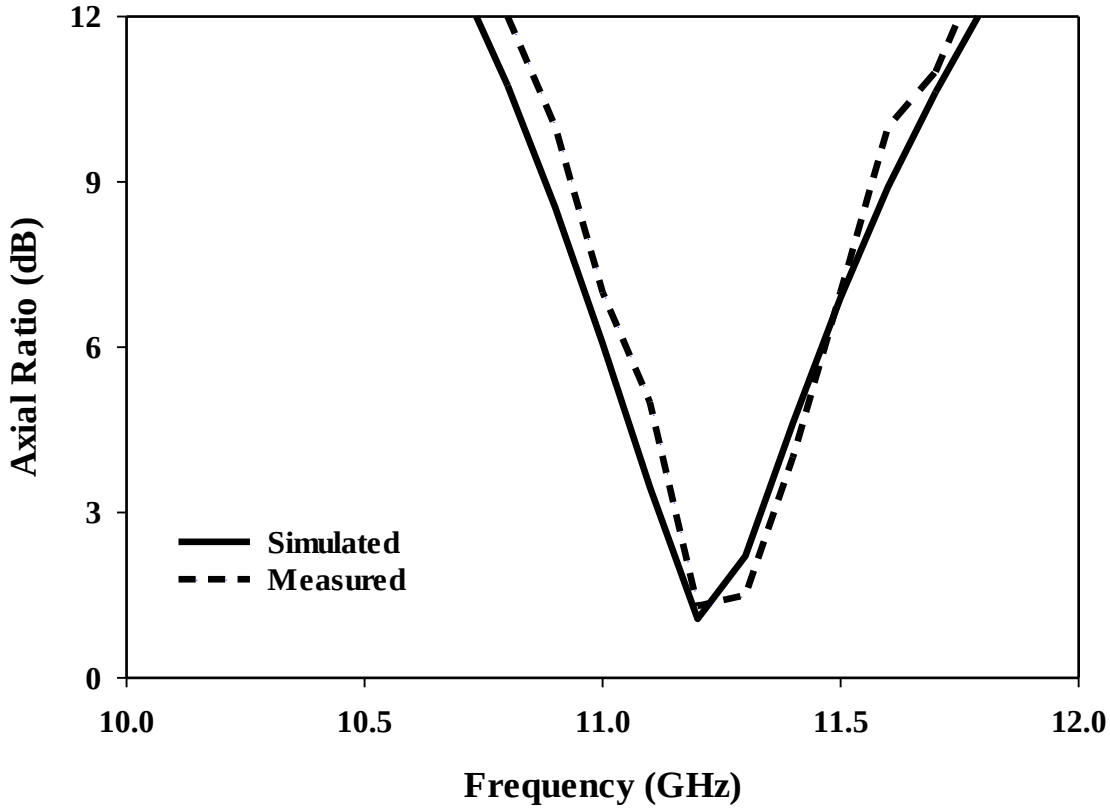

Figure 3.23: Simulated and measured axial ratios of higher order multi-mode TE_{117} DRA.

3.6.2 Two-layer Circularly Polarized Higher Order Mode RDRA

In this section, single and layered circularly polarized RDRAs will be investigated experimentally. Figure 3.24 illustrates the proposed layered RDRA configuration and its feed network, where a cross slot has been employed to excite the antenna [61, 84]. The rectangular DRA of the last section has been re-used in this experiment. Additionally, unequal slot lengths have been used in order to excite two near-degenerate orthogonal modes of equal amplitude and 90^0 phase difference that are needed to generate the CP radiation [84]. The coupling cross slot element lengths have the same width of $w_{s1} = w_{s2}$=1mm and unequal lengths of l_{s1}=4.4mm and l_{s2}=5mm. In addition, an open stub length of l_{stub}=2.5mm has been utilized for optimum matching. Furthermore, a double sided adhesive copper tape has been employed to eliminate the potential air-gaps between the DRA and ground plane [116]. The reflection coefficient has been measured using an E5071C vector network analyser, whereas the radiation patterns and gain have been measured using an NSI system.

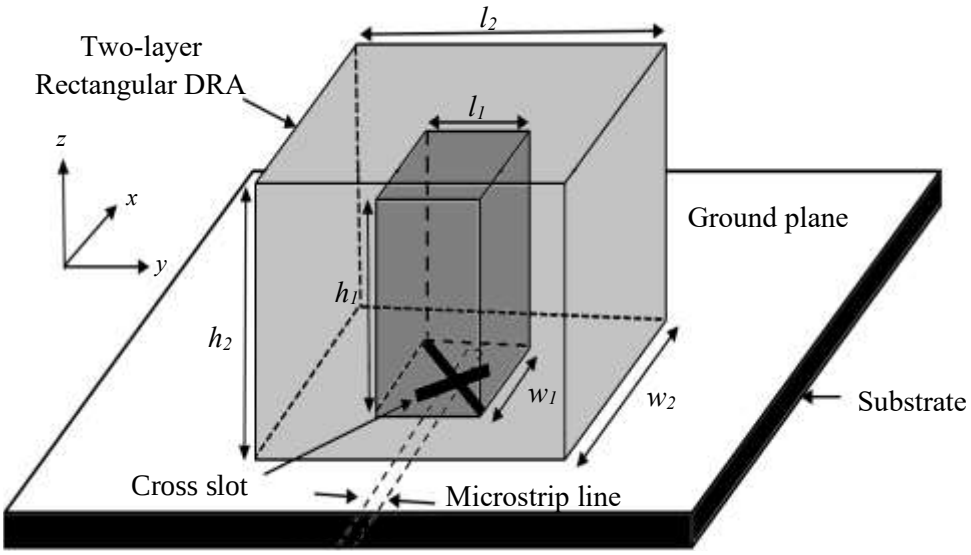

(a)

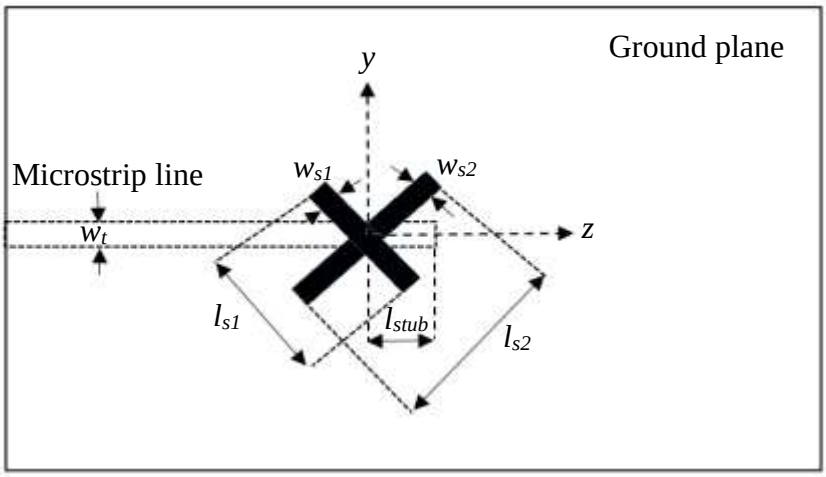

(b)

Figure 3.24: Geometry of the configuration (a) Layered rectangular DRA (b) Top view of the feed network.

A prototype of a two-layer DRA has been fabricated and measured in order to demonstrate the potential of such antenna. The magnetic field distribution inside the DRA is illustrated in Figure 3.25 , where it can be observed that the separation distance between adjacent short magnetic dipoles (S) is 6.6mm for the $TE_{11,11}$ mode at 11.3GHz, which exceeds 0.44λg. Therefore, a higher gain of 11.1dBic has been achieved at this frequency point. Similarly, it can be noted that for the $TE_{11,13}$ mode, the separation distance is 5.6mm, which corresponds to less than ~0.4λ_g at 12GHz, hence a lower broadside gain of ~7.6dBic has been achieved at this frequency. Figure 3.26 presents the reflection coefficient of the layered

DRA with a close agreement between simulated and measured bandwidths of ~21% and ~18.5%, respectively. This represents a significant bandwidth enhancement compared to that of a single layer DRA. In addition, it is evident from these results that the layered DRA supports a multi-mode operation where the $TE_{11,11}$ and $TE_{11,13}$ modes have been excited at 11.3 and 12GHz, respectively, which also contributes to the bandwidth enhancement.

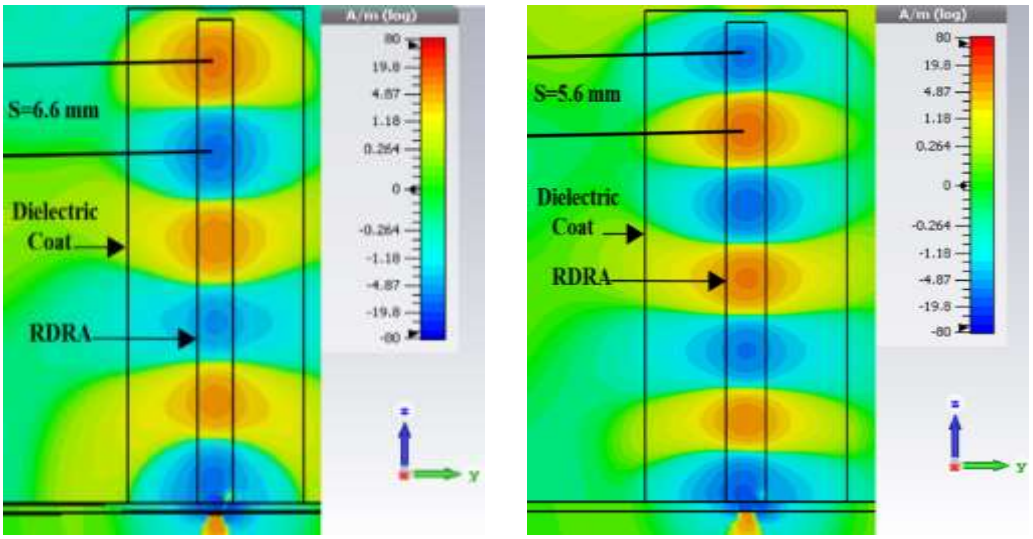

(a) (b)

Figure 3.25: Magnetic field distribution inside the layered DRA that operates in the (a) $TE_{11,11}$ at 11.3 GHz (b) $TE_{11,13}$ at 12 GHz resonance modes.

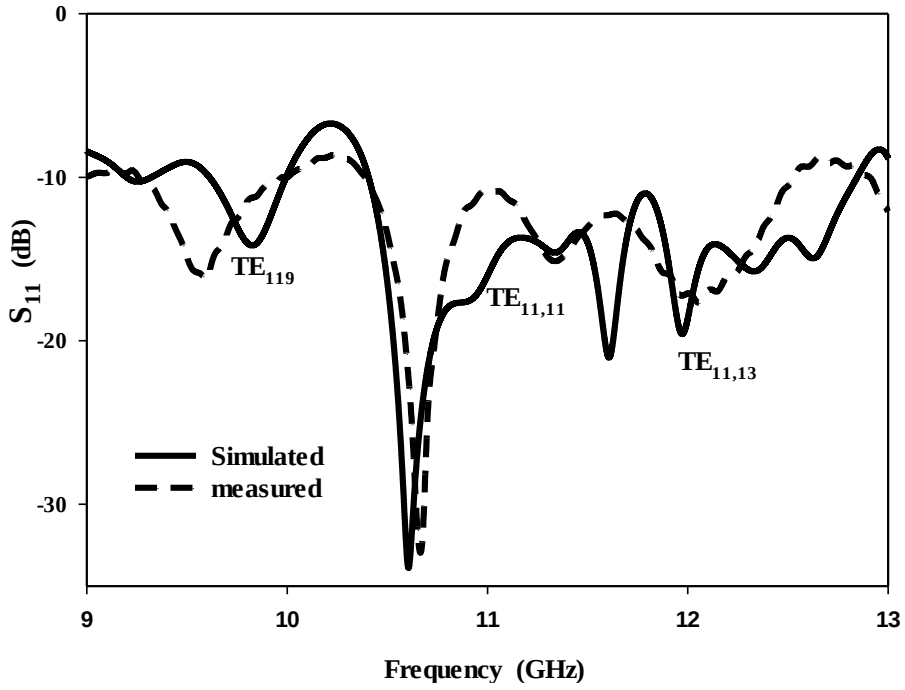

Figure 3.26: Reflection coefficient of a circularly polarized layered RDRA operating in multi-higher order modes.

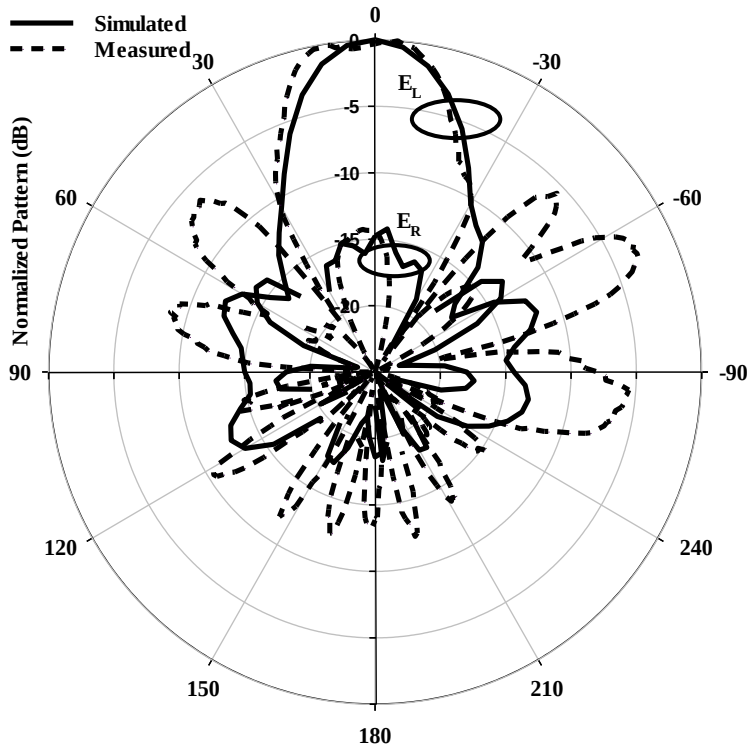

(a)

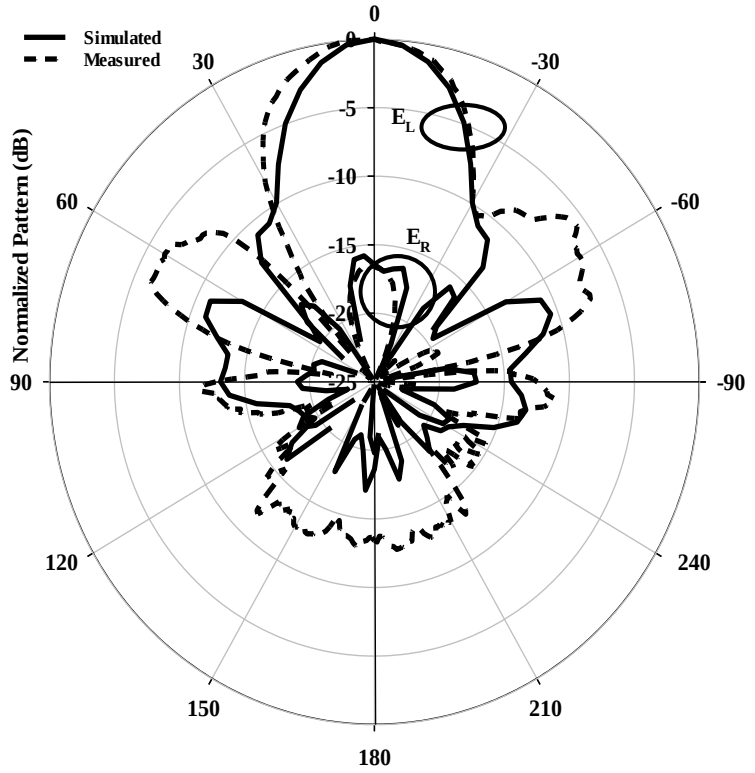

(b)

Figure 3.27: Radiation patterns of a circularly polarized layered DRA excited in the $TE_{11,11}$ mode at 11.3 GHz a) ϕ=0 b) ϕ=90.

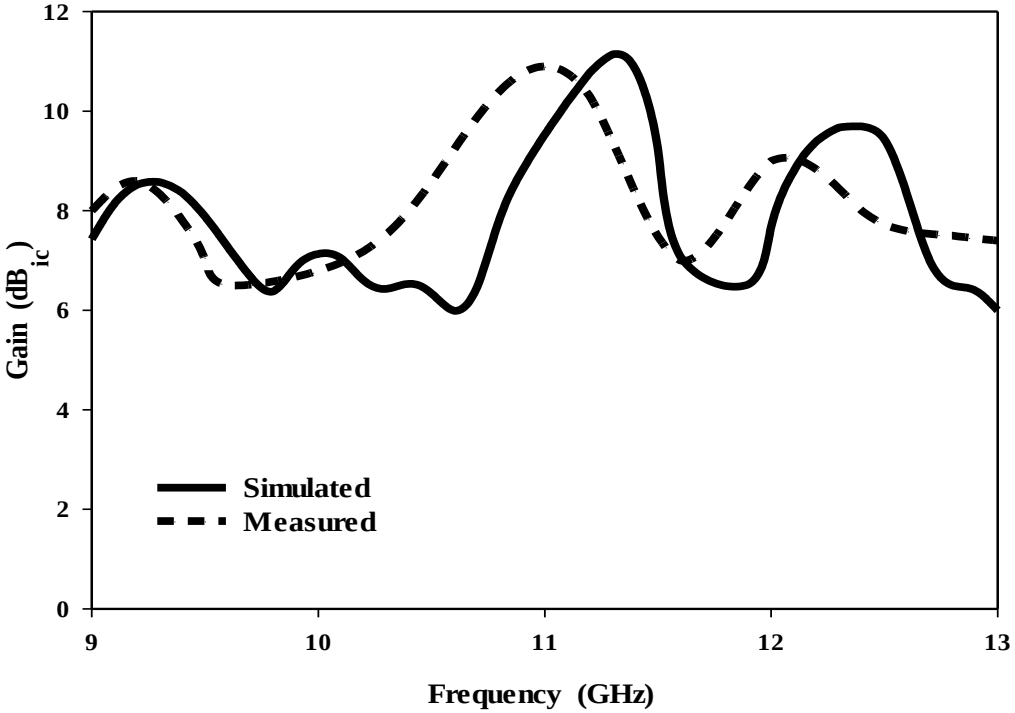

Figure 3.28: Gain for a circularly polarized higher order mode layered RDRA.

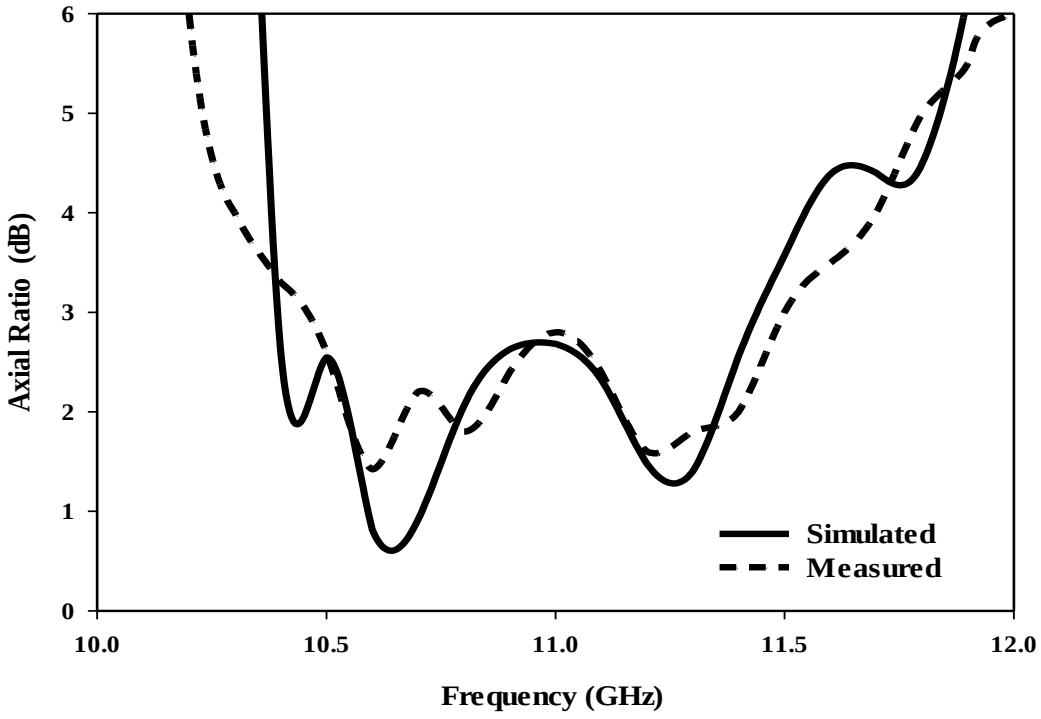

Figure 3.29: Axial ratio of a circularly polarized higher order mode layered RDRA.

Figure 3.27 illustrates a reasonable agreement between the measured and simulated radiation patterns of the layered DRA at 11.3GHz, where it can be noticed that a left-hand CP radiation has been achieved since the E_L field component is greater than the E_R component by 15dB. It is worth mentioning that a left-hand circular polarization sense, LHCP, has been achieved

due to the fact that the length of the l_{s2} arm of the cross slot is shorter than l_{s1} as demonstrated in Figure 3.24 (b). Similarly, right-hand circular polarization, RHCP, can be achieved by swapping the cross-slot arms so that l_{s1} is longer. The measured and simulated gains are presented in Figure 3.28 with close agreement. However, a slight drop in the measured gain to ~10.6dBic can be observed compared to a maximum simulated gain of 11.1dBic, which may be attributed to experimental errors as well as the existence of un-eliminated air-gaps spots between the DRA and the dielectric coat. In addition, the permittivity of the dielectric coat could have been slightly altered during the 3D printing process, which may contribute to this discrepancy. The simulated and measured axial ratio of the layered DRA are depicted in Figure 3.29, where it can be observed that a circularly polarized radiation has been achieved over a frequency range of 10.4 to 11.44GHz, which corresponds to a 3-dB axial ratio bandwidth of 9.5% compared to a measured counterpart of 9.1%. It is worth mentioning that the length of the slots has been altered slightly to l_{s1}=4 mm and l_{s2}=5.6 mm in order to achieve a wider CP bandwidth.

3.7 Conclusions

Higher order mode linearly and circularly polarized layered RDRAs have been considered theoretically and experimentally, where a dielectric coat has been incorporated in the configuration. As expected, the inclusion of a dielectric coat improved the impedance bandwidth and gain in combination with lower DRA profile as well as a minimized impact of fabrication errors. For example, a two-layer linearly polarized RDRA operating in the $TE_{11,11}$ mode offers impedance bandwidth of ~12% compared to 2.18% for a DRA working at TE_{117} the absence of the outer layer. Moreover, for circular polarization, the inclusion of a dielectric coat increases the impedance bandwidth considerably. This is combined with a significant enhancement in the far field radiation characteristics such as axial ratio bandwidth and gain. For instance, a two-layer RDRA operating in the $TE_{11,11}$ mode offers respective impedance and axial ratio bandwidths of ~21% and 9.5%. Additionally, the $TE_{11,11}$ mode provided a higher gain of 11.1dBic compared to 7.5dBic for the single layer DRA operating in the TE_{117} mode, which also offers narrower impedance and circular polarization bandwidths. Furthermore, the presence of the second layer provides a stronger physical support to the original RDRA since a long and thin ceramic DRA can be fragile. Furthermore, a close agreement has been achieved between the measured and simulated results for layered

rectangular DRAs. Furthermore, the simulated results demonstrated that, the dielectric coat is not suitable for rectangular DRAs that have dimension supports single higher order modes because the overlapping took place resulting no enhancement of gain as well as there is no adjacent modes close to each other for bandwidth enhancement. Although the DRA has been designed at the X frequency band, the demonstrated high gain and wide bandwidths represent appealing radiation characteristics for applications in the mm-wave and Terahertz higher frequency bands.

Chapter 4

Higher Order Mode Layered Cylindrical Dielectric Resonator Antenna

4.1 Introduction

A cylindrical DRA is one of three regular geometries that have been used throughout this study since it offers a useful design flexibility in terms of structure simplicity compared to hemispherical and rectangular counterparts. In this Chapter, a cylindrical DRA that operates in a higher order mode is considered. Similar to the layered rectangular DRA discussed earlier, the proposed antenna consists of two dielectric layers having different radii and dielectric constants. Once again, the outer layer has a lower permittivity, which is less than half that of the inner layer. Moreover, the inner and outer layers have been chosen based on commercially available materials, where a ceramic Alumina, with ε_r=10, has been chosen to fabricate the DRA while the outer layer has been fabricated with the aid of 3D printing technology using a polyimide powder with a dielectric constant of ε_r=3.5. It should be noted that the proposed multilayer DRA configuration offers enhancement of the CP and impedance bandwidths as well as a higher broadside gain.

The cylindrical geometry offers a single degree of design freedom, where both the resonance frequency and radiation Q-factor are completely dependent on the radius, *a*, to height, *h*, aspect ratio [117]. Therefore, for a given dielectric constant, a wide and short DRA can be designed to resonate at the same frequency as that of a tall and slender DRA. As a result, antenna designers have the option of choosing different antenna profiles to achieve the desired resonance frequency. Furthermore, a proper feeding mechanism is needed in order to excite particular resonance modes. In this research a slot aperture has been employed for multiple reasons that have been explained in Chapter 2,

This Chapter is focused on demonstrating the potential of a layered higher order mode cylindrical DRA for linear and circular polarizations. As has been demonstrated for the rectangular DRA, higher order resonance mode operation provides a higher gain with a narrower bandwidth for a single layer configuration, which necessities the incorporation of an outer dielectric layer. Therefore, this Chapter presents theoretical and experimental work for a layered cylindrical DRA configuration with wider impedance and axial ratio

bandwidths in conjunction with a higher gain. The outline of the Chapter is illustrated in Figure 4.1.

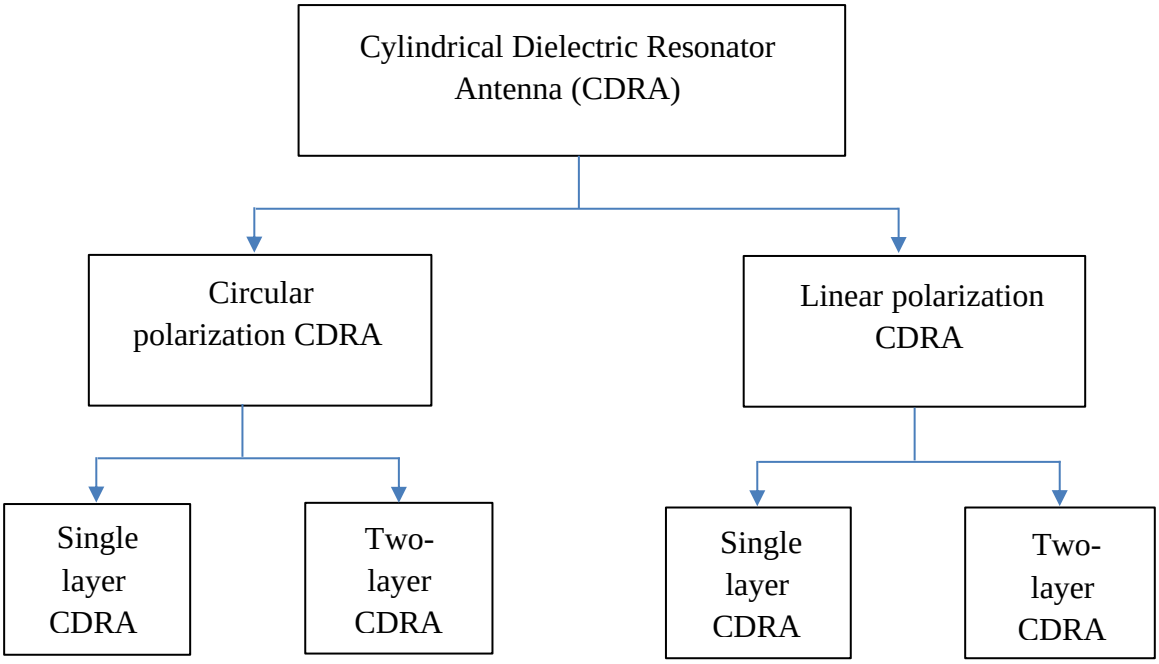

Figure 4.1: Chapter four overview.

4.3 Cylindrical DRA Resonance Modes

Figure 4.2 illustrates a 3D view of a cylindrical DRA mounted on a metal ground plane, where three distinct mode types can be generated; TE (E_Z=0), TM (H_Z=0) and hybrid modes. For the TE and TM modes, the electromagnetic fields are axially symmetric without azimuthal, ϕ, variations [118]. On the contrast, the fields of hybrid modes exhibit ϕ variations, and can be further categorized into two groups, HE and EH modes [117, 119]. At the same time, hybrid modes are antisymmetric and represent a superposition of the TE and TM modes' field. Based on the Debye potential, Ez and Hz need to construct an angular dependent solution in the cylindrical dielectric waveguide [118].

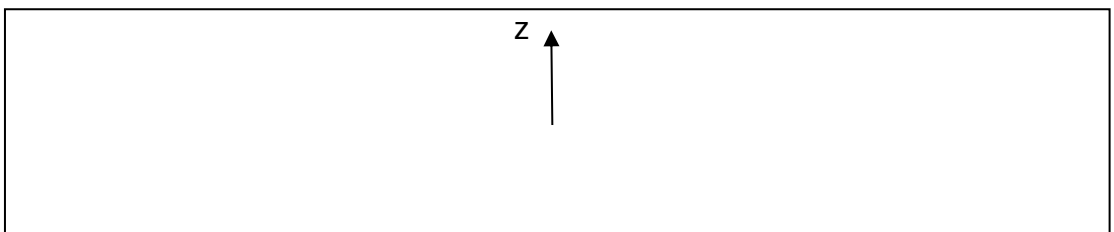

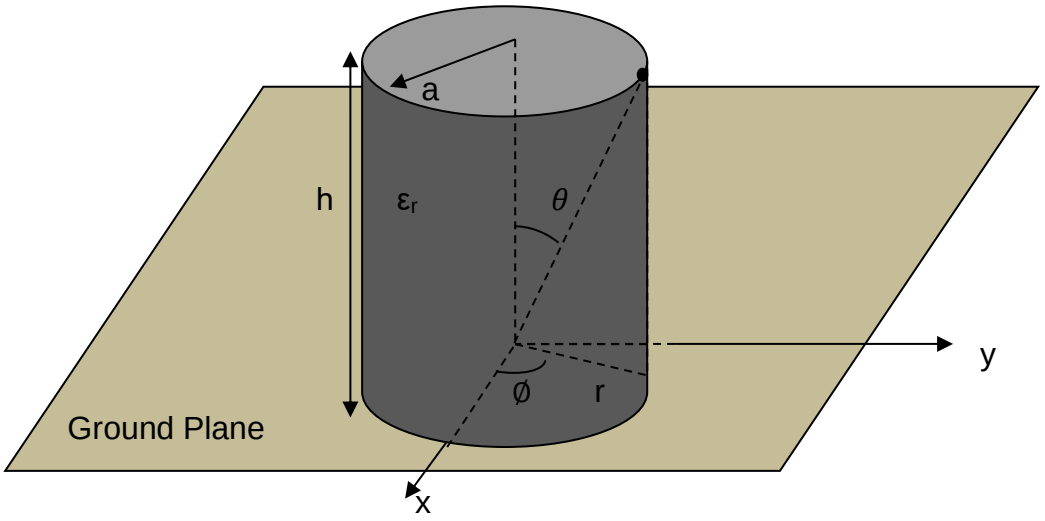

Figure 4.2: A cylindrical DRA placed on a ground plane.

The resonance modes are assorted as TE_{mnp}, TM_{mnp}, HE_{mnp} and EH_{mnp}., where the *m*, *n*, and *p* subscripts indicate field variations in azimuthal (ϕ), radial (*r*) and axial (*z)* directions, respectively. For example, the index *m* indicates the number of full wavelength cycles in the azimuth direction, while *n* and *p* denote the number of half-wavelength field variations along the radial and axial directions, respectively. Unlike the rectangular DRA, precise higher order modes resonance frequencies for a cylindrical DRA cannot be determined due to the complex mathematical modelling [6]. However, the resonance frequencies of these modes can be determined with the help of the CST MWS Eigen mode solver. On the other hand, resonance frequencies of lower order modes can be predicated approximately based on the radius, height and dielectric constant ε_r. For instance, when the aspect ratio is in the range of $0.4 \leq \frac{a}{h} \leq 6$, the $HEM_{11\delta}$ mode resonance frequency can be obtained as [6];

$$k_0 a = \frac{6.324}{\sqrt{\varepsilon_r + 2}}\left[0.27 + 0.36\left(\frac{a}{2h}\right) - 0.02\left(\frac{a}{2h}\right)^2\right] \qquad (4\text{-}1)$$

In which the free space wave number is given by $k_0 = \frac{2\pi f_0}{c}$, *c* is the speed of light, *fo* is the resonance frequency and $0 \leq \delta \leq 1$, δ which approaches 1 for high values of dielectric permittivity .Similarly, in the range of $0.33 \leq \frac{a}{h} \leq 5$, the resonant frequency of the $TE_{01\delta}$ mode can be calculated as [120].

$$k_0 a = \frac{2.327}{\sqrt{\varepsilon_r + 1}}\left[1.0 + 0.2123\left(\frac{a}{h}\right) - 0.00898\left(\frac{a}{h}\right)^2\right] \quad (4\text{-}2)$$

Finally, when $0.33 \leq \frac{a}{h} \leq 5$ the expression for the resonance frequency of the $TM_{01\delta}$ mode is given by [121].

$$k_0 a = \frac{2\pi f_0 a}{c} = \frac{\sqrt{3.83^2 + \left(\frac{\pi a}{2h}\right)^2}}{\sqrt{\varepsilon_r + 2}} \quad (4\text{-}3)$$

4.4 Linearly Polarized Higher Order Mode CDRA

4.4.1 Antenna Configuration

Figure 4.3 illustrates the proposed two-layer cylindrical DRA and feed network configuration. The inner layer represents a cylindrical DRA that has been fabricated by T-Ceram using Alumina with ε_{r1}=10 and a loss tangent of 0.002 with a fabrication precision of 0.05mm. The outer dielectric layer has been fabricated with the aid of 3D printing technology at the University of Sheffield using a polyamide with a dielectric constant of ε_{r2} = 3.5 and a loss tangent of 0.002. The proposed antenna has been placed on a 150×100mm^2 ground plane on top of a dielectric substrate with a thickness of 0.8mm that has been fabricated using a Roger material, RO4350B, with a dielectric constant of 3.48 and a loss tangent of 0.0037. Additionally, a slot aperture has been etched on the ground plane with dimensions of 1×6 mm^2. Further, a microstrip line has been printed on the bottom of the substrate with an open stub length of l_{stub}=5mm for optimum matching.

Simulated data that investigates the impact of varying the outer layer radius are illustrated in Table 4-1, where it can be observed that increasing the outer layer radius up to δa =17mm, which is equivalent to ~1.14λ_g, provides the maximum bandwidth of 16% in conjunction with a maximum gain of 13.8dBi compared to 4.9% and 7.4dBi at the absence of the outer dielectric layer. Moreover, increment of the gain can be attributed to that fact that increasing the thickness of the outer dielectric layer leads to the maximum energy confinement inside the dielectric resonator layer [83]. CST MWS has employed in order to confirm this point, where a number of probes have been attached at height of 7mm and located along the *x*-axis at distances of 0, 3, 6, 9 and 12mm from the CDRA center. The E-field strength is illustrated in Figure 4.4, where it can be noted that it is declined outside the central CDRA by increasing

the outer layer thickness. This confirm that the field confinement has been improved by increasing the outer layer thickness up to 20mm. More discussions on the impact of the outer layer thickness beyond δa =17 mm will be presented in Section 4.5. The short magnetic dipoles representation of the H-field inside the CDRA are illustrated in Figure 4.5, where it can be noted that the $HE_{11,11}$ has been excited for various outer layer's thicknesses.

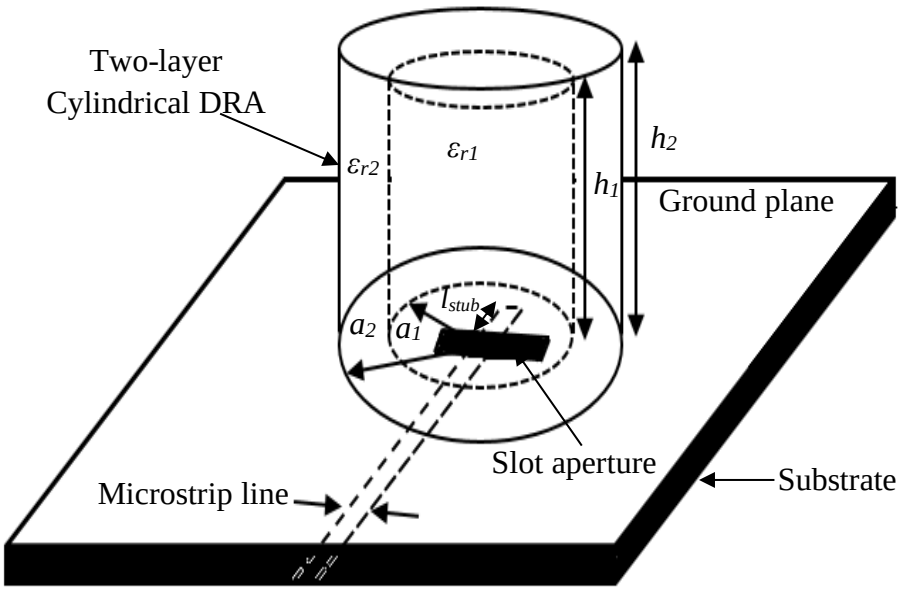

Figure 4.3: Layered cylindrical DRA fed by rectangular slot.

Table 4-1: Impedance bandwidth and gain with various outer layer radii for a linearly polarized CDRA

a_1 (mm)	a_2 (mm)	$\delta a=(a_2-a_1)$ (mm)	$\delta a/\lambda_g$	Bandwidth %	Gain dBi
3	0	0 (no coating)	0 (no coating)	4.98	7.4
3	5	2	0.13	6.10	7.17
3	10.5	7.5	0.5	13.5	9.1
3	15	12	0.81	14.65	11
3	18	15	1	13.9	12.3
3	20	17	1.14	16	13.8

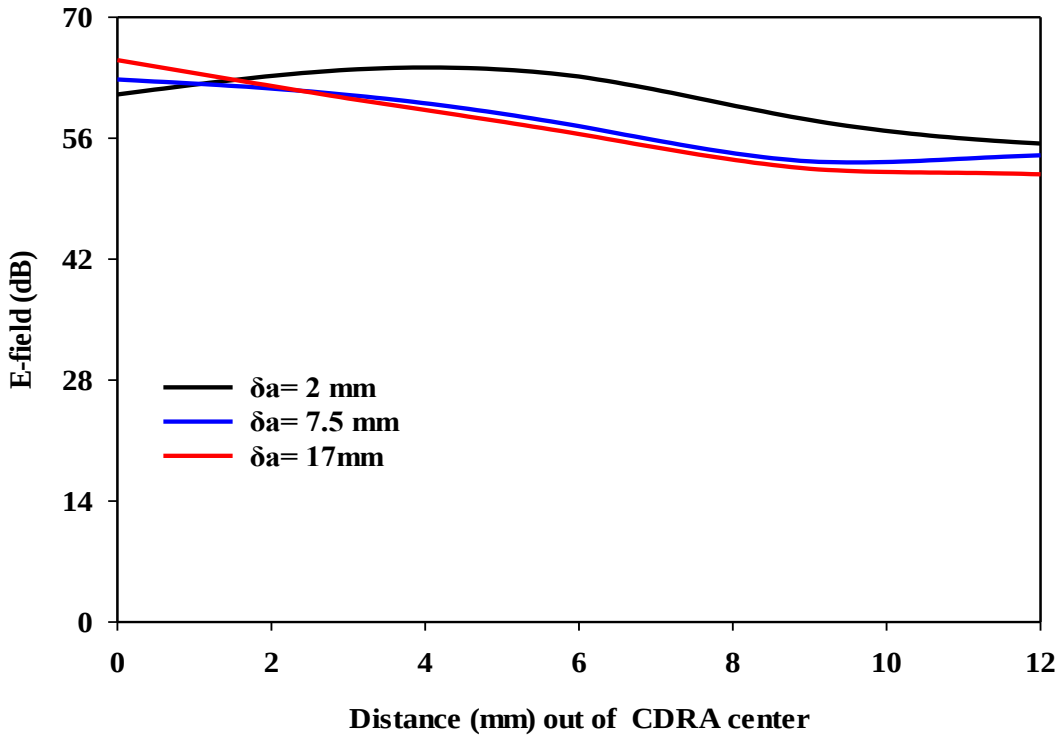

Figure 4.4: E-field strength around the LP LCDRA for various outer layer radii at 9.6GHz when δa =2mm and 11GHz when δa =7.5 and 17mm.

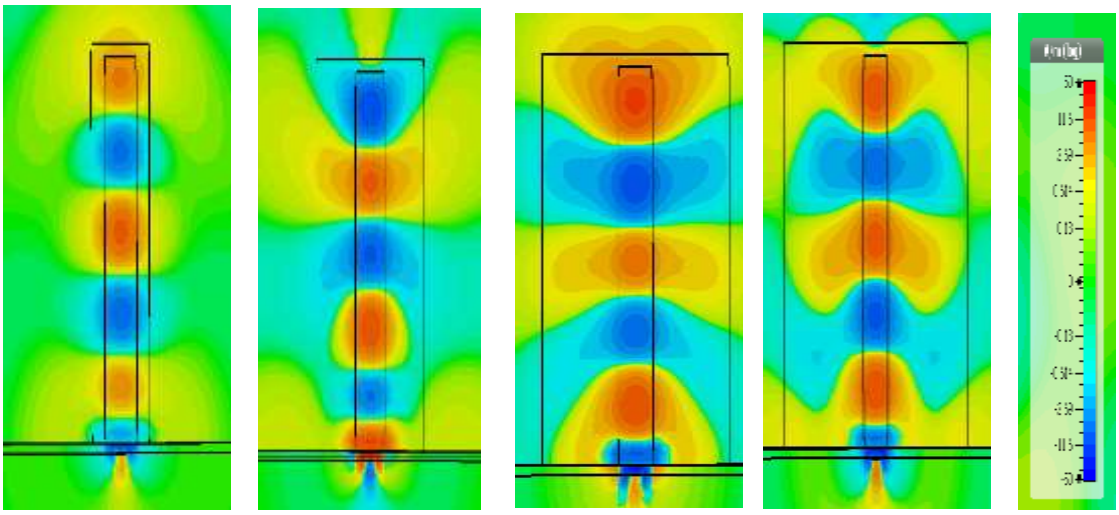

δa = 2mm δa = 7.5mm δa = 12mm δa = 17mm

Figure 4.5: H-field distribution inside the LP cylindrical DRA with varying outer layer thickness at 11GHz.

The impact of fabrication errors has also been investigated by studying the mode's resonance frequency variation for fabrication errors of 0.05, 0.1 and 0.2mm in case of outer layer that has thickness of δa =7.5 and 17mm. In each case the error has been added to the cylindrical DRA radius and the resonance frequency has been tracked for a fixed coat dimension. As can be noted from Table 4-2, the increment of the outer layer thickness minimizes the impact

of fabrication errors, This can be attributed to the fact that for the layered CDRA, the dimensions variation is taking place in the of vicinity reduced wave reflections at the cylindrical DRA surface compared to the case of a single layer DRA, which means an improved fabrication tolerance.

Table 4-2: Impact of fabrication errors on the resonance frequency of the layered CDRA

Fabrication error (mm)	Single layer CDRA (no coating) Δf (%)	Two-layer CDRA (δa=7.5 mm) Δf (%)	Two-layer CDRA (δa=17 mm) Δf (%)
0.05	0.696	0.264	0.164
0.1	1.427	0.768	0.546
0.2	2.89	1.25	0.600

4.4.2 Single Layer Linearly Polarized CDRA Configuration

A cylindrical DRA prototype has been fabricated with dimensions that support the HE_{115} and HE_{117} modes at 10.6 and 11.5GHz, respectively, with a radius of a_1=3mm and a height of h_1=32mm. The comparison between simulated and measured reflection coefficients are depicted in Figure 4.6 at the absence of the dielectric coat, where it can be noted that the respective simulated and measured respective impedance bandwidths are 5% over a frequency range of 10.3-10.85GHz and 4.3% at 10.5-11GHz for the HE_{115} resonance mode. Similarly, measured and simulated bandwidths of 4.98% have been achieved over a frequency range of 11.3–11.9GHz when the HE_{117} resonance mode is excited. These results demonstrate a close agreement between measurements and simulations. The magnetic field distributions are illustrated in Figure 4.7, where it is evident that the expected modes have been excited. Next, the radiation patterns and gain have been measured in an anechoic chamber as demonstrated in Figure 4.8 and 4.9, respectively. A good agreement between simulated and measured gains of 10.2 and 7.5dBi have been achieved for the HE_{115} and HE_{117}, respectively. It is worth mentioning that a slight drop of antenna gain is evident at the HE_{117} resonance frequency point of 11.6GHz that can attributed to the fact that a new short magnetic dipole has been generated inside the CDRA, which results in an overlapping between the short magnetic dipoles and, hence, reducing the gain [23, 122]. Based on these results, it can be concluded that the existence of overlapping short magnetic dipoles represents a key limitation of the higher order mode operation. Therefore, the antenna height need to be increased in order to maintain a higher gain. However, this usually result in impractical antenna dimensions with questionable robustness since a thin and tall ceramic

antenna is fragile. Similar to the RDRA design, a layered CDRA needs to be established in order to overcome these higher order mode limitations.

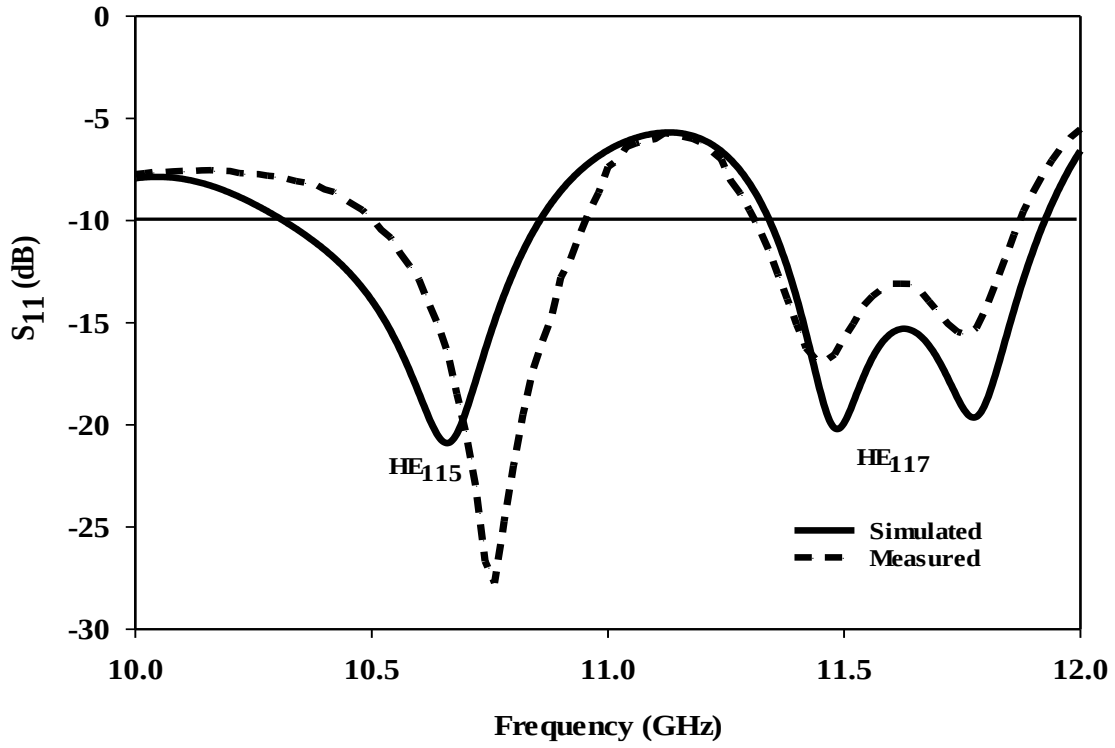

Figure 4.6: Reflection coefficient of a single-layer CDRA operating in the HE_{115} and HE_{117} modes.

Plane EM field component	Top surface, E_z	H_x (*yz* plane)	H_x (*xz* plane)
HE_{115} at 10.2 GHz	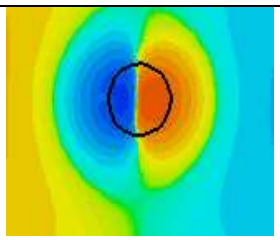	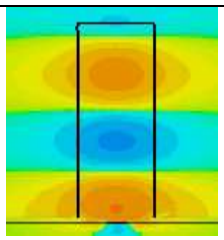	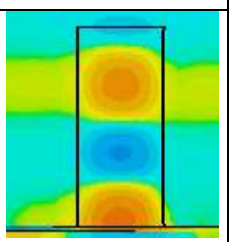
HE_{117} at 11.6 GHz	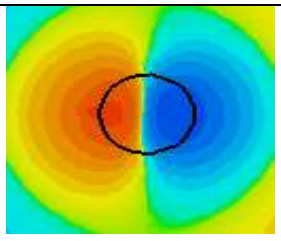	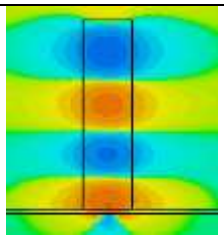	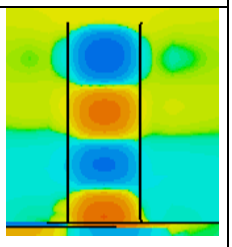

Figure 4.7: E-field and H-field distributions of higher-order modes linearly polarized single-layer cylindrical DRA.

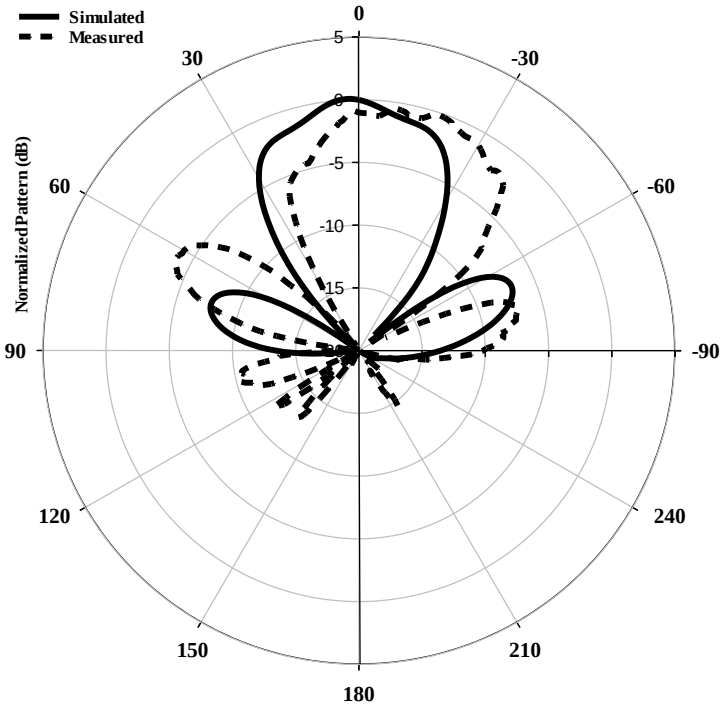

(a)

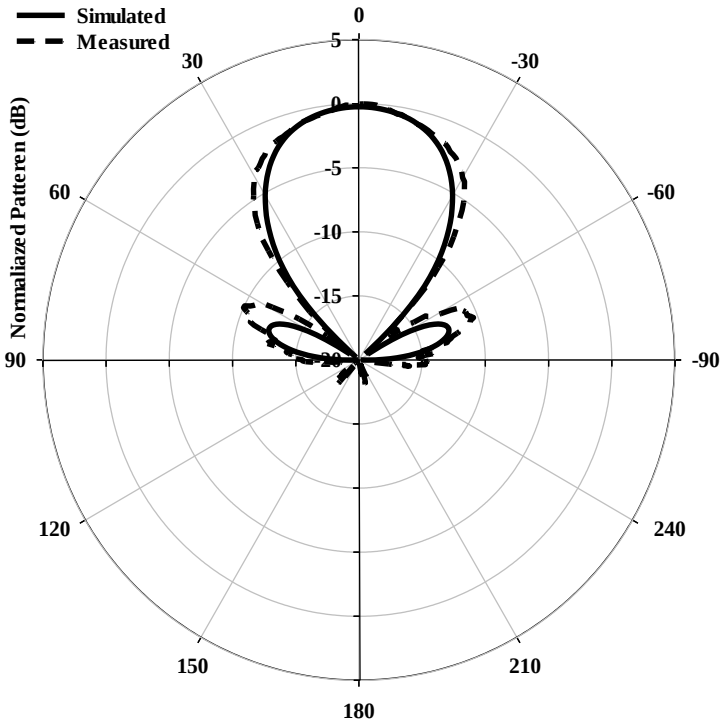

(b)

Figure 4.8: Radiation patterns of single layer LP CDRA excited in the HE_{117} mode at 11.6 GHz (a) $\phi=90^0$, (b) $\phi=0^0$

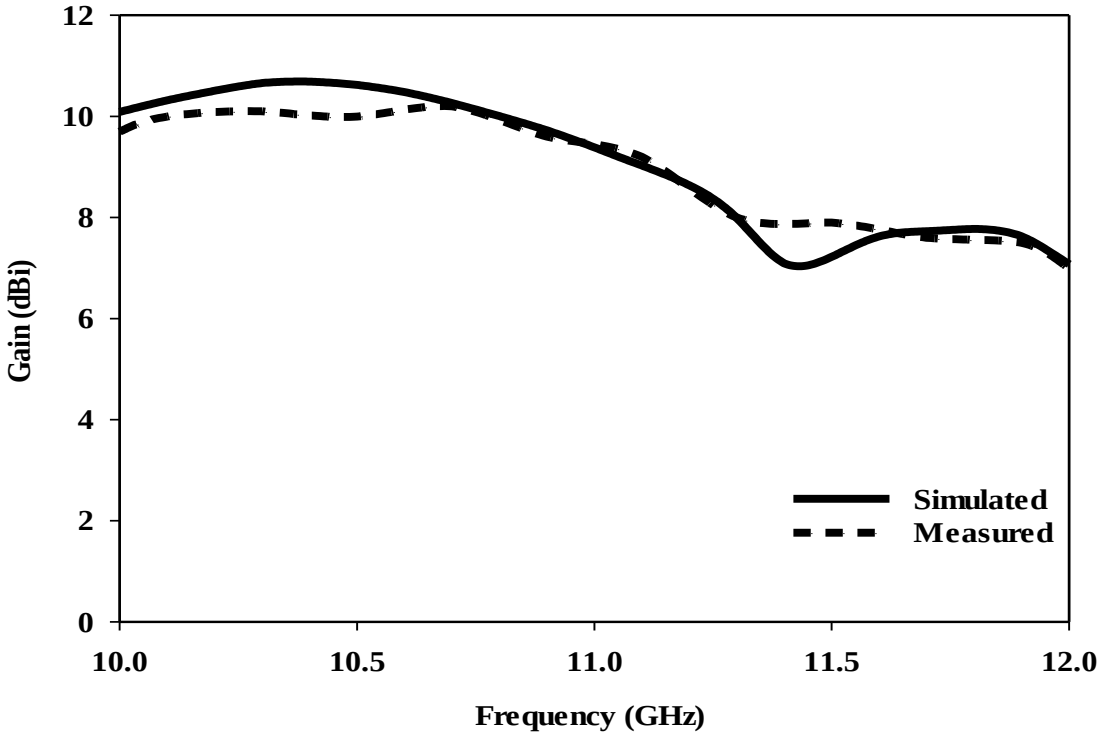

Figure 4.9: Broadside gain of a single layer LP CDRA.

4.4.3 Two Layer Linearly Polarized CDRA Configuration

As mentioned earlier, coating the antenna with a relative permittivity of ε_{r2} creates a transition region between the DRA and air, which improves the impedance bandwidth. The single layer CDRA has been coated by cylindrical dielectric coat has a respective inner and outer radius of 3 and 10.5mm, i.e. a layer thickness of δa= 7.5mm. The outer layer height, h_2, has been chosen as 33mm with a relative permittivity of ε_{r2}= 3.5 and loss tangent 0.00027. Figure 4.10 presents the simulated and measured reflection coefficients of a layered LP CDRA, with good agreement. As can be observed from these results, the respective simulated and measured bandwidths are 13.6% over a frequency range of 9.72-11.15GHz and 13.5% over 9.64-11GHz. It is worth mentioning that, new higher order modes HE_{119} and $HE_{11,11}$ have been generated at 9.8 and 10.9GHz frequency points with respective gains of 7.7 and 9.1dBi as illustrated in Figure 4.11. Further enhancement of layered CDRA gain will be investigated later in this Chapter. Figure 4.12 illustrates the measured and simulated radiation patterns of the linearly polarized layered CDRA that

operating at the $HE_{11,11}$ resonance mode at 10.9GHz with good agreement between the two data sets.

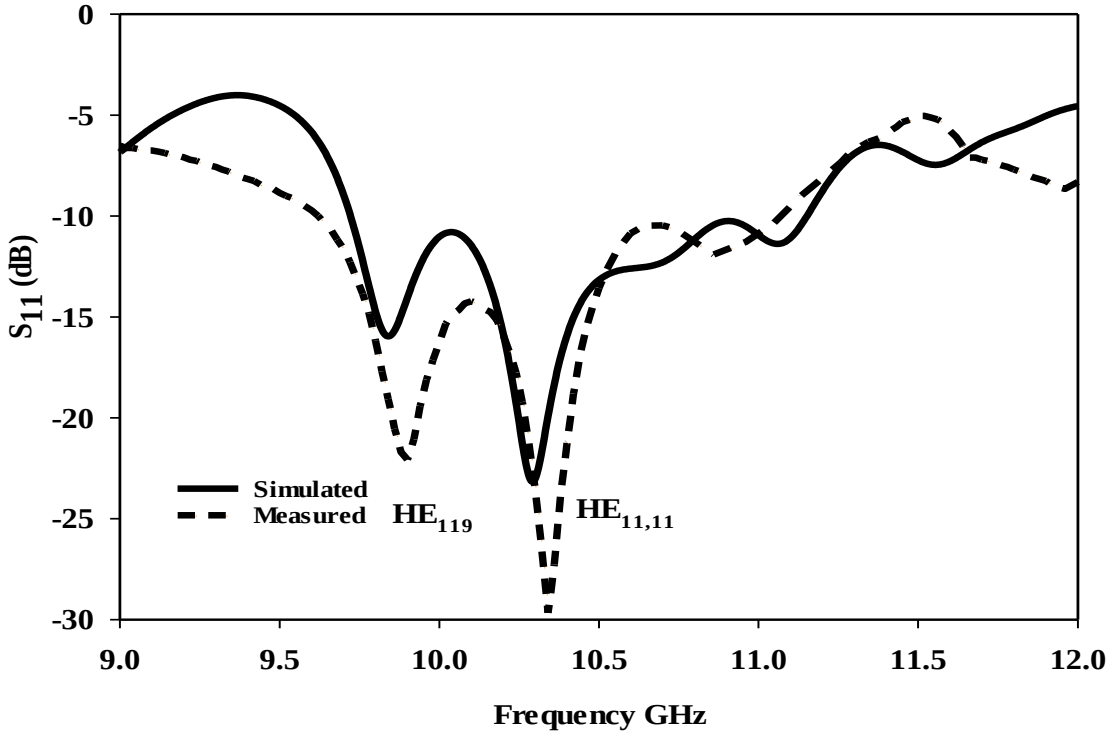

Figure 4.10: Reflection coefficient of linearly polarized two-layer CDRA.

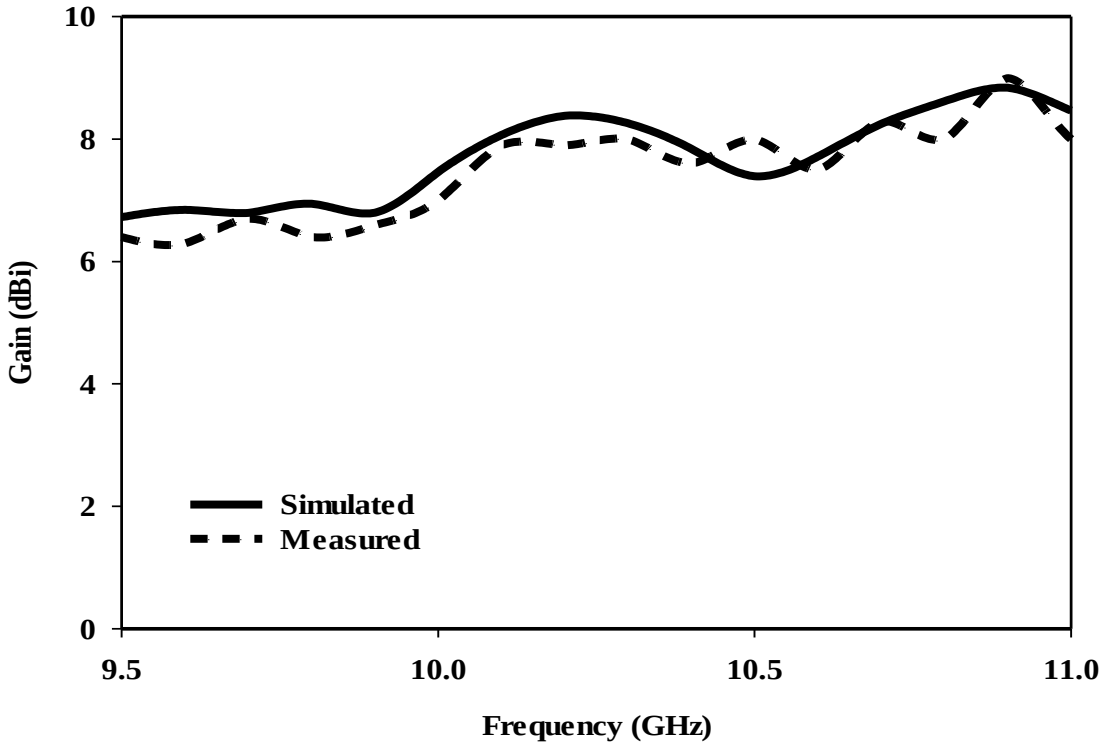

Figure 4.11: Gain of a two-layer linearly polarized cylindrical DRA.

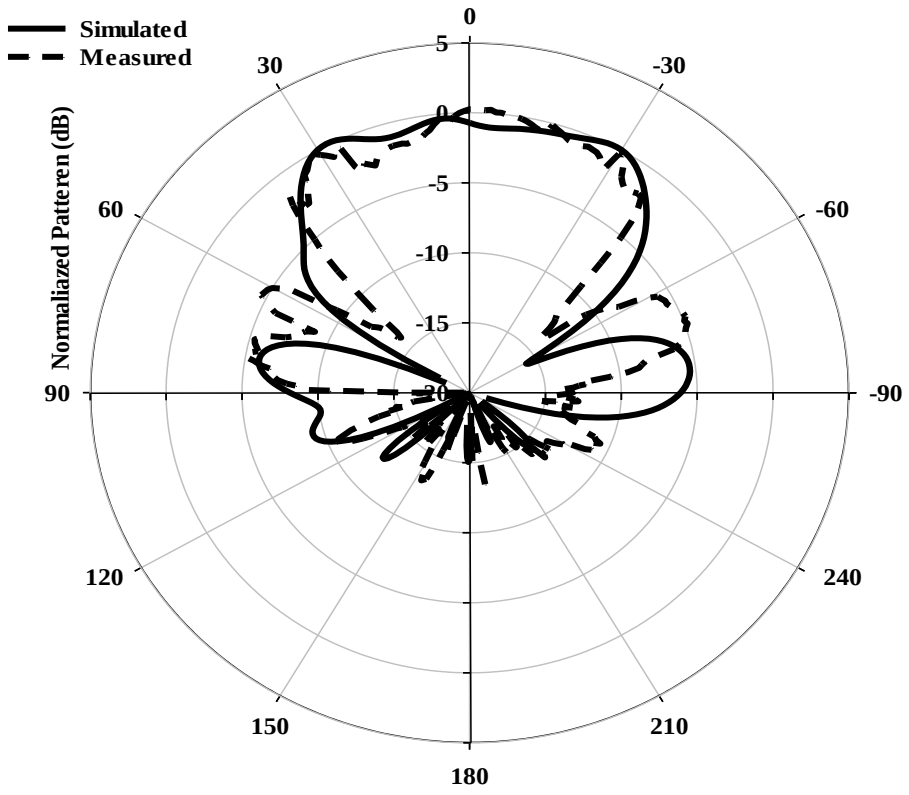

(a)

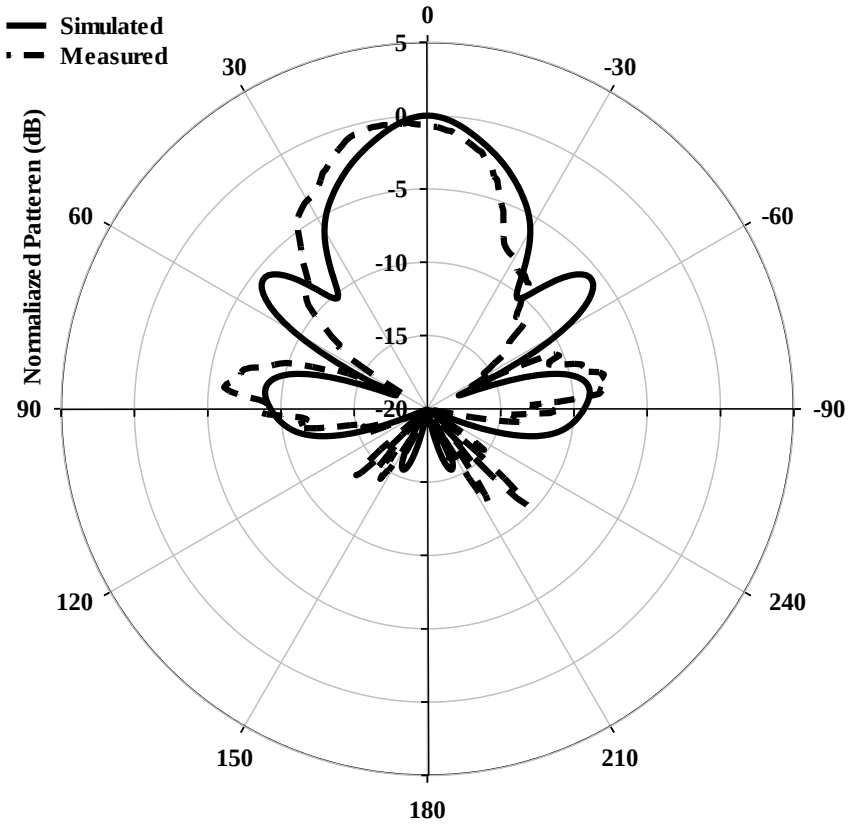

(b)

Figure 4.12: Radiation patterns of the wideband two-layer LP CDRA $HE_{11,11}$ at 10.9GHz (a) $\phi = 0^0$. (b) $\phi = 90^0$.

4.5 Circularly Polarized Higher Order Mode CDRA

4.5.1 Antenna Configuration

In this section, a higher order mode circularly polarized two-layer cylindrical DRA is investigated, where a special attention has been given to study the influence of the outer layer thickness. Figure 4.13 illustrates prototypes of the cylindrical DRA and the outer layer. Additionally, Figure 4.14 (a) and (b) illustrate the layered CDRA and its feed network, where the optimized DRA dimensions have been chosen as a_1=3mm, a_2=10.5mm, δa=7.5 mm, h_1=32mm and h_2=33mm. In addition, the proposed antenna has been placed on a 150×100mm^2 ground plane with same arrangements mentioned earlier. Further, a cross-slot has been itched on the ground plane with identical arm widths of w_{s1} = w_{s2} = 0.7mm and unequal arm lengths of l_{s1} = 4.4mm and l_{s2} = 6.2mm. Once more, the whole structure has been fed using a microstrip line that has been printed on the bottom of the substrate with an open stub length of l_{stub} =2.5mm for optimum matching. Unequal lengths of cross-slot arms have been chosen in order to excite two near-degenerate orthogonal modes of equal amplitude and 90^0 phase difference close to that of the fundamental mode of the cylindrical DRA, which leads to the generation of CP radiation [61, 84, 123].

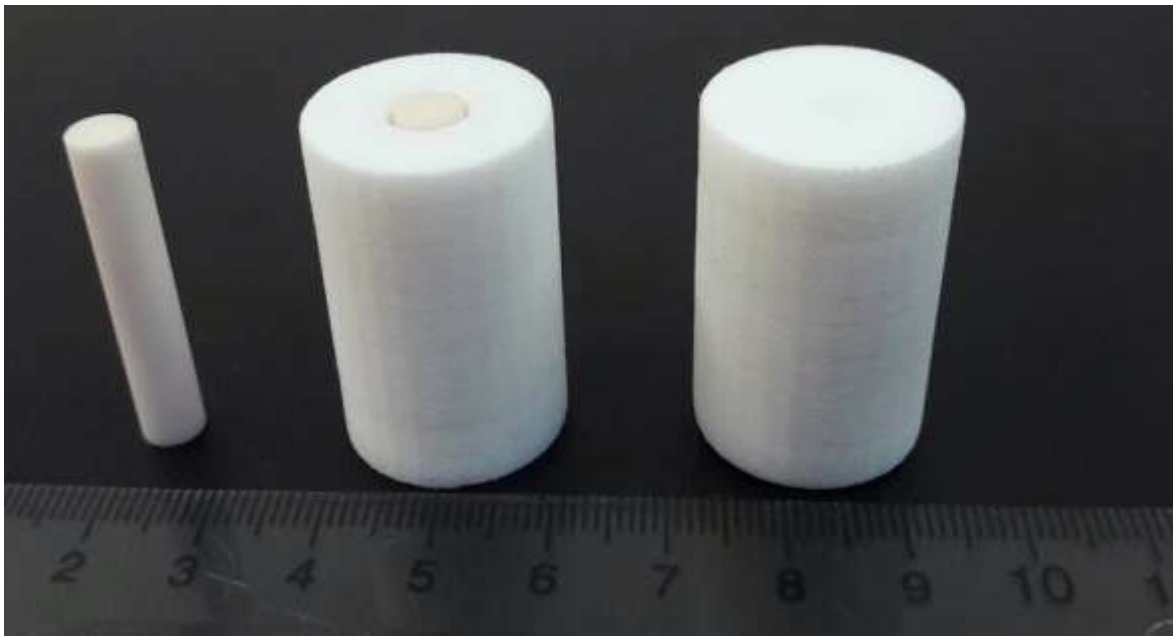

Figure 4.13: The outer dielectric coat and cylindrical DRA before and after assembly.

4.5.2 Parametric Study

The parametric sweep of CST MWS has been utilized to optimize the slot arms' length while keeping the outer layer thickness constant and vice-verse. The effects of the first slot length, l_{s1}, variations on the return losses and axial ratio are illustrated in Figure 4.15 when the second stub length is kept constant as 4.4mm. In the case of $l_{s1} = l_{s2} = 4.4$mm, the axial ratio is ~40dB, which indicates that the required two orthogonal modes have not been excited, hence a linear polarization has been achieved with a maximum impedance bandwidth of 8.33%. On the other hand, by increasing l_{s1} to 6.2mm, a significantly wider impedance and axial ratio bandwidths of 23.5% and 6.79%, respectively, have been achieved.

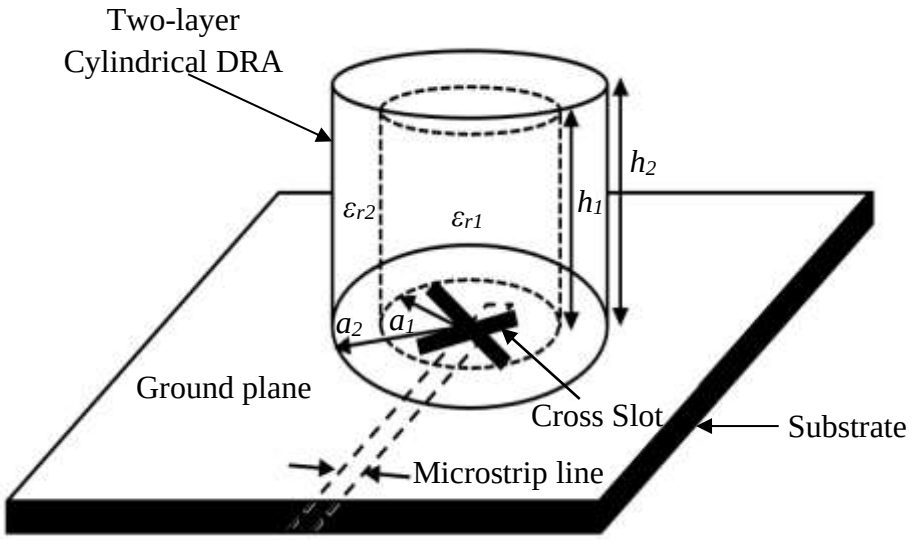

(a)

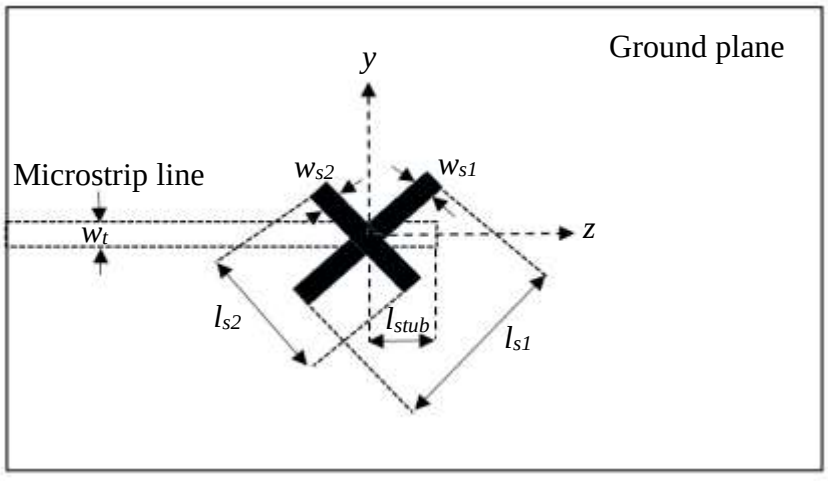

(b)

Figure 4.14: Geometry of the configuration (a) Layered cylindrical DRA (b) Top view of the feed network.

Next, the effects of varying outer layer thickness have been studied as illustrated in Figure 4.16, and 4.17 as well as Table 4-3, with l_{s1} and l_{s2} fixed as 6.2 and 4.4mm, respectively. From these results it can be observed that thicker outer layer (δa=17 mm) provides a significant improvement in the impedance and axial ratio bandwidths as well as gain to 28.34%, 9.52%, 13.9dBic, respectively, compared to 5.96%, 0.86%, and 6.6dBic for a single layer configuration. The improved characteristics can be attributed to the fact that the outer layer acts as a transition layer between the DRA and free space, which improves the matching bandwidth. This is in addition to merged bandwidth due to multi-mode excitation at adjacent resonance frequencies. Similarly, the gain has been improved owing to multiple reasons such as exciting the higher order modes of HE_{119} and $HE_{11,11}$ at 10.6GHz and 12GHz, respectively, compared to only the HE_{117} mode at 11.55GHz for a single layer configuration. Figure 4.18 demonstrate that increasing the outer layer thickness improves the energy confinement inside the dielectric resonator layer resulting in the gain increment as explained earlier. Again, several probes have been utilized in the simulations to study the E-field variation inside the DRA when the outer layer thickness is varied. The simulated results confirm that the E field strength around the CDRA diminishes for a thicker outer. The magnetic field distribution inside the CP CDRA is illustrated in Figure 4.19 for various outer layer thicknesses at 11GHz.

Moreover, with reference to Figure 4.20 the maximum bandwidth is consistently achieved using an outer layer radius of δa=17mm. it is well known that using higher permittivity material can confine more energy inside it, hence the radiation efficiency will be reduced, in this case, the low permittivity material has been used for the outer layer in order to avoid that. However, the increasing outer layer thickness beyond $1.14\lambda_g$ could lead to confine more energy inside the outer layer than release it as demonstrated in Figure 4.18 which indicated that the gain goes down. Figure 4.21 depicts the simulated H-field and E -field distributions of the hybrid modes in several planes of the resonator as acquired from the CST MWS and as excited within the designed CP two-layer cylindrical DRA at multiple targeted frequencies. The comparison clearly demonstrated the presence of the modes inside the cylindrical DRA.

Table 4-3: Radiation characteristics for various outer layer radii

a_1 mm	a_2 mm	$\delta a=(a_2-a_1)$mm	S_{11} bandwidth %	AR bandwidth %	Gain dBic
3	0	0 (no coating)	5.9	0.86	6.6
3	5	2 ($0.13\lambda_g$)	9.3	1.7	7.5
3	10.5	7.5 ($0.5\lambda_g$)	23.5	6.79	8.6
3	15	12 ($0.81\lambda_g$)	26.13	8.6	11
3	18	15(λ_g)	28.34	8.6	12.27
3	20	17($1.14\lambda_g$)	28.34	9.52	13.9
3	26	23($1.5\lambda_g$)	28.24	3.2	9.6
3	33	30($2\lambda_g$)	22.4	1.6	8.5

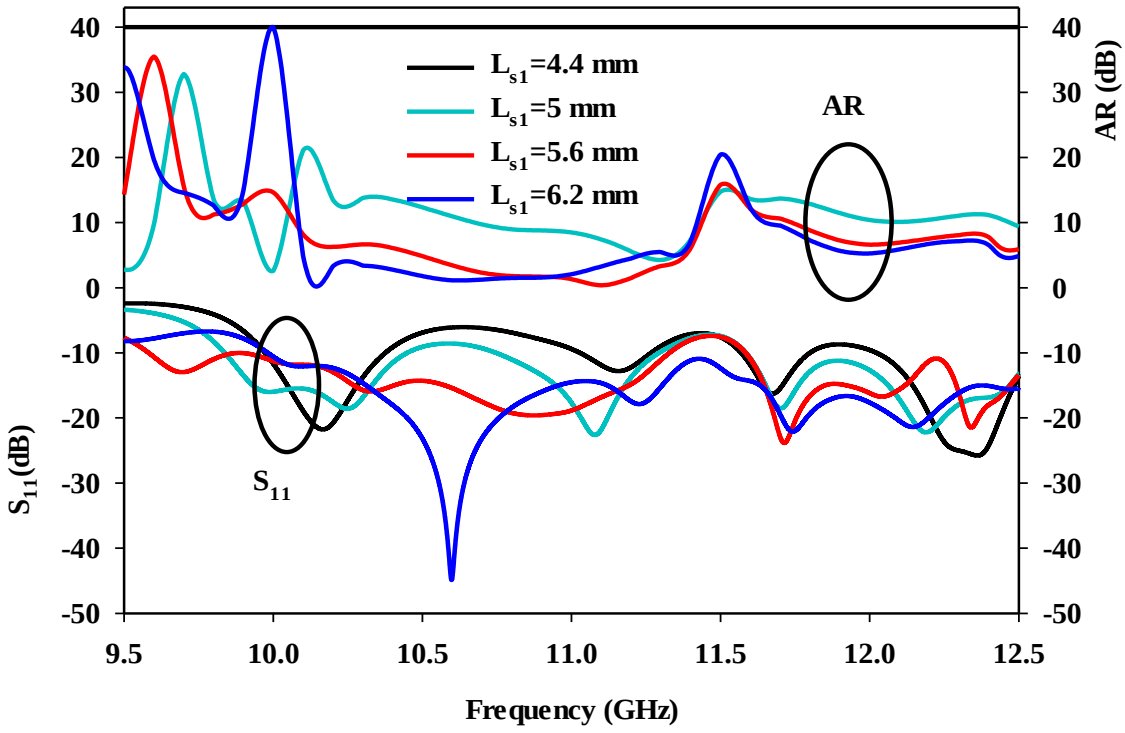

Figure 4.15: Simulated S_{11} and axial ratio of two-layer CP CDRA for various l_{S1} lengths

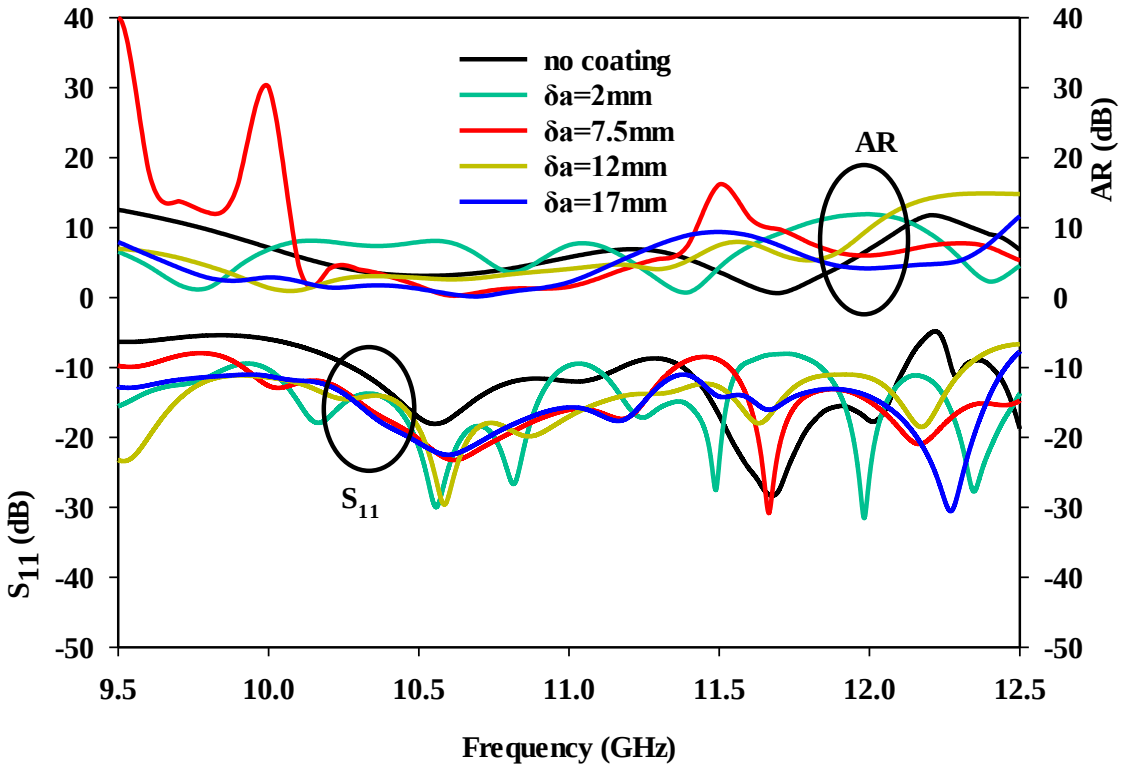

Figure 4.16: Simulated S_{11} and AR of a two-layer CP CDRA for various δa radii.

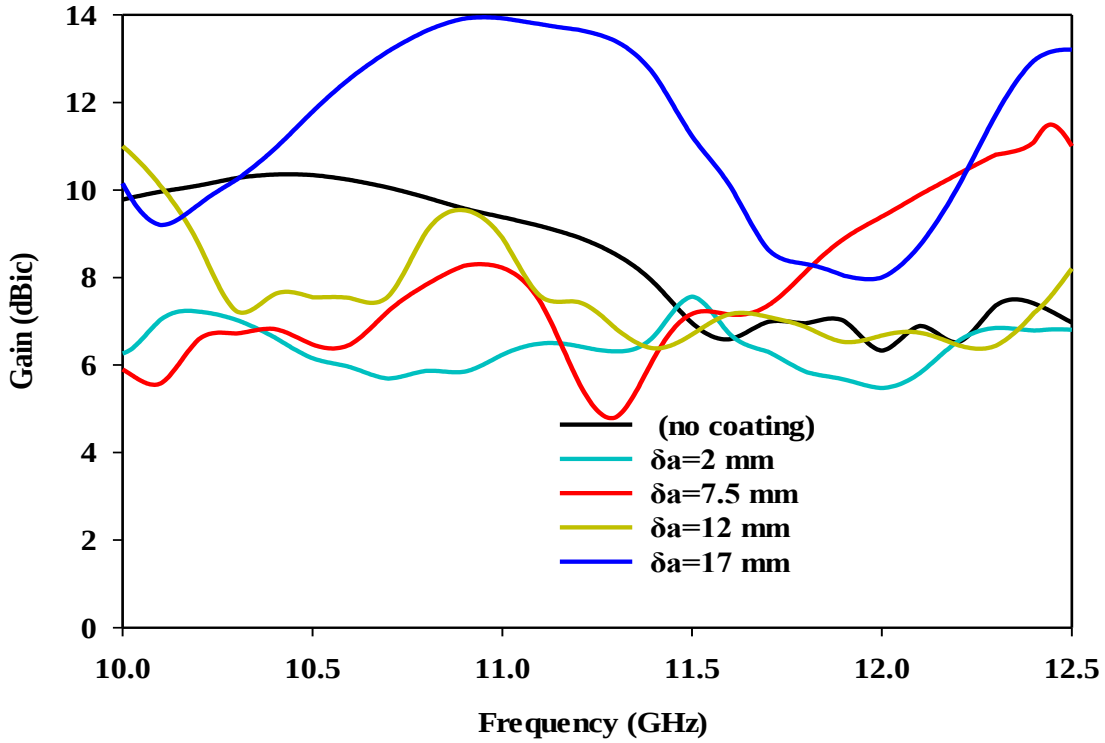

Figure 4.17: Simulated gain of two-layer CP CDRA for various δa radii.

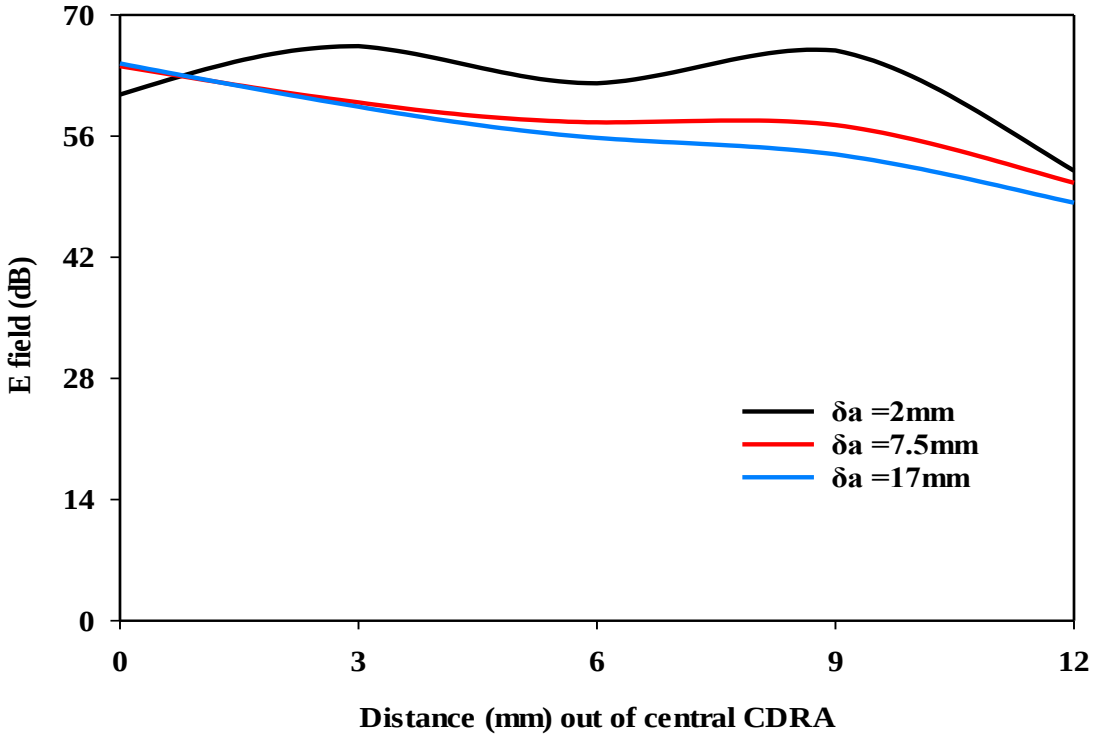

Figure 4.18: Strength of E-field around the CP LCDRA at 11GHz.

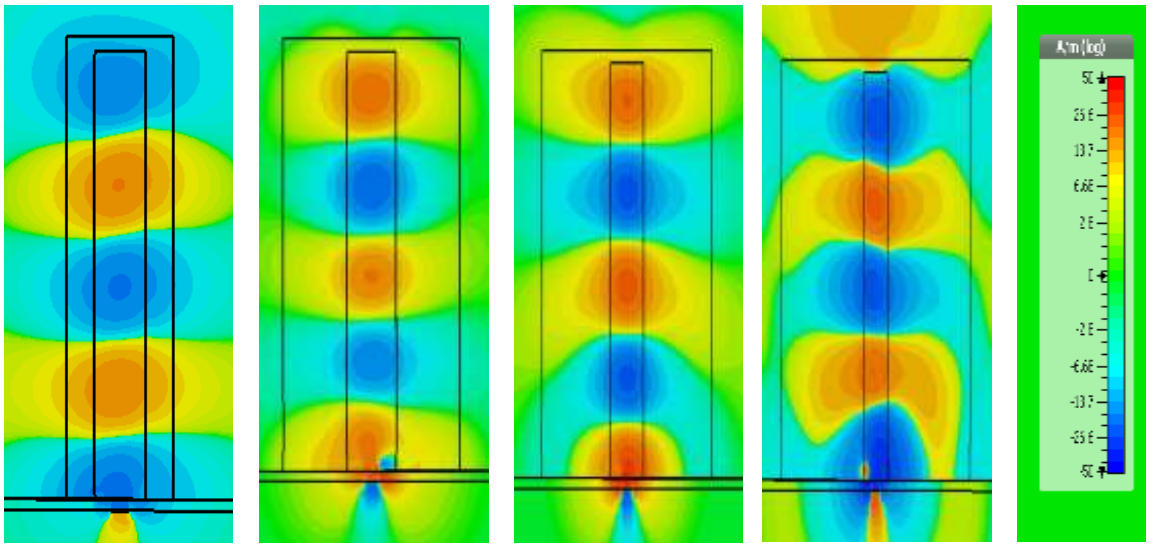

δa = 2mm *δa* = 7.5mm *δa* = 12mm *δa* = 17mm

Figure 4.19: The short magnetic dipoles representation of the H-field inside CP cylindrical DRA with varying outer layer thickness at 11GHz.

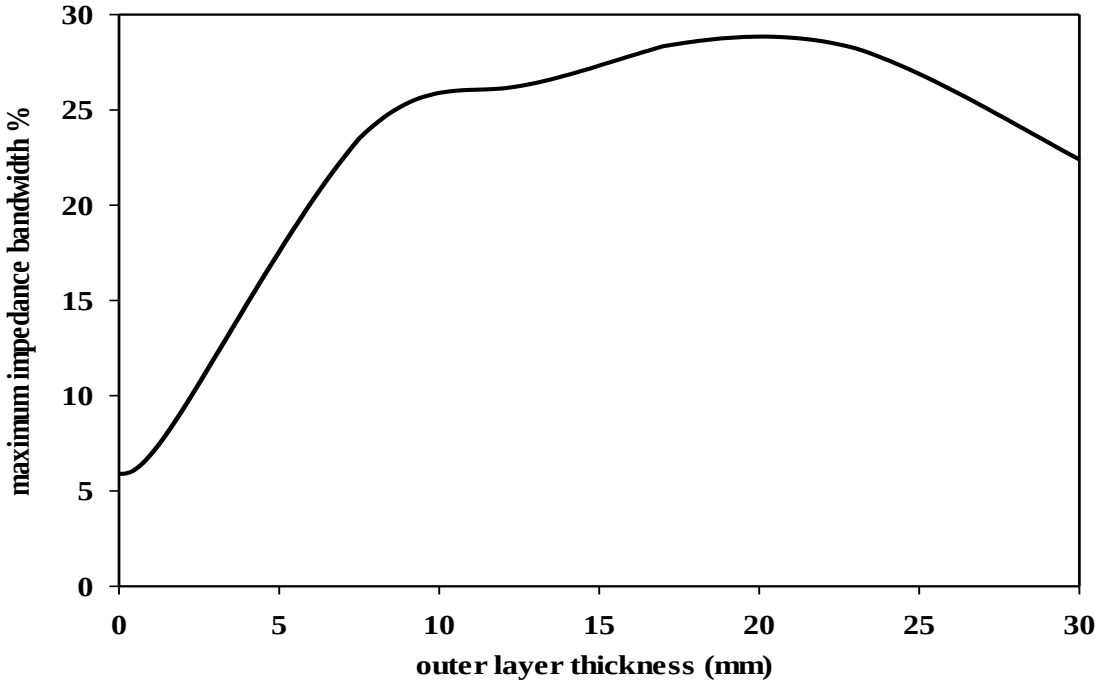

Figure 4.20: Maximum bandwidth as function of the outer layer thickness.

Plane EM field component	Top surface, E_z	H_x (*yz* plane)	H_y (*xz* plane)
single layer CP CDRA HE_{117} at 11.55GHz	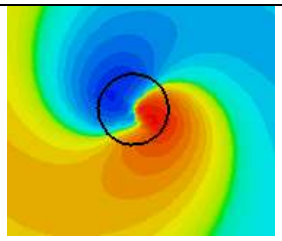	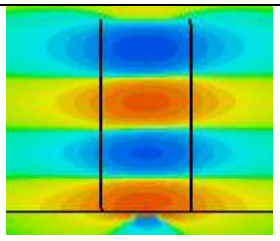	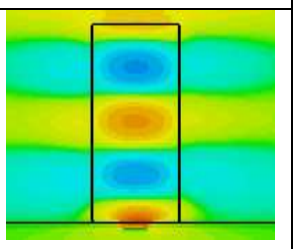
Multi- layer CP CDRA HE_{119} at 10.6GHz	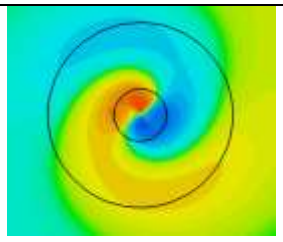	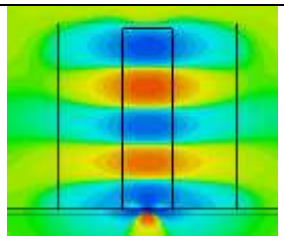	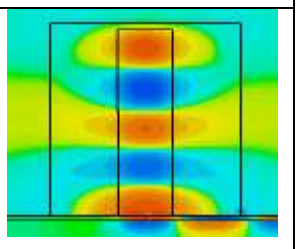
Multi- layer CP CDRA $HE_{11,11}$ at 12GHz	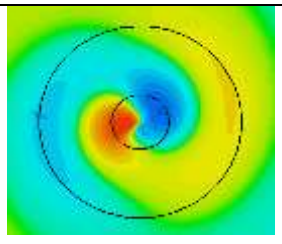	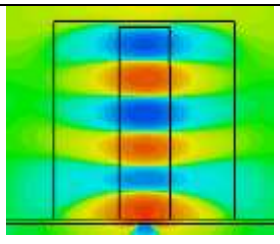	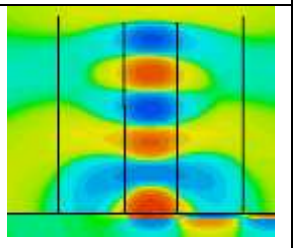

Figure 4.21: E-field and H-field distributions of higher-order modes circularly polarized single and multi-layer cylindrical DRA.

4.5.3 Single Layer Circularly Polarized CDRA Configuration

In order to verify the aforementioned simulations, a cylindrical DRA has been fabricated following the process described in Section 4.4.1, where the antenna has been fed using a cross-slot with two arms that have identical width of w_{s1}=w_{s2}=1mm and unequal lengths l_{s1}= 4.8mm and l_{s2}= 6.4mm. The single layer CP cylindrical DRA supports the HE_{117} mode. The simulated and measured S_{11}, gain, and axial ratio results are depicted in Figure 4.22 , 4.23, and 4.24, respectively. The respective simulated and measured impedance bandwidths are 6%and 5.8%, where the former extends from 11.36–12GHz and the latter covers a frequency range of 11.4–12.1GHz. The measured and simulated gains are 6.6dBic at 11.55 GHz, while both of the simulated and measured axial ratio bandwidths are 0.86% over a frequency range of 11.5 to 11.6GHz. The simulated and measured radiation patterns for the HE_{117} mode, at 11.55GHz, are illustrated in Figure 4.25, where it can be noticed that this is a left-hand circularly polarized, LHCP, antenna since the broadside E_L is stronger than the E_R counterpart by more than 15dB. Based on these results, it can be concluded that the narrower bandwidth represents the key limitation of a higher order mode operation. Therefore, a layered CDRA needs to be established for bandwidth enhancement.

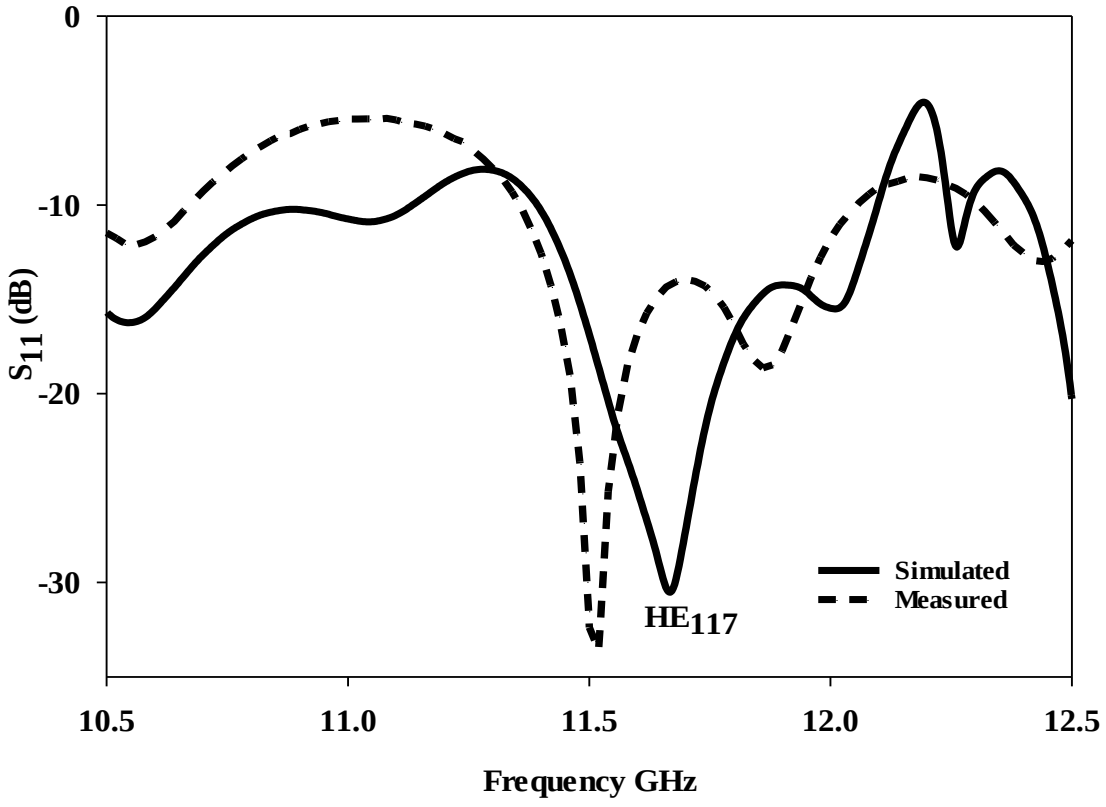

Figure 4.22: Reflection coefficient of a single-layer CP CRDRA operating in the HE_{117} mode.

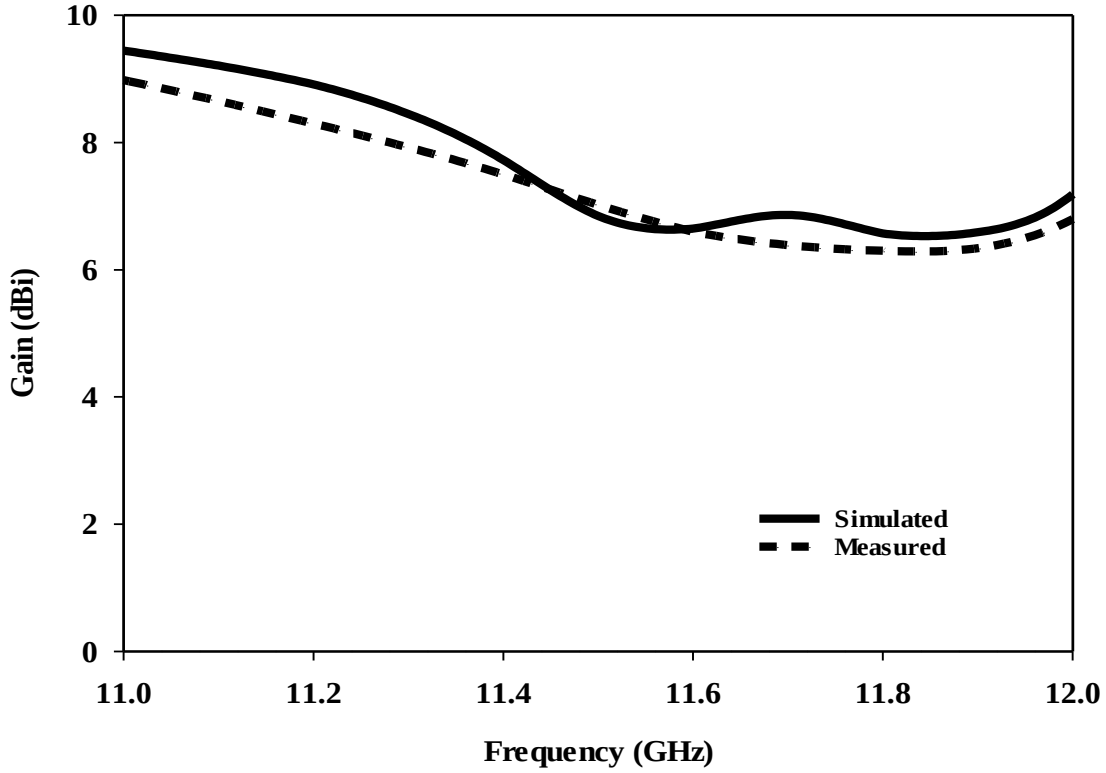

Figure 4.23: Simulated and measured boresight gains of a single-layer CP CRDRA.

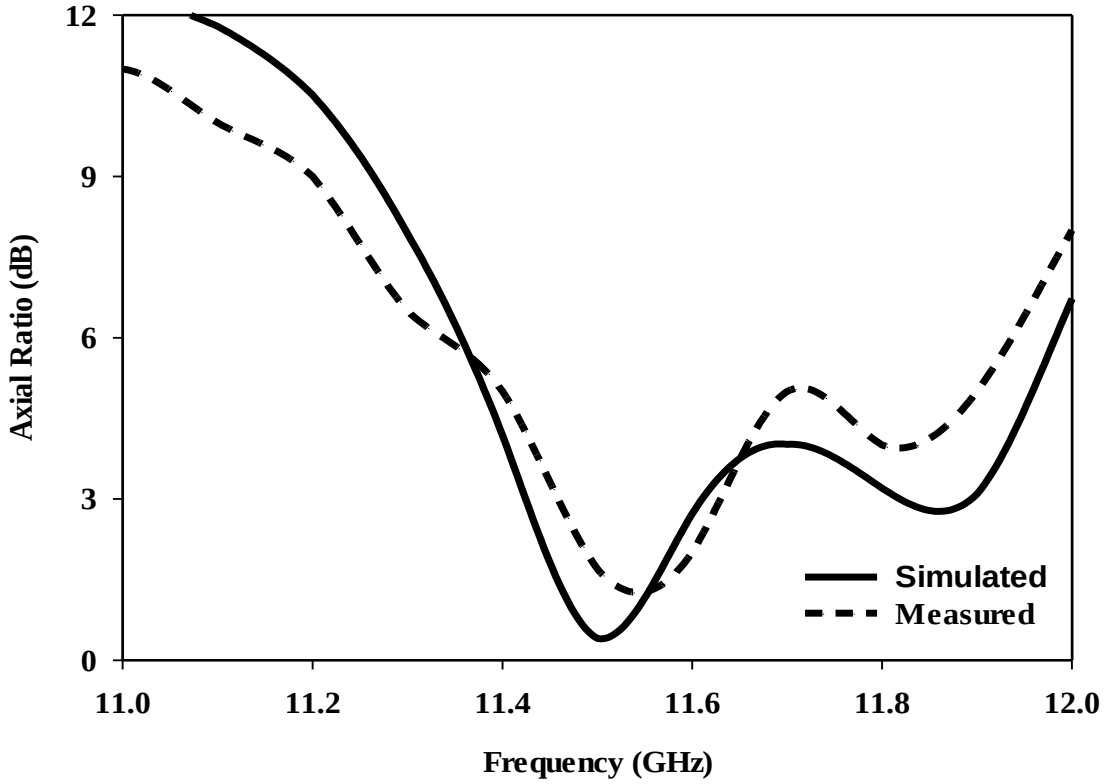

Figure 4.24: Simulated and measured AR of a single-layer CP CDRA operating in the HE_{117} mode.

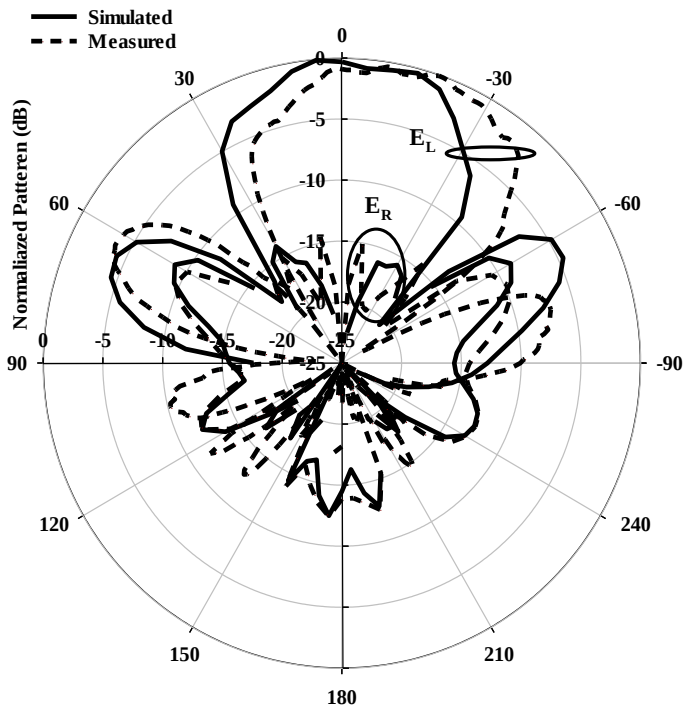

(a)

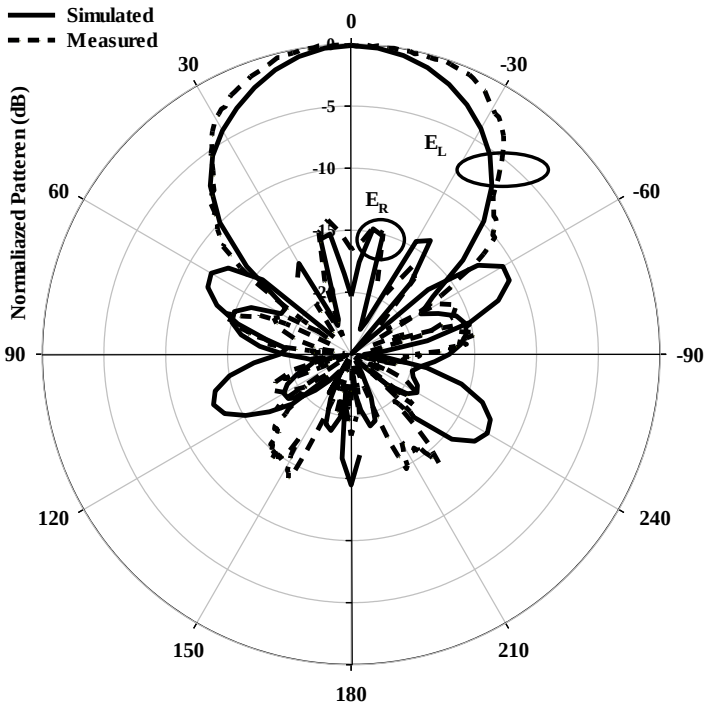

(b)

Figure 4.25: Radiation pattern of a single-layer CP CDRA excited in the HE_{117} mode at 11.55GHz (a) ϕ=0° (b) ϕ=90°.

4.5.4 Two Layer Circularly Polarized CDRA Configuration

The single layer cylindrical DRA has been coated by an outer dielectric layer fabricated using a 3D printing in order to address the narrower impedance and AR bandwidths as well as improving the gain further. Figure 4.26 presents the simulated and measure S11 in the case of δa=7.5mm, where it can be observed that the simulated impedance bandwidth is 23.5%, and extends from 10–12.64 GHz, agrees well with the measured counterpart of 22% over a frequency range of 10–12.6 GHz. It is worth mentioning that the two resonance modes of HE_{119} and $HE_{11,11}$ have been generated at 10.6 and 12 GHz, respectively. These modes contributed to increasing the antenna gain to 8.6dBic for the HE_{119} mode and 11dBi at the $HE_{11,11}$ resonance mode, as shown in Figure 4.27.

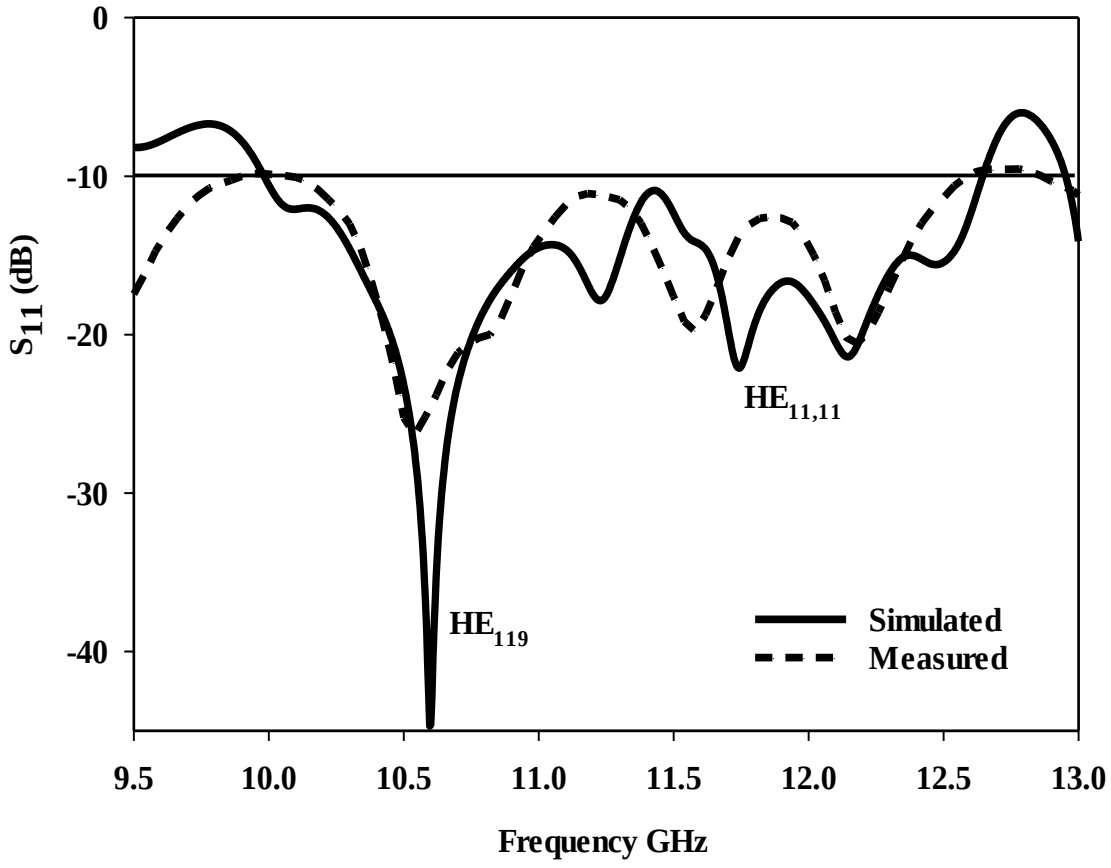

Figure 4.26: Reflection coefficient of a multi-layer CP CDRA with δa=7.5mm.

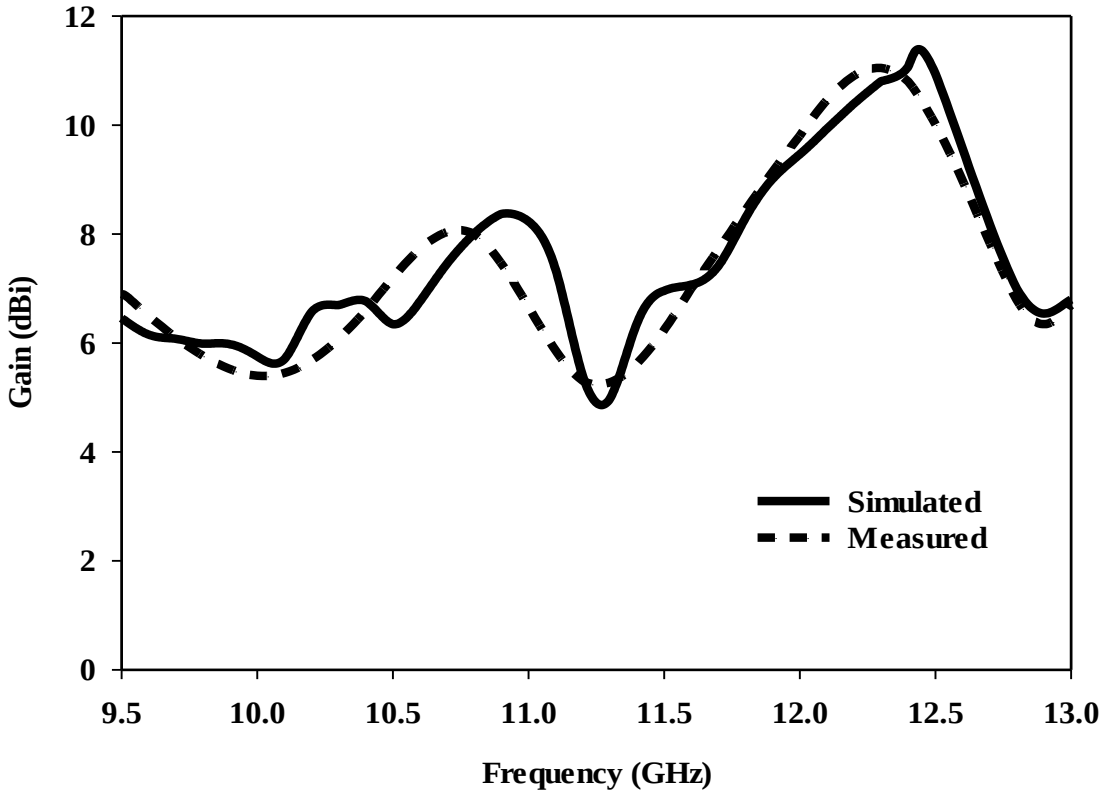

Figure 4.27: Gain of a multi-layer CP CDDRA when δa=7.5mm.

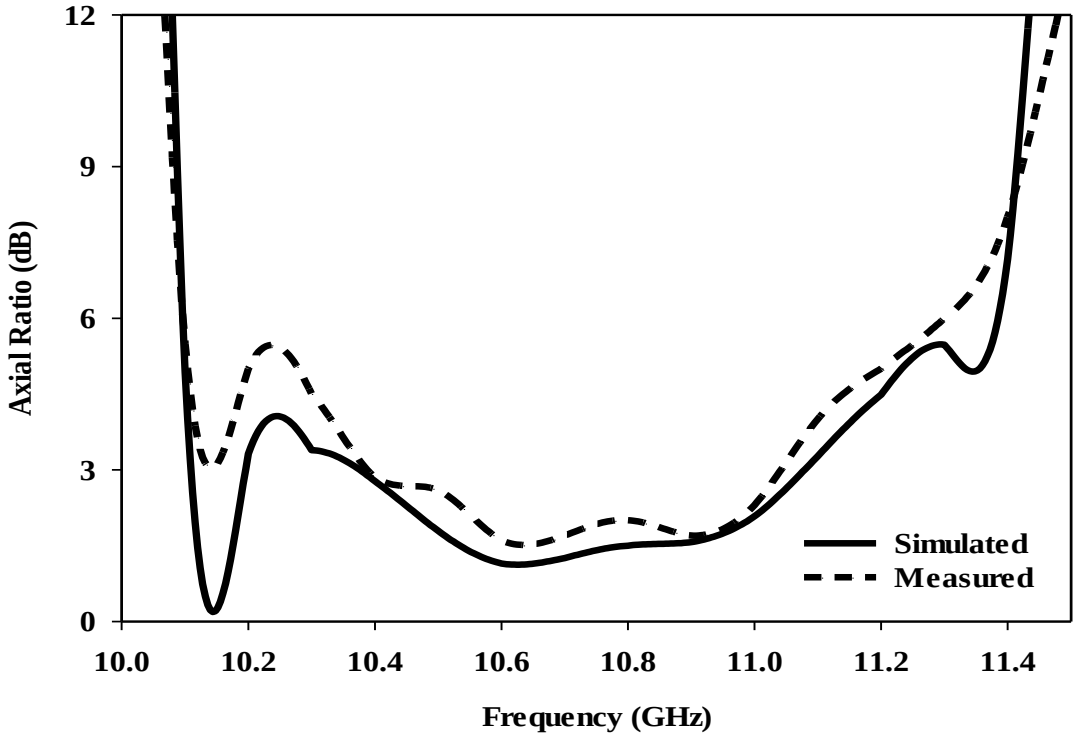

Figure 4.28: Axial Ratio as function of frequency of a multi-layer CP CDRA when δa=7.5mm.

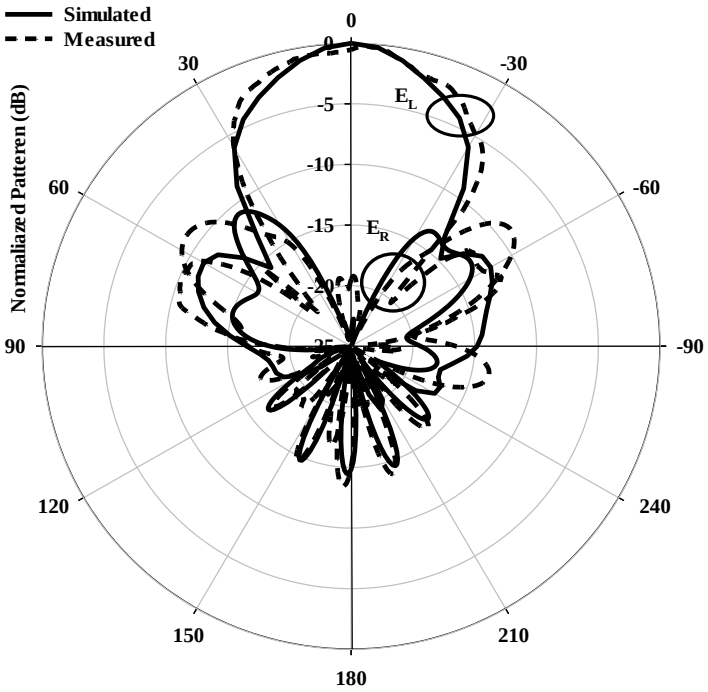

(a)

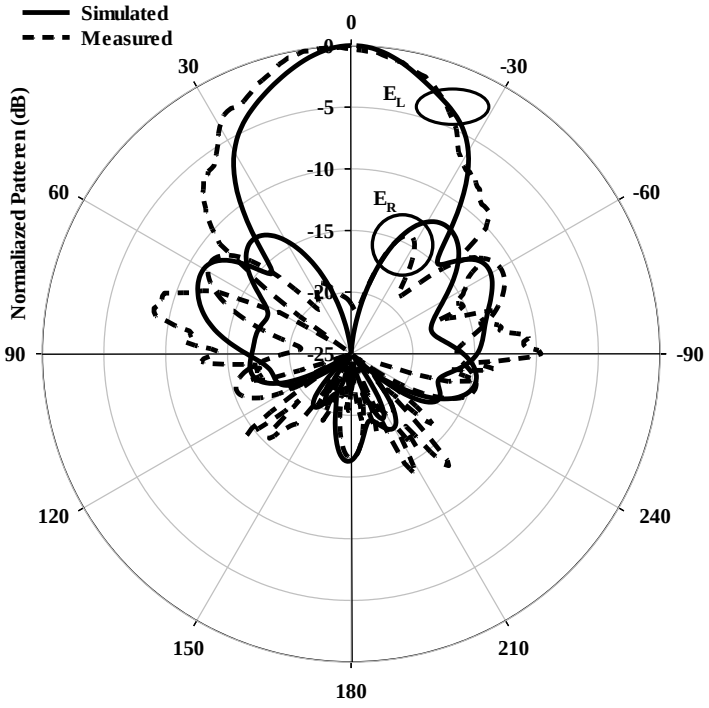

(b)

Figure 4.29: Radiation patterns of a multi-layer CP CDRA when δa=7.5mm at 10.6GHz (a) $\phi=0^0$ (b) $\phi=90^0$.

The axial ratio has been simulated and measured at the boresight, $\theta=0^0$, as function of frequency as depicted in Figure 4.28. For the axial ratio, the simulation predicts a

broadside 3-dB AR bandwidth of 6.79%, 10.4 to 11GHz, which is close to the corresponding measured counterpart. Figure 4.29 illustrates the radiation patterns of the proposed CP CDRA with an outer layer thickness of δa=7.5mm for the HE_{119} mode at 10.6GHz within the axial ratio bandwidth. With reference to the far field patterns, a left-hand CP (LHCP) exists since the boresight E_L magnitude is greater than the E_R counterpart by more than 20dB.

4.6 Further Performance Improvements

As mentioned earlier, the antenna performance in terms of axial ratio and impedance bandwidths, as well as gain, can be improved by altering the outer layer thickness. Therefore, the second optimum design using an outer layer radius of δa=17mm has also been chosen for measurements. However, the width of the cross slot has been altered to w_{s1}=w_{s2}=0.8mm while the unequal slot arm lengths have not been altered. Figure 4.30 presents the simulated and measured reflection coefficients of the thicker circularly polarized layered CDRA, where it can be noted that the simulated impedance bandwidth of 28.3%, which covers a frequency range of 9.36–12.45GHz, agrees well with the measured counterpart of 28.3% that extends from 9.27 to 12.3GHz. Once again, two resonance modes of HE_{119} and $HE_{11,11}$ have been generated at 10.6 and 12.2GHz respectively. It should be noted that these modes have contributed to improving the gain to 13.8dBic for the HE_{119} resonance mode, and 11.7dBic for the $HE_{11,11}$ resonance mode as illustrated in Figure 4.31. The far field radiation patterns are illustrated in Figure 4.32 for the HE_{119} resonance mode at the minimum axial ratio frequency point of 10.6GHz. The left-hand circularly polarized, LHCP, has been maintained since the E_L field components in the boresight direction is more than the E_R by more than 23dB. Figure 4.33 presents the simulated and measured axial ratio with measured and simulated bandwidths of 9.5% over a frequency range of 10 to11GHz. These results confirm that by increasing the outer layer radius from δa=7.5 to 17mm, the gain can be increased from 8.6 to 13.8dBic, respectively. Once more, this enhancement can be attributed to that fact that increasing the thickness of the outer dielectric enhances the maximum energy confinement inside the dielectric resonator layer [83].

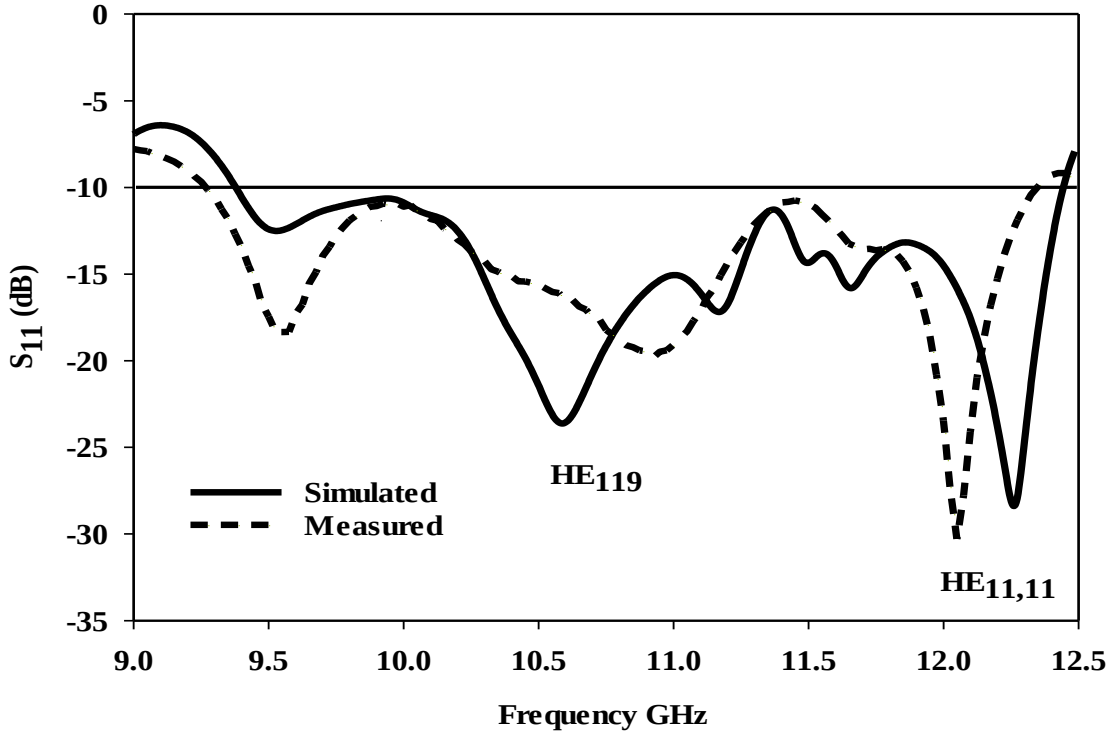

Figure 4.30: Reflection coefficient of circularly polarized layered CDRA with an outer layer radius of δa=17 mm.

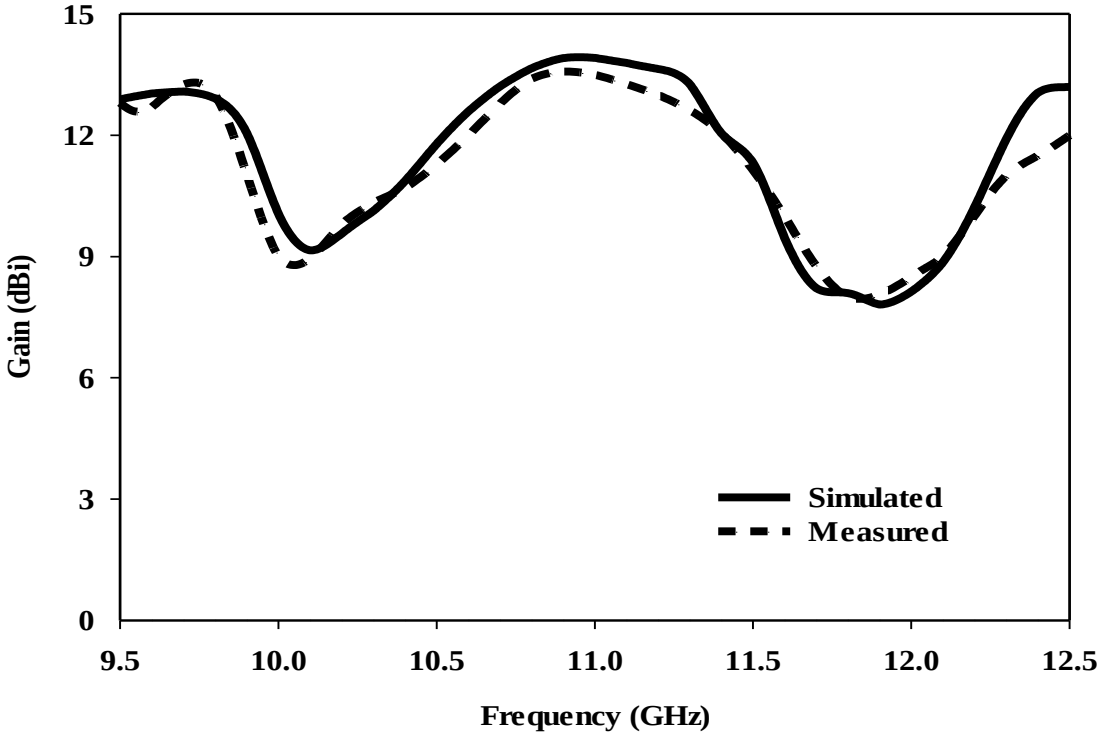

Figure 4.31: Gain of a circularly polarized layered CDRA with an outer layer radius of δa=17 mm.

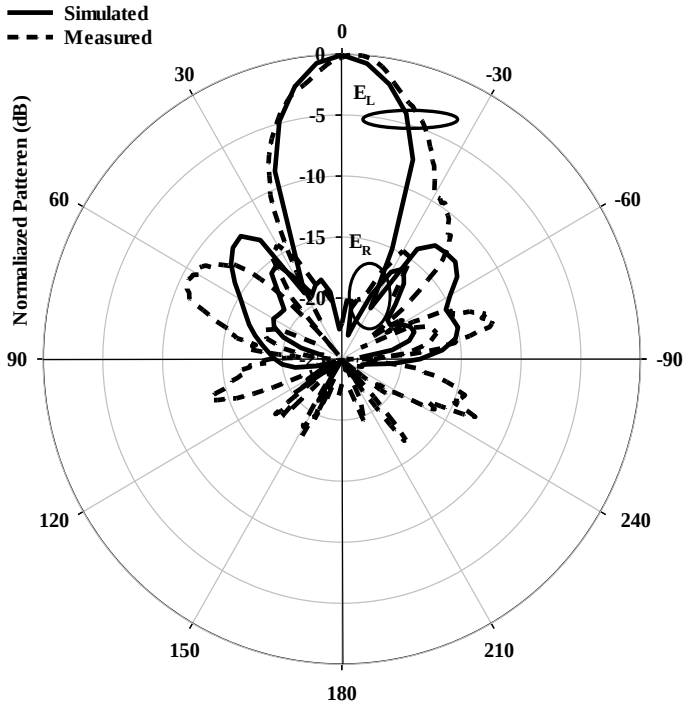

(a)

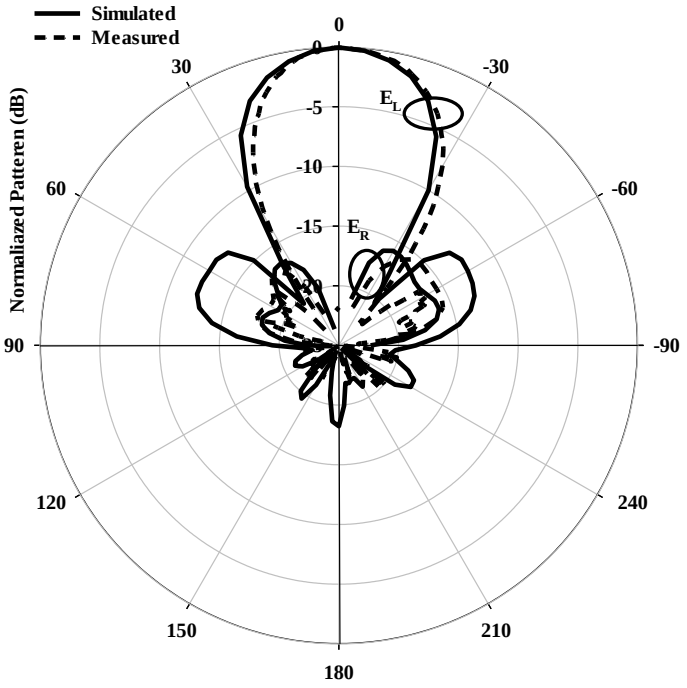

(b)

Figure 4.32: Radiation pattern of a circularly polarized layered CDRA with an outer layer radius of δa=17mm excited in the HE_{119} mode at 10.6 GHz (a) $\phi=0^0$. (b) $\phi=90^0$.

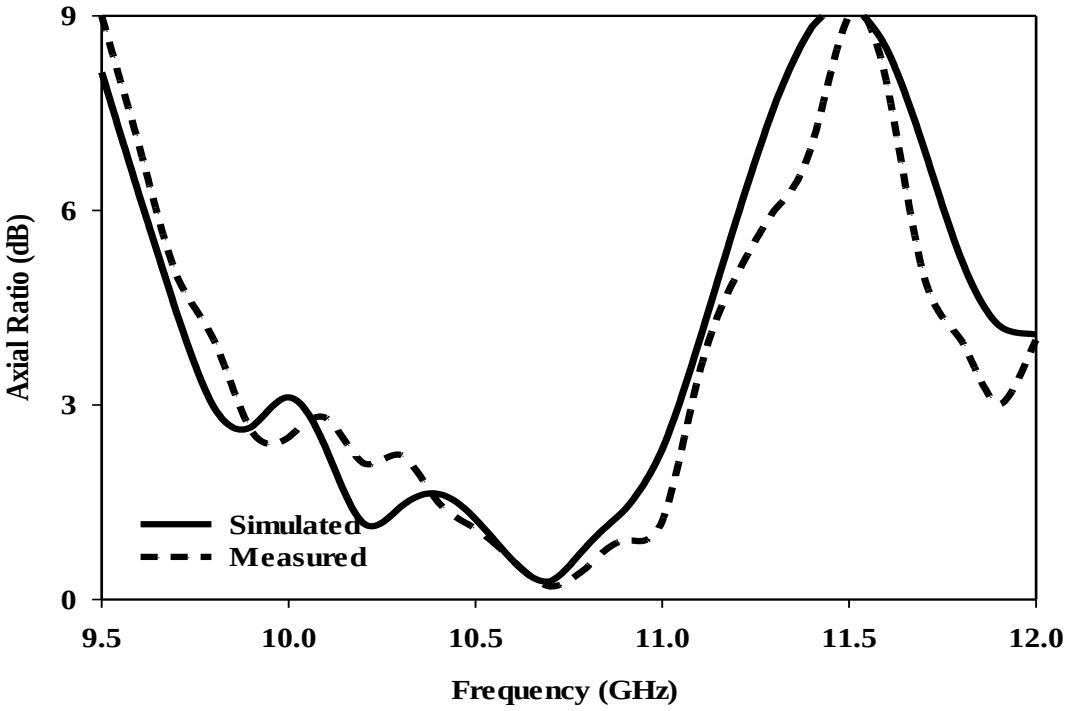

Figure 4.33: Axial ratio of a layered CDRA with an outer layer radius of δa =17mm.

Based on the aforementioned analyses and results, by increasing the outer layer radius, all the radiation characterises as well as fabrication tolerance can be improved. However, the radius of 20mm, which is equivalent~1.14λ_g, increases the physical, and electrical, antenna size considerably, which may not be appealing for applications at the considered frequency range. However, as the frequency increases, the physical antenna size will be substantially reduced. For example, at frequencies of 40 and 60GHz, the inner DRA radius will be reduced to 0.9 and 0.6mm, receptively. Therefore, the ceramic DRA will be fragile and easy to break. At the same time, the thicker outer layer radii are 6 and 4mm at 40 and 60GHz, respectively. These thicknesses will provide an extra physical support as well as the particularly needed higher gain, which represents the most important requirement from mm wave antenna. These topics will be investigated further in Chapter5. A comprehensive comparison between the proposed CP layered CDRA and the previously studied designs is summarised in Table 4-4, where it can be observed that the proposed antenna offers a wide impedance and axial ratio bandwidths, higher gain in a simple structure. It should be noted that, this is the first antenna design that offers a combination of these attractive radiation characteristics.

Table 4-4. Comparison between the proposed CP LCDRA and previously reported designs

Reference	Impedance BW	AR BW	Outer layer size	Gain dBi_c	Resonance Mode	Feeding mechanism
Proposed antenna δa =7.5mm	23.5%	6.79%	$0.5\lambda_g$	8.6	HE_{119}	Cross slot
Proposed antenna δa = 17mm	28.3%	9.52%	$1.17\lambda_g$	13.9	HE_{119}	Cross slot
[61]	28%	4.7%	-	3.5	$HE_{11\delta}$	Cross slot
[62]	9%	4%	-	3.5	-	Coaxial probe
[63]	34.5%	25.9%	-	5	-	strip feed
[64]	5.7%	1.8%	-	-	TM_{110}	probe
[65]	23.5%	7.4%	-	7	HE_{113}	Slot aperture
[66]	25.36%	3.23%	-	6.5	-	probe
[83]	88%	-	$0.77\lambda_g$	8.35	-	probe
[124]	18%	-	$0.77\lambda_g$	-	$TM_{01\delta}$	probe
[125]	45%	-	$0.85\lambda_g$	-	$TM_{01\delta}$	probe

4.8 Conclusion

In this chapter, a linearly and circularly polarized layered cylindrical DRAs have been considered theoretically and experimentally. For the linearly polarized antenna, adding the outer layer has improved the impedance bandwidth and gain to 15.8% and 13.8dBi compared to impedance bandwidth of 4.7% and gain of 7.5dBi in the absence of outer layer. Similarly, for the circularly polarized antenna, adding the outer dielectric layer provides wider impedance and axial ratio bandwidths as well as a high gain in one simple design. The two-layer CP CDRA operates in the HE_{119} mode and offer respective impedance and axial bandwidths of ∼28.3% and 9.52% in conjunction with a high gain up to 13.8 dBic, which could have not been achieved at absence of outer layer. Increasing the impedance bandwidth by coating the antenna a layer with low permittivity is expected and have been

reported in the literature. However, gain enhancement, wider axial ratio bandwidth and improved fabrication tolerance have not been demonstrated earlier for a layered antenna. Furthermore, two prototypes with outer layer radii of δa= 7.5 and 17 mm have been considered. A gain of 13.9dBic has been achieved when the thicker outer layer has been utilized. The potential of this design could be exploited further at high frequencies, for example at 60GHz where the outer layer radius will be reduced from 20 to 3mm.

Chapter 5

High Gain Wide-Band Millimetre wave DRAs

5.1 Introduction

This chapter presents simulated and measured results of mm wave layered rectangular and hemispherical DRAs. The rectangular DRA is based on that reported earlier for the x-band layered configuration, albeit with further performance improvements owing to additional optimization of the coat layer as well as the feed network. In addition, a three-layer hemispherical DRA has been considered. In contrast with its rectangular and cylindrical counterparts, hemispherical DRA has one degree of freedom, since both the resonance frequency and the radiation Q-factor are exclusively dependent on the DRA radius and permittivity. This result in a more complex design and fabrication compared to other DRAs shapes. As has been highlighted in Chapter 1, the layered hemispherical DRA has been the subject of much work in recent years for impedance bandwidth enhancement. However, the gain enhancement of hemispherical DRAs have not been investigated earlier. In this Chapter, higher order modes of a single layer hemispherical DRA will be considered first. This is followed by the design of a high gain wide-band three dielectric layers HDRA. The layer materials have been chosen based on the commercial availability having dielectric constants ε_{r1}=20, ε_{r2}=10 and ε_{r3}=3.5, for the inner, intermediate and outer layers, respectively. Both of presented hemispherical and rectangular DRAs operate over a frequency range of 20 to 31 GHz. It should be noted that mm-wave hemispherical DRAs have not been considered in the literature yet. The Chapter's plan is illustrated in Figure 5.1.

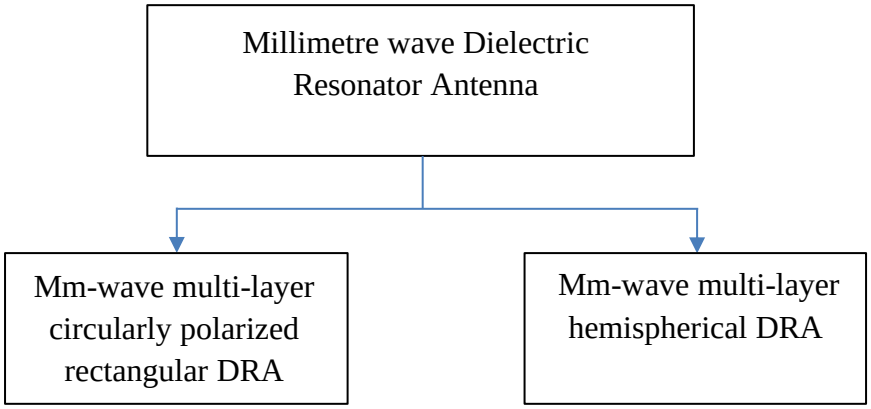

Figure 5.1: Chapter five overview.

5.2 Mm-wave Circularly Polarized Rectangular DRA

In this phase of the work, a mm-wave rectangular DRA that is working at higher order modes is designed and measured. It is worth pointing that the DRA configuration of Chapter three has been scaled down and optimized to work at the mm-wave band. Figure 5.1 illustrates the proposed RDRA geometry with an inner layer dimensions of l_1=w_1=2mm and h_1=10mm as well as a relative permittivity of ε_{r1}=10. Once more, the DRA has been coated by a Polyimide outer layer that have dimensions of l_2=w_2=12mm and h_2=11mm with a dielectric constant of ε_{r2}= 3.5. The proposed antenna has been placed on a Rogers RO4535 substrate having size of 20×20mm^2, thickness of 0.5 mm and dielectric constant of 3.5. In addition, a cross-slot with unequal arm lengths of 2.6 and 1.9 mm and identical width of 0.5 mm has been itched on the ground plane in order to generate two near resonant modes having an equal amplitude and 90^0 phase difference that are required to generate the circular polarization [61, 84]. The reflection coefficient has been measured using an E5071C vector network analyzer thorough a 50 Ω coaxial cable. A2.92 mm SMA has been utilized between the coaxial cable and the feeding strip line. The calibration has been carried out using the Agilent's 85052D calibration kit. Whereas the radiation patterns have been measured using the SNF-FIX-1.0 Spherical Near-field mm-Wave Measurement System.

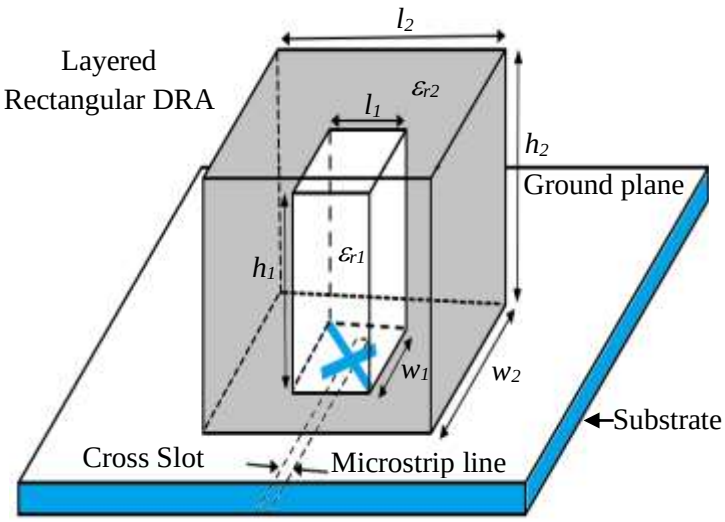

Figure 5.2: Mm-wave Layered Rectangular DRA excited by cross slot.

Figure 5.3 demonstrated a close agreement between the simulated and measured return losses with respective bandwidths of 36.3% and of 37.8% over a simulated frequency range of 21.5 to 31.1 GHz that agree well with a measured range of 21.14 to 31 GHz. From these results, it can be noted the DRA supports a multi-higher order modes operation since the following resonance modes have been excited; TE_{115}, TE_{117} and TE_{119} at 22.5 GHz, 27 GHz and 29.5 GHz, respectively. Figure 5.4 illustrates the normalized E-plane and H-plane far field patterns with close agreement between simulated and measured results that demonstrate a right hand circularly polarized (RHCP) antenna since E_R is considerably higher than E_L. However, the minor discrepancy between the simulated and measured H-plane patterns could be attributed to fabrication and measurements tolerances. The simulated and measured axial ratios agree well with each other as demonstrated in Figure 5.5. It can be noted that both of the measured and simulated CP radiations have been acquired over a frequency range of 23.4-26.7 GHz, which corresponds to an AR bandwidth of 13.73%. From Figure 5.6, it can be noted the broadside gain dropped down after 27 GHz, which can be could be attributed to the fabrication and measurements tolerances. Furthermore, Table 5-1 presents a comparison between the performances of the layered DRA to that of several reported DRA arrays [126-128]. From the tabulated data, it can be noted that the performance of the presented DRA is comparable to that of an array albeit with the advantage of utilizing a single element, which results in a smaller overall size as well as the absence of an array feed network.

Table 5-1: Comparison of the proposed antenna's performance with those of a number of DRA arrays.

Reference	Number of elements	Frequency (GHz)	Gain (dBi)	Bandwidth %	
				CP	S_{11}
Proposed DRA	1	21.5-31	12.5	13.7	36.3
[126]	4	10.5-12.5	12	16	19
[127]	6×8	59-61	18	1.64	3.33
[128]	4	27-33	12.4	-	20

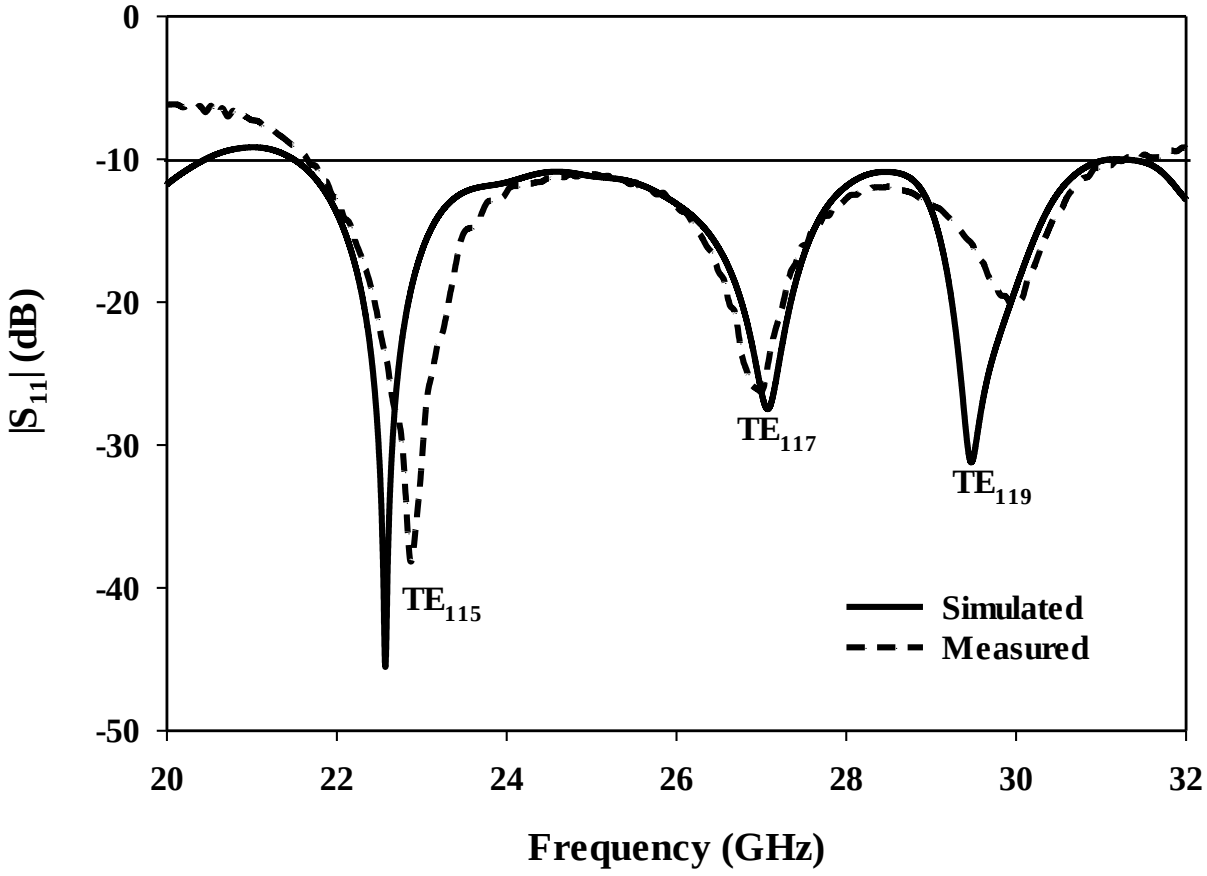

Figure 5.3: Simulated and measured return loss Reflection coefficient of a layered mm-wave RDRA.

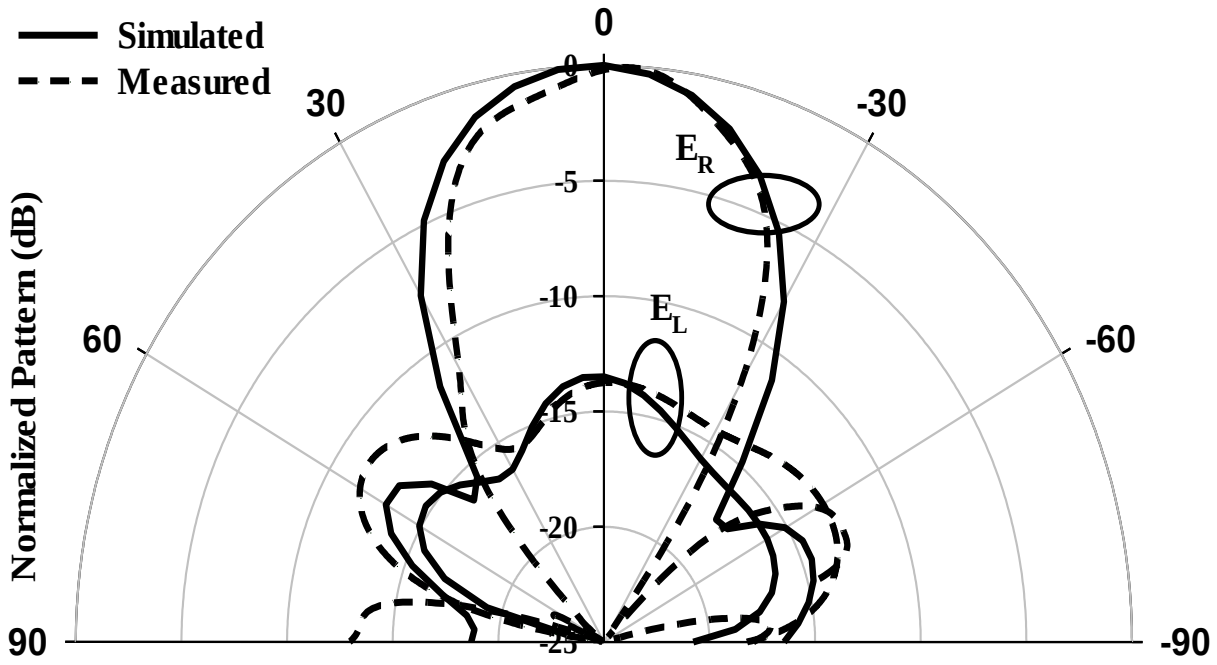

(a)

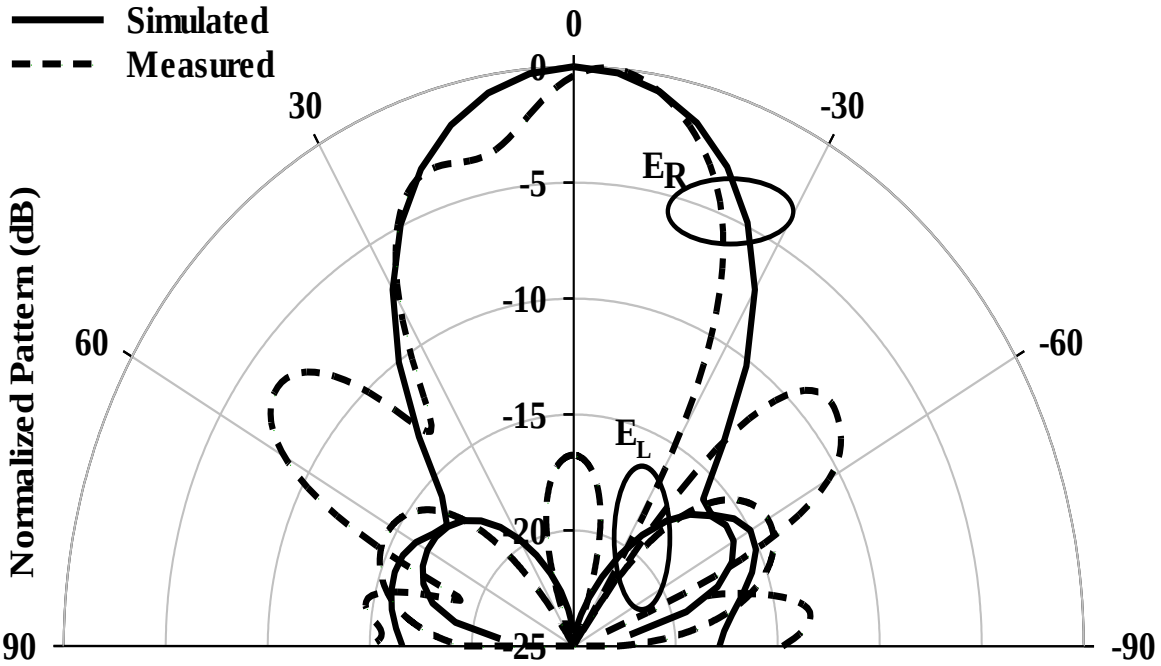

(b)

Figure 5.4. Simulated and measured of radiation 24 GHz a) phi=0^0, b) phi=90^0.

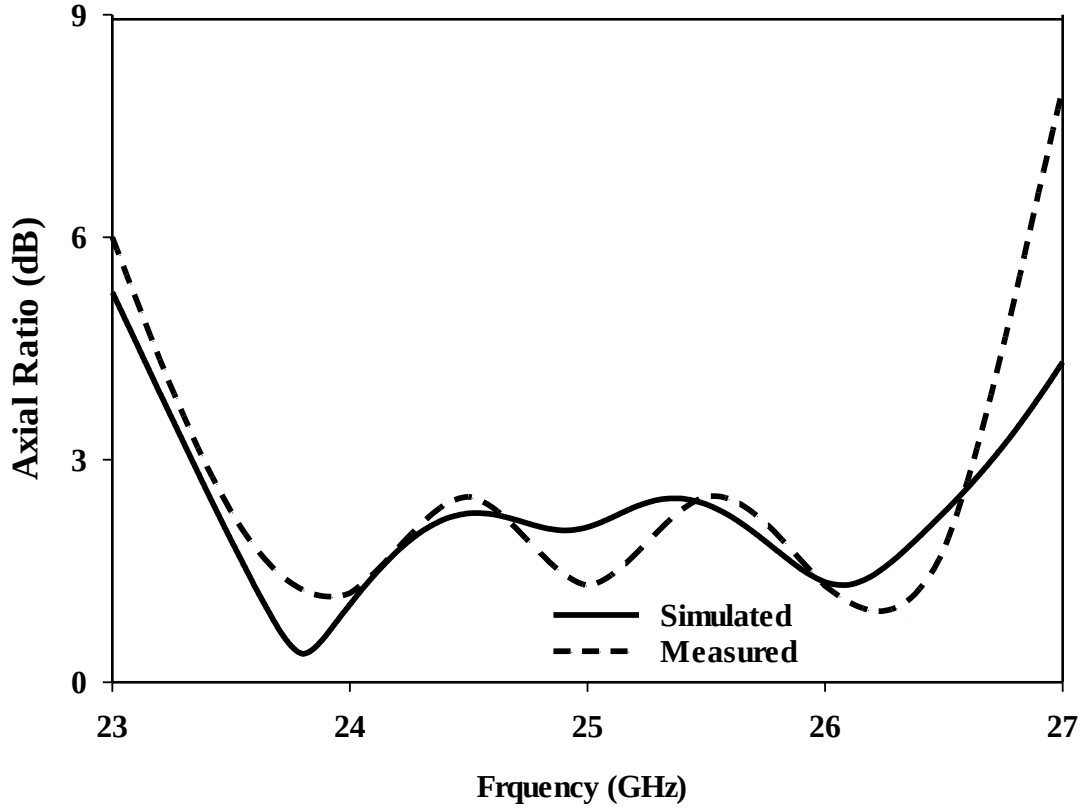

Figure 5.5 Simulated and measured axial ratios for layered mm-wave RDRA.

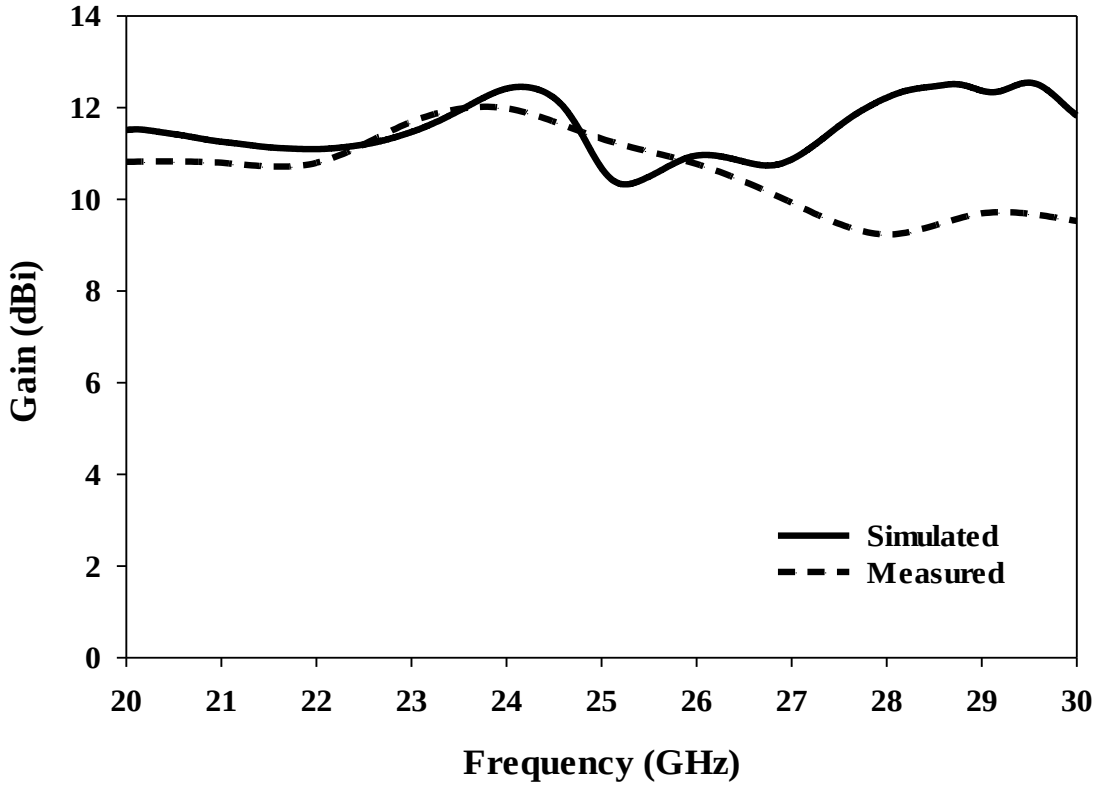

Figure 5.6: Simulated and measured of broadside gain of layered mm-wave RDRA.

5.3 Hemispherical DRA excitable modes

Figure 5.7 shows a hemispherical DRA geometry is defined by a radius of *a* and a dielectric constant ε_r with an aspect ratio of 0. As a result, the resonance modes are exclusively dependent on the DRA's radius and dielectric constant. Therefore, HDRAs exhibit the least flexibility with respect to the choice of design parameters. Furthermore, the fabrication of a hemispherical DRA is relatively difficult and more expensive compared to other regular DRA geometries. Similar to the cylindrical and rectangular DRAs counterparts, the power can be coupled to the HDRAs throughout probe [129], slot aperture [130] and conformal strip line [67]. Due to the small dimensions at the mm-wave band, a probe feeding is unsuitable due to the need of drilling a hole inside a solid ceramic structure, which results in unavoidable air-gap dimensions that can considerable with respect to the shorter wavelength. However, a slot feeding mechanism is more favourable at high frequencies sine it is easier to fabricate and isolates the antenna from the feed network, which eliminates any spurious radiation. In addition, HDRAs can support only two modes based on the chosen feed mechanism. For example, when the HDRA is fed using a slot aperture, transverse electric modes (TE_{mpn}) will be dominated [130]. On the other hand, transverse magnetic (TM_{mpn}) field modes will be achieved when the hemispherical DRA is fed using a probe [131]. The mode indices, *m, p, n* denote the variation of the fields in the elevation, azimuth and radial directions, respectively,. Furthermore, the lowest order TE mode is the TE_{111}, which is equivalent to a short horizontal magnetic dipole that it is equivalent to a short electric monopole when TM_{101} is the lowest order mode of TM modes [1]. It is worth mention that, the lowest order mode TE_{111} resonance frequency can be calculated from the following equation [132]

$$\frac{J_{1/2}\left(\sqrt{\varepsilon_r}k_0a\right)}{J_{3/2}\left(\sqrt{\varepsilon_r}k_0a\right)} = \frac{H^{(2)}_{1/2}\left(k_0a\right)}{\sqrt{\varepsilon_r}H^{(2)}_{1/2}\left(k_0a\right)} \tag{5-1}$$

where $J_{(x)}$ is the first kind Bessel function and $H^{(2)}_{(x)}$ is the second kind Henkel function *[132]*. Once the solution of k_o, being determined, the expected resonance frequency f_0 can be determined by

$$f_0 = \frac{4.7713\,\mathrm{Re}\left(k_0a\right)}{a} \tag{5-2}$$

In this research CST MWS is utilized for investigating the mode order due to the complexity of HDRA Eigen mode equations.

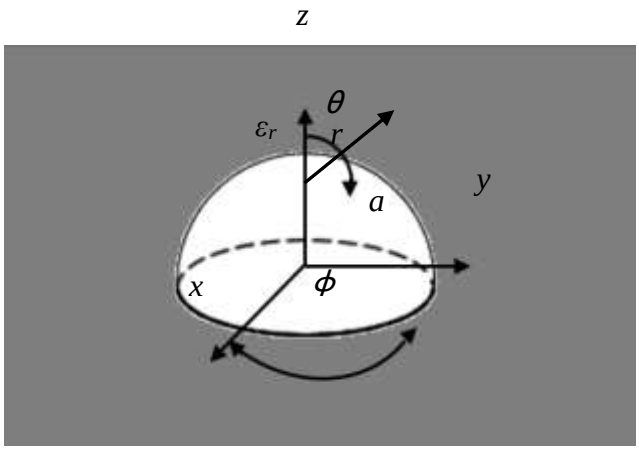

Figure 5.7: Geometry of Hemispherical DRA.

5.4 Higher Order Mode mm-wave Hemispherical DRAs

In this section, exciting a higher order mode to increase the antenna gain will be investigated. Therefore, a hemispherical DRA that has a relative permittivity of 10 and radius of 11 mm has been chosen and placed above a ground plane placed on the top of a 25 mm^2 Roger RO4003 substrate with thickness of 0.4 mm and ε_r of 3.38. The DRA has been excited by etching a cross-slot aperture in the metal ground plane. The cross-slot has two arms with equal widths and lengths of 1.35 mm and 3 mm, respectively. With reference to Figure 5.8, it can be observed that the proposed antenna supports three higher order resonance modes of TE_{919}, $TE_{11,1,11}$ and $TE_{13,1,13}$ at 21.3 GHz, 24.6 GHz and 29.5 GHz, respectively, which provide respective impedance bandwidths of 3.3% , 2.4% and 2.7% as well as gains of 6.8 dBi, 8.8 dBi and 10.7 dBi respectively. The radiation patterns of the $TE_{13,1,13}$ mode are presented in Figure 5.9 with a maximum gain of 10.7 dBi that has been has been achieved due to the increased number of short magnetic dipoles of a higher order mode operation as can be observed inform Figure 5.10. In addition, the HDRA has also been simulated with a size of 15mm to excite the $TE_{15,1,15}$ mode at 28.6 GHz that offered a slight gain increment to 11.2 dBi in conjunction with a narrow impedance bandwidth of 0.1%. As mentioned earlier in Chapter 1, the DRAs size is proportional to $\frac{\lambda_0}{\sqrt{\varepsilon_r}}$. Therefore, the antenna permittivity will

be increased in order to decrease the antenna size while maintaining the higher gain higher. As expected, the achieved high gain is associated with a narrow bandwidth that cannot meet the 5G requirements. Further, the DRA footprint is relatively large and may impose a limit on the applicability of the proposed high gain DRA. Therefore, a higher DRA relative permittivity of 20 and an optimized radius of 4.5 mm has been considered in order to design a smaller high gain hemispherical DRA.

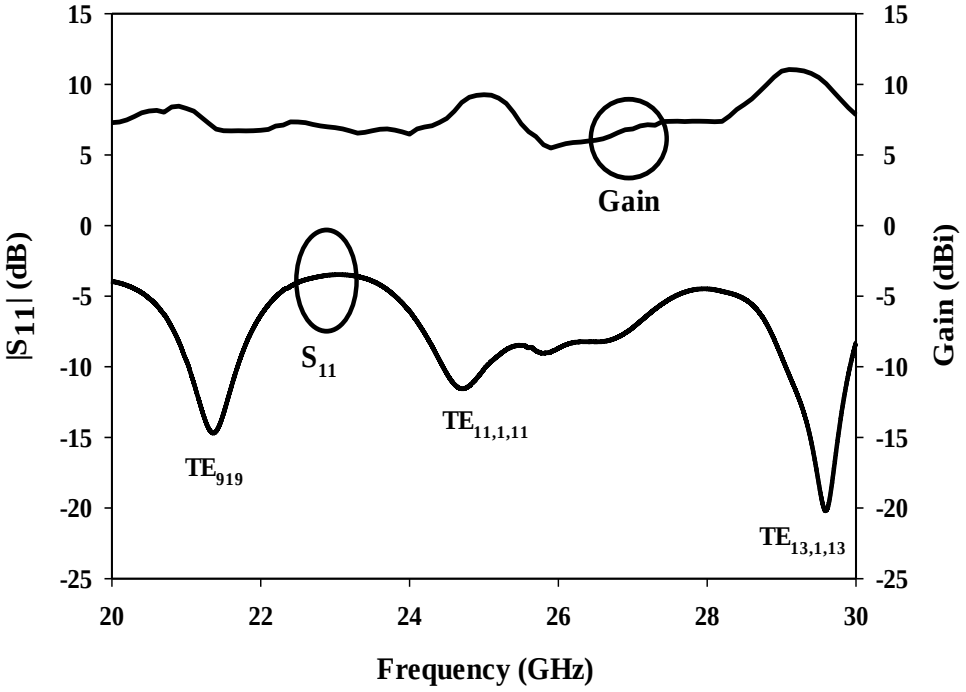

Figure 5.8: Reflection coefficient and gain of a single layer HDRA with ε_r=10.

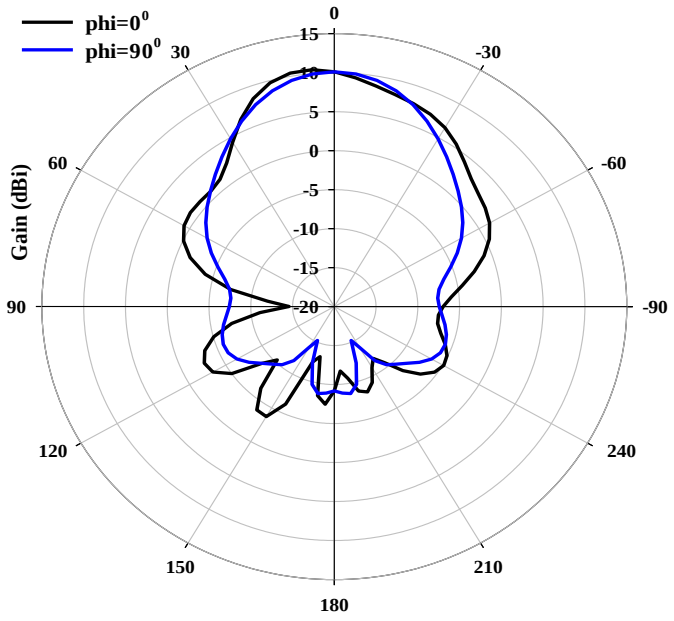

Figure 5.9: Radiation patterns of $TE_{13,1,13}$ mode at 29.9 GHz in the phi=0^0 and phi=90^0 planes.

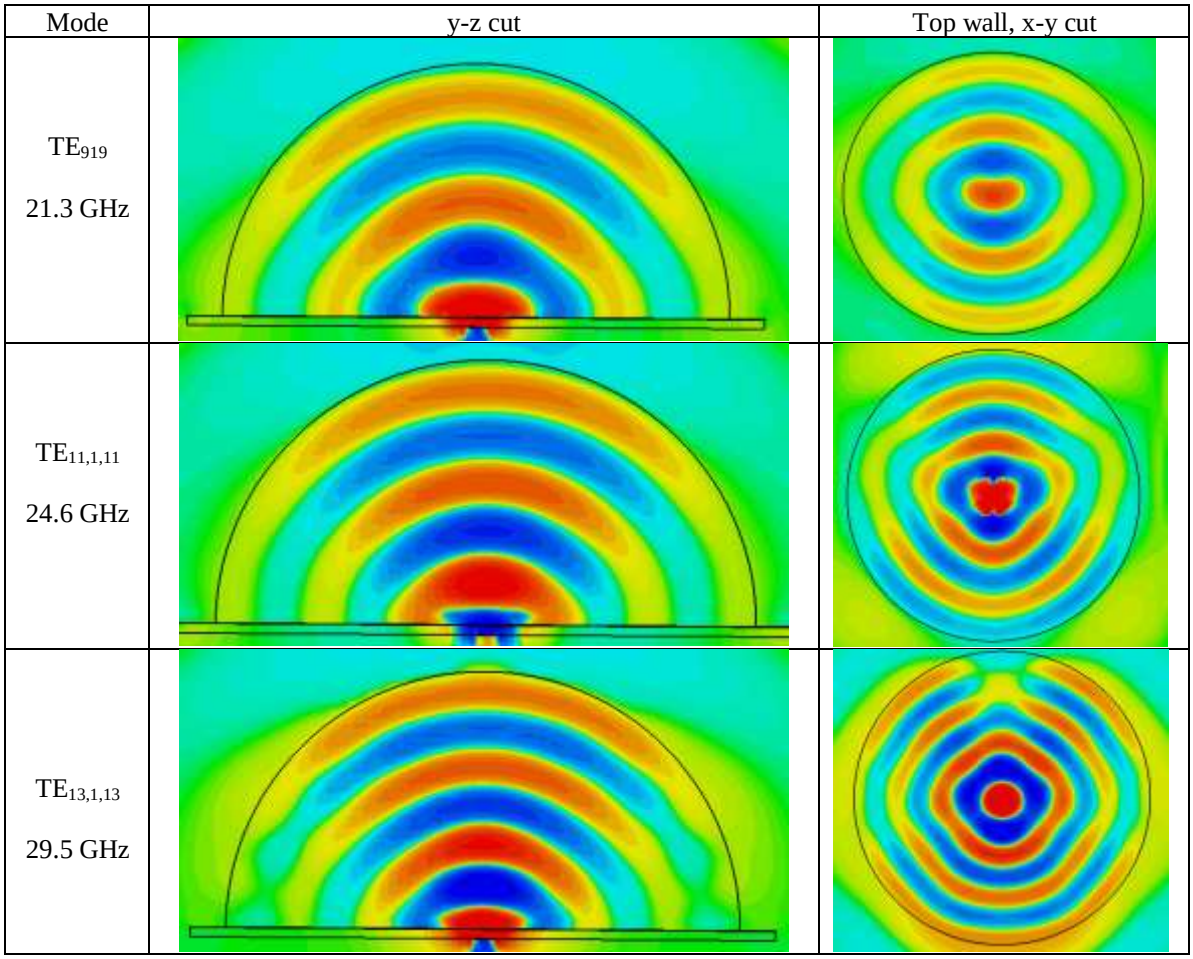

Figure 5.10: Magnetic field distribution inside a hemispherical DRA of ε_r=10 excited in TE_{919} $TE_{11,1,11}$ and $TE_{13,1,13}$ resonance modes.

In addition, the cross-slot arms' length and width have been optimized to 5 mm and 1.35 mm, respectively, and used in conjunction with a stub length of 1.25 mm for optimum matching. The reflection coefficient is presented in Figure 5.11, where it can be noted the TE_{515} and TE_{717} modes have been excited at 21.5 GHz and 28.5 GHz, with an impedance bandwidths of 5.46% and 4.5%, respectively. It should be noted these bandwidths are wider than those Figure 5.8, which can be explained as a result exciting lower order modes due to the smaller DRA size. The magnetic field distribution for the TE_{515} and TE_{717} resonance modes at 21.5 and 28.5 GHz are depicted in Figure 5.12. In addition, Figure 5.13 presents the radiation patterns of the proposed smaller hemispherical DRA at 21.5 and 28.5 GHz where it can be noted that the excited DRA modes offer gains of ~ 10 dBi for both the TE_{515} and TE_{717} modes, which are comparable to those of the lower permittivity larger size DRA considered earlier.

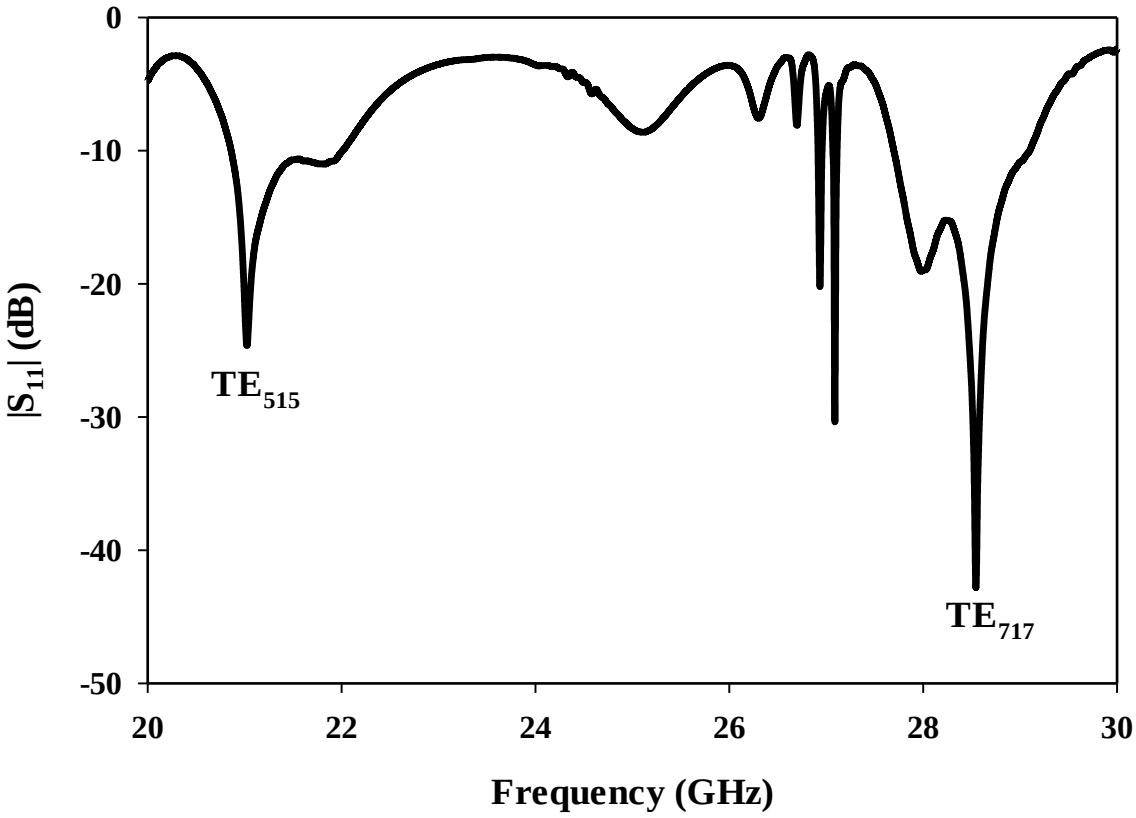

Figure 5.11: Simulated S-parameters of a single layer hemispherical DRA when ε_r=20.

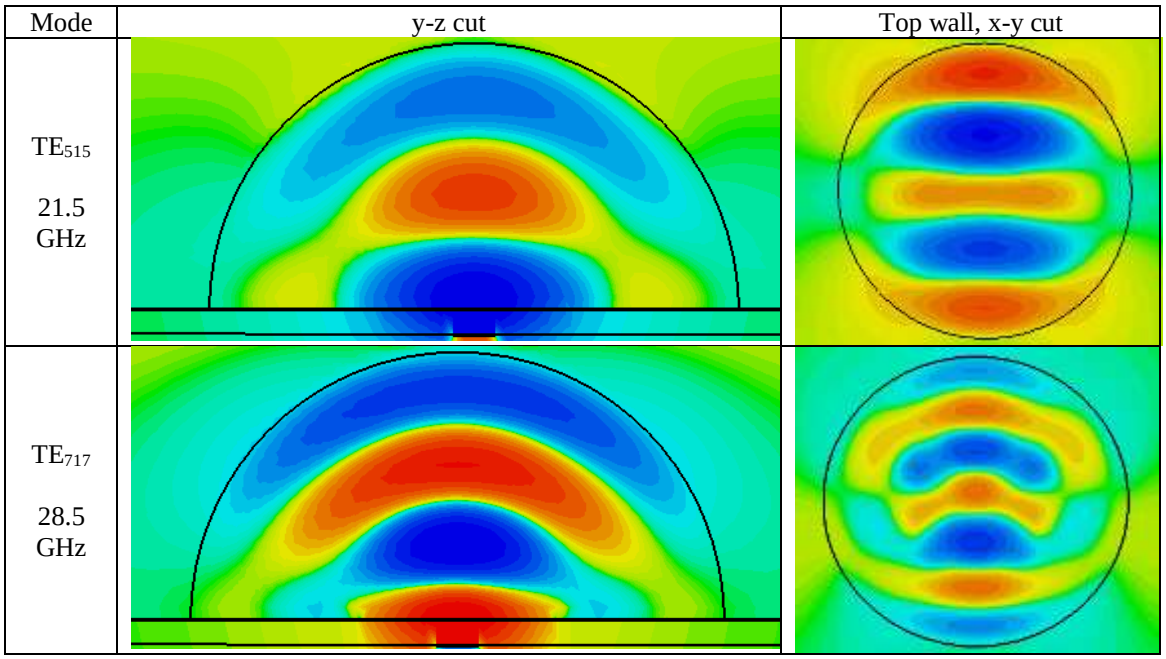

Figure 5.12: Magnetic field distribution inside a hemispherical DRA of ε_r=20 excited in TE_{515} and TE_{717} resonance modes.

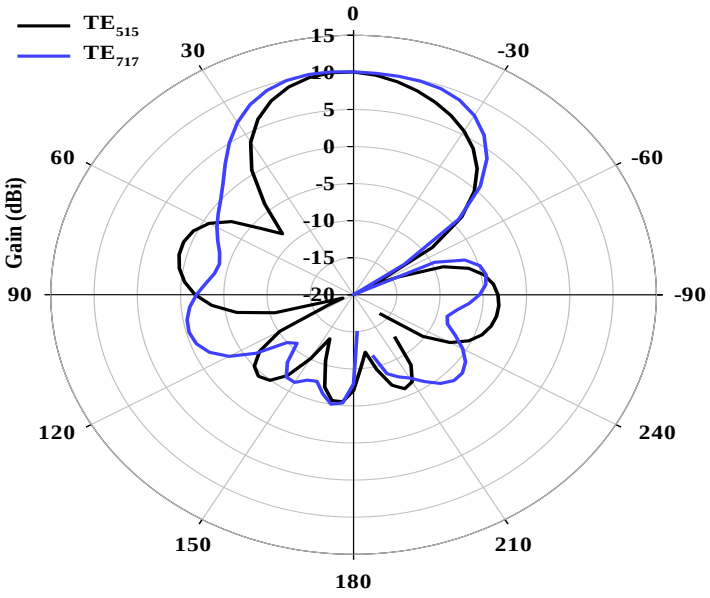

(a)

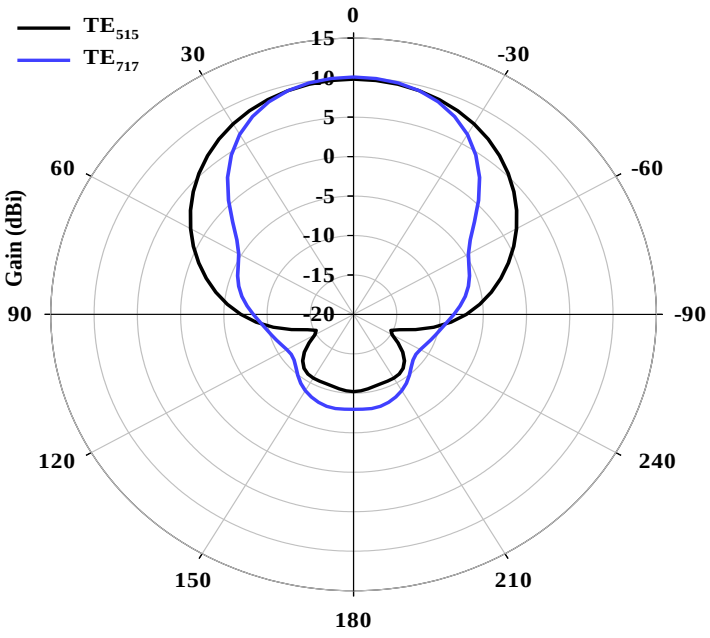

(b)

Figure 5.13: Radiation patterns of a single layer HDRA operating at the TE_{515} and TE_{717} modes at 21.5 and 28.5GHz. (a) $\phi=0^0$. (b) $\phi=90^0$.

To sum up, high gains have been acquired for both low and high DRA permittivities, albeit with approximately half the DRA in the latter case. In addition, although the smaller size DRA offered almost double the bandwidth, it is still relatively narrow to meet the requirements of the high data rates in 5G communication systems. This challenge will be addressed in the next section.

5.5 Multi-layer Millimetre Wave HDRA

5.5.1 Two-layer Configuration

In this section, a lower permittivity dielectric coat will be incorporated in the proposed hemispherical DRA of section 5.4. The main goal of this investigation is to enhance the impedance bandwidth, while maintain a high gain, for a higher order mode hemispherical DRA. The cross-slot fed two-layer hemispherical DRA configuration is illustrated in Figure 5.14, where, once more, the inner and outer layers permittivities have been chosen based on availability of the dielectric materials. With reference to Table 5-2 and Figure 5.15, it can be observed that for a hemispherical DRA with ε_{r1}=10 and coated by an outer layer of ε_{r2}=3.5, wider impedance bandwidth of 18.8% has been achieved in conjunction with lower gain and larger size compared to that of a DRA counterpart with ε_{r1}=20. On the other hand, increasing ε_{r1} to 20 has provided a higher gain with a lower impedance bandwidth. It should be pointed that using a material with ε_{r2}=3.5 to provide a coat for hemispherical DRA of ε_{r1}=20 reduces the reflections at the coat-air interface, while maintaining strong wave reflections at the coat-DRA interface due to the considerable differences in the two materials permittivity. Similarly, coating the same DRA with a layer of Alumina, ε_r=10, reduces the wave reflections at the DRA-coat interface albeit with stronger reflections at the coat-air interface. As a result, utilizing a DRA with ε_{r1}=20 with a coat layer of ε_{r2}=3.5 improves the bandwidth and reduces the gain compared to that of a single layer DRA. On the other hand, if the same DRA is coated by a material with ε_{r2}=10 then higher gain with narrower impedance bandwidth are achieved. Therefore, a multiple coat layers configuration needs to be considered in order to accomplish a high gain wide-band hemispherical DRA. The multi-layer coat acts as a multi-stage transition region between free space and the DRA element with minimised wave reflections at all dielectric interfaces. This analysis will be demonstrated in the next section in conjunction with experimental results.

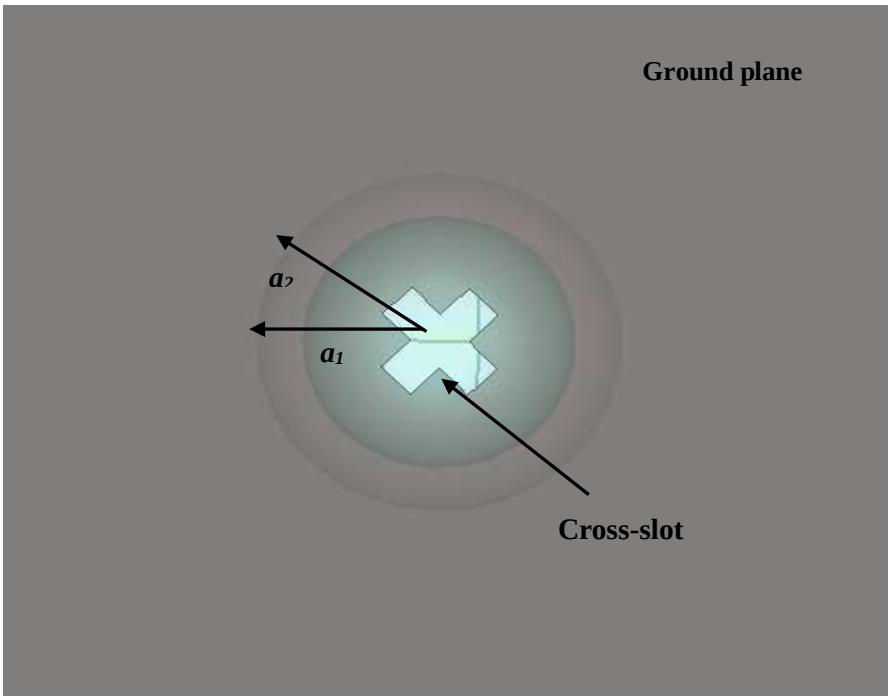

Figure 5.14: Two-layer HDRAs fed by cross-slot.

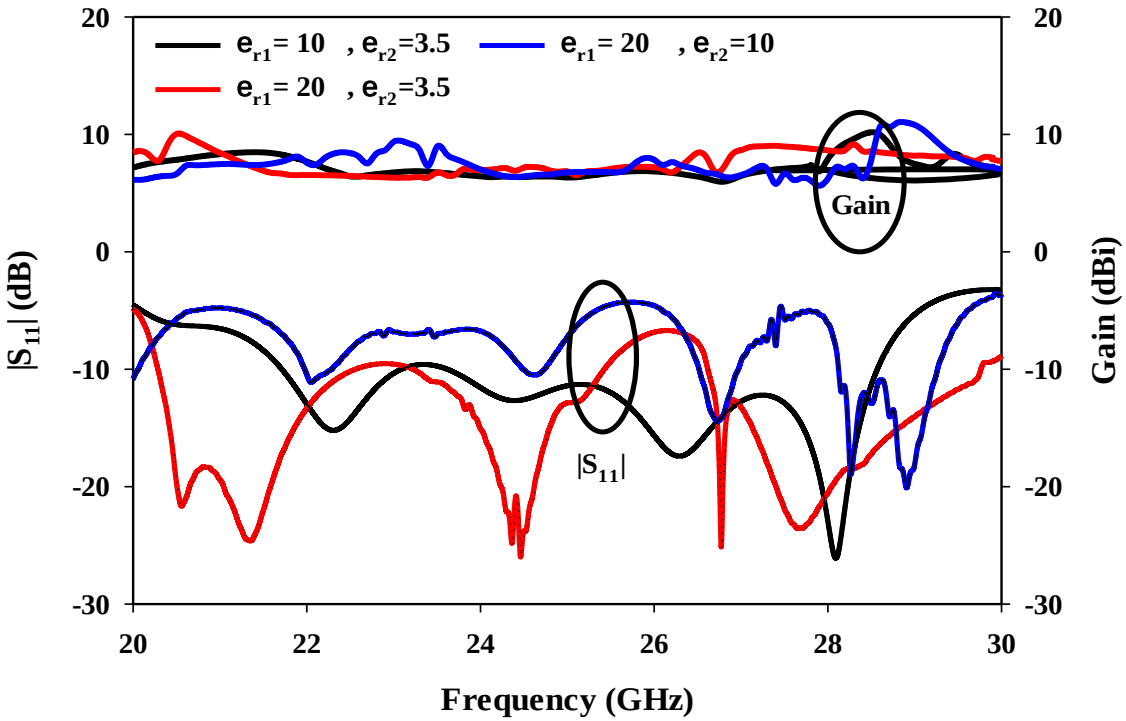

Figure 5.15: Return loss and various dielectric constants for the inner and outer layers of the proposed hemispherical DRA.

Table 5-2: Companion the performances of various layered hemispherical DRA configurations with different ε_{r1} and ε_{r2}.

Dielectric constant		radius (mm)		Gain dBi	Impedance bandwidth %
ε_{r1}	ε_{r2}	a_1	a_2		
10	1	11	-	10.7	2.7
10	3.5	4.5	10	7	18.8
20	1	4.5	-	10	5.46
20	3.5	4.5	6	8.2	11.1
20	10	4.5	6	11	4

5.5.2 Three-layer mm-wave Hemispherical DRA.

A three-layer hemispherical DRA is presented in Figure 5.16with a cross slot feed. The cross-slot arm lengths and widths have been optimised as l_{s1}=l_{s2} = 4 mm and w_{s1}=w_{s2} =1.35 mm, respectively. The optimum practical relative permittivities of the three layers have been chosen as ε_{r1}= 20, ε_{r2}=10 and ε_{r3}=3.5. These dielectric constants have been chosen in order to achieve the wide bandwidth and high gain combination. The inner layers have been fabricated using E-20 ceramic and Alumina while the outermost layer has been fabricated using 3D printing technology. The layers radii have been chosen as a_1=4.5mm, a_2=6.5m, and a_3=8mm. Furthermore, the outer two dielectric layers have not been glued to each other during the fabrication process. In order to ensure optimum matching, the open stub length has been chosen as ls_{tub}=1.25 mm.

A prototype has been mounted on ground plane, where a double-sided adhesive copper tape has been utilized in order to eliminate the potential air-gaps and keep the antenna stable with respect to the feed network, otherwise the antenna may be shifted due to the smaller size.

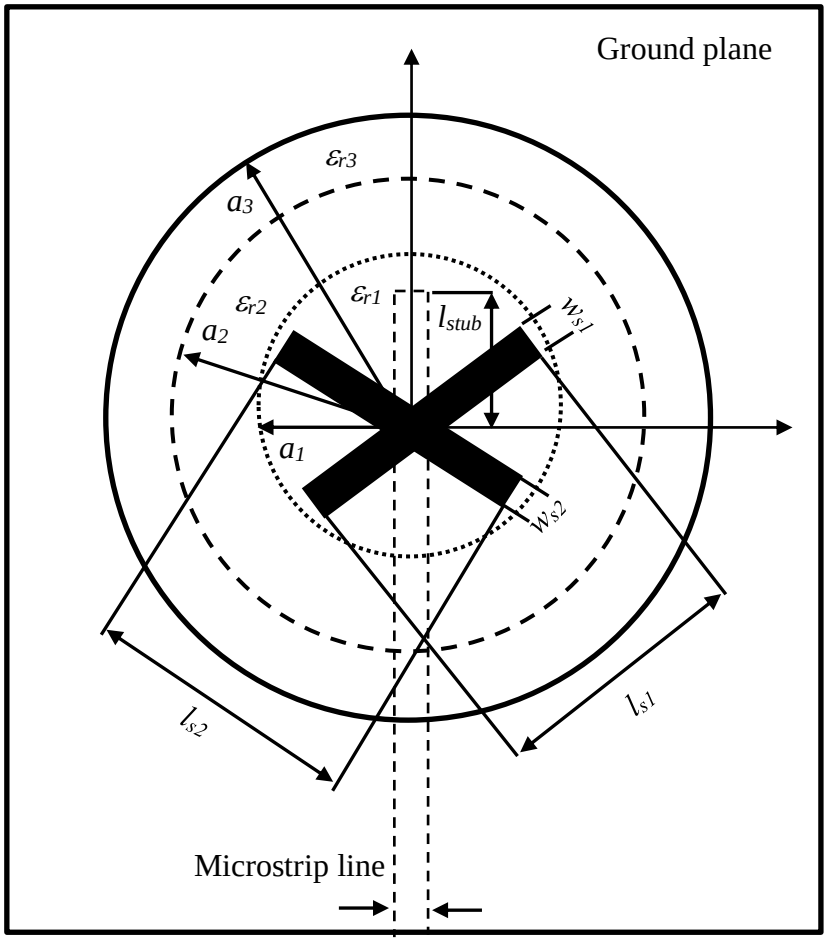

(a)

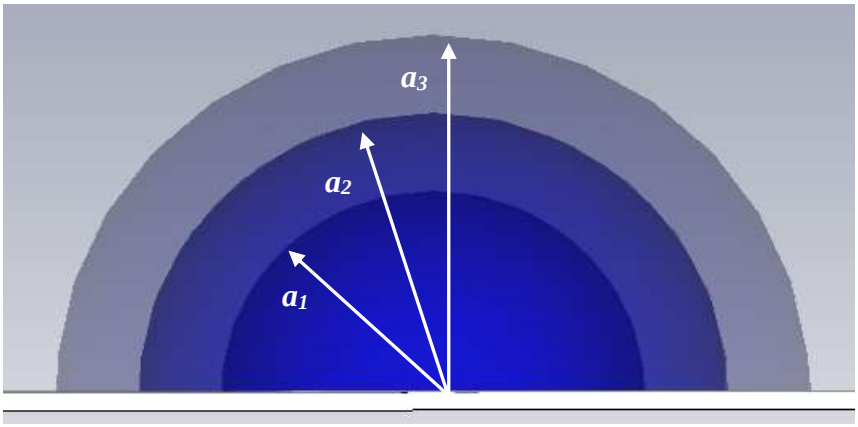

(b)

Figure 5.16: The configuration of three layers hemispherical DRA excited by cross slot (a) top view, (b) side view.

The CST MWS [103] has been utilized to optimize the three layer thicknesses in order to come up to final design. It is worth pointing that the proposed HDRA supported the TE_{515} and TE_{717} higher order modes. Figure 5.17 presents the porotype of the designed multilayer

hemispherical DRA and its feed network. Meanwhile, a small air gab has been noted between the first two layers that can be attributed to the subtractive manufacturing process that used for fabrication. The measured and simulated reflection coefficients are presented in Figure 5.18. The results correlated well with each other, where a simulated bandwidth of 35.8% has been achieved over a frequency range of 20.8 to 29.9 GHz, compared to a measured bandwidth of 35.5% over a frequency range of 20.5 to 29.4 GHz. The magnetic field distribution inside the three layers hemispherical DRA is presented in Figure 5.19. The simulated and measured radiation patterns of the TE_{515} and TE_{717} modes are depicted in Figure 5.20 and 5.21 in both principle E and H plane and s at 21.9 29 GHz. Reasonable agreement has been achieved between experimental and simulated data with minor degradation at the E-plane side lobes that could be attributed to measurement or fabrication tolerances[25]. Furthermore, close agreement has been achieved between measured and simulated gains as demonstrated in Figure 5.22. A comprehensive comparison between the proposed antenna against those reported in the literature is tabulated in Table 5-3, where it can be observed that, even though the proposed design is slightly larger, it combines higher gain and wider bandwidth, which outperforms the earlier deigns that generally offer wider bandwidth in conjunction with a lower gain. Therefore, it can be concluded that the first mm-wave hemispherical DRA has been reported with a gain that considerably exceeds those of lower frequencies counterparts while maintaining a wideband operation.

Figure 5.17: Prototype of a multi-layer mm-wave hemispherical DRA before and after assembly.

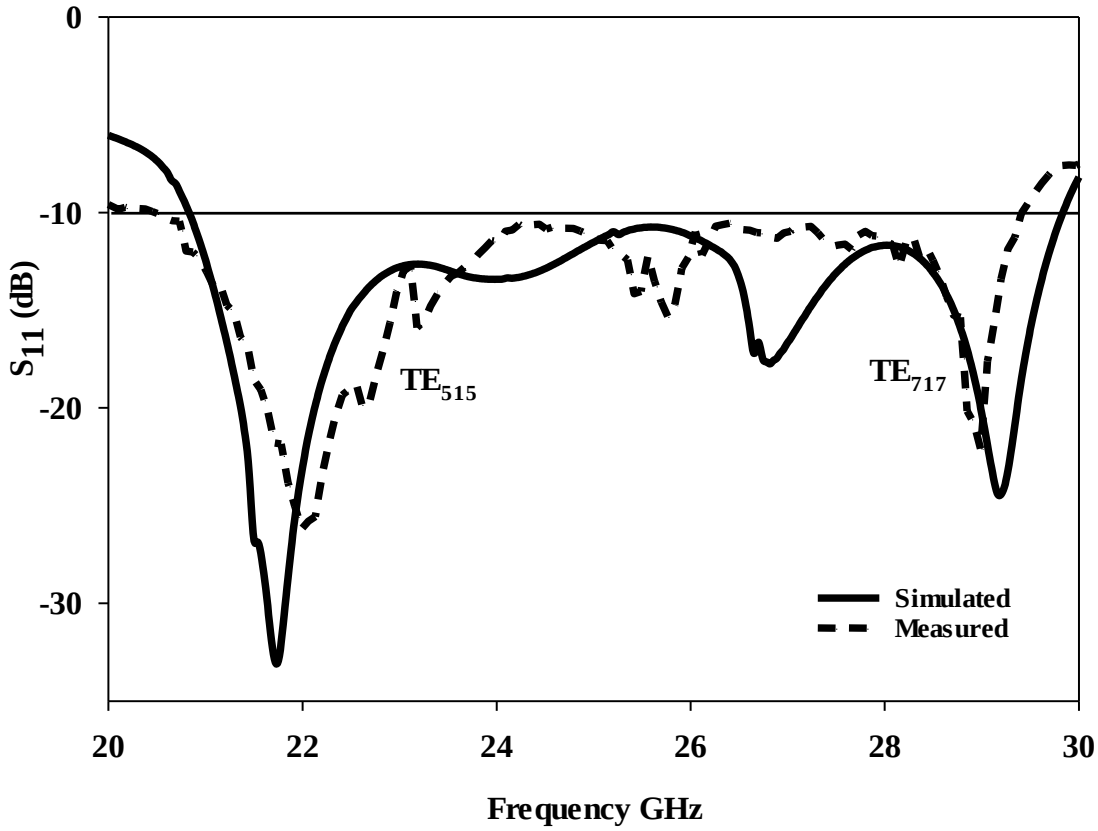

Figure 5.18: Return losses of a three-layer hemispherical DRA.

Mode	y-z cut	Top wall, x-y cut
TE_{515} 21.9 GHz	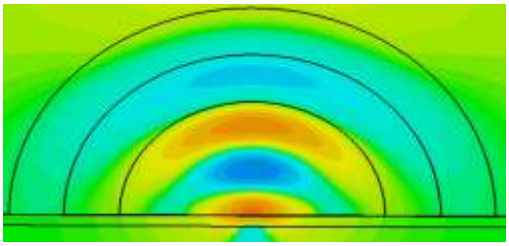	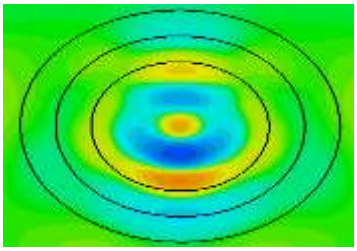
TE_{717} at 29 GHz	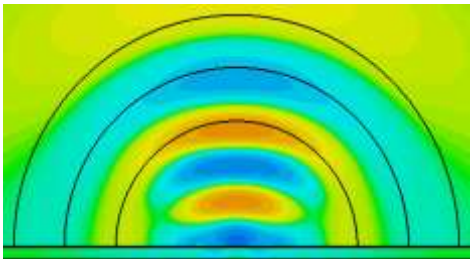	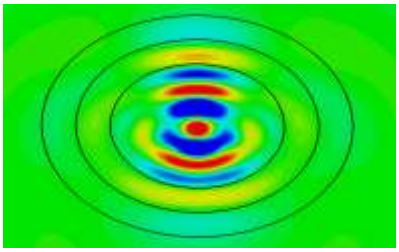

Figure 5.19: Magnetic field distribution inside the three layers hemispherical DRA for the TE_{515} and TE_{717} resonance modes.

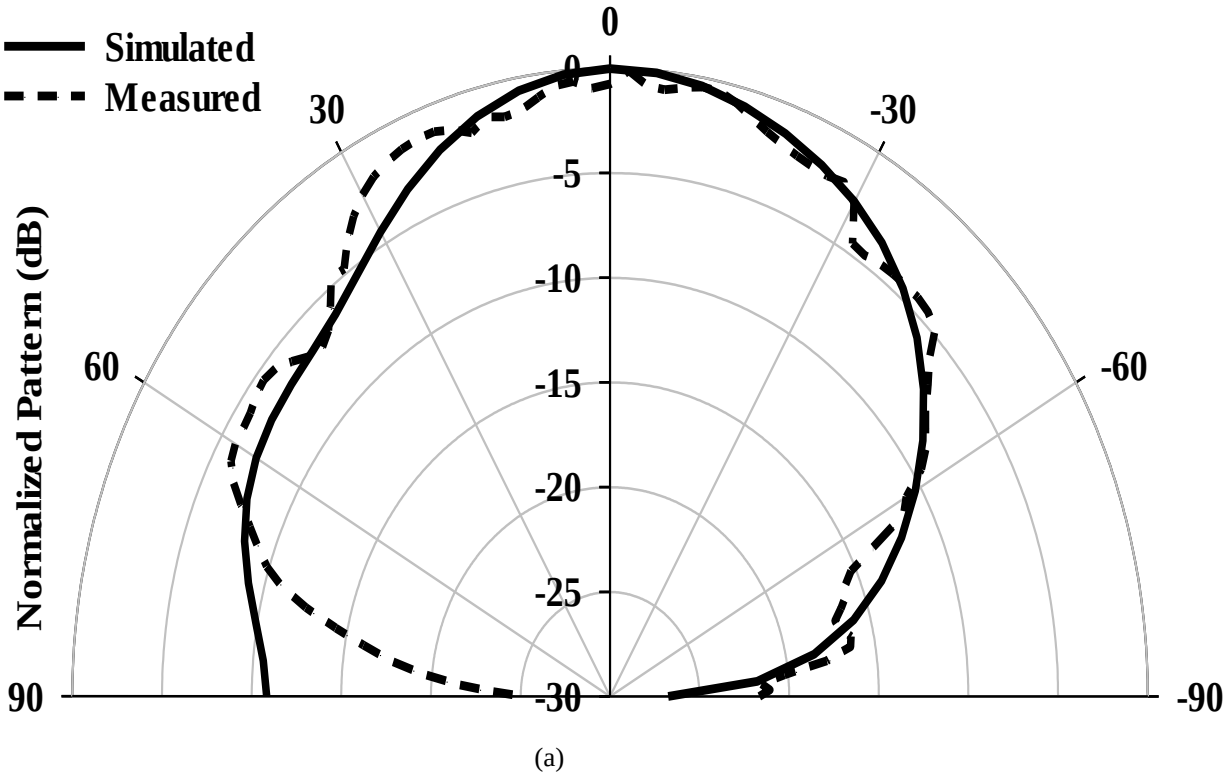

(a)

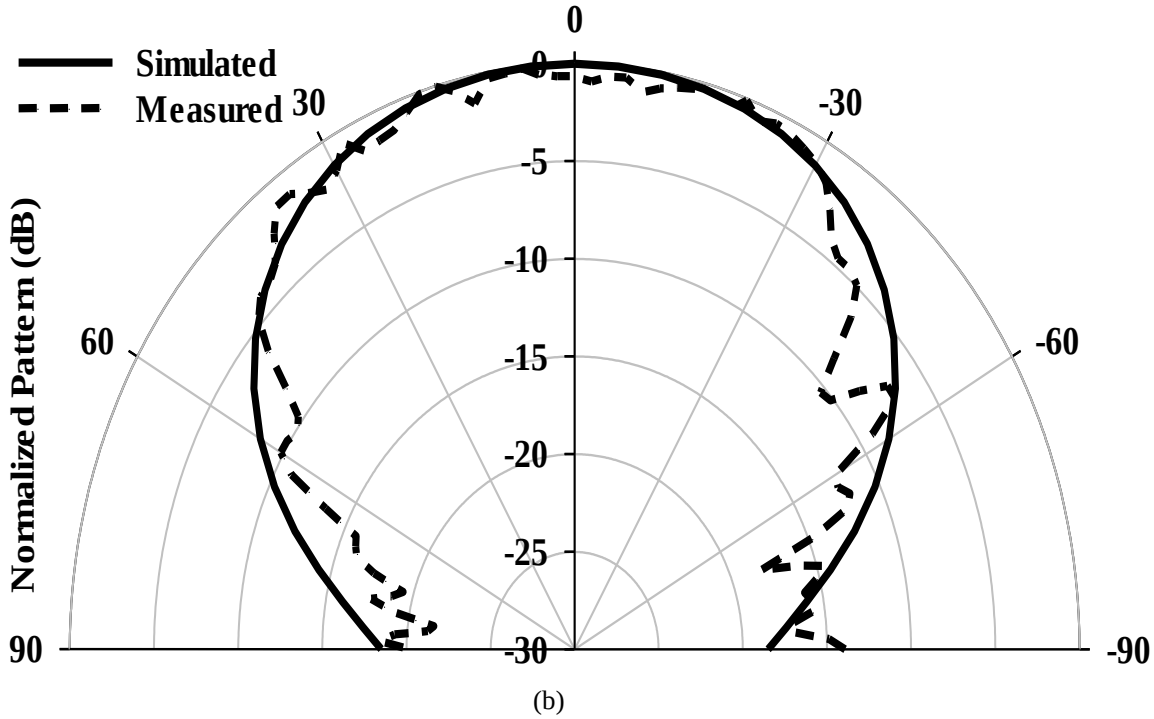

(b)

Figure 5.20: Radiation patterns of mm-wave HDRA excited in the TE_{515} mode at 21.9 GHz. (a) $\phi=0^0$, (b) $\phi=90^0$.

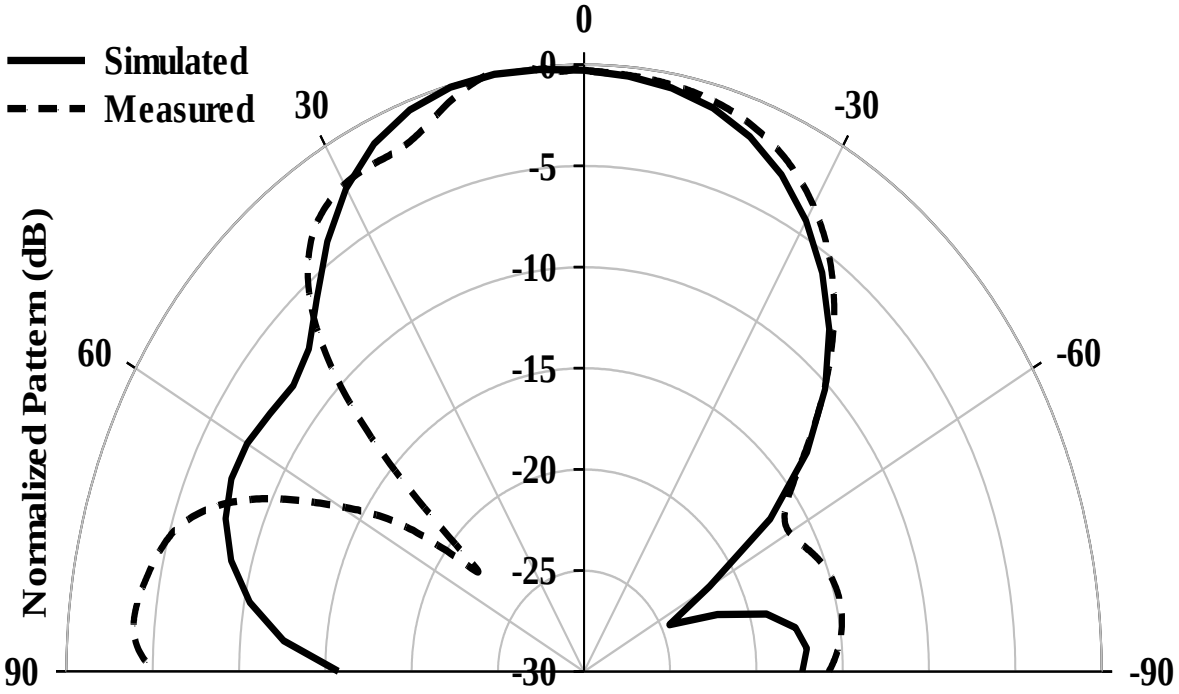

(a)

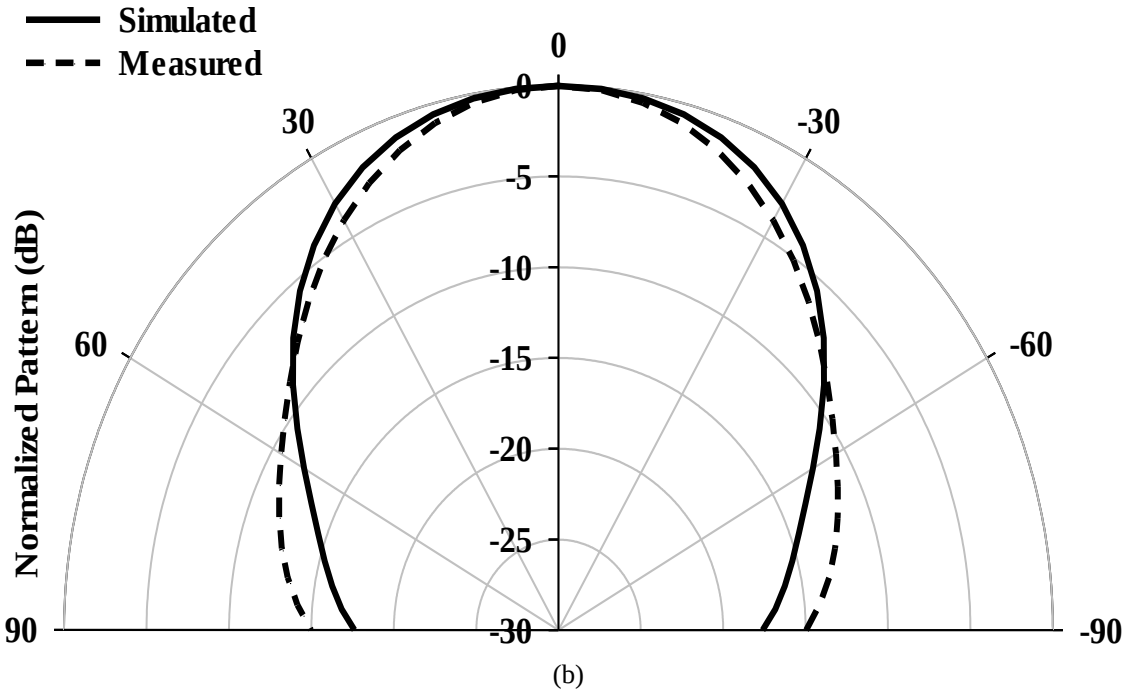

(b)

Figure 5.21: Radiation patterns of mm-wave HDRA excited in the TE_{717} mode at 29 GHz. (a) $\phi=0^0$, (b) $\phi=90^0$.

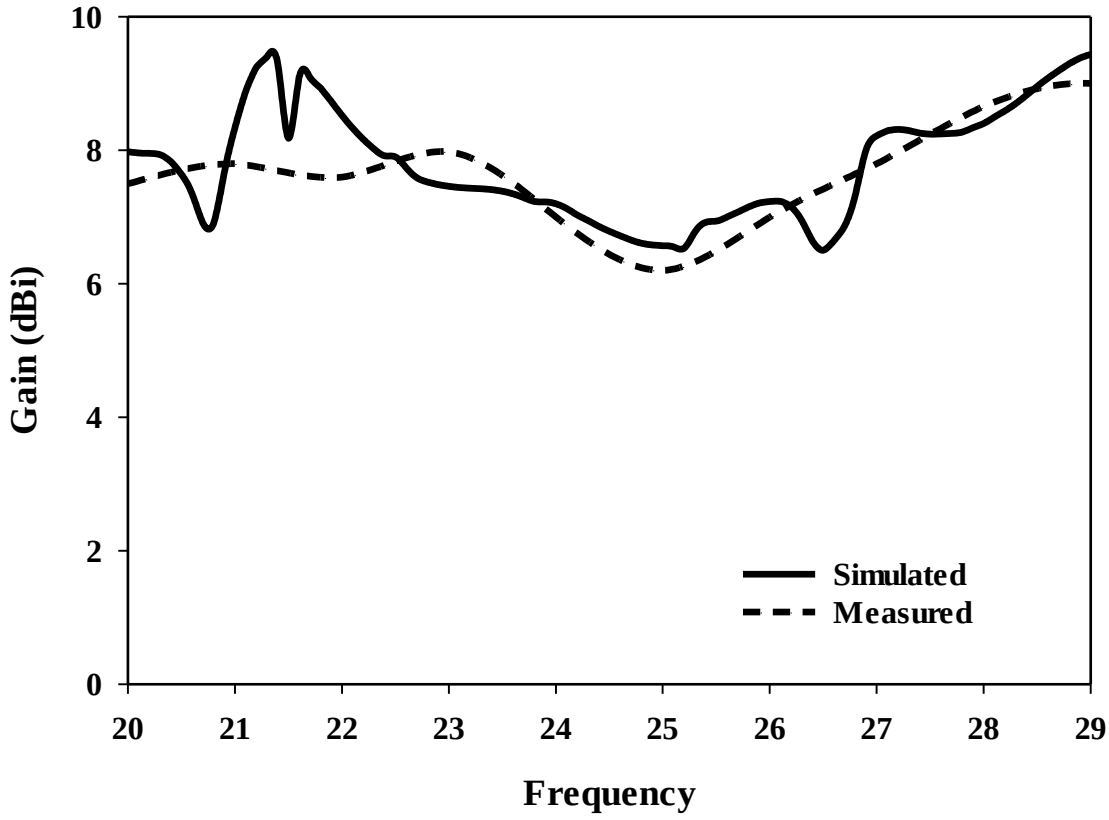

Figure 5.22: Simulated and measured gain of three-layer hemispherical DRA

Table 5-3: Comparison between the proposed high gain wide bandwidth HDRA and previously proposed designs.

Reference	Number of layers	Overall Size (λ_0)	Frequency range (GHz)	Gain (dBi)	Bandwidth %
Proposed antenna	Three	0.6	21-30	9.45	35.8
[72]	Two	0.48	5.1-7.42	-	52
[73]	Three	0.5	7.5-10.8	3.28	62.6
[74]	Three	0.72	8.4-9.5	6.4	9.6
[75]	Three	0.25	2.8-3.25	-	25.79
[76]	Three	0.45	4.5-6.5	4.5	36
[77]	Two	0.35	2.8-3.9	2.5	31.9

5.6 Conclusion

Layered rectangular and hemispherical DRA configurations have been designed for mm-wave applications. Mm-wave circularly polarized higher order mode rectangular DRA has been investigated experimentally. The proposed antenna offered a maximum gain of 12.5 dBic gain in conjunction with 36.8% and 13.73% impedance and axial ratio bandwidths. These appealing features will play main role for 5G applications that require higher gain and wider bandwidth. Furthermore, the layered RDRA performance is comparable to that of a typical DRA array.

In addition, based on the acquired HDRA results, it can be concluded that, fundamental and lower order HDRA modes offered lower gain due to the broad beam-width that result from the uniform short magnetic dipoles representation throughout the hemispherical surface. In order to increase the gain, extremely higher order resonance modes need to be excited, which requires considerably larger DRA dimensions. As a result, higher dielectric constants have been considered as an option to maintain practical DRA dimensions while improving the gain. However, the combination of higher DRA dielectric constants with higher order mode operation results in an extremely narrow bandwidth. It is well-known that adding a dielectric coat provides a transition region between the DRA and free space, which enhances the impedance bandwidth considerably. This approach has been intensively utilized with Alumina DRA, $\varepsilon_r \approx 10$ that has been covered by coats with typical relative permittivity of 3.5. However using such a material to provide a coat for a DRA with $\varepsilon_r = 20$ will reduce the reflections at the coat-air interface, while maintaining strong wave reflections at the coat-DRA interface due to the considerable differences in the two materials permittivity. Similarly, coating the DRA with of Alumina, $\varepsilon_r = 10$, reduces the wave reflections at the DRA-coat interface with stronger reflections at the coat-air interface. Therefore, multiple coat layers has been considered in order to provide a multi-stage transition regions between free space and the DRA element with minimised wave reflections at all interfaces. As a result of incorporating two outer layers, the impedance bandwidth has been improved to 35.8% compared with ~5.5% for a single layer hemispherical DRA along with a maximum gain of 9.45 dBi. In both of the rectangular and hemispherical DRA configurations, the outer layer provided a physical support to the smaller size DRA element. Furthermore, close agreement between simulated and measured results have been accomplished.

Chapter 6

Conclusions and Future Work

The focus of this thesis focused is on the design of wideband high gain circularly polarised layered DRAs that can be adopted for X band and mm-wave applications. Chapter one has provided an introduction to the research topic, objectives, literature review of existing approaches for DRA gain and impedance bandwidth enhancements and lists the thesis novelty and contributions. Chapter two presented numerous well-known gain enhancement approaches that have been utilized with a rectangular DRA. For example, utilizing a single higher order mode operation requires a single layer DRA aspect ratio that falls between ~0.3 and 1.5. Such an aspect ratio reduces the antenna profile and provides wider impedance bandwidth in conjunction with a lower gain due to the overlap between the adjacent magnetic field maxima, i.e. short magnetic diploes, which can be avoided when a multi-higher order mode approach is adopted. However, designing a rectangular DRA for a multi-higher order mode operation results in higher gain due to the elimination of overlapping between adjacent short magnetic dipoles, which is combined with key limitations such as higher DRA profile and narrower impedance bandwidth. Furthermore, using a dielectric superstrate for gain enhancement has been investigated experimentally, where a maximum gain of ~16.2 dBi has been achieved along with a narrow impedance bandwidth of 2% that represents the main drawback of this approach. Moreover, using antenna arrays resulted in a high gain of ~17dBi and wider impedance bandwidth of ~7% when six rectangular DRAs are utilized and separated by distance of 22 mm which corresponding to ~$0.8\lambda_0$. The increased size as well as potential ohmic losses, cost and complexity of the feed network represent the main challenges that are associated with the adopting the array approach.

Chapter two challenges have been addressed in Chapter three, where it has been demonstrated that the incorporation of the outer dielectric layer has reduced the required antenna profile and increased the gain and impedance bandwidth considerably. As a result, a novel structure of higher order mode layered rectangular CP DRA has been utilized that combines the advantages of higher gain along with wide impedance and axial ratio bandwidth as well as an improved physical support due to the fragility of the inner ceramic

DRA layer. For example, a two-layer rectangular DRA operating in the $TE_{11,11}$ mode offers respective impedance and axial ratio bandwidths of ~21% and 9.5% as well as a gain of 11.5 dBi, which could have not been achieved at the absence of the dielectric coat. More importantly, the proposed layered RDRA is less affected by fabrication errors compared to both single and multi-higher order mode single layer approaches. Furthermore, based on simulations that have been conducted using CST MWS, it has been noted that layered DRA configuration is most suitable for a multi-higher order mode operation. This can be understood by noting the fact that in a single higher order mode operation there is no adjacent modes that can be merged together when a dielectric coat is incorporated, hence less bandwidth enhancement is expected. In addition, an improvement of the bandwidth has been achieved when a layered rectangular cross-section DRA is designed. However, the slight improvement of the gain could be attributed to short magnetic diploes overlapping.

In Chapter four, circularly polarized layered cylindrical DRAs have been designed and measured with different dielectric coat thicknesses, where it has been demonstrated that incorporating an outer dielectric layer provides wider impedance and axial ratio bandwidths as well as high gain in a simple design. In addition, the effects of the outer dielectric layer on the gain enhancement has been examined in more details, where it has been observed that increasing the outer layer thickness results in a stronger electric filed confinement inside the inner DRA layer that leads to a narrower beam-width and hence the increment of the broadside gain. For example, two practical designs have demonstrated that a maximum gain of ~ 13.9 dBic can be achieved when the outer layer thickness is 20 mm compared to 11 dBic for a thickness of 10 mm. Even though the outer layer results in a slightly bigger size, the potential of this design could be exploited further at higher frequencies, for example at 60GHz where the outer layer radius will be reduced to 4mm. Another important point that should be taken to account with respect to the equivalent array gains of 14dBi that has been achieved in Chapter 2 by utilizing a four DRA array with an overall size of 76mm, which is almost double that of a single layered cylindrical DRA that offers comparable gain and other advantages such as the wider impedance and CP bandwidths as well as the absence of the array feed network.

In Chapter five, two practical mm-wave designs have been investigated experimentally, where, once more, wider impedance bandwidths have been achieved in conjunction with higher gain that meet the 5G application requirements. The CP mm-wave layered

rectangular DRA offered a gain of 12.5 dBic, which resulted in a smaller overall size and improved fabrication tolerance. Furthermore, based on analysis of a hemispherical DRA, it can concluded that in order to increase the gain, the higher order mode need to be excited, which implies a larger size with narrow impedance bandwidth. Therefore, the antenna permittivity needs to be increased in order to minimize the antenna size. However, even if the gain can be enhanced, the impedance bandwidth still extremely narrow. Therefore, a multi-stage dielectric coat has been considered in order to lower the quality factor and improve the bandwidth. For example, when the Alumina DRA, $\varepsilon_r \approx 10$, has been covered by a coat with a typical $\varepsilon_r = 3.5$, a wideband has been achieved in conjunction with a low gain. However, increasing the dielectric constant of the hemispherical DRA to $\varepsilon_r = 20$ with an Alumina coat, high gain and lower bandwidth have been obtained. Therefore, multiple coat layers has been considered in order to provide a multi-stage transition regions between free space and the DRA element with minimised wave reflections at all interfaces. As a result a 9.5 dBi gain has been achieved by coating the hemispherical DRA coated by two layers, which is considerably higher than typical gains of ~5dBi that have been reported in the literature. Furthermore, such a high gain has been accomplished with a wide impedance bandwidth of ~36 %. Finally, it can be concluded that, in context with the literature review, this thesis demonstrated robustness high gain wideband DRAs that are applicable for both X-band and mm-wave applications.

Future Work

This section exhibits some new areas of potential research for future work based on this thesis findings. The investigations process of this thesis has observed that using layered DRAs offered the challenging combination of high gain and wide bandwidth as well as a an improved physical support due to the fragility of the long and thin inner ceramic DRA layer. This features can be exploited at high frequencies such as 40 GHz and 60 GHz, where wider bandwidths and higher gains are key requirements in order to achieve high data rate for mm-wave communications. However, at such high frequencies any air gaps between the layers can impact the performance significantly. Therefore, novel manufacturing techniques need to be considered such the 3D printing of the Alumina DRA layer as well as the coat layer in a single process in order to ensure the elimination of any potential air gaps that may exist between the two layers. Additionally, 3D printing improves the fabrication tolerance, which is especially important at 40 and 60 GHz since the dimensions will be too small for a precise fabrication using traditional methods. Furthermore, the possibility of printing the feed substrate and the ground planed are strong because of availability of 3D printing machine and raw materials at the University of Sheffield. In addition, the circularly polarized multi-layer hemispherical DRA represents another promising area for further investigation since the utilization of a higher permittivity DRA impose a significant limitation on the generated CP bandwidth. Furthermore, in this thesis unequal lengths cross-slot feeding has been considered. In order to achieve wider axial ratio bandwidth other feeding mechanisms can be considered such as a spiral slot and parasitic patch that represent promising approaches. Moreover, as from DRA, a smaller size can be achieved when a higher permittivity is employed. Applying this concept to cylindrical and rectangular DRA represents a promising area for further investigation. Besides, the experience of designing layered DRA elements, the single layer DRA that has been investigated in this research can be developed to be form arrays, where placing multiple DRA elements inside one dielectric coat can achieve higher gain and maintains the wider impedance bandwidths.

References

[1] K. Luk and K. Leung, *Dielectric Resonator Antennas Research Studies Press Limited*, 2002.

[2] L. Z. Thamae and Z. Wu, "Broadband bowtie dielectric resonator antenna," *IEEE Transactions on antennas and Propagation*, vol. 58, pp. 3707-3710, 2010.

[3] G. Makwana and D. Ghodgaonkar, "Wideband stacked rectangular dielectric resonator antenna at 5.2 GHz," *International Journal of Electromagnetics and Applications*, vol. 2, pp. 41-45, 2012.

[4] T. S. Rappaport, R. W. Heath Jr, R. C. Daniels, and J. N. Murdock, *Millimeter wave wireless communications*: Pearson Education, 2014.

[5] J. Karjalainen, M. Nekovee, H. Benn, W. Kim, J. Park, and H. Sungsoo, "Challenges and opportunities of mm-wave communication in 5G networks," in *Cognitive Radio oriented Wireless networks and communications (CROWNCOM), 2014 9th International Conference on*, pp. 372-376, 2014.

[6] S. Long, M. McAllister, and L. Shen, "The resonant cylindrical dielectric cavity antenna," *IEEE Transactions on Antennas and Propagation*, vol. 31, pp. 406-412, 1983.

[7] M. Birand and R. Gelsthorpe, "Experimental millimetric array using dielectric radiators fed by means of dielectric waveguide," *Electronics Letters*, vol. 17, pp. 633-635, 1981.

[8] M. Haneishi and H. Takazawa, "Broadband circularly polarised planar array composed of a pair of dielectric resonator antennas," *Electronics Letters*, vol. 21, pp. 437-438, 1985.

[9] A. Kishk, A. Glisson, and G. Junker, "Bandwidth enhancement for split cylindrical dielectric resonator antennas," *Progress In Electromagnetics Research*, vol. 33, pp. 97-118, 2001.

[10] B. Li and K. W. Leung, "Strip-fed rectangular dielectric resonator antennas with/without a parasitic patch," *IEEE Transactions on Antennas and Propagation,* vol. 53, pp. 2200-2207, 2005.

[11] A. A. Kishk, X. Zhang, A. W. Glisson, and D. Kajfez, "Numerical analysis of stacked dielectric resonator antennas excited by a coaxial probe for wideband applications," *IEEE transactions on antennas and propagation,* vol. 51, pp. 1996-2006, 2003.

[12] A. Abumazwed, "Broadband dielectric resonator antennas for WLAN applications," Concordia University, 2009.

[13] G. Das, A. Sharma, and R. K. Gangwar, "Dual port aperture coupled MIMO cylindrical dielectric resonator antenna with high isolation for WiMAX application," *International Journal of RF and Microwave Computer-Aided Engineering,* vol. 27, p. e21107, 2017.

[14] R. A. Kranenburg, S. A. Long, and J. T. Williams, "Coplanar waveguide excitation of dielectric resonator antennas," *IEEE Transactions on Antennas and Propagation,* vol. 39, pp. 119-122, 1991.

[15] C. S. DeYoung and S. A. Long, "Wideband cylindrical and rectangular dielectric resonator antennas," *IEEE Antennas and Wireless Propagation Letters,* vol. 5, pp. 426-429, 2006.

[16] A. P. Kumar, "Higher order mode of a microstripline fed cylindrical dielectric resonator antenna," in *AIP Conference Proceedings,* p. 020027, 2016.

[17] N. Gupta, S. Rout, and K. Sivaji, "Characteristics of Cylindrical Dielectric Resonator Antenna," *Microwave Review,* pp. 29-32, 2009.

[18] M. Al Salameh, Y. M. Antar, and G. Seguin, "Coplanar-waveguide-fed slot-coupled rectangular dielectric resonator antenna," *IEEE Transactions on Antennas and Propagation,* vol. 50, pp. 1415-1419, 2002.

[19] Q. Lai, G. Almpanis, C. Fumeaux, H. Benedickter, and R. Vahldieck, "Comparison of the radiation efficiency for the dielectric resonator antenna and the microstrip

antenna at Ka band," *IEEE Transactions on Antennas and Propagation,* vol. 56, pp. 3589-3592, 2008.

[20] R. Khan, "MultiBand-Rectangular Dielectric Resonator Antenna," 2014.

[21] A. Petosa, A. Ittipiboon, Y. Antar, D. Roscoe, and M. Cuhaci, "Recent advances in dielectric-resonator antenna technology," *IEEE Antennas and Propagation Magazine,* vol. 40, pp. 35-48, 1998.

[22] A. Petosa and S. Thirakoune, "Design of a 60 GHz dielectric resonator antenna with enhanced gain," in *Antennas and Propagation Society International Symposium (APSURSI), 2010 IEEE*, pp. 1-4, 2010.

[23] A. Petosa and S. Thirakoune, "Rectangular dielectric resonator antennas with enhanced gain," *IEEE Transactions on Antennas and Propagation,* vol. 59, pp. 1385-1389, 2011.

[24] R. S. Yaduvanshi and H. Parthasarathy, *Rectangular dielectric resonator antennas*: Springer, 2016.

[25] Y.-M. Pan, K. W. Leung, and K.-M. Luk, "Design of the millimeter-wave rectangular dielectric resonator antenna using a higher-order mode," *IEEE Transactions on Antennas and Propagation,* vol. 59, pp. 2780-2788, 2011.

[26] S. Maity and B. Gupta, "Closed form expressions to find radiation patterns of rectangular dielectric resonator antennas for various modes," *IEEE Transactions on Antennas and Propagation,* vol. 62, pp. 6524-6527, 2014.

[27] M. Mrnka and Z. Raida, "Linearly polarized high gain rectangular dielectric resonator antenna," in *Antennas and Propagation (EuCAP), 2016 10th European Conference on*, pp. 1-4, 2016.

[28] N. H. Shahadan, M. R. Kamarudin, M. H. Jamaluddin, and Y. Yamada, "Higher-order mode rectangular dielectric resonator antenna for 5G applications," *Indonesian Journal of Electrical Engineering and Computer Science,* vol. 5, pp. 584-592, 2017.

[29] D. Guha, A. Banerjee, C. Kumar, and Y. M. Antar, "Higher order mode excitation for high-gain broadside radiation from cylindrical dielectric resonator antennas," *IEEE Transactions on Antennas and Propagation,* vol. 60, pp. 71-77, 2012.

[30] Y. X. Sun and K. W. Leung, "Dual-band and wideband dual-polarized cylindrical dielectric resonator antennas," *IEEE Antennas and Wireless Propagation Letters,* vol. 12, pp. 384-387, 2013.

[31] O. Avădănei, M. Banciu, and L. Nedelcu, "Higher-order modes in high-permittivity cylindrical dielectric resonator antenna excited by an off-centered rectangular slot," *IEEE Antennas and Wireless Propagation Letters,* vol. 13, pp. 1585-1588, 2014.

[32] A. Banerjee, C. Kumar, D. Guha, and Y. M. Antar, "Microstrip line (s) as new feed for exciting a cylindrical DRA with higher order HEM 12δ mode," in *Antennas and Propagation Society International Symposium (APSURSI), 2014 IEEE*, pp. 1990-1991, 2014.

[33] D. Guha, A. Banerjee, C. Kumar, and Y. M. Antar, "New technique to excite higher-order radiating mode in a cylindrical dielectric resonator antenna," *IEEE Antennas and wireless Propagation letters,* vol. 13, pp. 15-18, 2014.

[34] M. Mrnka and Z. Raida, "Enhanced-gain dielectric resonator antenna based on the combination of higher-order modes," *IEEE Antennas and Wireless Propagation Letters,* vol. 15, pp. 710-713, 2016.

[35] M. Mrnka and Z. Raida, "Gain improvement of higher order mode dielectric resonator antenna by thin air gap," in *Broadband Communications for Next Generation Networks and Multimedia Applications (CoBCom), International Conference on*, pp. 1-3, 2016.

[36] P. Hu, Y. Pan, X. Zhang, and S. Zheng, "Broadband filtering dielectric resonator antenna with wide stopband," *IEEE Transactions on Antennas and Propagation,* vol. 65, pp. 2079-2084, 2017.

[37] A. Sharma, K. Khare, and S. Shrivastava, "Simple and Enhanced Gain Dielectric Resonator Antenna for Ku band Application," *International Journal of Scientific & Engineering Research,* vol. 4, 2013.

[38] A. S. Al-Zoubi, A. A. Kishk, and A. W. Glisson, "Analysis and design of a rectangular dielectric resonator antenna fed by dielectric image line through narrow slots," *Progress In Electromagnetics Research,* vol. 77, pp. 379-390, 2007.

[39] F. Kazemi, M. H. Neshati, and F. Mohanna, "Design of rectangular dielectric resonator antenna fed by dielectric image line with a finite ground plane," *International Journal of Communications, Network and System Sciences,* vol. 3, p. 620, 2010.

[40] S. Fakhte, H. Oraizi, and L. Matekovits, "High gain rectangular dielectric resonator antenna using uniaxial material at fundamental mode," *IEEE Transactions on Antennas and Propagation,* vol. 65, pp. 342-347, 2017.

[41] A. S. Mekki, M. N. Hamidon, A. Ismail, and A. R. Alhawari, "Gain enhancement of a microstrip patch antenna using a reflecting layer," *International Journal of Antennas and Propagation,* vol. 2015, 2015.

[42] S. J. Franson and R. W. Ziolkowski, "Gigabit per second data transfer in high-gain metamaterial structures at 60 GHz," *IEEE Transactions on Antennas and Propagation,* vol. 57, pp. 2913-2925, 2009.

[43] H. Vettikalladi, L. Le Coq, O. Lafond, and M. Himdi, "High-efficient slot-coupled superstrate antenna for 60GHz WLAN applications," in *Proceedings of the Fourth European Conference on Antennas and Propagation*, pp. 1-5, 2010.

[44] Y. Coulibaly, M. Nedil, I. B. Mabrouk, L. Talbi, and T. A. Denidni, "High gain rectangular dielectric resonator for broadband millimeter-waves underground communications," in *2011 24th Canadian Conference on Electrical and Computer Engineering (CCECE)*, pp. 001088-001091, 2011.

[45] T. Elkarkraoui, G. Y. Delisle, N. Hakem, and Y. Coulibaly, "Hybrid Broadband 60-GHz Double Negative Metamaterial High Gain Antenna," *Progress in Electromagnetics Research,* vol. 58, pp. 143-155, 2015.

[46] M. Haneishi and B. Wu, "Array antenna composed of circularly polarized dielectric resonator antennas," in *Antennas and Propagation Society International Symposium, 1999. IEEE*, pp. 252-255, 1999.

[47] M. Keller, M. Oliver, D. Roscoe, R. Mongia, Y. Antar, and A. Ittipiboon, "EHF dielectric resonator antenna array," *Microwave and optical technology letters,* vol. 17, pp. 345-349, 1998.

[48] A. Buerkle, K. F. Brakora, and K. Sarabandi, "Fabrication of a DRA Array Using Ceramic Stereolithography," *IEEE Antennas and Wireless Propagation Letters,* vol. 5, pp. 479-482, 2006.

[49] J. Svedin, L.-G. Huss, D. Karlen, P. Enoksson, and C. Rusu, "A micromachined 94 GHz dielectric resonator antenna for focal plane array applications," in *Microwave Symposium, 2007. IEEE/MTT-S International*, pp. 1375-1378, 2007.

[50] F. Wee, F. Malek, F. Ghani, S. Sreekantan, and A. Al-Amani, "High gain and high directive of antenna arrays utilizing dielectric layer on bismuth titanate ceramics," *International Journal of Antennas and Propagation,* vol. 2012, 2012.

[51] N. M. Nor, M. H. Jamaluddin, M. R. Kamarudin, and M. Khalily, "Rectangular Dielectric Resonator Antenna Array for 28 GHz Applications," *Progress In Electromagnetics Research C,* vol. 63, pp. 53-61, 2016.

[52] B. Rana and S. K. Parui, "Direct microstrip line-fed dielectric resonator antenna array," *Journal of ElEctromagnEtic WavEs and applications,* vol. 30, pp. 1521-1531, 2016.

[53] M. Mrnka, M. Cupal, Z. Raida, A. Pietrikova, and D. Kocur, "Millimetre-wave dielectric resonator antenna array based on directive LTCC elements," *IET Microwaves, Antennas & Propagation,* vol. 12, pp. 662-667, 2018.

[54] M. R. Nikkhah, J. Rashed-Mohassel, and A. A. Kishk, "High-gain aperture coupled rectangular dielectric resonator antenna array using parasitic elements," *IEEE Transactions on Antennas and Propagation,* vol. 61, pp. 3905-3908, 2013.

[55] K. Gong, X. H. Hu, P. Hu, B. J. Deng, and Y. C. Tu, "A series-fed linear substrate-integrated dielectric resonator antenna array for millimeter-wave applications," *International Journal of Antennas and Propagation,* vol. 2018, 2018.

[56] M. R. Nikkhah, A. A. Kishk, and J. Rashed-Mohassel, "Wideband DRA array placed on array of slot windows," *IEEE Transactions on Antennas and Propagation*, vol. 63, pp. 5382-5390, 2015.

[57] W. Mazhar, D. Klymyshyn, G. Wells, A. Qureshi, M. Jacobs, and S. Achenbach, "Low profile artificial grid dielectric resonator antenna arrays for mm-wave applications," *IEEE Transactions on Antennas and Propagation*, 2019.

[58] B. Li, C.-X. Hao, and X.-Q. Sheng, "A dual-mode quadrature-fed wideband circularly polarized dielectric resonator antenna," *IEEE Antennas and wireless propagation letters*, vol. 8, pp. 1036-1038, 2009.

[59] H. San Ngan, X. S. Fang, and K. W. Leung, "Design of dual-band circularly polarized dielectric resonator antenna using a higher-order mode," in *Antennas and Propagation in Wireless Communications (APWC), 2012 IEEE-APS Topical Conference on*, pp. 424-427, 2012.

[60] X.-C. Wang, L. Sun, X.-L. Lu, S. Liang, and W.-Z. Lu, "Single-feed dual-band circularly polarized dielectric resonator antenna for CNSS applications," *IEEE Transactions on Antennas and Propagation*, vol. 65, pp. 4283-4287, 2017.

[61] G. Almpanis, C. Fumeaux, and R. Vahldieck, "Offset cross-slot-coupled dielectric resonator antenna for circular polarization," *IEEE Microwave and Wireless Components Letters*, vol. 16, pp. 461-463, 2006.

[62] L. Chu, D. Guha, and Y. Antar, "Comb-shaped circularly polarised dielectric resonator antenna," *Electronics Letters*, vol. 42, pp. 785-787, 2006.

[63] K.-W. Khoo, Y.-X. Guo, and L. C. Ong, "Wideband circularly polarized dielectric resonator antenna," *IEEE Transactions on Antennas and Propagation*, vol. 55, pp. 1929-1932, 2007.

[64] A. Malekabadi, M. H. Neshati, and J. Rashed-Mohassel, "Circular polarized dielectric resonator antennas using a single probe feed," *Progress In Electromagnetics Research C*, vol. 3, pp. 81-94, 2008.

[65] X. S. Fang and K. W. Leung, "Linear-/circular-polarization designs of dual-/wide-band cylindrical dielectric resonator antennas," *IEEE Transactions on Antennas and Propagation,* vol. 60, pp. 2662-2671, 2012.

[66] A. Malekabadi, M. H. Neshati, and J. Rashed-Mohassel, "Circular Polarized Dielectric Resonator Antenna for Portable RFID Reader Using a Single Feed," *Progress In Electromagnetics Research C,* vol. 3, pp. 81-94, 2008.

[67] H. Ng and K. Leung, "Circular-polarized hemispherical dielectric resonator antenna excited by dual conformal-strip," in *Antennas and Propagation Society International Symposium, 2002. IEEE,* pp. 442-445, 2002.

[68] K. W. Leung and H. K. Ng, "Theory and experiment of circularly polarized dielectric resonator antenna with a parasitic patch," *IEEE Transactions on Antennas and Propagation,* vol. 51, pp. 405-412, 2003.

[69] K. W. Leung and H. K. Ng, "The slot-coupled hemispherical dielectric resonator antenna with a parasitic patch: Applications to the circularly polarized antenna and wide-band antenna," *IEEE Transactions on Antennas and Propagation,* vol. 53, pp. 1762-1769, 2005.

[70] R. Chowdhury, R. Kumar, and R. K. Chaudhary, "A coaxial probe fed wideband circularly polarized antenna using unequal and adjacent-slided rectangular dielectric resonators for WLAN applications," *International Journal of RF and Microwave Computer-Aided Engineering,* vol. 28, p. e21210, 2018.

[71] J. Wen, Y. C. Jiao, Y. X. Zhang, and J. Jia, "Wideband circularly polarized dielectric resonator antenna loaded with partially reflective surface," *International Journal of RF and Microwave Computer-Aided Engineering,* p. e21962, 2019.

[72] K. W. Leung and K. K. So, "Theory and experiment of the wideband two-layer hemispherical dielectric resonator antenna," *IEEE Transactions on Antennas and Propagation,* vol. 57, pp. 1280-1284, 2009.

[73] A. B. Kakade and B. Ghosh, "Mode excitation in the coaxial probe coupled three-layer hemispherical dielectric resonator antenna," *IEEE Transactions on Antennas and Propagation,* vol. 59, pp. 4463-4469, 2011.

[74] A. Kakade and B. Ghosh, "Analysis of the rectangular waveguide slot coupled multilayer hemispherical dielectric resonator antenna," *IET microwaves, antennas & propagation,* vol. 6, pp. 338-347, 2012.

[75] A. B. Kakade and M. Kumbhar, "Wideband circularly polarized conformal strip fed three layer hemispherical dielectric resonator antenna with parasitic patch," *Microwave and Optical Technology Letters,* vol. 56, pp. 72-77, 2014.

[76] B. Ghosh and A. B. Kakade, "Mode excitation in the microstrip slot-coupled three-layer hemispherical dielectric resonator antenna," *IET Microwaves, Antennas & Propagation,* vol. 10, pp. 1534-1540, 2016.

[77] X. S. Fang and K. W. Leung, "Design of wideband omnidirectional two-layer transparent hemispherical dielectric resonator antenna," *IEEE Transactions on Antennas and Propagation,* vol. 62, pp. 5353-5357, 2014.

[78] S. Fakhte, H. Oraizi, and R. Karimian, "A novel low-cost circularly polarized rotated stacked dielectric resonator antenna," *IEEE Antennas and Wireless Propagation Letters,* vol. 13, pp. 722-725, 2014.

[79] Y. Pan and S. Zheng, "A low-profile stacked dielectric resonator antenna with high-gain and wide bandwidth," *IEEE Antennas and Wireless Propagation Letters,* vol. 15, pp. 68-71, 2016.

[80] S. Shum and K. Luk, "Numerical study of a cylindrical dielectric-resonator antenna coated with a dielectric layer," *IEE Proceedings-Microwaves, Antennas and Propagation,* vol. 142, pp. 189-191, 1995.

[81] W. Huang and A. Kishk, "Compact wideband multi-layer cylindrical dielectric resonator antennas," *IET Microwaves, Antennas & Propagation,* vol. 1, pp. 998-1005, 2007.

[82] R. K. Chaudhary, K. V. Srivastava, and A. Biswas, "Four element multilayer cylindrical dielectric resonator antenna excited by a coaxial probe for wideband applications," in *Communications (NCC), 2011 National Conference on*, pp. 1-5, 2011.

[83] R. K. Chaudhary, K. V. Srivastava, and A. Biswas, "Two-layer embedded half-split cylindrical dielectric resonator antenna for wideband applications," in *Radar Conference (EuRAD), 2012 9th European*, pp. 489-491, 2012.

[84] R. D. Maknikar and V. G. Kasabegoudar, "Circularly polarized cross-slot-coupled stacked dielectric resonator antenna for wireless applications," *International Journal of Wireless Communications and Mobile Computing*, vol. 1, pp. 68-73, 2013.

[85] Y. Sun, X. Fang, and K. W. Leung, "Wideband two-layer transparent cylindrical dielectric resonator antenna used as a light cover," in *Computational Electromagnetics (ICCEM), 2015 IEEE International Conference on*, pp. 286-287, 2015.

[86] C.-X. Wang, F. Haider, X. Gao, X.-H. You, Y. Yang, D. Yuan, *et al.*, "Cellular architecture and key technologies for 5G wireless communication networks," *IEEE Communications Magazine*, vol. 52, pp. 122-130, 2014.

[87] Y. Niu, Y. Li, D. Jin, L. Su, and A. V. Vasilakos, "A survey of millimeter wave communications (mmWave) for 5G: opportunities and challenges," *Wireless Networks*, vol. 21, pp. 2657-2676, 2015.

[88] N. H. Shahadan, M. H. Jamaluddin, M. R. Kamarudin, Y. Yamada, M. Khalily, M. Jusoh, *et al.*, "Steerable Higher Order Mode Dielectric Resonator Antenna With Parasitic Elements for 5G Applications," *IEEE Access*, vol. 5, pp. 22234-22243, 2017.

[89] J.-G. Kim, H. S. Lee, H.-S. Lee, J.-B. Yoon, and S. Hong, "60-GHz CPW-fed post-supported patch antenna using micromachining technology," IEEE microwave and wireless components letters, 15(10), pp.635-637,2005.

[90] R. K. Gangwar, S. Singh, and D. Kumar, "Comparative studies of rectangular dielectric resonator antenna with probe and microstrip line feeds," *Archives of applied science research*, vol. 2, pp. 1-10, 2010.

[91] L. Y. Feng and K. W. Leung, "Millimeter-wave wideband dielectric resonator antenna," in *Infrared, Millimeter, and Terahertz waves (IRMMW-THz), 2015 40th International Conference on*, pp. 1-2, 2015.

[92] Y. Coulibaly, M. Nedil, L. Talbi, and T. Denidni, "Design of a mm-wave broadband CPW-fed stacked dielectric resonator antenna for underground mining communication," in *Antennas and Propagation Society International Symposium (APSURSI), 2010 IEEE*, pp. 1-4, 2010.

[93] A. Perron, T. A. Denidni, and A. R. Sebak, "Circularly polarized microstrip/elliptical dielectric ring resonator antenna for millimeter-wave applications," *IEEE Antennas and Wireless Propagation Letters,* vol. 9, pp. 783-786, 2010.

[94] A. Rashidian, D. M. Klymyshyn, M. Tayfeh Aligodarz, M. Boerner, and J. Mohr, "Development of polymer-based dielectric resonator antennas for millimeter-wave applications," *Progress in Electromagnetics Research,* vol. 13, pp. 203-216, 2010.

[95] Y. Coulibaly, M. Nedil, L. Talbi, and T. Denidni, "High gain cylindrical dielectric resonator with superstrate for broadband millimeter-wave underground mining communications," in *Antenna Technology and Applied Electromagnetics & the American Electromagnetics Conference (ANTEM-AMEREM), 2010 14th International Symposium on*, pp. 1-4, 2010.

[96] M. Laribi and N. Hakem, "Hight-gain circular polarised hybrid DRA for millimeter-wave," in *Antennas and Propagation (APSURSI), 2016 IEEE International Symposium on*, pp. 141-142,2016.

[97] A. Elboushi, O. Haraz, A. Sebak, and T. Denidni, "A new circularly polarized high gain DRA millimeter-wave antenna," in *Antennas and Propagation Society International Symposium (APSURSI), 2010 IEEE*, pp. 1-4, 2010.

[98] J. Oh, T. Baek, D. Shin, J. Rhee, and S. Nam, "60-GHz CPW-fed dielectric-resonator-above-patch (DRAP) antenna for broadband WLAN applications using micromachining technology," *Microwave and Optical Technology Letters,* vol. 49, pp. 1859-1861, 2007.

[99] W. M. A. Wahab, D. Busuioc, and S. Safavi-Naeini, "Low cost planar waveguide technology-based dielectric resonator antenna (DRA) for millimeter-wave applications: Analysis, design, and fabrication," *IEEE Transactions on Antennas and Propagation,* vol. 58, pp. 2499-2507, 2010.

[100] N. Ojaroudiparchin, M. Shen, and G. F. Pedersen, "Mm-Wave dielectric resonator antenna (DRA) with wide bandwidth for the future wireless networks," in *Microwave, Radar and Wireless Communications (MIKON), 2016 21st International Conference on*, pp. 1-4, 2016.

[101] H. Chu and Y.-X. Guo, "A novel approach for millimeter-wave dielectric resonator antenna array designs by using the substrate integrated technology," *IEEE Transactions on Antennas and Propagation,* vol. 65, pp. 909-914, 2017.

[102] Y. Liu, Y. C. Jiao, Z. Weng, C. Zhang, and G. Chen, "A novel millimeter-wave dual-band circularly polarized dielectric resonator antenna," *International Journal of RF and Microwave Computer-Aided Engineering,* p. e21871, 2019.

[103] M. Studio, "Computer Simulation Technology (CST)," *Online: www. cst. com,* 2015.

[104] M. Mrnka, "Perforated dielectrics and higher-order mode dielectric resonator antennas," Ph. D. dissertation, Brno University of Technology, Brno, Czech Republic, 2017.

[105] A. Petosa, *Dielectric resonator antenna handbook*: Artech House Publishers, 2007.

[106] B. Y. Toh, R. Cahill, and V. F. Fusco, "Understanding and measuring circular polarization," *IEEE Transactions on Education,* vol. 46, pp. 313-318, 2003.

[107] S. Gregson, J. McCormick, and C. Parini, *Principles of planar near-field antenna measurements* vol. 53: IET, 2007.

[108] H. Yang and N. Alexopoulos, "Gain enhancement methods for printed circuit antennas through multiple superstrates," *IEEE Transactions on Antennas and Propagation,* vol. 35, pp. 860-863, 1987.

[109] Y. Coulibaly, M. Nedil, L. Talbi, and T. A. Denidni, "Design of high gain and broadband antennas at 60 GHz for underground communications systems," *International Journal of Antennas and Propagation,* vol. 2012, 2012.

[110] S. K. K. Dash, T. Khan, B. K. Kanaujia, and N. Nasimuddin, "Wideband cylindrical dielectric resonator antenna operating in HEM11δ mode with improved gain: a study

of superstrate and reflector plane," *International Journal of Antennas and Propagation*, vol. 2017, 2017.

[111] K. L. Wong and N. C. Chen, "Analysis of a broadband hemispherical dielectric resonator antenna with a dielectric coating," *Microwave and Optical Technology Letters*, vol. 7, pp. 73-76, 1994.

[112] N. C. Chen, H. C. Su, K. L. Wong, and K. W. Leung, "Analysis of a broadband slot-coupled dielectric-coated hemispherical dielectric resonator antenna," *Microwave and Optical Technology Letters*, vol. 8, pp. 13-16, 1995.

[113] K. P. Esselle, "Circularly polarised higher-order rectangular dielectric-resonator antenna," *Electronics Letters*, vol. 32, pp. 150-151, 1996.

[114] A. Sharma, K. Khare, and S. Shrivastava, "Simple and Enhanced Gain Dielectric Resonator Antenna for Ku band Application." International Journal of Scientific & Engineering Research, 4(9), pp.1066-1070,2013.

[115] M. I. Sulaiman and S. K. Khamas, "A singly fed rectangular dielectric resonator antenna with a wideband circular polarization," *Ieee antennas and wireless propagation letters*, vol. 9, pp. 615-618, 2010.

[116] K. W. Leung, "Conformal strip excitation of dielectric resonator antenna," *IEEE Transactions on Antennas and Propagation*, vol. 48, pp. 961-967, 2000.

[117] K. M. Luk and K. W. Leung, *Dielectric resonator antennas*. Baldock, Hertfordshire, England; Philadelphia, PA; Williston, VT: Research Studies Press ; Distribution, North America [by] AIDC, 2003.

[118] A. Kapoor and G. Singh, "Mode classification in cylindrical dielectric waveguides," *Journal of lightwave technology*, vol. 18, pp. 849-852, 2000.

[119] J. Sethares and S. Naumann, "Design of microwave dielectric resonators," *IEEE Transactions on Microwave Theory and Techniques*, vol. 14, pp. 2-7, 1966.

[120] R. De Smedt, "Correction due to a finite permittivity for a ring resonator in free space," *IEEE transactions on microwave theory and techniques*, vol. 32, pp. 1288-1293, 1984.

[121] M. Tsuji, H. Shigesawa, and K. Takiyama, "Analytical and experimental investigations on several resonant modes in open dielectric resonators," *IEEE transactions on microwave theory and techniques,* vol. 32, pp. 628-633, 1984.

[122] A. A. Abdulmajid, Y. Khalil, and S. K. Khamas, "Higher Order Mode Circularly Polarised Two-Layer Rectangular Dielectric Resonator Antenna," *IEEE Antennas and Wireless Propagation Letters,* 2018.

[123] C.-Y. Huang, J.-Y. Wu, and K.-L. Wong, "Cross-slot-coupled microstrip antenna and dielectric resonator antenna for circular polarization," *IEEE Transactions on Antennas and Propagation,* vol. 47, pp. 605-609, 1999.

[124] S. Shum and K. Luk, "Stacked annular ring dielectric resonator antenna excited by axi-symmetric coaxial probe," *IEEE Transactions on Antennas and Propagation,* vol. 43, pp. 889-892, 1995.

[125] S. H. Ong, A. A. Kishk, and A. W. Glisson, "Wideband disc-ring dielectric resonator antenna," *Microwave and Optical Technology Letters,* vol. 35, pp. 425-428, 2002.

[126] N. M. Nor, M. H. Jamaluddin, M. R. Kamarudin, and M. Khalily, "Rectangular dielectric resonator antenna array for 28 GHz applications," *Progress In Electromagnetics Research,* vol. 63, pp. 53-61, 2016.

[127] H. Kaouach, L. Dussopt, J. Lanteri, T. Koleck, and R. Sauleau, "Wideband low-loss linear and circular polarization transmit-arrays in V-band," *IEEE Transactions on Antennas and Propagation,* vol. 59, pp. 2513-2523, 2011.

[128] J.-H. Lin, W.-H. Shen, Z.-D. Shi, and S.-S. Zhong, "Circularly polarized dielectric resonator antenna arrays with fractal cross-slot-coupled DRA elements," *International Journal of Antennas and Propagation,* vol. 2017, 2017.

[129] K. Leung, K. Luk, and K. Lai, "Input impedance of hemispherical dielectric resonator antenna," *Electronics Letters,* vol. 27, pp. 2259-2260, 1991.

[130] K.-W. Leung, K.-M. Luk, K. Y. Lai, and D. Lin, "Theory and experiment of an aperture-coupled hemispherical dielectric resonator antenna," *IEEE Transactions on Antennas and Propagation,* vol. 43, pp. 1192-1198, 1995.

[131] K. Leung, K. Ng, K. Luk, and E. Yung, "Simple formula for analysing the centre-fed hemispherical dielectric resonator antenna," *Electronics Letters*, vol. 33, pp. 440-441, 1997.

[132] M. Gastine, L. Courtois, and J. L. Dormann, "Electromagnetic resonances of free dielectric spheres," *IEEE Transactions on Microwave Theory and Techniques*, vol. 15, pp. 694-700, 1967.